Centre for Doctoral Training in Energy Storage and its Applications

Department of Chemical and Biological Engineering

A Techno-Economic Analysis of Lithium-Ion and Vanadium Redox Flow Batteries for Behind-the-Meter Commercial/Industrial Applications with a Focus on Achievable Efficiency and Degradation Rates.

Thesis submitted for the degree of Doctor of Philosophy

Diarmid Roberts

d.roberts1@sheffield.ac.uk

August 4, 2022

Declaration

I, Diarmid Roberts, confirm that the work presented in this thesis is my own. Where information or methods have been derived from other sources, I confirm that this has been indicated in the thesis. I also confirm that this work has not been submitted - in its entirety or in part - at any other institution to obtain an academic qualification.

Abstract

This thesis concerns vanadium redox flow batteries (VRFB), and whether their posited advantages over the more commercially advanced lithium-ion battery (LIB) can translate to improved economic outcomes in realistic use-cases.

The key advantage of the VRFB is increased lifetime; the energy storage medium (and major cost component) is simply two solutions of vanadium at differing oxidation states hence here is no scope for the myriad permanent degradation mechanisms that exist in LIB. As such, over a project lifetime VRFB will potentially have lower economic and environmental costs than LIB. A second posited advantage of the VRFB was the low incremental cost of storage duration, allowing longer durations to be more cost competitive.

However, VRFB are disadvantaged by lower round-trip efficiency and a higher power capacity cost due to the relatively complex power generating apparatus.

In this thesis, bottom up cost modelling for a state of the art VRFB predicted that following cost reductions in LIB over the last 5 years, the cost of incremental usable duration would now be very similar for the two technologies, negating one of the posited benefits.

For the full cost-benefit analysis, it was hence important to rigorously define the use-cases and resulting cycle rates. The chosen case study was a commercial/industrial facility in South California. This region is a very promising market for stationary electrical storage, and as such was considered an arena in which VRFB and LIB are likely to compete in the near future.

In order to thoroughly explore the thesis two differing archetypal use-case were formulated. In use-case A, the battery was called upon to reduce the electricity bill at the facility by time-shifting power imports to cheaper hours, reducing the peak power consumption each month, and generate revenue by providing spinning reserve and frequency response

to the grid operator. The objective was strictly economic; to maximise the net present value of a ten year project.

In use-case B, the battery was deployed in conjunction with a PV array in order to achieve self-sufficiency in power. In this case the self-sufficiency objective is in competition with the economic objective (to minimise the levelised cost of electricity), hence a multi-objective optimisation was used to size the battery and PV array.

An important contribution made by this thesis was the incorporation of detailed degradation models for both VRFB and LIB. For VRFB, previous case studies had assumed zero degradation, whereas in practice regular intervention is required to avoid electrolyte imbalance. For LIB, similar case studies had employed models attributing all degradation to cycling, whereas continual temperature dependent aging is also important. The latter was modelled in this work.

A novel mixed integer-quadratic programming (MIQP) method was introduced that allowed the VRFB operation to be optimised while accounting for the considerable variation in efficiency with power input/output. This is an improvement over previous VRFB case studies where a constant efficiency is assumed. In use-case A this resulted in the discovery of an energy saving strategy whereby the charging was performed at moderate power in order to track the peak efficiency as closely as possible. In a further novel contribution, this model was used to demonstrate the benefit of operating multiple VRFB modules as an ensemble. The benefit arises when a low load must be covered, and some modules may be idled to reduce parasitic losses.

In use-case A, it was concluded that VRFB may compete with LIB under certain scenarios at 4 h duration, although the most profitable system is a shorter duration LIB. Both were predicted to break even at 6 h duration when current long duration storage incentives were included.

For use-case B, both systems were predicted to achieve a SSR of 0.95 at under ¢21.5 $\mathrm{kW^{-1}\,h^{-1}}$. Although the costs overlap depending on the scenario, VRFB were estimated to be more likely to be cheaper up to 0.9 SSR, above which reducing cycle rates

favoured LIB. This level of self-sufficiency called for a usable duration of 6 h - 7.5 h. An important finding for project developers is hence that 6 h would be a sensible duration for both LIB and VRFB systems as this would cover both use cases effectively.

Another novel contribution of this work to estimate the benefit of a hybrid LIB/VRFB system, the hypothesis being that the LIB could be used to cover the less frequent high charge/discharge power events. In use-case B this had the hypothesised effect of increasing the LIB lifetime, but there was negligible predicted effect on the overall levelised cost of electricity.

Lastly, a number of important findings were made relating to practical operation of both LIB and VRFB, which should be of interest to asset owners. Firstly, in use-case A, it is unlikely that bidding for regulation provision would be feasible alongside demand charge reduction, as performing the former can result in a loss in the latter. Maintenance timing was predicted to be important for VRFB in use-case A where available revenue varies seasonally, and the capacity should be replenished prior to the peak revenue periods of the summer months. For LIB, it was predicted that managing state of charge will prolong life considerably in use-case B, and climactic variations across Southern California may strongly affect lifetime in both cases.

Acknowledgements

I would like to thank the EPSRC for funding my PhD via the Centre For Doctoral Training in Energy Storage and its Applications. I would also like to thank Drax Power for making an additional contribution.

Next I would like to thank my supervisor Sol Brown for helping me get started in modelling, for reassurance on many occasions, for pushing me to write papers, for lots of interesting conversations, and last but not least for reviewing my chapters in a timely fashion!

I would also like to say thanks to my colleagues on the CDT, especially those in the Kroto building, for four really enjoyable years. Among these I'd like to thank Rachel Lee for all the coffee break conversations and for answering my endless questions about electrical grids, markets and project economics.

Finally, I'd like to thank my wife Annie, and boys Laurie and Morgan, who appeared while the following work was in progress. Doing the following work, I've had to think like an accountant at times, so it's been great to get home and spend time with priceless people. Special thanks go to Annie who has been incredibly patient and supportive, especially in the last few months when I've been writing up on most evenings.

List of Publications

The following research articles have been published as a direct results of the work undertaken for this thesis:

- D. Roberts, S. F. Brown, "Flow batteries for energy management: Novel algebraic modelling approaches to properly assess their value." *Journal of Energy Storage*, vol. 26, 2019.
- D. Roberts, S. F. Brown, "DC to Turnkey: an analysis of the balance of costs for behind the meter BESS at commercial/industrial sites." *Energy Reports*, vol. 7, 2021.
- D. Roberts, S. F. Brown, "The economics of firm solar power from Li-ion and vanadium flow batteries in California", *MRS Energy & Sustainability*, 2022.

The first publication concerns the application of the MIQP model introduced in Chapter 6 to deliver a meaningful improvement in energy price arbitrage revenue compared to typical LP methods. The second publication describes the balance of system cost model developed for the techno-economic analyses performed in this thesis, and discusses the limitations of the data available. The third article is a technoeconomic analysis based on the work described in Chapter 7, including the novel hybrid LIB/VRFB system modelling.

Additionally, the following article based on the multiple module RFB optimisation introduced in Chapter 6 is currently under review:

- D. Roberts, J. Baker, J. Searle, T. Griffiths, R. Lewis, S. F. Brown, "Overcoming performance limitations of hybrid redox flow batteries with modular operation."

Contents

Declaration **i**

Abstract **ii**

Acknowledgements **iii**

List of Publications **iv**

Chapter 1: Introduction **10**

1.1 Context 10

1.2 Structure of Thesis 13

Chapter 2: Literature Review **15**

2.1 Redox Flow Batteries 15

2.1.1 RFB Technical Considerations 18

2.1.2 Classification of RFB Systems 21

2.1.2.1 Degree of Symmetry 21

2.1.2.2 Hybrid Systems 21

2.1.2.3 Metal/non-Metal 22

2.1.2.4 Aqueous/non-Aqueous Solvent 23

2.1.2.5 Separation Method 24

2.1.3 The Vanadium RFB 26

2.1.3.1 VRFB Degradation Processes 29

2.1.3.2 Commercial VRFB Offerings 31

2.2 Techno-Economic Analysis 31

2.2.1 TEA Methods Specific to ESS 33

2.2.2 Methodology for Review of TEA on RFB Systems 34
2.2.3 Costs of RFB Systems 36
2.2.3.1 Bottom up Cost Models 36
2.2.3.2 Cost Trend Analysis 37
2.2.4 Benefit Analysis of RFB Systems 37
2.2.4.1 Application Definition 37
2.2.4.2 Optimisation Approaches 39
2.2.5 LIB Degradation in TEA 44
2.3 Conclusions 46
2.4 Summary of Research Challenges and Novel Contributions 48

Chapter 3: Methodology **51**
3.1 Introduction 51
3.2 Defining the Power and Duration of the BESS 52
3.3 Enhanced Degradation Models 53
3.3.1 VRFB Stack Lifetime, Capacity Fade and Electrolyte Decay 53
3.3.2 LIB Degradation Model with Calendar Aging and Temperature Dependence 57
3.4 Economic Analyses 59
3.4.1 Discounted Cash Flow Model 59
3.4.2 Levelised cost of Storage and Levelised Cost of Energy Calculations 60
3.4.3 DC Module Definition 61
3.4.4 VRFB DC Price Model 61
3.4.4.1 RFB Price Model Terms 63
3.4.4.2 Base Scenario VRFB Parameters 66
3.4.5 LIB DC Price Model 70
3.4.6 Balance of Upfront Costs for Turnkey BESS 70
3.4.7 Operation and Maintenance Costs 75
3.5 Conclusions 76

Chapter 4: The Co-optimisation of Revenue Streams Behind the Meter in the CAISO Market. 77

4.1 Introduction 77

4.2 Methods 78

4.2.1 Model Assumptions 79

4.2.2 Linear Programming Model Described by Fisher *et al.* 80

4.2.3 Novel Extensions to Fisher Model 86

4.2.3.1 Quantifying BESS Usage for Accurate Degradation Modelling 86

4.2.3.2 Accounting for Regulation Throughput in Degradation . . 88

4.2.3.3 Regulation Signal Parameters 90

4.2.3.4 Enforcement of the CAISO Continuous Energy Requirement 92

4.2.4 Data Sources and Processing Methods 93

4.3 The Revenue Stack 93

4.4 Sensitivity of Optimal BESS Operation to Degradation Penalty and Demand Charge Weighting 96

4.5 The Impact of the CAISO Continuous Energy Requirement 99

4.6 Managing Risk Caused by Regulation Dispatch Uncertainty 100

4.6.1 Risk of Ejection from the Regulation Market 103

4.6.2 Risk to Peak Demand Charge Avoidance 109

4.7 Conclusions 112

Chapter 5: Comparing the NPV of LIB and VRFB Projects at Site 281 using State of the Art Degradation Models. 114

5.1 Introduction 114

5.2 Methods 115

5.2.1 Model Assumptions 115

5.3 CAPEX Requirements for Turnkey Systems 117

5.4 The Impact of Degradation 120

5.4.1 A Comparison of the Ciez and Whitacre and the Schmalstieg Degradation models . . . 120
5.4.2 Optimising the Revenue/Lifetime Trade-off . . . 122
5.4.3 Managing SOC to Extend LIB Lifetime . . . 123
5.4.4 Optimisation of VRFB Maintenance Timing . . . 124
5.5 NPV Comparison of VRFB and LIB of Varying Duration at Site 281 . . . 125
5.5.1 Impact of 4 Hour Duration Resource Adequacy Payments . . . 126
5.5.2 An Economic Sensitivity Study on External Variables and VRFB Efficiency. . . . 127
5.5.3 An Economic Sensitivity Study of the No-Spinning-Reserve Scenario 130
5.6 Conclusions . . . 133

Chapter 6: Optimising the Operation of a VRFB with a Novel Algebraic Model for Dynamic Efficiency 135

6.1 Introduction . . . 135
6.2 Methods . . . 136
6.2.1 Model Assumptions . . . 136
6.2.2 Novel Mixed Integer-Quadratic Programming Model for Multiple VRFB Modules . . . 136
6.2.3 VRFB Parametrisation in the MIQP Model . . . 139
6.2.4 Maximum Cell Voltage Constraint . . . 141
6.2.5 Practicalities of Solving the MIQP Problem . . . 142
6.3 VRFB Dynamic Efficiency . . . 142
6.4 MIQP Optimal VRFB Operation . . . 144
6.5 Cost Benefit Analysis on Electrode Area . . . 145
6.6 Improving VRFB Efficiency With Independent Scheduling of Sub-Modules 149
6.6.1 Uncertainty in Fixed Losses . . . 152
6.7 The Impact of Voltage Constraints on High Current Operation . . . 154
6.8 Conclusions . . . 156

Chapter 7: A Comparison of LIB and VRFB Economics in Support of Self-Sufficiency from on-Site PV **158**

7.1 Introduction 158

7.2 Methods 160

7.2.1 Model Assumptions 160

7.2.2 MILP Formulation for Maximising PV Self-Sufficiency Ratio 162

7.2.3 MIQP Multiple VRFB Module Formulation 163

7.2.4 Hybrid System MILP Formulation 164

7.3 Economic Comparison of LIB and VRFB in a Constrained PV Scenario . . 164

7.4 A Comparison in a Non-Constrained PV Scenario 167

7.4.1 Base Scenario 168

7.4.2 Economic Sensitivity Study 170

7.4.3 Extending LIB lifetime by SOC control 172

7.5 Evaluating the Benefit of Hybrid LIB/VRFB Systems 174

7.6 Achievable VRFB Round Trip Efficiency While Providing Self Sufficiency . 178

7.7 Load Profile Dependence 180

7.8 Conclusions 182

Chapter 8: Conclusions **184**

8.1 Further Work 191

8.1.1 Temperature and Degradation Modelling 191

8.1.2 Non-Deterministic Modelling 193

8.1.3 Lithium Iron Phosphate Chemistry 194

List of Figures

1.1 Thesis Structure in Terms of Novel Contributions. 14

2.1 Schematic of a RFB. 17

2.2 Illustration of RFB Polarisation Curve 19
2.3 Generic Schematic of BESS Sizing Optimisation 39
2.4 Example of BESS Sizing Optimisation by Graphic Sensitivity Study 40

3.1 Comparison of LIB Installation Costs from Lazard and PNNL and Synthesis Applied in this Work 75

4.1 Site 281 Load Profile Showing Demand Charge Periods. 78
4.2 Clusters Found in Daily Profiles of CAISO Day-Ahead AS Prices 81
4.3 Clusters Found in Daily Profiles of CAISO Day-Ahead LMP Prices 82
4.4 Illustration of Appropriate Data Smoothing Resolution for Regulation Dispatch Signal 89
4.5 Regulation Signal Variability 90
4.6 Distribution of 15 min Averaged Regulation Signal 91
4.7 Snapshot of Optimal Operation of a 2 h LIB Behind the Meter in the CAISO Market 94
4.8 Annual Revenue Stacks for 2h and 4h LIB and VRFB 95
4.9 Sensitivity Study on Effect of LIB Throughput penalty on the Revenue Stack. 97
4.10 Sensitivity Study on Impact of Demand Charge Weighting on the Revenue Stack 99
4.11 Impact of CAISO 1 h Continuous Energy Requirement 100
4.12 Example Regulation Signal Data Showing Signal Imbalance at a Range of Time Resolutions. 102
4.13 Example of Simulated Regulation Provision Failure 105
4.14 Simulated Regulation Accuracy Across One Year for 2 h and 4 h] LIB and VRFB 106
4.15 Scatter-Plots Used to Determine Cause of Poorer Regulation Accuracy Observed for VRFB. 107
4.16 The trade-off Between Demand Charge Avoidance and Regulation. 110
4.17 Monthly Breakdown of Revenue for a 80 kW/4 h LIB. 111

4.18 Analysis of Demand Charge and Regulation Revenue Trade-off in March to May period 111

5.1 Price Breakdown of VRFB DC Module in \$ kW^{-1} and \$ kW^{-1} h 117

5.2 Turnkey Price Versus Duration for LIB and VRFB 119

5.3 Ambient Temperature Histograms for Locations Simulated in This Work . 120

5.4 Comparison of LIB Degradation Predicted by Cycle-Only Model and Model with Calendar Aging 121

5.5 The Effect on LIB Lifetime and Revenue of Varying the Throughput Penalty 122

5.6 Dependence of 10 Year LIB Project NPV on Throughput Penalty Term . . 123

5.7 The Degradation of VRFB Capacity Across One Year of Operation 125

5.8 Revenue and NPV Dependence on LIB and VRFB Duration 126

5.9 The Impact of the CAISO Resource Adequacy Payment 127

5.10 Sensitivity Study for Relative NPV of LIB and VRFB Systems with all Revenue Streams Included 129

5.11 An Illustration of the Impact of a SOC Penalty on the Optimal LIB Schedule 131

5.12 Sensitivity Study for Relative NPV of LIB and VRFB Systems Without Spinning Reserve Revenue Stream 132

6.1 Derivation of ASR and V_a Parameters from Experimental Data of Reed *et al.* 140

6.2 Simulated VRFB Efficiency and Experimental Data Across a Range of Current Density 143

6.3 An Example of the Difference Between VRFB Operation Optimised Using LP and MIQP Models 144

6.4 DC Boundary Price of 1 kW VRFB in Different Electrode Area Cases . . . 146

6.5 Dependence of Operational Efficiency and Project NPV on Electrode Area 147

6.6 Histograms Explaining Difference in Optimal Electrode Areas for VRFBs of 2 h and 4 h Duration 148

6.7 Sensitivity of Multiple Module Optimisation to Computing Time 150

6.8 Example of Optimal peak Shaving Operation with Two VRFB Modules . . 151

6.9 The Impact of Multiple Module Operation on the Optimal Electrode Area 152

6.10 Simulated VRFB Efficiency with Increased Coulombic Loss 153

6.11 The Importance of Multiple Module Operation in Increased Coulombic Loss Scenario 153

6.12 Incidence of High Cell Voltages During VRFB Operation 156

7.1 Model for LIB Efficiency at Greater than 4 h Duration 161

7.2 LCOS Comparison for LIB and VRFB when Installed to Increase Self-sufficiency from Existing Rooftop PV at Site 281 165

7.3 Approximate Pareto Fronts for Maximisation of Self-Sufficiency and Minimisation of Levelised Cost of Electricity at Site 281 169

7.4 Sensitivity Study on the Comparative Cost of Self-Sufficiency Provision from LIB and VRFB 171

7.5 Comparison of SOC profile of a 1080 kW/6 h LIB across one year of operation providing self sufficiency at site 281 when paired with a 1080 kWp PV array (120% over-sizing). a) 24 h optimisation. b) 48 h optimisation with penalty on mean SOC. 173

7.6 Impact of LIB SOC Minimisation Strategy on LCOE / Self-Sufficiency Pareto Front 174

7.7 Snapshot of Optimal Operation of LIB:VRFB Hybrid BESS 175

7.8 Cycle-Rate and Lifetime of a LIB in Various Combinations with a VRFB in a Hybrid System 176

7.9 A comparison of the economics of hybrid VRFB:LIB systems with those of the optimal single BESS systems. 0% VRFB indicates a 100% LIB system. 177

7.10 Histograms Showing Current Density During MIQP Optimal Operation for Self-sufficiency from PV 179

7.11 Site 767 Load Profile 181

7.12 Comparison of LIB and VRFB Pareto Fronts for LCOE and SSR at Site 767 181

List of Tables

2.1 VRFB commercial Offerings as of 2021 31
2.2 TEA Literature Review Methodology 35

3.1 VRFB Capacity Loss Parameters 56
3.2 VRFB Component Prices Assumed in Bottom up Model. 67
3.3 VRFB Technical Parameters Used in Bottom up Price Model for the Base Scenario. 69
3.4 Cost Estimates for Balance of Turnkey BESS 72

4.1 Retail Energy and Peak Demand Charges in 2015 and 2019 78
4.2 Regulation Signal Parameters Reported by Fisher *et al.* and Those Obtained in the Present work. 92

6.1 MIQP Model Base Scenario Parameter Values. 141
6.2 Electrode Area Scenarios Studied 146

7.1 Predicted Operational Efficiency of VRFB at Site 281 Under MIQP Self-Sufficiency Optimisation 178
7.2 Predicted Operational Efficiency of VRFB at Site 767 Under MIQP Self-sufficiency Optimisation 182

Chapter 1

Introduction

1.1 Context

Worldwide, the need to reduce CO_2 emissions is stimulating the development of a wide range of intermittent renewable energy sources (IRES). The growth of IRES is forecast to be highest in the electrical power sector, from 24% in 2017 to 30% in 2023. Although hydro power presently accounts for 50% of IRES generation, wind and solar are forecast to contribute most to this growth [1]. Indeed, in a number of large European economies, such as Germany, UK, Italy and Spain 23% to 30% of electrical energy was already obtained from non-hydro renewable power in 2017 [2]. In the US, Texas obtained around 17% of electrical energy supply from wind power in 2017, whereas California obtained 9% from wind and 10% from solar [3, 4].

To maintain hourly grid stability in these regions, the fluctuating output from wind and solar is supplemented to match demand primarily by varying output from fossil fuel powered thermal plant. In the UK, this is specifically achieved by closed cycle gas turbines and to a decreasing extent coal power [5]. For the industrialised nations that have pledged to achieve net-zero carbon emissions by 2050 or earlier [6], achieving these goals via IRES is going to require much of this thermal plant to be replaced with energy storage.

Battery energy storage systems (BESS), particularly lithium-ion batteries (LIB) have

attracted much media attention in the last five years as a potential solution to the IRES balancing problem. However, the highest profile battery, the 100 MW Hornsdale Power Reserve, is designed to perform short term responses to supply/demand imbalance and is hence only specified with a 129 MW h energy capacity, giving a 1.3 h duration [7].

Although provision of grid services like this are lucrative, the bulk time-shifting of electricity on its own is not [8]. This is because the BESS relies on charging at a low price and discharging at a high one, and the differential is not currently large enough.

Placing a BESS behind the meter at a site with high electrical consumption is an emerging BESS application that has the advantage of capturing multiple revenue streams [9]. In this application, not only can the power imports at the site be time-shifted to periods of lower price, but savings can be made by peak shaving to reduce peak power import. The latter can result in large savings in certain regions [10]. In some circumstances the BESS will also be able to provide grid support services like those performed by the Hornsdale Power Reserve. In addition, the BESS may also be used to increase the self-consumption of on-site IRES, most likely photovoltaics (PV). PV is an ideal IRES for pairing with BESS in lower latitude regions where the variability is primarily daily with less seasonal variation.

In addition to LIB, there is a wide range of competing BESS at various technological readiness levels (TRL). Redox flow batteries (RFB) are a class of BESS in which at least one of the chemical species is present as a liquid which may be pumped through a reactor to produce electricity. Of these, the all-vanadium system (VRFB) is at the highest TRL, with a number of companies offering products [11–15]. The commercial scale is not comparable with that of LIB however.

VRFB differ significantly from LIB across the majority of the metrics by which batteries are typically rated.

The LIB has both high power density and energy density (676 $\mathrm{W\,h\,L^{-1}}$), without which neither the smartphone nor the pure electric vehicle would have come to market [16]. The VRFB has a much lower energy density of 20 $\mathrm{W\,h\,L^{-1}}$ - 40 $\mathrm{W\,h\,L^{-1}}$, and hence is

mainly being considered for stationary applications [17]. That said, inland shipping is a possible application [18]. Here, weight is required anyway for ballast, the ability to recharge by pumping in pre-charged electrolyte is attractive, and the fire risk of LIB may be unacceptable.

The round trip efficiency of the LIB is 90+% whereas that of the VRFB is around 70-80% [19]. Although both values vary with the input/output, the VRFB shows a greater variation. At low power input/output, the efficiency falls steeply due to current leakage and electrolyte pumping [20]. The importance of efficiency depends on the application and the cost of the electricity available to charge the system, but a high figure always gives an advantage.

Lifetime is the key metric where VRFB has an advantage. While the two most common LIB variants have lifetimes of 1200-3000 cycles, the VRFB has been reported to achieve 10000-15000 cycles [21, 22] and is advertised to achieve over 20000 cycles [11–15]. However, there are costs associated with keeping the positive and negative electrolyte balanced [23], and individual components will need replacing during this lifetime [24, 25]. Additionally the benefit of this increased lifetime is highly dependent on the valuation of future cash flows via discount rates.

The VRFB is also claimed to be more recyclable [26]. The energy store is simply an acidic solution of vanadium oxides [17, 27] which is physically separated from the power system. This contrasts with LIB, where the energy store comprises thin layers of mixed metal oxides (cathode) and graphite (anode) coated on copper electrodes, both of which are soaked in a non-aqueous electrolyte. These would have to be separated at an elemental level as the materials themselves degrade. Additionally, current grid scale LIB are assembled from thousands of small cells, requiring disassembly.

Given that the two technologies differ in many ways, it is necessary to perform techno-economic analyses (TEA) on particular applications to understand which is more suitable once the estimated upfront and ongoing costs of both systems are considered.

1.2 Structure of Thesis

In Chapter 2 the existing academic research providing context and motivation for the work that follows were reviewed and critiqued. The first part of the literature review focused on the key figures of merit for describing RFB, with a particular focus on the VRFB due to its high TRL. The second part focused on TEA that have already been carried out on VRFB and LIB. At the end of this chapter, the research challenges to be undertaken in this thesis are summarised, and the novelty of the approaches employed discussed.

In Chapter 3 the definitions of the models applied generally in the thesis are given, leaving models specific to a research challenge or use-case to dedicated method sections in the relevant chapters.

In Chapter 4, the short-run optimal operation of LIB and VRFB system is compared for the CAISO market use case. One problem with posing the optimisation is that there are timescale mismatches, not only between the realisation of the different revenue streams, but between the revenue accrual and the longer term degradation of the BESS. Steps are taken to optimise the necessary weightings. The feasibility of performing regulation from behind the meter is then analysed as is the impact of a 1 h service provision constraint imposed by CAISO.

In Chapter 5 the economics of LIB and VRFB are compared across a ten year project for the CAISO market use case. A comparison is first made between the LIB lifetime predicted using a cycle-only model, and that predicted with calendar aging included at different climactic locations. A number of approaches to minimise the impact of degradation on both LIB and VRFB economics are then introduced and assessed. Lastly, economic sensitivity studies are performed in order to determine the impact of performance, cost and environmental factors on the relative economic merit of LIB and VRFB.

In Chapter 6 a novel mixed integer-quadratic programming (MIQP) method is introduced that optimises the VRFB operation while accounting for the variability of efficiency with power input/output (via current density). This model is parametrised using a well defined pilot scale VRFB system reported in 2016 that is taken to represent the state of

Figure 1.1: A schematic giving a non-exhaustive overview of the methodology components and information flows that are novel to be generated.

the art [28]. The efficiency achieved by this method is compared to that assumed in the preceding economic analysis. The model is then applied to determine the optimal electrode area for a given power rating, and to study the benefit of independently controlling sub-modules.

In Chapter 7 a PV self-sufficiency case study is introduced. This analysis employs the levelised cost of electricity (LCOE) metric which is commonly used to give an average price of electricity produced from an IRES installation across its lifetime in today's money. Although the VRFB has a lower round trip efficiency than the LIB, the impact will depend upon the availability of PV power. For this reason a grid search is performed for each in three dimensions: PV installation size, BESS power and BESS duration. From this data an approximate Pareto front is obtained for each BESS, showing the best case economics across a range of self-sufficiency ratios. The operation of a hybrid system is then modelled to determine whether a lower LCOE can be obtained by prioritising the VRFB for the regular cycling. Lastly, the same analysis is rerun for a different site with a differing load profile to check the consistency of the results.

Conclusion are drawn in Chapter 8 and recommendations made for future research directions.

Given that a number of modelling innovations were made in this thesis, resulting in original contributions across two use cases and BESS technologies, a schematic showing the novel contributions is shown in Figure 1.1 below.

Chapter 2

Literature Review

This literature review attempts to describe the state of the art in redox flow battery (RFB) systems and the methods used to perform TEA on them at the time of writing. Section 2.1 contains descriptions of the general features of RFB systems, the figures of merit by which they should be judged, the various sub-classes of systems and a more detailed discussion of the vanadium RFB (VRFB), particularly the key figures of merit required to accurately model its operation. Section 2.2 deals with TEA, starting with a general overview before reviewing metrics that have been developed specifically for energy storage. The modelling of both the costs of RFB systems and the benefits in the context of particular applications is then reviewed in more detail. Lastly recent work on TEA of lithium ion batteries is reviewed and discussed with a focus on the developments in incorporation of degradation modelling in the last five years.

2.1 Redox Flow Batteries

The objectives for this section of the literature review are:

- To identify the characteristics of RFB systems that distinguish them from other ESS.

- To identify the key figures of merit by which RFB system performance should be judged.

- To identify the sub-classes of RFB systems that exist.

- To obtain performance data for the VRFB in order to be able to calculate \$ kW^{-1} h^{-1} and \$ kW^{-1} costs, and accurately pose the benefit optimisation problems applied in this thesis.

The focus will be on literature reporting experimental performance data for well-defined systems, rather than the theoretical approach used by Dmello *et al.* [29], which considers the possible design space as being continuous. This approach is based on a desire to focus on systems at high TRL and avoid overoptimistic estimates.

A schematic of an all-solution RFB system is shown in Figure 2.1. It consists of two tanks, containing solutions of redox active species, connected by flow channels to an electrochemical cell. One of the tanks contains the anolyte (or negolyte) and during discharge, electrons flow via an external circuit to reduce the active species in the catholyte (or posolyte) with a charge balancing ion (e.g. a proton) passing across the ion conducting interface.

During operation the electrolyte is pumped in a circulating fashion, and the flow rate must be sufficient that the change in state of charge (SOC) through the cell (δ_{SOC}) is limited, in order to avoid a significant potential across the electrode. Weber *et al.* [30] assume a δ_{SOC} of 0.2, implying the flow of chemical energy must exceed the electrical power by a factor of 5.

There are number of details left out from Figure 2.1 for the sake of simplicity:

- Cell stacking: the stacking of multiple cells is required in order to achieve a high voltage. This is necessary for efficient DC to AC conversion, and to minimise the current in the wiring to minimise ohmic losses. In the stack, individual cells are separated by conductive carbon bipolar plates and fed from a common flow manifold.

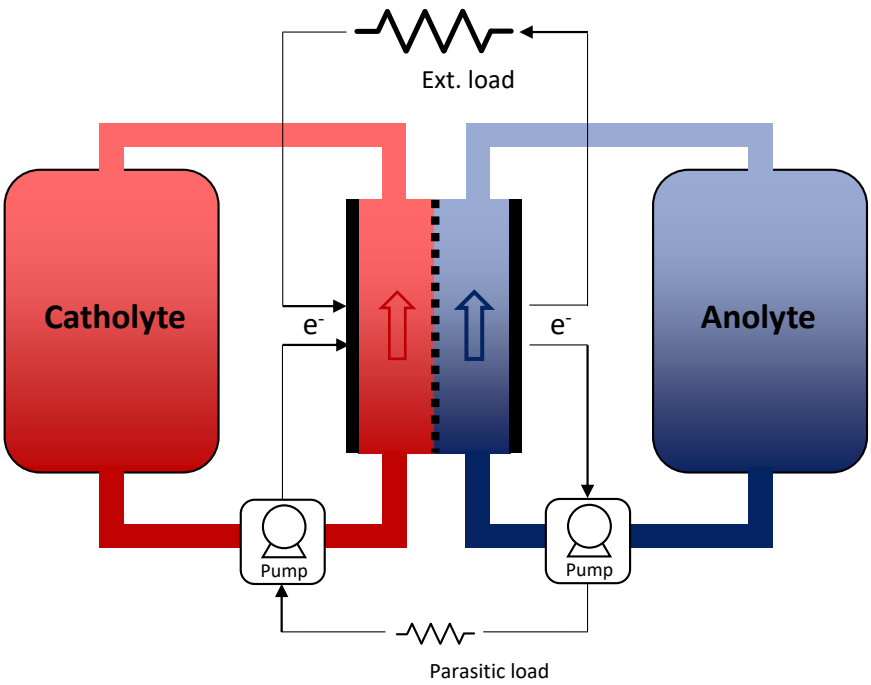

Figure 2.1: Simplified schematic of a RFB system operating in discharge mode.

- Electrode structure: the above figure displays the electrodes as if they were flat plates. In reality, carbon fibre matts are used, which give higher contact area for electron transfer. In fact, the electrode may occupy the whole flow channel, reducing diffusion length [31].

There are a number of characteristics that distinguish the all-solution RFB system from other battery energy storage systems (BESS):

- Fully decoupled energy and power rating: as the energy is held in tanks outside the electrochemical stack, the store may be scaled independently. While it is true that the energy to power ratio in a LIB cell (or a lead acid cell) could be increased by making the cathode and anode layers thicker [32], this would involve developing a new cell design and manufacture protocol; for the RFB it is a case of adding another tank of electrolyte. This decoupling is a feature the RFB shares with other forms of energy storage such as hydrogen (electrolysis & fuel cells) and compressed or liquefied air storage.

  It is important to note however, that in many applications the duration of a LIB

may be increased by placing more modules behind the inverter, effectively reducing the power that any one cell can output. Although the cells may be over-specified from a power perspective, this would not cause practical problems.

- Absence of phase change: during normal operation of the VRFB system (as with other all-solution RFBs) the redox active species remain in solution at all times and there is no phase change during the redox reaction [33]. This is in contrast to LIB where the cathode structure changes upon de-lithiation, or lead acid batteries where new lead and lead (II) oxide must be formed each time the battery is charged. This is advantageous, as the phase change comes with a risk of material loss, dendrite formation or conversion to an inactive form.

Hybrid RFB systems do not exhibit the above characteristics, as discussed in more detail in Section 2.1.2.2.

2.1.1 RFB Technical Considerations

At the cell level, there are a number of chemistry-dependent figures of merit that will ultimately influence the capital cost of an RFB system. The four most important are given below:

- Open circuit voltage: this is the combined potential of the redox couple at the concentrations present in the electrolytes. In principle, a higher standard cell potential will allow greater power output for a given current, and typically allow a smaller (and hence cheaper) stack, and smaller system footprint. It is important to note that the practical cell potential is limited by the requirement that neither electrode is outside the stability window of the solvent.

- Cell over-potential: when the RFB is discharged, the voltage at the DC contacts is the open circuit voltage minus various losses. Figure 2.2 shows qualitatively the order in which these losses appear as discharge current increases (adapted from Aaron *et al.* [34] and Chen, Gerhart and Aziz [35]).

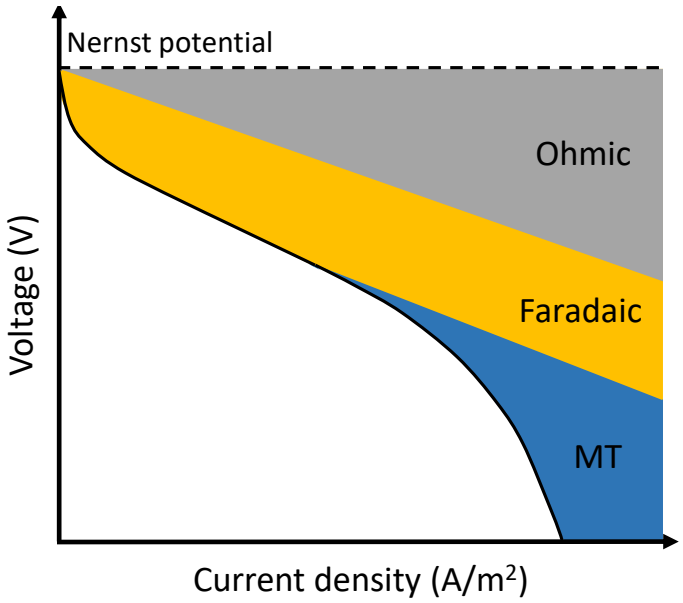

Figure 2.2: Illustration of a discharge polarisation curve (black line) showing the contribution of various mechanisms to voltage drop at varying current density. MT = mass transport.

The Faradaic losses (aka activation, or electrode polarization losses) arise due to the kinetics of electron transfer between the redox species and the electrodes. The ohmic losses are due to electrical resistance in the electrode and other electron conducting parts, and ionic resistance in the electrolyte and the membrane/separator. These are proportional to the current density (as in Ohm's law). There may also be pseudo-ohmic resistances (linear contribution) due to mass-transport limitations. These may be distinguished from the true ohmic resistance by Electrical Impedance Spectroscopy (EIS). At high current density the polarisation curve becomes increasingly non-linear as the rate of mass transport (that is, movement driven by concentration gradients rather than electrical potential) of redox active species becomes unable to satisfy the current draw, leading to a drop in concentration in the proximity of the electrodes [34].

Minimising all of these losses is a crucial factor in increasing the power that may be extracted from an RFB at a given voltaic efficiency (or the converse).

- Active Species Crossover Rate: in order to complete the electrical circuit, counter-ions must be able to move across the boundary between each half of the cell. However,

crossover of the active redox species is undesirable; it leads to a loss of coulombic efficiency, but more importantly, causes a capacity fade that is either irreversible or necessitates periodic re-balancing depending on the RFB. This is discussed further in Section 2.1.2.5.

- Active species solubility: a higher solubility is generally desirable, as it reduces the work required to circulate the anolyte/catholyte (leading to lower pumping losses) and the volume of the electrolyte reservoir.

The above figures of merit are not strictly parameters, rather functions of other variables that are highly interrelated overall. For this reason, experimental investigation is of great importance. For example, Weber *et al.* found that increasing the concentration of HBr in the catholyte of a hydrogen\bromine RFB reduced the volume of liquid (and hence the pump and tank cost), but that this benefit was eventually outweighed by increased ohmic resistance due to dehydration of the Nafion^{TM} membrane [30]. As another example, reducing the thickness of a membrane will reduce the ohmic resistance but increase the active species crossover rate.

The conductivity of the electrolyte is also an important parameter, but was not included in the above figures of merit as it is not clear that it should be maximised. When comparing electrolytes of differing conductivity (for example, Wei *et al.* [36] report conductivities of $825\,\mathrm{mS\,cm^{-1}}$ for a $3\,\mathrm{mol\,L^{-1}}$ H_2SO_4 solution and a $4.6\,\mathrm{mol\,L^{-1}}$ KOH solution respectively) the benefits of increased ionic conductivity in support of the redox reaction must be weighed against the increase in shunt currents. Shunt currents occur when individual cells connected in series to increase the stack voltage are supplied by a common flow manifold. The difference in potential between cells drives a current through the electrolyte flow channel, resulting in reduced coulombic efficiency and the possibility of corrosion of materials [37]. There is a trade off to be made between minimising flow resistance and minimising shunt currents, as investigated by Konig, Suriyah and Leibfried [38].

The above examples show that caution must be taken when extrapolating the performance of single cell experiments to large scale systems.

2.1.2 Classification of RFB Systems

The above description of a flow battery is provided as an introduction, and does accurately represent many of the systems described in the literature. However, many of the systems described in the literature differ sufficiently that further classification is useful, and is provided in the following subsections.

2.1.2.1 Degree of Symmetry

Potash *et al.* [39] define a symmetric RFB as one in which the active species in the anolyte and in the catholyte are the same when the system is fully discharged. The stated advantages of a symmetric system are the absence of potential across the cell in the discharged state (long shelf life), the low impact of active species crossover and the ability to switch cell polarity periodically, leading to longer life. The VRFB is not truly symmetric, but the asymmetry is only due to differing ionic states of vanadium. Although species crossover leads to a penalty in coulombic efficiency and a fade in capacity, there is no permanent degradation; the system may be rebalanced. This is not the case with systems where different elements (or molecules) are used in the catholyte and anolyte, as crossover would necessitate some form of chemical separation in order to renew the capacity. The degree of unwanted crossover depends on the nature of the interface and the redox active species.

2.1.2.2 Hybrid Systems

A more obvious deviation from the classical RFB system is the hybrid RFB. Here the anolyte is replaced by an anode on which metal is plated out during charging. One attraction of such a system is the ability to use lithium (with its attractively low standard electrode potential of $-3.04\,\mathrm{V}$) and zinc, which yields two electrons. These metals have limited oxidation states, and hence it is not possible to support redox reactions while maintaining a soluble ionic form. Replacing the anolyte with a solid has the potential to increase the energy density of the system, and reduce balance of plant costs. A fundamental

limitation of this type is the lack of decoupling between the energy and power rating of the battery. This is because the energy stored is proportional to the electrode area, which is proportional to the power. In their study of RFB manufacturing costs, Gallagher and Ha [40] state that a hybrid lithium/polysulfide system would hence be unable to access all of the benefits associated with an all-solution RFB. This constraint is also mentioned in regard to $Zn\backslash Br_2$ hybrid RFB systems in an economic analysis carried out by the asset management company Lazard [41]. The plating process also carries risks of dendrite formation and loss of material by flaking. In order to maintain consistent plating, Redflow stipulate a periodic full discharge and "strip" procedure for their $Zn\backslash Br_2$ system in order to reset the electrodes [42]. The 2 to 3 h required for this process represents a reduced availability for service provision, or if multiple modules are employed, a reduced capacity. However, electrolyte rebalancing in the vanadium system may have an analogous impact on availability, and the relative impact will depend on the specifics of each system.

The $Zn\backslash Br_2$ system is at a high TRL. In addition to Redflow, Arenas *et al.* [43] list four other manufacturers; EnSync Energy Systems (USA), Zbest Power Co. Ltd. (China), Lotte Chemical Cop. (Korea) and Primus Power (USA).

The $H_2\backslash Br_2$ system reported by Weber *et al.* in 2013 [30] is difficult to categorise; it employs a gas on one side, and a solution on the other, but has the full decoupling of energy and power seen in an all-solution RFB.

2.1.2.3 Metal/non-Metal

In a very useful 2017 review Winsberg *et al.* attempt to classify the many RFB systems reported so far on chemical grounds [44]. The review divides the history of RFB research into "The Metal Age" and "Rise of the Organic Materials". In their conclusion the authors make high-level recommendations on RFB chemistry selection. Systems employing transition metals are considered a stepping-stone on the way to large-scale energy storage, which instead would employ organic species that would be synthesised rather than mined, thus avoiding the pitfall of finite resources. However, the authors do not provide quantitative

arguments to back up this generalisation regarding resources. For example, iron - a metal - is abundant. Organic redox species are also credited with faster kinetics, reducing the Faradaic losses described in Section 2.1.1.

It is beyond the scope of this review to detail the wide range of aqueous RFB chemistries that have been reported in the preceding 30 years. The Winsberg review, and a review by Noack *et al.* [45] are both recommended for this purpose. The Fe\Cr system deserves a particular mention as its conception preceded the VRFB, and it has subsequently been improved upon in order to achieve high power performance [46]. The polysulphide\bromine system is based on cheap raw materials, and a 15 MW \120 MW h was built by Regenysys in the UK in 2002, but never commissioned [47]. An economic analysis of the system has been carried out by Scamman, Reade and Roberts [48]

Finally, the ferrocyanide\2,6-dihydroxyquinone system reported by Lin *et al.* [49] and the all organic AQDS\Br_2 system reported by Huskinson *et al.* [50] stand out among systems that have emerged in the last five years, by merit of their combination of cheap chemical energy and low toxicity with promising power performance.

2.1.2.4 Aqueous/non-Aqueous Solvent

In the aforementioned review by Winsberg et al [44], aqueous electrolytes are favoured over those based on organic solvents. Although organic solvents can tolerate higher cell voltages, and hence support greater energy densities, their lower ionic conductivities result in lower current densities and hence higher stack area requirements for a given power output. For example, Yang, Zheng and Cui [51] reported a hybrid system with a lithium anode, and a solution of lithium polysulfides in dioxolane/dimethoxyethane as the catholyte. The high cell voltage of 2.3 V combined with the high solubility of Li_2S_8 leads to an energy density of 159 W h L^{-1}, approximately five times higher than that of a typical vanadium system. The system displays a high cell resistance however, with an overall energy efficiency of 80% only achievable at the very low current density of 6 mA.cm^{-2}. Such low current densities are shared by LIB cells, with Gallagher *et al.* [32] recommending a maximum charge

current density of $4\,\mathrm{mA\,cm^{-2}}$. However, in a LIB cell the low current density is not so problematic as there is no need to flow liquid through the cell hence large cell areas may be packed into a small volume.

It is worth noting that, like the above example, the majority of non-aqueous RFB systems are also hybrid systems. This is because the research is motivated by the appeal of the high redox potential of lithium, which can't be realised in aqueous solution.

2.1.2.5 Separation Method

The VRFB systems reported in the literature typically employ Nafion^{TM} , a perfluorosulfonic acid membrane, which gives excellent conductivity to the protons that complete the electrical circuit while restricting crossover of vanadium ions and providing high stability [52]. Unfortunately this material is expensive; Weber *et al.* [30] and Viswanathan *et al.* [24] used prices of $\$350\,\mathrm{m^{-2}}$ and $\$500\,\mathrm{m^{-2}}$ in their respective cost calculations. 3M [53] and Asahi Glass Company [54] now manufacture similar membranes (the former targeting the RFB market), so prices are likely to decrease. Minke and Turek published a review of cost projections for various VRFB components which showed future estimates for Nafion^{TM} 212 averaging to €48 $\mathrm{m^{-2}}$.

In the meantime, the cost of Nafion^{TM} has motivated research into alternative separation methods.

Wang *et al.* [55] compared the performance of a microporous polymer separator with the Nafion^{TM} NR 212 membrane in an iron-vanadium RFB. At a current density of $50\,\mathrm{mA\,cm^{-2}}$ the systems displayed energy efficiencies of 70% and 80% respectively. Although both the voltaic and coulombic efficiencies of the polymer system were lower, the coulombic efficiency was the larger factor. The authors attribute the poor coulombic efficiency of the polymer system to active species crossover, although there was no indication that the capacity degrades faster than that of the Nafion^{TM} system.

Janoschka *et al.* [56] tackled the separator issue by immobilising the redox active species in polymers. A low cost dialysis membrane could then be employed while minimising

crossover (with a coulombic efficiency of 95 to 99% depending on current density). However, the system did suffer from high voltaic resistance across the membrane, leading to an energy efficiency of approximately 64% at $20\,\mathrm{mA\,cm^{-2}}$, a low current density.

Here it is important to note that although the Nafion^{TM} membrane will likely be the single most expensive component in any stack where it is used, the other costs are not negligible. A 2007 EPRI report [25] on the VRFB estimates that Nafion^{TM} contributes 41 % of the total stack cost (including manufacture). Therefore systems using cheap separators must still display a reasonable current density or the $\$\mathrm{kW^{-1}}$ cost will become prohibitive. On this basis, the $20\,\mathrm{mA\,cm^{-2}}$ displayed by the Janoschka system would not give a $\$\mathrm{kW^{-1}}$ cost that is competitive with the VRFB systems described in Section 2.1.3.

It is also worth noting the work of Gong *et al.* [57] who reported a Zn\Fe RFB with a claimed capital cost of less than $\$100\,\mathrm{kW^{-1}\,h^{-1}}$. This system combines cheap redox active species, high cell voltage and moderate current density. The key innovation is the use of a double membrane, with a third electrolyte in the middle which acts as a counter ion reservoir. The membrane on the catholyte (Fe^{3+}/Fe^{2+}) side is an anion conductor, and the membrane on the anolyte ($Zn/Zn(OH)_4^{2-}$) side side is a cation conductor, hence crossover of active species should be greatly limited. Because the anolyte is at high pH and the catholyte at low pH, the evolution of hydrogen is limited despite the high cell voltage of 1.99 V. This system is a hybrid RFB, as zinc is plated during charging (with the advantages and disadvantages discussed above). Unfortunately the specifics of the membranes are not revealed, making corroboration of the cost modelling difficult.

The $Zn\backslash Br_2$ system developed by Redflow is able to operate with a simple micro-porous separator, because the bromine evolved during charging is captured in an immiscible phase which cannot pass through the pores [42]. There is less literature data available on the current density performance of the $Zn\backslash Br_2$ hybrid system than the VRFB, but Arenas *et al.* [43] recently cited a limiting current density of $40\,\mathrm{mA\,cm^{-2}}$ due to dendrite issues (although $80\,\mathrm{mA\,cm^{-2}}$ may be achievable for limited periods of time). The point made above regarding the balance of stack costs also applies here.

2.1.3 The Vanadium RFB

Any discussion of RFB systems should cover the VRFB, which was introduced in the 1980s, and has been subject to more research and development than any other chemistry. The VRFB was first reported at the University of New South Wales in Australia by Skyllas-Kazacos and Grossmith [27]. It is also the RFB most commonly incorporated in the modelling of renewable energy systems.

Equation (2.1) and Equation (2.2) show the catholyte and anolyte redox reactions respectively [17]:

$$VO_2{}^+ + 2\,H^+ + e^- \underset{charge}{\overset{discharge}{\rightleftharpoons}} VO^{2+} + H_2O,\ E^0 = 1.00\,V \text{ vs. SHE} \tag{2.1}$$

$$V^{3+} + e^- \underset{discharge}{\overset{charge}{\rightleftharpoons}} V^{2+},\ E^0 = 0.26\,V \text{ vs. SHE} \tag{2.2}$$

The redox couple gives an overall standard cell potential of 1.26 V.

The Skyllas-Kazacos and Grossmith system employed a solution of 1.5M vanadium in 2M sulphuric acid (H_2SO_4) as electrolyte, and a sulphonated polyethylene membrane. The system was charged at $40\,mA\,cm^{-2}$, and discharged at current densities up to approximately $20\,mA\,cm^{-2}$, with a reported energy efficiency of 73%.

In 2011 Kim *et al.* [17] reported a hydrochloric acid (HCl) electrolyte with a vanadium concentration of 2.3M, which was tested alongside a 1.7M vanadium sulphuric acid electrolyte. The new electrolyte was less susceptible to precipitation of V_2O_5 which occurs at high temperatures, and the authors suggest the need for a heat exchanger would be removed. Both electrolytes were tested at $100\,mA\,cm^{-2}$ in a cell using the Nafion^{TM} N117 membrane. At this current density, the energy efficiencies of the 2.3M HCl and the 1.7M H_2SO_4 systems were 80% and 83% respectively; a considerable improvement in power density compared to the Skyllas-Kazacos Grossmith system. As well as providing improved energy density, the 2.3M HCl system also displayed slower capacity fade during cycling at $50\,mA\,cm^{-2}$, and the electrolyte was less viscous, in principle reducing pumping losses.

The potential downside of the system is the non-negligible vapour pressure of hydrochloric acid, which may pose corrosion and safety concerns.

Reed *et al.*, also at Pacific Northwestern National laboratory (PNNL), studied the impact of decreasing Nafion^{TM} membrane thickness in a 1 kW system [58]. The system used a mixed acid electrolyte (2M vanadium, 2M H_2SO_4, 5M HCl). Going from N115 (127 µm) to NR-212 (50 µm) allowed an increase from 160 mA cm^{-2} to 240 mA cm^{-2} while maintaining 75% round trip efficiency. Moving to the NR-211 membrane (25 µm) resulted in little further improvement, implying that the resistivity bottleneck was no longer at the membrane. The authors also commented that the NR-211 was difficult to manipulate unlike the NR-212. The reported coulombic efficiency (97-98 %) of the cell was not decreased in moving from the N115 membrane to the NR-212 membrane, and the rate of capacity fade was the same for all membranes (although rather high, losing 20% capacity in 20 cycles). Minke and Turek [59] claim that high active species crossover precludes the use of Nafion^{TM} membranes with a thickness less than 100 µm in VRFBs. It is not clear whether the capacity fade rate in the Reed study is due to crossover or another mechanism such as electrolyte decay discussed in [23].

In a subsequent study, using the same electrolyte, the authors developed an interdigitated flow architecture and modified the electrode structure of the system [28]. These improvements allowed an increase to approximately 300 mA cm^{-2} at 75 % energy efficiency using the same NR-212 membrane (from interpolation of Figure 17 in the cited text).

It is rare to find examples in the academic literature of systems that have been treated to the same level of engineering development as the VRFB stack at PNNL. The significant improvements to the NR-212 systems between the two publications should be considered when assessing other systems that have not been subject to such development. The study is also unusual in the detail with which the operational space is tested. For this reason, data from Reed *et al.* [28] are used to parametrise the scheduling model reported in Section 6.2.2.

An even higher current density was achieved by Zhou *et al.* who modified a carbon

paper electrode by etching with KOH and heating at 800 °C under nitrogen to form 5 nm pores in addition to the 10 µm pores already present [60]. Used in a cell in combination with the NR-212 membrane (and running an electrolyte of 1M vanadium, 3M H_2SO_4), a current density of $400\,\mathrm{mA\,cm^{-2}}$ was achieved at an energy efficiency of >80 % . The authors attributed the drop in resistance to improved mass transfer in the dual-scale porous electrode, and enhanced kinetic performance on the activated carbon. However, the cell was tested using a 1M vanadium solution based on sulphuric acid, a significantly lower concentration of vanadium ions than that used by Reed *et al.* [28]. The work of Zawodzinski *et al.* [61] showed that the conductivity of a Nafion™ N117 membrane dropped linearly as concentrations of V^{3+}, VO^{2+} and $VO_2{}^+$ increased, and that the conductivity dropped by approximately 25% going from 1M to 2M for each ion. It is therefore not clear whether the Zhou *et al.* electrode set-up is superior to that of Reed *et al.*

In the same report, Zawodzinski *et al.* report several VRFB embodiments with excellent current density performance. A system based on 1.7M vanadium in 3.3M "acid" that employs a SDAPP membrane displays is able to achieve a current density of between $400\,\mathrm{mA\,cm^{-2}}$ and $500\,\mathrm{mA\,cm^{-2}}$ at a voltaic efficiency of 80% with negligible Faradaic losses. The coulombic efficiency and stability of the system were not reported however.

Developments in the sulphuric acid based electrolyte were made in 2016 by Roe, Menictas and Skyllas-Kazacos who pushed the vanadium ion concentration to 3M using stabilising additives [62]. As well as reducing storage space requirements, increases in concentration also reduce the costs associated with pumping (both in CAPEX and parasitic losses).

It is foreseeable that further improvements to the performance of the VRFB are possible, but these will have to be weighed against costs of increased complexity, less durable membranes and other factors.

The primary drawback of the VRFB is the high cost of the metal when compared to other RFB chemistries. Huskinson *et al.* [50] calculated the chemical energy cost at $\$81\,\mathrm{kW^{-1}\,h^{-1}}$, compared to $\$27\,\mathrm{kW^{-1}\,h^{-1}}$ for their organic redox species. However, once

refined, the vanadium solution should not degrade, and may be classed as an asset.

The low energy density of the electrolyte will also pose a problem in some applications. The 39 W h L^{-1} of the improved electrolyte in [17] compares poorly with the 100 W h L^{-1} achieved by the Redflow ZBM2 zinc/bromine RFB [42], and both of these are well below the 676 W h L^{-1} achieved by a Panasonic NCR18650b lithium-ion cell [16]. Although VRFB manufacturers describe their systems as being capable of 100% depth of discharge (a marketing strategy to distinguish them from LIB), the full energy content of the electrolyte is not accessed during operation. Instead, the permitted SOC range is restricted, both to reduce the risk of V(V) precipitation at high SOC, and to avoid mass transfer limitations at both high and low SOC. Ranges of 0.05-0.85 [63], 0.15-0.85 [28] and 0.11-0.89 [24] have been considered appropriate by others researchers. In [28] the SOC is more constrained as high current densities are tested, hence voltage constraints are hit earlier.

2.1.3.1 VRFB Degradation Processes

The cost associated with degradation is a key characteristic of any BESS, but unlike a LIB, the VRFB is composed of multiple components, and it is possible that the system will be refurbished rather than replaced completely.

Eckroad suggests that valves are bearings will require replacement every 5 years, and pumps every 10-15 years [25]. Although Nafion ™ membranes are highly durable, they will degrade over time. This subject was reviewed by Yuan *et al.*, who state that the primary impact of membrane degradation is increased ionic crossover [64]. This will reduce coulombic efficiency and add to re-balancing cost. However, the literature reviewed is primarily fundamental research, and there has been little work carried out to understand the impacts at an engineering level. Another degradation mechanism is discussed by Yuan *et al.* is corrosion of the graphitic electrodes in the stack. The degradation of the stack components is accounted for by Viswanathan by limiting the stack life to ten years *et al.* [24]. This lifespan was corroborated by comments made by Adam Whitehead, Head of Research at Invinity Energy Systems at the 2020 UKRFB network conference. In response

to a question on the subject he stated that the expectation was that the stack would be replaced once in a projected 20 year life, but that the membrane may not be the first component to degrade to a degree that would necessitate replacement [65].

There are also processes that lead to a loss of energy capacity, although these are reversible. A 2020 article by Rodby *et al.* provides an overview of capacity fade and electrolyte decay, and a quantitative anaysis of rates based on a literature survey [23]. Capacity fade is primarily attributed to V(II) and V(III) ions in the anolyte moving to the catholyte via the membrane. Rather than being a function of energy throughput, the crossover is a function of charge/discharge duration, i.e. how long the electrolyte is in contact with the membrane for. Capacity fade due to crossover may be reversed without manual intervention by one of the following methods:

- Full rebalance: 1) VRFB discharged to give 3^+ mean oxidation state in anolyte and $<4^+$ in catholyte. 2) Full mixing and volume split giving $<3.5^+$ on both sides. 3) Full charge.
- Partial rebalance: 1) As above 2) Portion of catholyte transferred to anolyte such that oxidation states in each are equidistant from 3.5+ (under assumption that electrolyte volume in each tank is proportional to V inventory). 3) Fully charge.
- Continuous rebalance, e.g. overflow or shunt tube as described in [66].

Rodby *et al.* state that partial rebalancing is more efficient (coulombically and timewise) than full rebalancing, although there are issues with accurate online SOC measurement required to judge the volume to transfer. The continuous rebalance methods cited by Rodby *et al.* are relatively new and limited performance data is available.

The electrolyte decay is primarily attributed to an anode side reaction during charging. Electrons generated by the oxidation of V(IV) to V(V) in the catholyte reduce water to form hydrogen, rather than reducing V(III) to V(II). This leads to a net increase to the average oxidation state in the system, which is ideally 3.5. This decay can be reversed by adding a reductant such as oxalic acid to the catholyte to reduce some V(V) to V(IV).

Alternatively, an continual reduction process has been proposed in [67]

For the overall fade rate, the authors report an average of 0.44% per cycle (acknowledging that variability in the data will be due to different charge/discharge durations, as crossover is a function of electrolyte/membrane contact time among other factors). The authors corroborate their decay rate analysis with anecdotal data from industrial collaborators, who report that it is typical to perform a treatment with oxalic acid when the average oxidation state of the electrolyte reaches 3.6, corresponding to a capacity fade of 20%. Assuming a cycle per day, this corresponds to a decay rate of 0.055% per cycle.

2.1.3.2 Commercial VRFB Offerings

There are a number of companies offering VRFB products. Table 2.1 summarises the companies that have evidence of a physical product, and shows the range of scales being considered. UET and its Chinese sister company Rongke [68] both employ a higher energy density electrolyte related to that developed by Kim *et al.* [17].

Table 2.1: Commercial offerings of VRFB systems as of 2021 (non-exhaustive). SC is shipping container. The power rating is the minimum listed, assumed to be the basic module.

Company	**Power** (kW)	**Duration** (h)	**Advertised life**	**Format**	**Ref.**
CellCube	250	4-8	20000+ cycles, >25 years	SC	[11]
Invinity	78	2-12	20000+ cycles, >25 years	SC	[12]
Sumitomo	250	3-6	Unlimited cycles	SC	[13]
UET	14	3.2	20000+ cycles	0.9 m×1.8 m×2.1 m	[14]
VRB Energy	250	4-8	25000+ cycles, 25 years	SC	[15]

2.2 Techno-Economic Analysis

The Dow Centre for Sustainable Engineering Innovation [69] defines techno-economics as: *"...the evaluation of technologies using models of economic inputs, costs, and benefits to support applied research, development, and commercial decisions."*

In a guide to TEA methodology, Lauer [70] splits the information requirement into three sections; cost assessment, benefit assessment and risk assessment. For the first, he

states that:

"It is specific to research and technical development, that no exact data are known for the technologies to be developed or tested. So cost assessments can only be made on comparative basis looking at existing similar technologies or applications with data available."

The author also stated that TEA consistently underestimate costs, and that a contingency factor of 1.05 to 1.25 should be applied, depending on experience with the technology, and the complexity of the proposed project.

The benefit assessment is less uncertain, as a market for the output will already exist in most cases. It is however dependent on estimates of the performance of the system, and subject to uncertainty regarding future product prices and government regulation among other factors.

Regarding the risk assessment, Lauer cautions that *"Risk assessment is not methodically incorporated in TEA."* and recommends that sensitivity analyses be carried out by varying the various input parameters.

Lauer recommends the use of Net Present Value (NPV) as the economic framework for TEA, as it factors in discount rate (i.e. gives consideration to a dollar today being worth more than the promise of a dollar in n years). The net present value tells the investor what the cumulative profit (or loss) of a project will be, discounted to today's money. The NPV is calculated by:

$$NPV = \sum_{n} \frac{NCF_n}{(1+d)^n} - C_0 \tag{2.3}$$

Where NCF_n is the net cash flow (income minus outgoings) in year n, d is the fractional discount rate and C_0 the initial investment (where $n = 0$).

Where NCF_n is the net cash flow in year n and d is the discount rate. Depending on financing, the NCF may include the cost of interest payments on outstanding debt.

The discounted cash flow approach can also be expressed in terms of payback period, which is the number of years before the cumulative NPV becomes positive. This format

is used by Hu, Chen and Bak-Jensen [71] in their assessment of arbitrage revenue for a VRFB and a polysulfide\bromine RFB. A similar metric is internal rate of return, which is the discount rate at the project yields a NPV of 0.

2.2.1 TEA Methods Specific to ESS

In the field of energy storage, at least three TEA frameworks have emerged in order to facilitate comparisons of different technologies.

A form of static cost-benefit assessment (as defined by Lauer [70]) may been performed by dividing an estimated $\$\mathrm{kW}^{-1}\,\mathrm{h}^{-1}$ system cost by the product of the cycle life and the round trip efficiency. This returns the average lifetime $\$\mathrm{kW}^{-1}\,\mathrm{h}^{-1}$ of storage throughput (i.e. per electrical unit) to be calculated for a quick comparison of different systems.

Barnhart and Benson [72] developed an analogous metric in energy terms, Energy Stored on Invested (ESOI), defined by:

$$\mathrm{ESOI} = \frac{\text{Energy stored}}{\text{Embodied energy}} = \frac{(\text{capacity})\lambda\eta D}{(\text{capacity})\epsilon_{\text{gate}}} = \frac{\lambda\eta D}{\epsilon_{\text{gate}}} \tag{2.4}$$

where λ is the cycle life, η the round trip efficiency, D the depth of discharge and $\varepsilon_{\text{gate}}$ the energy embodied in manufacture (per unit storage capacity).

Given the difficulty in setting boundaries and obtaining embodied energy figures for components, there is an incentive to use money as a proxy. Weißbach *et al.*[73] give some justification for this approach when they comment that:
"Energetically, human labor is negligible but financially it dominates and represents the welfare of society...".

The construction of nuclear power plant (where the strict regulation incurs high white-collar labour costs) and solar power plant (where energy costs dominate) are given as examples where the use of energy and money would give different conclusions. The downside of money as a proxy for labour and energy is that it may be subject to political manipulation (such as subsidies, or regulation), leading to a loss of information.

A more application-centric framework is the levelised cost of storage (LCOS) which takes into account the intensity of usage for the ESS in a finite project timescale, and discounts future costs. The LCOS is an evolution of the levelized cost of energy (LCOE), which divides the total discounted NCF by the total discounted energy production to give a price per delivered unit energy in today's money. The framework has been used by Lazard [9] in order to compare the economics of different ESS for realistic applications, although they do not lay out the formulation formally. A clear definition of LCOS is given by Jülch [19]. The formulation includes the cost of the electricity used to charge the ESS, so the framework can be used to combine generation with storage. The inclusion of residual value of the ESS is important to note, as it will undoubtedly be an important consideration for VRFB where the vanadium solution consists a significant part of the CAPEX and does not degrade.

The cost-per-unit-energy format of LCOS is not as useful for applications where available power capacity if at least as important as consumption of electrical units, for example industrial power use, or electrical grid services. Here, benefits may accrue on a $\$kW^{-1}$ basis. In this case it would be more sensible to use NPV, or a similar cash flow based metric.

2.2.2 Methodology for Review of TEA on RFB Systems

A literature review of TEA on RFB systems was carried out at the end of 2017 by performing the searches outlined in Table 2.2, with any purely electrochemical treatments removed.

Table 2.2: TEA Literature Review Methodology. WoS: Web of Science, GS: Google Scholar. *Hits not already captured in previous search

Search Terms	Platform	Filter?	Hits	RFB Specific*
Redox Flow Battery Cost Model	WoS	-	90	42
Energy Storage Optimization	GS	Sort by Relevance	first 50	0
Energy Storage Optimization Sizing	GS	Sort by Relevance	first 50	2
Wind Power Flow Battery	WoS	Articles and Reviews	302	11
Techno Economic Analysis Flow Battery	WoS	Articles and Reviews	21	0

It can be seen from the Google Scholar searches that optimisation studies dealing with RFB systems comprise a small fraction of the overall literature.

Within the above results there was a subset of articles dealing with power-quality issues and control strategies for RFB systems, and containing no techno-economic analysis [74–77]. These are considered to be outside the scope of the current work.

Within the remaining results, there is a broadly even split in accordance with the two main components of a TEA as described above:

- Cost-centric: where the primary objective is to deliver a capital cost for an RFB system - 26 results.
- Benefit-centric: where the primary objective is to quantify the economic benefit of an RFB system in a realistic application - 23 results.

There is limited overlap between the two areas; some of the cost-centric articles use a simplified application model to generate a levelised cost, most of the benefit-centric models only take capital costs ($\$kW^{-1}$ and $\$kW^{-1}\,h^{-1}$) and charge/discharge efficiencies to represent the RFB. These areas of research are discussed in more detail in Section 2.2.3 and Section 2.2.4.

Despite the long history of VRFB systems, the bulk of modelling and optimisation studies have been performed on other BESS, such as lead acid, lithium-ion and sodium sulfur (as evidenced by the small number of results in the non-RFB specific searches shown in Table 2.2).

2.2.3 Costs of RFB Systems

2.2.3.1 Bottom up Cost Models

Bottom-up cost models are a popular method for establishing an approximate capital cost for a RFB system, either in $\$\mathrm{kW}^{-1}$ or $\$\mathrm{kW}^{-1}\,\mathrm{h}^{-1}$ or, ideally, both. In such models an inventory of components and their respective quantities is constructed following assumed performance parameters. For example, the area of electrode may be calculated approximately as the target discharge power divided by the discharge voltage and the maximum current density. Costs may then be allocated to each item based on best estimates. Such models have been used to estimate the system costs of particular RFB embodiments [24, 30, 46, 57, 78, 79].

Some of these articles involve a degree of system optimisation, for example the work of Weber *et al.* [30] mentioned previously, where the influence of catholyte concentration on $\$\mathrm{kW}^{-1}\,\mathrm{h}^{-1}$ cost is investigated by graphic sensitivity study. The model of Viswanathan *et al.* [24] includes shunt current losses and pumping losses, and an iterative approach was used to achieve the lowest $\$\mathrm{kW}^{-1}\,\mathrm{h}^{-1}$ system cost. The authors also translate the system cost into estimated LCOS, although the assumptions regarding the usage of the RFB are not described in the article.

Darling *et al.* [80] very clearly present a model for system cost, based on the sizing of components. This model was effectively used in reverse, in order to generate mappings of allowable cost versus performance figures for various RFB chemistries under a target system cost $\$120\,\mathrm{kW}^{-1}\,\mathrm{h}^{-1}$ (excluding installation) in line with US DOE targets. This model is adapted for the present purpose in Section 3.4.4. The same model was used in a similar way by Dmello *et al.* [29] in a more general comparison of aqueous and non-aqueous RFB systems.

The bottom-up approach has the advantage of allowing the benefit of design changes to be tested, and the duration of the system to be varied, both of which are important for a thorough optimisation.

2.2.3.2 Cost Trend Analysis

An interesting empirical approach to the determination of RFB system costs (or those of any manufactured product) is the use of experience (or learning) rates. The basis of this method is the historic tendency of the logarithms of prices of many products to decrease linearly with the logarithms of volumes of production. Schimdt *et al.* [81] applied this approach to energy storage technologies in order to estimate the investment required to meet 1 TW h of storage capacity. Unfortunately only four data points were available for VRFB systems. Disadvantages of this approach are the inability to model step changes (e.g. the shift to a new cheaper membrane), and the reliance on quoted price as an accurate proxy for cost.

2.2.4 Benefit Analysis of RFB Systems

2.2.4.1 Application Definition

There are several ways in which to classify the research on modelling the benefit of ESS within real applications. A useful high-level classification may be made according to the timescale over which the ESS must be charged/discharged. van der Linden used the following categories in 2006 [82]:

- Power quality: milliseconds to seconds
- Bridging power: seconds to minutes
- Energy management: hours

Such a classification is useful in the selection of ESS, which are classified according to power and energy capacity (or time to discharge at rated power), as often shown on a Ragone plot. In the UK, the electrical system operator National Grid tenders for services in each of these categories. Enhanced Frequency Response is an example of the first, Fast Reserve the second and Short Term Operating Reserve the third [83]. Analogous services are procured in other industrialised nations. Sabihuddin, Kiprakis and Mueller

[84] provide a comprehensive list of applications within the above classes, and extend the energy management time-scale from hours to months in the case of seasonal storage.

Another important distinction may be made between whole-system modelling (e.g. off-grid, micro-grid, islanded grid) and market participant modelling. In the former, all reliability criteria (such as spinning reserve) should be costed in to the system and posed as constraints in the model, as done by Chen *et al.* [85]. Arbabzadeh *et al.* relax these constraints in order to focus on the cost of reduction in CO_2 emissions (including embodied emissions) using wind power and VRFB to displace natural gas power [86]. They found that installing excess capacity of wind power was more economical than using VRFBs up until the very lowest CO_2 intensity targets.

In the market-participant scenario, the owner of ESS or other generation plant may choose which services they bid to provide. Here it is important to note that ESS are typically modelled as price-takers i.e. they may buy or sell energy without influencing the price - although only a few works mention this explicitly [71, 87, 88]. This assumption is sufficiently accurate for considering a project at a given moment in time. In reality there is a finite demand for grid services, and every additional ESS installation will reduce the price differential for subsequent participants.

Another important application is behind-the-meter peak-shaving for large-scale users of electricity. These users are billed according to both the electrical consumption, and the maximum power demand. According to Oudalov, Cherkaoui and Beguin, the power demand component can contribute up to one half of an industrial electrical bill [89]. There is therefore a strong financial incentive to store energy off-peak in order to reduce the import requirement at peak times.

The challenging economics of energy storage have necessitated the "stacking" of multiple services in order to increase revenue. For example, both Vaca *et al.* [90] and Johnston *et al.* [91] looked at the combination of the mandatory frequency response service with arbitrage in the context of transmission-level wind power in the UK. A standout work is that of Fisher *et al.* who in 2019 modelled behind-the-meter LIB and VRFB performing electrical

price arbitrage, peak demand reduction, regulation and spinning reserve in California's CAISO market [10]. It was shown that 2 h systems are more profitable than 4 h systems, and that a VRFB would have to be cheaper than a LIB due to the higher efficiency of the latter.

2.2.4.2 Optimisation Approaches

In order to perform a valid TEA, it is necessary to optimise the ESS for the application, so that its benefit is maximised. This process should consider the specification of the ESS (i.e. what capacity must be installed) and its scheduling (e.g. what is the charge/discharge profile that minimises costs and maximises revenue). If this is not done then a fair comparison cannot be made between two ESS. In some circumstances, for example where power flow constraints exist on a network, a spatial optimisation may also be appropriate.

Figure 2.3 shows a flowchart representation of the sizing optimisation framework most frequently encountered in this literature review. The process is iterative, with the optimisation of schedule performed for a range of energy and power capacities until the global optimum is found.

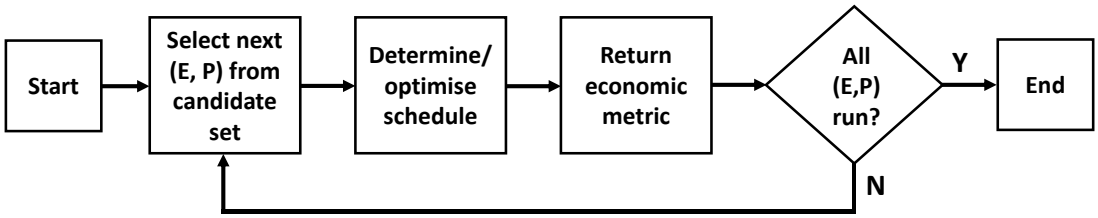

Figure 2.3: Generic representation of the optimisation process most commonly applied in the RFB techno-economic analyses encountered during this literature review.

Oudalov *et al.* [89] explain the necessary iterative approach to the sizing component as follows:

"The nature of the variable "operating schedule" is completely different from that of the battery size. Therefore, in this optimisation problem, there are two sub-problems: the battery size optimisation... and the operating schedule optimisation."

The output of this process may be interpreted as a graphic sensitivity study, where the

optimum is found by visual inspection. Figure 2.4 shows an example, taken from Chen *et al.* [85].

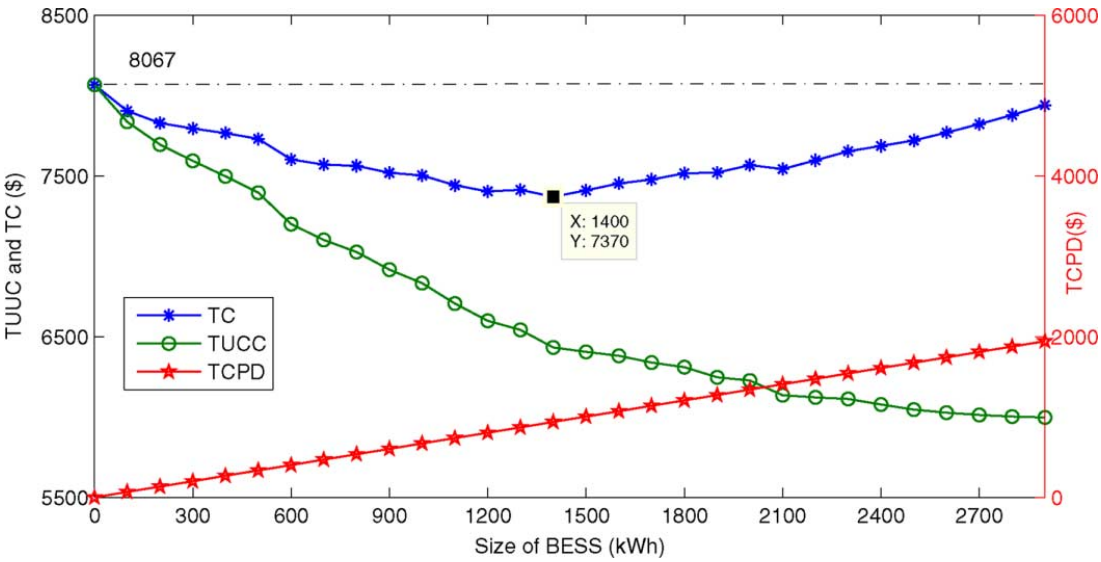

Figure 2.4: Graphic sensitivity study for an islanded micro-grid, showing incremental cost per day (TC) as a function of ESS cost (TCPD) and optimised balance of generation cost (TUCC). Reproduced from [85].

The nature of the sizing operation depends on the application studied. In a pure arbitrage application the absolute kW h capacity of the ESS is not important (assuming the system is a price-taker as described above and that there are no gird constraints or fixed costs). Where the ESS complements an existing generator, such as a wind farm, or supports an islanded grid, then the absolute capacity is obviously more important. For an all-solution RFB the decoupling of energy and power should however oblige the optimisation of the E/P ratio in all applications. Mellentine and Culver [92] explored the NPV for scenarios involving a 2 MW VRFB specified with different E/P ratios and used in the provision of area regulation (classed as bridging power in the above definitions), but concluded that the decoupling of energy and power was not relevant in this application. The aforementioned work of Fisher *et al.* considered two VRFB durations, but did not vary the power rating [10].

In whole system studies, optimisation of the BESS scheduling may not be necessary, as dispatch may be dictated by the hard supply/demand constraints that exist rather than being encouraged by price differentials. For example, in [86] the VRFB was simply

discharged if the SOC was greater than zero, and the demand exceeded the wind power supply in the system, and charged if wind exceeded demand and the SOC was less than 1 (with backup provided by gas generation).

Where schedule optimisation is required, the problem is commonly posed as a unit commitment problem, where the charge and discharge power of the ESS are continuous variables indexed over a set of time periods [20, 71, 85, 89–91, 93]. This formulation is common in electrical power engineering, where daily and hourly scheduling of generators must be optimised to minimise system cost. In the case of generating plant, where there are shut-down/start-up costs it may be necessary to use mixed integer-linear programming (MILP) to capture the discrete on-off behaviour. This is not necessary for a high level treatment of RFB system power output, and linear programming (LP) may be used for a basic analysis. Different conventions are used across the literature cited above, but for a simple arbitrage example, the objective is to maximise the revenue, defined by:

$$R_{Arbitrage} = \tau \sum_{t} P_t p_t \tag{2.5}$$

where P_t is the power flow between the RFB and the market in period t (with a positive value indicating discharge), τ the time-step (length of period t) and p_t is the price of electrical energy in the same period. The above function is subject to a constraint on the SOC of the RFB, defined by:

$$\begin{aligned} Discharge : SOC_t &= SOC_{t-1} - \frac{\tau P_t}{E_{RFB}\eta_{Dis}} \\ Charge : SOC_t &= SOC_{t-1} - \frac{\tau P_t \eta_{Chg}}{E_{RFB}} \end{aligned} \tag{2.6}$$

where E_{RFB} is the capacity of the RFB and η_{Dis} and η_{Chg} are the discharge and charge efficiencies respectively. The specific implementation of the above formulae are not always made explicit in the cited articles, and it is not clear whether separate variables for charge and discharge power are specified. If a single variable is defined with a range spanning negative and positive values then a linear solver would always drive the power to the most

extreme value permitted, resulting in excessive charge/discharge. This is likely to be the reason why Hu, Chen and Bak-Jensen [71] used a non-linear approach to solve a problem posed in terms of a single power variable.

Variable efficiency

A number of researchers have attempted to improve the fidelity of RFB modelling within the schedule optimisation. One source of inaccuracy in the typical LP approach is the use of a fixed parameter for efficiency, which in reality is a function of SOC and charge/discharge power. Nguyen *et al.* address this by introducing a non-linear function relating the efficiency of charging and discharging to the power input/output and the SOC [20] . As the optimisation involves a back-and-forth between the objective function and the SOC constraint, the problem becomes non-convex, which means that the global optimum is not guaranteed to be found by a gradient based algorithm with a single start point. Hence a search algorithm must be employed, which is typically more computing intensive. The authors used a dynamic programming approach, which splits the problem into sub-problems in order to obtain a tractable problem. They don't make a comparison of the introduced approach with a LP approach in terms of either outcome or computing time. Although the treatment of efficiency is thorough within the chosen operational space, this space is limited to the maximum rated power (where energy efficiency is 75%), so the benefits of allowing high power/low efficiency operation are not studied.

Lei and Gong [94] adopted the above approach in their own analysis of VRB operation in distribution networks for wind and solar applications. In an earlier publication, Oudalov, Cherkaoui and Beguin [89] also allude to the use of dynamic programming in order to incorporate variable resistance in the scheduling of lead acid and VRFB systems for peak shaving but the article does not provide comparable detail to that of Nguyen *et al.* [20].

Degradation cost

An important factor that has not been covered in detail in the TEA of RFB is degradation. The most basic approach is to simply set the project life as the anticipated calendar life of the RFB. Sayfutdinov *et al.* rightly point out that the lifetime (in years) is a function of the intensity of usage [95]. Implementing this condition leads to a non-convex problem,

and a global search algorithm is used to find an apparent optimum . One shortcoming of the work is that the time value of money is not factored in to the TEA (i.e. it is a static assessment as defined by Lauer [70]). As a result, in the case of a Zn\Br_2 RFB, when the calendar life is not constrained, the optimum project life is found to be 107 years, with only 0.08 cycles per day on average. Despite this, the approach is potentially very useful for planning RFB projects.

Johnston *et al.* [91] pose the problem differently, by defining a cost of degradation per unit energy throughput as the ESS cost divided by the cycle life ($\$ \, kW^{-1} \, h^{-1}$) . This term is then included as a negative coefficient in the objective function for revenue, providing a disincentive to use the battery when the revenue is small. Vaca *et al.* [90] employ a similar approach in a TEA comparing the performance of a VRFB, super-capacitors and a hybrid system in provision of mandatory frequency response at a wind farm.

Outside of RFB specific articles, Bordin *et al.* [96] present a number of strategies for incorporating the degradation of ESS into the optimisation of scheduling. One of these is to count the degradation cost according to the minimum SOC in each day. He *et al.* He *et al.* incorporated the cost of degradation as a function of SOC in an algorithmic optimisation of bids on multiple markets [88]. Sarker *et al.* used a piece-wise approach to incorporate the degradation cost of a LIB as a function of the power input/output [97].

Non-deterministic approaches to scheduling

In the articles described so far, the optimisation is deterministic, i.e. across the optimisation period there is perfect knowledge of the price of electricity (in arbitrage), or the demand that must be met (in a whole system). With the exception of the Danish spot market example [71] where spot price is known 24h ahead, the deterministic optimisation can only provide a best case economic scenario - in reality imperfect forecasting will lead to reduced revenue. A second category of scheduling optimisation relates to the use of control methodologies that are able to maximise the value of ESS while looking toward a given time horizon. Brekken *et al.* [98] analysed the efficacy of different control algorithms for a Zn\Br_2 RFB used to make up the difference between forecast and actual wind farm output (where deviations incur a penalty). This was combined with an iterative RFB

sizing approach. They found that an artificial neural network (ANN) was able to achieve the same revenue as a simple or fuzzy controller with a smaller energy capacity of RFB installed (although not installing RFB capacity was the most economical option overall).

Stochastic treatment A stochastic approach is one in which a distribution of parameter data is fed into a model in order to gauge the impact of uncertainty on the model predictions. Such a sensitivity study is a necessary step in understanding the risk of a project according to Lauer [70]. The approach of Sayfutdinov *et al.* [95] is stochastic in that a large number of electrical price profile scenarios are fed into the schedule optimisation programme.

2.2.5 LIB Degradation in TEA

The body of literature on LIB TEA is approximately consistent with that on VRFB, albeit richer. Providing a full review of the literature is outwith the scope of this thesis, and the following review is instead limited to degradation, where LIB require additional model formulation.

Battery degradation is of the utmost importance when determining the economic value of a LIB project. Maheshwari *et al.* provide a useful classification of the treatments of degradation within TEA of LIB, and distinguish between studies where degradation is simply modelled after the schedule has been optimise, and those in which it is defined in the objective function [99]. Shi *et al.* [100] provide a useful classification of approaches to the latter:

- Linear model: all throughput is modelled as having equal degradation, which is attributed a representative cost.
- Cycle-based model: individual cycles are identified by a rainflow counting algorithm, and the throughput in each is weighted by the depth of discharge.

They note that the cycle-based models are more difficult to incorporate as the rainflow algorithm is not a closed function, and proceed to give a mathematical definition of a

convex form for such. Although Shi *et al.* refer to degradation as an operational cost, this is not strictly true, as no money must be paid, unless the battery is augmented continually to compensate for the loss of capacity. The degradation cost in the optimisation process is really a penalty term, which may be adjusted in order to find the optimum behaviour over a longer period.

Fisher *et al.* applied the non-linear depth of discharge sensitive model of Ciez and Whitacre [101] in a linearised form to penalise LIB cycling during schedule optimisation [10]. This was done by taking a representative depth of discharge from operation up until the day in question. By increasing the degradation penalty term (via the battery replacement cost parameter), the authors were able to extend the lifetime of the LIB to match the 10 year project term. The SOC range was also constrained to 0.15-0.95 to preserve the lifetime, although the reason for picking this range was not discussed.

None of the aforementioned works consider the calendar aging of LIB, which continues regardless of cycling and is sensitive to both temperature and SOC. The experimental work of Schmalstieg et al. showed that the rate of capacity loss depends approximately linearly with SOC, and displays an Arrhenius type relationship to temperature [102]. It also yielded a more complex empirical cycle aging function, where the degradation per unit throughput is a function of both depth of discharge and the average state of charge on which the cycle is centred. They also showed that a NMC cathode LIB would lose 10% of its initial capacity after 3 years at 35 °C, corresponding to 50% of it's available lifetime if 80% of initial capacity is taken as end of life. Even at 25 °C (based on extrapolation of the reported Arrhenius behaviour), the same loss would occur in 7 years.

Reniers *et al.* employed this model within the objective function of an energy price arbitrage problem, but commented that the solution time was 1000 times greater than for a linear degradation model [103].

Recently, [99] reported a similar cycle aging behaviour to that in [102]. They also report a method for optimising operation while considering this behaviour alongside the influence of current, but neglect calendar aging on the grounds that it is less important

than cycle aging. The degradation model is represented in a piece-wise fashion, rather than as a closed function like those derived in [102].

The practical impact of computation time is not typically discussed in the literature, and computation time is usually deployed as a metric to evidence progress relative to previous work. In techno-economic studies, where it is desirable to simulate long periods of operation, long computation times are a nuisance as they restrict the number of scenarios that can be run, making sensitivity studies or stochastic approaches difficult. They also disrupt project workflow. However, in a control system, it is likely that an optimisation model might be run once a day or less frequently, e.g. for intra-day trading. Optimising shorter time periods but doing so more frequently reduces the computational burden, as integer programming problems grow super-linearly with number of variables, and he number of variables is usually a linear function of the number of time-steps.

2.3 Conclusions

This literature review has shown that a huge variety of RFB systems have been demonstrated at the bench scale, and some of these have the potential to offer lower $\$\mathrm{kW}^{-1}\,\mathrm{h}^{-1}$ costs, or higher energy densities than the VFRB. However, most of these systems demonstrate lower power densities at the stack, which would lead to higher $\$\mathrm{kW}^{-1}$ costs. This is particularly true of systems based on non-aqueous solvents. It is anticipated that the power performance may be improved by engineering efforts, and system optimisation as indicated by the work of Reed *et al.* [28]. For the purpose of accurate TEA, similarly in-depth experimental studies on promising alternative chemistries would be very valuable.

TEA of RFB systems tend to focus on either the system cost (with a simple application assumed), or the revenue calculated from scheduling optimisation (citing $\$\mathrm{kW}^{-1}$ and $\$\mathrm{kW}^{-1}\,\mathrm{h}^{-1}$ capital costs from elsewhere). Having a true bottom up TEA tool would be very useful for understanding the economic impact of system modifications in the context of a particular application.

While a number of researchers have attempted to improve the fidelity of the representation of RFB systems within scheduling problems there is more work to be done in this area. The approach of Nguyen *et al.* to accurately formulating the variation in efficiency with power output is very interesting, but relies on a non-convex problem formulation with an associated increase in computing cost.

Regarding VRFB degradation, the only TEA on this subject is the recently published work of Rodby *et al.*, but this only includes a levelised cost analysis in the context of maintenance frequency [23].

For LIB, a range of techniques have been employed to include the degradation cost in the optimisation. The linear approach employed by [10] is attractive from a computational perspective, but does not capture calendar aging, which Schmalstieg *et al.* showed to be a significant component of the total aging [102]. The work of Reniers *et al.* is exemplary, but the non-linear model considerably more computationally intensive [103].

Given the higher TRL of VRFB, if was decided to focus on this type of flow battery. Based on the preceding literature review on VRFB and LIB TEA, the following were identified as focus areas for generating original findings:

- Combining a bottom up cost model for VRFB with a detailed case-study rather than a basic LCOS analysis.
- Applying the VRFB degradation model reported in [23] and the LIB model reported in [102] to such case studies, and studying the role of local temperature for the latter. The challenge in this area was to integrate these models with the operational model in order to generate accurate results.
- Developing a model for variable VRFB efficiency in such case studies, that runs quickly enough to be able to obtain results for a large set of scenarios. The challenge in this case was to determine which are the most important components of efficiency in order to reduce complexity without introducing errors.

For the first case study, the model of [10] was chosen, as it allows several services to be

studied in one application. The linear LIB degradation model is retained in the objective function, but for tracking degradation the model of Schmalstieg *et al.* [102] is applied.

For the second case study an application focusing on renewable energy facilitation like that of [86] was desired for variety. As the first case study was based behind the meter at commercial/industrial sites in Calfiornia, a case study was defined in which the site would aim to achieve self-sufficiency using PV and an LIB, VRFB or hybrid system.

2.4 Summary of Research Challenges and Novel Contributions

The objective of this thesis was to determine whether the posited advantages of VRFB (long life and low incremental cost of energy capacity) translate to economic benefits in commercially relevant applications. LIB were chosen as the technology to compare to. These are maturing as MW scale energy storage for short duration applications such as frequency control, and as such may be considered the incumbent large scale BESS. However, they are not necessarily suitable for longer durations as the cost of incremental energy capacity is high. Additionally, they exhibit permanent degradation during operation which limits their lifetime. Once degraded, there is no commercially established route to recycling, hence their use poses a sustainability challenge which the VRFB avoids. The primary downsides of the VRFB are higher power capacity costs - which lead to high system costs for short durations - and lower round trip efficiency, which increases the cost of charging.

In order to perform the comparison of the two technologies rigorously, considering each of the above differences in characteristics, the following research challenges were overcome. In each case these resulted in novel contributions to the field.

- Research challenge: to study economics rigorously required estimates for total installed system cost (turnkey) of VRFB at various durations, and the ability to modify individual cost components, e.g. in the case of electrolyte leasing.

Approach: Construction of a full bottom up model for VRFB cost by adapting existing DC level model and combining with a balance of system (to AC) model synthesised from two sources

- Research challenge: as the efficiency of the VRFB varies significantly with power input/output, it was important to model this behaviour and allow for optimisation of operation to accommodate this.
  Approach: A novel MIQP optimisation model was developed, which approximates the losses due to pumping, shunt currents and ohmic and kinetic overpotentials. Additionally it allows idling of the VRFB when appropriate to reduce parasitic losses.

- Research challenge: to understand the longer term performance of VRFB and LIB, it was necessary to model degradation processes more accurately than had previously been done in detailed realistic use-case studies.
  Approach: for VRFB a 2020 degradation model was implemented for the first time to work in combination with a rainflow counting algorithm for cycle logging. For the LIB, a degradation model describing both cycle aging and temperature dependent calendar aging was implemented.

In order to develop a deeper understanding of the potential benefit of the VRFB, the models developed were applied to simulate two use-cases:

- Use-case A: Performing peak demand charge avoidance, electricity price arbitrage and ancillary service provision across a 10 year project.

- Use-case B: Increasing the electrical self-sufficiency of the site when combined with photovoltaic panels across a 20 year project.

The cases differ in the level of duty the BESS must perform. In use-case A the BESS may opt to perform a services if the revenue justifies it, or simply sit idle. In use-case B, the BESS is obliged to support the site load, hence is more likely to have a high cycle rate.

The novelty of the above contributions has been evidenced by the successful publication of articles on both the modelling developments and the techno-economic assessment as detailed in the list of publications.

The key novel contributions of the thesis and the techniques used to achieve these are outlined graphically in Figure 1.1 on the following page.

Chapter 3

Methodology

3.1 Introduction

In this chapter the modelling methods used throughout this thesis are described. Models specific to a particular use-case or research problem are defined in a dedicated methods section at the start of the relevant chapter. For a graphical representation of the key components of the methodology, and how these were employed to generate novel findings, the reader is referred back to Figure 1.1 in Chapter 1.

In the first section of this methodology, an important description of the definition of BESS duration is made in Section 3.2.

Analysis of BESS degradation is an important component of this thesis. The methods used to apply recently published degradation models within the optimisation framework are described for the VRFB in Section 3.3.1 and the LIB in Section 3.3.2.

In Section 3.4, the methods used to generate the economic comparisons between VRFB and LIB are defined. The definition of net present value for the CAISO market case study is given in Section 3.4.1, and the definitions of levelised cost of storage (LCOS) and levelised cost of electricity (LCOE) used in the self-sufficiency case-study are given in Section 3.4.2. The models used to estimate the price of VRFB and LIB systems at the DC boundary are given in Section 3.4.4 and Section 3.4.5 respectively. In Section 3.4.6 the

model used to estimate the balance of costs to deliver a turnkey system is introduced.lastly, the operation and maintenance cost assumptions are given in Section 3.4.7.

3.2 Defining the Power and Duration of the BESS

Before describing the optimisation models in detail, it is important to formalise the definitions of BESS power and duration that will be used as there is potential for confusion in this area. For example, say a 50 kW / 4 h system is desired, then one definition of such a system might be 200 kW h of LIB energy capacity placed behind a 50 kW inverter. There are two problems with this. Firstly, in the likely case that the SOC range will be capped at both ends in order to prolong the life of the cells, the usable duration will be reduced. In the present work the SOC range of 0.8 would yield an accessible duration of 3.20 h. Secondly, this reduced capacity is further reduced by losses within the DC boundary. For a round trip efficiency (RTE) of 0.95, as assumed for an LIB in the work of Fisher *et al.* cited herein, the energy capacity that may be retrieved and converted to AC power is 3.20 h X $\sqrt{0.95}$ = 3.12 h. Minor losses also occur at the inverter, and at 0.96 RTE, 3.06 h of discharge would be achievable.

While these results could be internally consistent if the pricing is calculated correctly, there is an issue when comparing different BESS. A VRFB with an accessible SOC range of 0.7 and an RTE of 0.75 would only have an AC duration of 2.38 h. Given that the incremental revenue generated falls as the duration is extended, this approach would falsely inflate the economic performance of the VRFB, as the LIB has a longer usable duration.

To avoid this issue, the BESS durations in this work are accessible durations, defined as the gross duration divided by the SOC range. Hence, for the LIB, a 4 h duration would require 50 kW x 4 h / 0.8 = 240 kW h of cells.

There will be some difference in the actual duration of a VRFB and an LIB due to the difference in efficiency mentioned above, but given that efficiency is a variable that is studied in this work, it was not deemed appropriate to fix it in the definition of duration.

Regarding power, for the LIB it is assumed that in the present case studies, where the duration is never less than 2 h, the cells will always be able to satisfy the power requirement, hence no over-sizing is required in this dimension. For the VRFB, the size of the stack is scaled to cover losses and still output the rated system AC power. This is formalised in Section 3.4.4.

3.3 Enhanced Degradation Models

In previous studies, including that of Fisher, the degradation of a VRFB is typically not considered when assessing project economics. In Section 3.3.1, the adaptation of a newly published model for the reversible degradation that occurs in a VRFB to the case studies is described. In Section 3.3.2, the implementation of a more up to date LIB degradation model is defined, which includes calendar aging, the aging that occurs regardless of energy throughput.

3.3.1 VRFB Stack Lifetime, Capacity Fade and Electrolyte Decay

In this work, three forms of degradation affecting the VRFB are considered. The first of these, component wear is addressed firstly by assuming that the stack will require replacement after 10 years (covering both membrane degradation and component corrosion) after [24, 65]. Secondly, the replacement of minor parts as indicated in [25] is assumed to be covered by the $10\,\mathrm{kW}^{-1}$ O & M cost described in Section 3.4.7.

As discussed in section 2.1.1 there are two capacity loss mechanisms, capacity fade (due to ionic crossover) and electrolyte decay (due to the hydrogen evolution side reaction). Although both of these are reversible, the former may be managed by an automated rebalancing routine whereas the latter may require a site visit in which a reductant is added to the tanks. Rodby *et al.* reported an optimal (minimum LCOS) capacity fade limit of 20% between interventions. Below this, the lowering of the average working

capacity increases the LCOS [23]. Above this value the LCOS increases steeply, but this is because the authors apply the same capacity cut off for the two mechanisms, and there is a fixed cost associated with a site visit to reverse the electrolyte decay, which discourages more regular reversible. There is nothing in the formulation to suggest rebalancing more frequently costs more; the rebalancing cost is solely due to the cost of electricity required to transfer a portion of the catholyte to the anolyte tank and modify the oxidation state in each tank, which will be the same regardless of the frequency.

By assuming that the rebalancing may be superimposed on an already scheduled charging event, and hence not impinge on revenue, the cost may simply be expressed as an operating cost, defined by:

For the reversible capacity fade, it is assumed as in [23] that a fade of f % is due to f % of the vanadium in the anolyte (average oxidation state 2.5) crossing the membrane and reacting with f % of the catholyte (average oxidation state 4.5) to give 2 f vanadium with an oxidation state of 3.5. The resultant deficit in the oxidation state of the catholyte in the discharged state is hence defined by:

$$\delta^{Ox.}_{catholyte} = 4 - \frac{2f \cdot 3.5 + (100 - f) \cdot 4}{100 + f} \tag{3.1}$$

In this work, it is assumed that the VRFB would need to be cycled anyway on the day in which the rebalancing is performed, hence the cost of the rebalancing operation is simply that of the incremental charging. Because the redox reaction in the VRFB involves the transfer of one electron, the cost of the energy (kW h) required to rebalance 1 kW h of capacity may be defined by:

$$cost^{rebalance}_{kWh} = \frac{\delta^{Ox.}_{catholyte}(LMP_r + EC_r)}{\sqrt{\eta_{AC}}}(1 - f_{ED}) \tag{3.2}$$

Where LMP_r and EC_r are the average wholesale and retail energy prices in the rebalancing period r. In order to simplify the analysis, it is assumed that the rebalancing will be performed between the hours of 00:00 and 08:00 in order to capitalise on low

electricity rates (see Figure 4.2) and coincide with typical charging behaviour as shown in Figure 4.5b. As in Rodby *et al.* the maximum capacity is reduced by f_{ED}, the cumulative electrolyte fade since the last maintenance visit .

It may be inferred from Equation (3.2) that the cost of rebalancing based on a per cycle capacity fade rate of less than 1 % per cycle is very low compared to even arbitrage revenue, hence it is not necessary to optimise the scheduling of this task based on price signals, and an O & M approach is sufficient. There may be additional constraints that would apply in practice to the rebalancing operation, but these have not been disclosed in the literature to the best of the author's knowledge. It is assumed that rebalancing is performed frequently that there is no meaningful decrement to the VRFB capacity due to this process, hence it is not tracked in the application model, but the cost is logged daily.

The capacity fade rate for the PNNL IDD2s embodiment used to parametrise the VRFB model in the base scenario was not reported for the PNNL system [28], however, such data were published the previous year by the same research group for a system using the same Nafion NR-212 mebrane, but with a more basic electrode structure [58]. The capacity of the system fell to 70 % of the original in 40 cycles, or 0.75% per cycle. This is fast compared to the average rate of 0.44 % that Rodby *et al.* reported in their literature review. The thinness of the Nafion membrane used in the PNNL system would be an obvious reason for the high fade rate, but the same rate was reported for the thicker N-115 membrane and the still thinner NR-211 membrane. Another explanation is that the high electrolyte temperature in the PNNL system leads to increased membrane permeability.

Alternatively, the relatively high charging voltage cutoff of 1.75 V in [58] may have caused accelerated electrolyte decay, and this degradation would be independent of membrane choice. As the PNNL system was not subjected to a rebalance procedure, the fraction of the overall capacity loss attributable to electrolyte decay is not knowable hence the estimate made by Rodby *et al.* is used. They reported the electrolyte decay in two ways - as the % of capacity lost per cycle (0.055 % per cycle), and as the % of overall capacity loss attributed to this process (12.5 % per cycle). The latter definition has been applied in this case, as it gives a more conservative figure when applied to the

Table 3.1: VRFB capacity loss per cycle assumptions for PNNL system; total loss, loss due to capacity fade, loss due to electrolyte decay.

Capacity loss (%)	f (%)	f_{ED} (%)
0.75	0.66	0.09

0.75% per cycle total capacity loss seen in [58]. This may still be an underestimation of the electrolyte decay that occurred in [58], but in a real application if is likely that high voltage can be avoided by appropriate scheduling. This matter is discussed further in Section 6.2.4. The total capacity loss applied to the PNNL system is therefore broken down as shown in Table 3.1.

The maintenance cost associated with electrolyte decay was defined by Rodby *et al.* as the sum of a site visit cost of $\$10\,\mathrm{kW}^{-1}\,\mathrm{h}^{-1}$ and the cost of reductant material required to return the anolyte oxidation state to 3.5. Using the reductant cost formulation in Rodby *et al.*, and their rough assumption of 20 % loss of capacity a year due to electrolyte decay, the cost of oxalic acid is calculated to be $\$0.5\,\mathrm{kW}^{-1}\,\mathrm{h}^{-1}$ which is considered negligible and hence not included in the O & M cost. It is assumed that the corrective maintenance may be performed at the same time as the generic maintenance covered by the $\$10\,\mathrm{kW}^{-1}\,\mathrm{h}^{-1}$ in Section 3.4.7, and hence no extra cost is incurred.

The impact of electrolyte decay on the working capacity of the VRFB is however important, as it will impact the revenue of the project between maintenance visits. For this reason the loss of capacity is calculated at the end of each optimisation period as the product of the equivalent full cycles performed and the electrolyte decay rate given in Table 3.1. Given the seasonality of the revenue streams in the chosen application, an analysis of maintenance scheduling is made in Section 5.4.

3.3.2 LIB Degradation Model with Calendar Aging and Temperature Dependence

The literature review identified several degrees of fidelity when modelling the degradation of LIB. The two key features of modelling degradation are the tracking of degradation through the project lifetime, and the optional imposition of a degradation cost when optimising the operation. The former may be achieved more easily, as it is easy to calculate the degradation once the operation is known. The latter is more challenging, as the degradation is itself a non-linear function of state parameters, notably SOC.

It is also important to note that the degradation model of Ciez and Whitacre, by only considering the number of cycles to reach end of life, linearises what is actually a non-linear process [101, 102]. In addition to the Ciez and Whitacre degradation model, a more comprehensive degradation model reported by Schmalstieg *et al.* was also implemented. Four functions are provided, describing calendar and cycle ageing with regard to both coulombic capacity loss and resistance increase. The latter is not investigated here, primarily due to scope constraints, but also because Schmalstieg *et al.* concluded that resistance aging is a far slower process and the LIB starts with excellent efficiency.

The capacity of the battery relative to the initial value is defined by Schmalstieg *et al.* as:

$$C = 1 - \alpha_{cap} \cdot t^{0.75} - \beta_{cap} \cdot \sqrt{Q} \tag{3.3}$$

In the first term, describing calendar aging, t is the time in days since the start of service and α_{cap} is the calendar aging factor. The second term describes the cycle aging in terms of cycle equivalents Q and the cycle aging factor β_{cap}.

α_{cap} is defined by:

$$\alpha_{cap} = (7.543V - 23.75) \cdot 10^6 \cdot e^{-6976/T} \tag{3.4}$$

where T is the cell temperature (K) and V the cell voltage is approximated by:

$$V = a \cdot SOC + b \tag{3.5}$$

where a and b are empirically derived parameters.

β_{cap} is defined by:

$$\beta_{cap} = 7.348 \cdot 10^{-3} \cdot (\bar{V} - 3.667)^2 + 7.600 \cdot 10^{-4} + 4.081 \cdot 10^{-3} \cdot \Delta DOD \tag{3.6}$$

where $\bar{V}$ is the mean cell voltage across the cycle, and ΔDOD the depth of discharge, equivalent to SOC_{swing} in the terminology used in Section 4.2.2.

For the purposes of the present work, where it is necessary to calculate the degradation following each implemented schedule, it is necessary to take the derivatives of the calendar and cycle aging expressions. The derivative of the calendar aging expression with respect to time, and the derivative of the cycle aging expression with respect to cycles are defined respectively by:

$$\frac{\mathrm{d}C}{\mathrm{d}t} = -0.75 \cdot \alpha_{cap} \cdot t^{-0.25} \tag{3.7}$$

and

$$\frac{\mathrm{d}C}{\mathrm{d}Q} = -0.5 \cdot \beta_{cap} \cdot Q^{-0.5} \tag{3.8}$$

It is assumed that the length of the optimisation period and the energy throughput are sufficiently small relative to the project history, so that the change in gradient across the schedule may be ignored. It is also assumed that because the average cell voltage does not change with time, the coulombic expression of Schmalstieg *et al.* (A h) may be directly converted to energy (kW h). Lastly, as in Schmalstieg *et al.*, it is assumed that cycle aging and calendar aging are independent processes. The absolute degradation in a schedule of length d days, where W whole cycles and H half cycles are performed may hence be

defined by:

$$\Delta_C = C_0 \cdot \left(0.75 \cdot \alpha_{cap} \cdot t^{-0.25} \cdot d + 0.5 \cdot Q^{-0.5} (\sum_W \beta_{C,w} \cdot \Delta DOD_w + \cdot \sum_H \beta_{C,h} \cdot 0.5 \cdot \Delta DOD_h) \right) \tag{3.9}$$

Where C_0 is the starting capacity of the LIB in kW h. The calendar aging was calculated on an hourly basis, under the assumption that the cell temperature is equal to the ambient temperature. This assumption is discussed in Chapter 5.

After each day of operation, the battery capacity was decremented according to Equation (3.9).

3.4 Economic Analyses

3.4.1 Discounted Cash Flow Model

In this work,net present value is used to compare different BESS projects in the CAISO market case study, as defined in Equation (2.3).

Choosing an appropriate discount rate is important. For example, in comparing two BESS that have identical performance excepting that one will last 10 years in the application and one 20. At a discount rate of 10%, the revenue generated by the longer lived BESS in the extra ten years is discounted by 76% on average. At a discount rate of 5%, the discounting is reduced to 51%.

A discount rate of 10% is common for recent TEA of BESS in the academic literature [80, 102, 104, 105]. This figure lies between the 8% p.a. cost of debt and 12% cost of equity assumed by Lazard, so is used in the CAISO case study here [9]. Where BESS are being compared purely for the provision of firm power from intermittent renewable sources, and not other services, the payback periods tend to be longer and lower discount rates are often applied. For the PV self-sufficiency case study a discount rate of 5% is used, after [106].

In this work the impact of tax is ignored, as project financing typically has the goal of using debt to spread the upfront costs and offset revenue across the project. In order to keep the findings general, the impact of incentives such as tax breaks for BESS projects are ignored.

The project life is fixed at ten years, as this is warranty period for several commercial inverters [107]. As such a decision would likely be made at this point regarding the cost/benefit of extending the project.

Inflation is assumed to be 2% p.a., however this is only applied to the O& M cost. The revenue/avoided cost for the BESS operation cannot be assumed to simply increase in line with inflation.

Lastly, where the lifetime of the BESS exceeds the project life, a residual value is calculated and added as an income in the final year. For the Li-ion system, the residual value is the initial DC module CAPEX multiplied by the fraction of life left following the calculation of degradation. This is an approximation which assumes a linear decrease in capacity. For the VRFB, the residual value is that of the electrolyte, assuming as with the LIB that there will be a direct market for it. We ignore the residual value of the balance of system.

3.4.2 Levelised cost of Storage and Levelised Cost of Energy Calculations

In Chapter 7 where the BESS are combined with PV in order to provide self-sufficiency to commercial-industrial sites, levelised cost of storage (LCOS) and levelised cost of electricity (LCOE) are used as metrics. The former is used where a BESS is added to an existing PV installation. In this case, the LCOS is calculated after the definition of Julch [19], with the charging cost set to 0, under the assumption that the surplus PV would not be used otherwise. Residual BESS value was included as in the NPV calculation.

For the LCOE calculation, the LCOS definition was applied as above, but the CAPEX associated with the PV was added in year 0. The electrical output on the LCOE denomi-

nator was calculated by comparing the original load to the net load after including PV and BESS output.

3.4.3 DC Module Definition

For both LIB and VRFB the boundary is drawn around the components that allow DC power production. Control of the system is accounted for in the balance of system hardware (BOSH) figure defined in section 3.4.6. In the VRFB, the heat exchanger is included in the DC module, as this is required to move heat from the electrolyte into the container. In the following subsections the methods for estimating VRFB and LIB DC module prices are described.

3.4.4 VRFB DC Price Model

In order to calculate the price of a VRFB of a given specification it is necessary to calculate the material requirements and multiply these by the associated prices. For the material requirements, the model introduced by Darling *et al.* has been used [80]. The formulation has however been changed so that the model returns \$ kW^{-1} and \$ $kW^{-1} h^{-1}$ prices that may be used as input for the CAPEX entry in the DCF analysis under different sizing scenarios. For this reason, the discharge time parameter used by Darling *et al.* is removed. Also, Darling *et al.* do not explicitly calculate the electrolyte flow rate, as they consider pumping costs to be part of the balance of plant, which is given a separate \$$kW^{-1}$ cost. In the following work, it was desirable to have a bottom up cost model for electrolyte pumping, and the calculations around this component are informed by the work of Viswanathan *et al.* [24].

For the overall price model, the approach of Ha and Gallagher has been adopted, which takes the perspective of an RFB manufacturer which purchases components and adds its own costs and profit margin to arrive at the product price [40]. The approach used here errs on the conservative side by applying profit margins to any components where the data used is described as a cost.

The following assumptions/simplifications have been made while constructing the model:

- Discharge voltage: it is assumed that cell voltage during discharge is linear w.r.t. SOC within the allowed range and hence the cell voltage at 50% SOC is taken to represent the average discharge voltage.

- Symmetry of losses: it is assumed that the discharge and charge efficiency are equal (both voltaic and coulombic), and hence the one way efficiency may be calculated as the square root of the round-trip figure.

- Single cell: The RFB component requirements are calculated as if it were a single cell, with no stacking of cells

- Non-discretised pump rating: the pump rating uses a continuous linear price function for simplicity, following Weber *et al.* [30].

- Round-trip efficiency: The power output of an RFB may be increased at the cost of resistive losses. Therefore an accurate system cost ($\$kW^{-1}$, $\$kW^{-1}\,h^{-1}$) can only be specified at a particular round trip efficiency. Here, as in [80], a round-trip DC efficiency of 0.75 at the maximum charge/discharge power is targeted, and the current density that allows this efficiency is used in Equation (3.11). This condition is formally defined by:

$$\eta_{DC} = \eta_V \eta_C (1 - l_{BOP})^2 \geq 0.75 \tag{3.10}$$

  where η_V and η_C are respectively the voltaic and coulombic round-trip efficiencies of the cell/stack, and l_{BOP} is the fractional power loss due to balance of plant (primarily pumping) during either charge or discharge.

- Round trip efficiency: it is assumed that the stated round trip energy efficiency (η_{DC}) is constant across the allowed SOC range.

- Although Ha and Gallagher's analysis of "Unit Price Less materials" (UPLM) fixes the BESS duration at 5 h, it is assumed that this price component scales with power, as the stack and other power components are where the manufacturing complexity lies.

3.4.4.1 RFB Price Model Terms

The stack area A_s (m^2) of each VRFB module required to supply the specified AC output on the BESS kW is defined by:

$$A_s = \frac{1000 P_{Inv.}}{\bar{I}^d OCV_{50\%} \sqrt{\eta_V}(1 - l_{BOP})\sqrt{\eta_{Inv.}} N_S} \tag{3.11}$$

where $P_{inv.}$ is the inverter rating which defines the maximum BESS output (kW), $\bar{I}^d$ is the maximum discharge current density (A/m^2), $OCV_{50\%}$ the open cell voltage at 50% SOC, η_V the round-trip voltaic efficiency, $\eta_{Inv.}$ the round trip inverter efficiency and N_s the number of modules making up the system. This definition assumes all the VRFB modules have the same properties.

The maximum flow rate (and hence pump rating, $L\,s^{-1}$) for the catholyte is determined by:

$$Q_+^{max} = \frac{A_s \bar{I}^d r_{flow}}{C_+ min(SOC_{min}, 1 - SOC_{max}, \delta_{SOC})\sqrt{\eta_C}} \tag{3.12}$$

where r_{flow} is the ratio describing the over-supply of flow to avoid diffusion limitations, SOC_{min} is the lowest permitted SOC, SOC_{max} the highest, δ_{SOC} the maximum permitted change in SOC through the cell per pass, η_C the coulombic efficiency and C_+ the coulombic concentration ($C\,L^{-1}$) of the catholyte, defined as:

$$C_+ = \frac{n_e F c_+}{s_+} \tag{3.13}$$

where n_e, the number of electrons transferred in the redox reaction and s_+, the number

of species participating in the reaction (stoichiometry) are both 1. F is the Faraday constant ($96\,485\,\mathrm{C\,mol^{-1}}$) and c_+ is the concentration of the catholyte redox active species ($\mathrm{mol\,L^{-1}}$).

The presence of η_C on the denominator in Equation (3.12) ensures sufficient charge is supplied in chemical form to cover the coulombic losses due to active species crossover and shunt currents.

The inclusion of the minimum of SOC_{min}, SOC_{max} and δ_{SOC} on the denominator of eq. (3.12) adds a level of stringency above that of Viswanathan *et al.*, who applied only the SOC_{min}. This reflects the fact that active species depletion during charging, and the need to maintain a maximum drop in SOC across the stack can also lead to inflation of the required flow rate. It is assumed that the coulombic flow in the electrolyte is equal to that required at the electrode. This assumption is tested by reference to the Reed *et al.* system later in this section.

The calculation shown in Equation (3.12) is repeated for the anolyte flow $Q_{-,max}$ using c_- and s_-.

The inventory of catholyte species (mol) required to satisfy one hour of discharge is then defined by:

$$m_+ = \frac{3.6 \cdot 10^6 P_{Inv.} c_+}{OCV_{50\%}(SOC_{max} - SOC_{min})C_+} \tag{3.14}$$

The inventory of each supporting counter ion species (mol) may be calculated for the catholyte by:

$$m_{CI,+,n} = \frac{m_+ c_{CI,+,n}}{c_+} \tag{3.15}$$

where $c_{CI,+,n}$ is the concentration of the nth counter ion (allowing for mixed acid electrolytes) in the catholyte. An analogous calculation is performed for the anolyte. In the case of the VRFB it is assumed that the concentrations of counter ions are the same on both sides of the membrane.

The volume of storage required for the catholyte (L) was calculated by:

$$V_+ = \frac{m_+}{c_+} \tag{3.16}$$

an analagous calculation was used for the anolyte.

The total price of the power basis components is then defined by:

$$price_{kW} = A \cdot price_{areal} + (Q_+ + Q_-)price_{Pump} + price_{HEX} + UPLM \tag{3.17}$$

where $price_{pump}$ is the pump price ($\$L^{-1}\,s$). Ha and Gallagher used a bottom up model to estimate the "Unit Price Less Materials" (UPLM) for a VRFB with a 5 h duration, and compared this to that of a LIB with the same specification (using the Argonne BatPac model for the latter) [40]. It is assumed that the UPLM will scale with power rating, as the article mentions number of stacks per year as the scale. For a given capacity output per annum, they report a lower UPLM for the VRFB, attributed to the higher current density of the latter and the resultant lower area specific costs. The current density assumed by Ha and Gallagher (approx 190 $mA\,cm^{-2}$) for the VRFB is similar to that of the VRFB in the present base case scenario (219 $mA\,cm^{-2}$), so the stack manufacturing requirements captured in the UPLM should be appropriate. The area specific price $price_{areal}$ ($\$m^{-2}$) is defined according to the cell components representing a repeating unit in a stack by:

$$price_{areal} = price_{Memb.} + 2price_{CE} + price_{BPP} + price_{areal,other} \tag{3.18}$$

where the terms on the right hand side represent, respectively, the cost of the membrane/separator, the carbon felt electrodes and the bipolar plate.

In this model the cost of end plates is ignored, as these would represent a small fraction of the cost for a 105 V stack (the voltage considered in [40]).

The total price of components on an energy basis are then calculated by:

$$price_{kWh} = ((m_{+} \cdot price_{+} + m_{-} \cdot price_{-} + \sum_{n} m_{CI,n} \cdot price_{CI,n}) \cdot MC_{E} + (V_{+} + V_{-}) price_{tank}) PM_{RFB} \tag{3.19}$$

where $price_{+}$ and $prices_{-}$ are the prices of the redox active species in the catholyte and anolyte respectively, $price_{CI,n}$ the price of the nth supporting species (all in $\$\mathrm{mol}^{-1}$), MC_{E} the electrolyte manufacturer cost factor (e.g. 1.1 for 10%) and $price_{tank}$ the price of chemical storage ($\$\mathrm{L}^{-1}$). As the UPLM parameter is assumed to scale with power, the energy component prices are multiplied by PM_{RFB}, an assumed profit margin factor for the RFB manufacturer. It is assumed that the electrolyte is manufactured by the same entity that manufactures the RFB. If this were not the case, an additional profit margin would need to be applied to the total electrolyte cost.

3.4.4.2 Base Scenario VRFB Parameters

The approach to price model parametrisation for the base case VRFB was to collect as much pertinent data from the literature as possible, and generate average values for present day and future scenarios. This task was aided by the 2018 review of Minke and Turek which collated cost data for key stack components [108]. For the data taken from Viswanathan *et al.*, "Near term" was used for the present case, as this shows better agreement with other sources than the "Present" values do [24]. Nafion NR212 is used as the membrane in the model VRFB, as this material was used in the system from which performance parameters are drawn [28]. Although potentially cheaper due to the reduced material requirements, the thinner Nafion NR211 did not show improved performance, and was described as being difficult to handle [58]. As the sources tend to use "cost", a profit margin of 12% is applied to each component in order to avoid underestimating the RFB manufacturer's costs [109]. The data obtained are shown in Table 3.2

Other area specific costs is the average of those given in the two sources. Under pump costs, a figure of $\$900\,\mathrm{L}^{-1}\,\mathrm{s}$ was reported in [30] for an acid compatible unit. This cost is higher than the current price of the pump used in the VRFB reported by [28]. According

Table 3.2: VRFB Component Price Parameters. *Present/future.

Scaling	Component	Cost unit	Cost*	$ exchg.	PM	Price*	Source
kW^{-1}	Nafion NR212		301/48	1.10		370/59	[108]
	Bipolar Plate	€ m^{-2}	100/50	1.10		123/62	[108]
	Felt electrode		53/16	1.10	12%	65/20	[108]
	Other Area Specific*	$\$m^{-2}$	8/3	1		9/3	[24, 80]
	Pump	$\$L^{-1}\,s$		1		500/400	[28]
	HEX	$\$kW^{-1}$	56/37	1		63/41	[24]
	UPLM	$\$kW^{-1}$		1		173/158	[40]
$kW^{-1}\,h^{-1}$	V	$\$mol^{-1}$		1		1.55/1.55	[110]
	HCl	$\$mol^{-1}$		1		0.021/0.021	[111]
	H_2SO_4	$\$mol^{-1}$		1		0.020/0.020	[112]
	MC_E					10%	[25]
	Tank (HDPE)	$\$L^{-1}$	0.09/0.08	1		0.10/0.09	[24]
	PM_{RFB}					10%	Estimate

to the brochure, that pump is capable of $1.25\,L\,s^{-1}$ at the base case stack pressure drop of 0.34 bar [113]. At the time of writing, this pump is available in the US for a price of $ 500, giving a pump price of $\$400\,L^{-1}\,s$. The large discrepancy between the two sources may be explained by the former source being 7 years old. For this reason, the Reed pump price is used for the present scenario, but a 25% contingency is added in case custom seal arrangements are necessary. For the future scenario, a price decrease of 20% is estimated to be achieved by volume discounting.

The inclusion of a price for a heat exchanger (HEX) is conservative. The mixed acid electrolyte used in the Reed system allows a higher electrolyte temperature to be reached before precipitation occurs, and in principle this will allow greater passive cooling [17]. Viswanathan *et al.* factored this in their cost estimates for sulphuric acid and mixed acid systems, removing the heat exchange cost component from the latter [24]. However the ability to operate without a heat exchanger is merely asserted, and a detailed study of the thermal management has not been carried out to the best of the author's knowledge. HEX is assumed to be a VRFB specific component of the DC module cost, and it is assumed that more generic heat management equipment required at the container level is included in the BOSH figure derived in section 3.4.6.

Future cost decreases are primarily attributed to economies of scale. Where the manufacturing scale scope of the study is stated, present day estimates are associated with

a scale of <300 MW and future scenarios with 1 GW - 2 GW [24, 40, 80].

A vanadium price of \$1.55 mol^{-1} is derived from a vanadium pentoxide price of \$17 kg^{-1}, this being the average European spot price from January 2006 to April 2020 (data are assumed to have been corrected to 2020 \$) [110]. Predicting a future price for vanadium is beyond the scope of this project hence the same price is assumed for the future scenario. A price of \$ 200 per wet ton for industry grade 35% HCl was used, based on prices shown on a Chinese commodity purchasing platform at the time of writing [111]. This price is assumed to include a shipping component, as prices at factory are typically considerably lower [114]. A price of \$200 per ton was also used for 98% industrial grade H_2SO_4 [112].

Minke and Turek mention reducing agents and additives as additional cost components in the electrolyte manufacture but do not report $\mathrm{kW}^{-1}\,\mathrm{h}^{-1}$ estimates for these [108]. The PNNL system used to parametrise this model did not include additives according to the experimental description, hence these are ignored. It is likely in any case that the contribution would be small relative to that of vanadium.

The performance parameters for the VRFB are predominantly taken from the system reported by Reed *et al.* in 2016 [28], except δ_{SOC} and l_{BOP} where a more generic approach is taken. Reed *et al.* tested various electrode flow architectures on a 1 kW VRFB stack based on a 50 µm Nafion NR212 membrane. In the base case scenario, performance data are taken from the test of the highest performing stack architecture (IDD2s) at an electrolyte flow rate of 400 $\mathrm{mL\,min}^{-1}$ per cell. This setup was tested at three current-densities: 160, 240 and 320 $\mathrm{mA\,cm}^{-2}$. At each test condition efficiency data were obtained as integrals over a cycle between 15% and 85% SOC.

In the parametrisation of the VRFB for the base case scenario the target for η_{DC} was fixed at 0.75. A coulombic efficiency (η_C) of 0.975 was derived as the average of the values reported by [28] at the three current-densities tested, which only varied between 0.974 and 0.976. For the base case system the η_{DC} requirement in Equation (3.10) is satisfied when the voltaic efficiency η_V is 0.801, which corresponds (by linear interpolation) to a current-density ($\bar{I}^d$) of 219 $\mathrm{mA\,cm}^{-2}$. $OCV_{50\%}$ was taken from a linear best fit line of data

in [17], where the OCV of a chloride electrolyte was reported at 20%, 50% and 80% SOC. Although a different electrolyte, based on a mixture of sulphuric acid and hydrochloric acid, was used in [28] the OCV data were not published.

Table 3.3 summarises the technical parameter values representing the VRFB in the bottom up price model.

Table 3.3: Parameters describing base scenario VRFB in the pricing model.

Parameter	**Value**	**Units**	**Source**
η_{DC}	0.75	-	Set
$\eta_{Inv.}$	0.96	-	[115]
η_V	0.801	-	
η_C	0.975	-	
$\bar{I}^d$	219	$\mathrm{mA\,cm^{-2}}$	
SOC_{min}	0.15	-	
SOC_{max}	0.85	-	[28]
c_+, c_-	2	M	
c_{HCL}	5	M	
$c_{H_2SO_4}$	2	M	
r_{flow}	1.12	-	
δ_{SOC}	0.2		[30]
$OCV_{50\%}$	1.47	V	[17]
l_{BOP}	0.02	-	[79, 80, 116]

The flow over-supply ratio r_{flow} was estimated by analysis of the experimental details in [28]. At the lowest permitted SOC during discharge, the concentration of unreacted vanadium would be 0.3 mol. At the flow rate of $400\,\mathrm{min}^{-1}$, a current of 193 A passes through each cell in chemical form [1]. The current required at the electrode is calculated as the product of I_{rated} and the cell area divided by the one way coulombic efficiency. For the reported cell area of $780\,\mathrm{cm}^2$ this figure is 173 A, hence the flow over supply is 12%.

An estimate for l_{BOP} is obtained by averaging the three sources. In [79] a 2.3% round trip pumping loss is interpreted here as a one way loss of 1.1%. The shunt current losses reported (1.1% round trip) are ignored, because in the Reed system these will be accounted for in the coulombic efficiency term. The figure in [80] is a generic estimate given in the form of charge/discharge system efficiencies of 0.94, giving l_{BOP} of 6%. However,

[1] It is assumed that this flow rate is used on both sides of the membrane, otherwise the flow would be insufficient

this includes PCS losses, which in this study are included at a one way value of 2%. To avoid double counting, this loss and the one way figure for the shunt loss in [79] are subtracted from this figure to give 3.4%. In [116] a pumping power of 20 W is required at the maximum flow rate tested for a 1.1 kW stack, giving a figure of 1.8%.

3.4.5 LIB DC Price Model

For the LIB DC module, figures published in 2020 by PNNL for NMC the DC storage block module were applied [21]. This unit includes rack and BMS, and is described as being similar to an electric vehicle pack. The 1 MW \4 MW h data were used: \$194 $\mathrm{kW^{-1}\,h^{-1}}$ in 2020 and \$116 $\mathrm{kW^{-1}\,h^{-1}}$ in 2030. These figures are assumed to be prices, rather than costs, hence no profit margin is applied. In the discounted cash flow analysis, the LIB DC price is interpolated linearly between the above years, then held constant after 2030. Hence in the CAPEX calculation for projects starting in 2025, the DC module price is \$155 $\mathrm{kW^{-1}\,h^{-1}}$, and a replacement after 4 years would be debited at 124 $\mathrm{kW^{-1}\,h^{-1}}$.

3.4.6 Balance of Upfront Costs for Turnkey BESS

An aspect of cost/benefit analysis that is neglected in most of the academic studies covered in Chapter 2 is the balance of costs associated with installing a BESS. In a highly detailed 2007 report "Vanadium Redox Flow Batteries: An In-Depth Analysis" Eckroad listed three types of upfront costs for a BESS project [25]:

- Costs that scale with power capacity.
- Costs that scale with energy capacity.
- Costs that do not scale with size.

Additionally, Eckroad highlighted the fact that there are cost gaps, where even the best informed analysts will be unaware of the current costs of items due to confidentiality or uncertainty.

When determining the optimum size for a behind the meter BESS installation, ideally the breakdown of costs along the above three categories would be available. Although it may be the case that a small battery with a low E:P ratio would deliver the highest revenue per kW h, the presence of fixed costs and costs that scale with power rating will change the picture. For a VRFB, where the incremental cost of energy capacity is relatively low at the module level, any installation costs that scale with energy capacity (for example site preparation) will reduce the net benefit of incremental capacity.

While the Eckroad study is an ideal resource, being focused on VRFB systems, it is somewhat outdated in that the VRFB is treated as a large unit similar to a chemical plant (hence the costings for pipes and a construction engineer). Currently, the trend appears to be towards modules with kW ratings in double figures (see Table 2.1). While some of these are described as "turnkey" there will inevitably be additional costs associated with installation.

In order to have as little uncertainty in the economic analysis as possible, a survey of upfront costs for BESS projects in the US was performed in order to obtain representative estimates of the various components. This proved difficult for multiple reasons:

- Data for industrial scale behind-the-meter systems is more scarce than utility scale and residential scale.
- Different studies use different terms and breakdowns.
- Some studies provide a limited number of absolute sizing cases with insufficient degrees of freedom to deconvolute the scale dependency of costs [117, 118].
- Different studies show costs scaling in different ways.
- Data come from different years.

The survey was restricted to standalone systems, i.e. those not paired with PV, and sources which publish properly deconvoluted per unit capacity costs. As the sector is subject to ongoing cost reductions [117], only data for installations in or after 2018 were included. The data obtained are shown in Table 3.4.

Table 3.4: Generic cost estimates for balance of turnkey BESS cost. BOP: balance of plant, BOS: balance of system hardware, C&C: construction and commissioning, EPC: engineering and procurement. *(Present/Future)

Source	**Ref.**	**Year**	**Scale**	**BESS**	**\$ kW^{-1}**	**\$ kW^{-1} h^{-1}**	**Other**
PNNL	[115]	2018/2025	Various	LIB	BOP (100/95)* PCS (288/211)	C&C (101/96)	-
				VRFB	BOP (100/95) PCS (350/211)	C&C (190/180)	-
Lazard	[9]	2019	1 MW/2 MW h	LIB	Inv. & AC system (205)	BOS (104)	EPC @ 51% of hardware costs.

Figures for inverter cost are in reasonable agreement between the Lazard study and the PNNL 2025 projection. The placement by Lazard of balance of system costs in the \$ kW^{-1} h^{-1} column is in contrast to both the PNNL study, and the aforementioned McKinsey and NREL reports, which show minimal dependence of this cost on energy rating. Lazard's expression of EPC as a fraction of the total hardware cost does seem reasonable, as there are likely to be both power and energy rating dependent components, e.g. the installation of cabling and the preparation of the site respectively. The Lazard figure is particularly high, even in comparison to its own estimates for a 100 MW utility scale project (EPC @ 15%) and a 6 kW residential project (EPC @ 19%). The EPC fraction used by Lazard for behind the meter Commercial projects has increased steadily since v2.0 in 2016. From v2.0 to v3.0 in 2017, the increase in EPC fraction from 16% to 25% was justified by reports from industry participants of cost increases [41, 119]. By contrast, Li *et al.* [120] applied an EPC cost of 21.5% of hardware for a flow battery, based on a synthesis of data contained in a 2015 DOE/EPRI report. However, Lazard also state that the cost of the hardware has fallen faster than the cost of installation, at least for LIB systems, hence the apparently high value for EPC as % of hardware may not be unrealistic.

In the PNNL study, the construction and commissioning costs are 88% higher for the VRFB, because the authors used energy density as a predictor of site area. This is a larger increment than the 54% reported by EPRI when comparing costs for a 20 MW/80 MW h system [121].

Given the limited data availability, the upfront costs for the present work are calcu-

lated by averaging the estimates obtained from both the Lazard and PNNL (2025) cost components. Although the PNNL report is more detailed and transparent, only one of the six sources surveyed concerns behind the meter installations ([122]), the rest being utility type installations. For this reason the two sources are given equal weighting.

The use by PNNL of the same BOP figure for both VRFB and LIB is worthy of further discussion. In an earlier work, Darling *et al.* assumed a lower cost of control system for a VRFB than for Li-ion ($60\,\mathrm{kW}^{-1}$ vs. $300\,\mathrm{kW}^{-1}$), due to the *" temperature sensitivity, large number of interconnects, and robust state-of-charge controls needed"* for the latter [80] . This assertion is not incorporated in the present work, as it is not self evident that the cooling requirements are lower for a VRFB. Firstly, the VRFB is also temperature sensitive, as high temperatures can cause the $VO_2{}^+$ species to precipitate. Secondly, the lower voltaic efficiency of the VRFB will result in greater waste heat generation. On the matter of interconnects and SOC controls in the LIB system, it is assumed here that these costs are kept low by standardised pack production.

The combined cost model for balance of turnkey costs (BTC) is defined by:

$$BTC = BOSH + EPC \tag{3.20}$$

where the balance of system hardware costs (BOSH) is defined by:

$$BOSH = (C_{Lazard}^{Inv.\&ACsystem} + C_{Lazard}^{BOS} + C_{PNNL}^{PCS} + C_{PNNL}^{BOP})/2 \tag{3.21}$$

and:

$$EPC = (C_{Lazard}^{EPC} + C_{PNNL}^{C\&C})/2 \tag{3.22}$$

Using the information summarised in table 3.4, BTC may be expressed in terms of system power P (kW) and energy E (kW h) by:

$$BTC = ((205 + 211 + 95)P + 104E + 0.51(205P + 104E + p_{DC}) + 96E \cdot FF)/2 \quad (3.23)$$

where p_{DC} is the DC module price, and FF is the footprint factor accounting for the lower volumetric energy density of a VRFB. This is set at 1 for LIB and 1.71 for VRFB based on the average of figures used by PNNL and EPRI [115, 121]. This differential is worthy of further study, given the large proportion of the installation footprint not occupied by the battery containers, as observed in large scale installations [123].

The Damato report cited by Mongird *et al.* would be an ideal resource, as it focuses on behind the meter application at the sub MW scale [122]. In principle the three instances could be used to deconvolute fixed, \$ kW^{-1} and \$ $\mathrm{kW}^{-1}\,\mathrm{h}^{-1}$ if such a structure existed, but an attempt to do so failed to yield positive values for each cost category. Judging by the PCS costs there are discontinuities between the scales, so it would be unsafe to over-interpret this data.

The available data were however used to corroborate the BTC model. A BTC cost for each of the LIB scenarios in [122] was calculated by the PNNL, Lazard and combined cost models. The results are shown in fig. 3.1[2]. As Lazard's EPC estimate is based on a fraction of total hardware, the LIB module price of \$300 $\mathrm{kW}^{-1}\,\mathrm{h}^{-1}$ from the same case study was used.

Overall, the BTC model combining the models of Lazard and PNNL gives a better agreement with the Damato estimates than either of the individual models does. For the 4 h system, the BOSH component from the Lazard model is notably higher than the other estimates.

Returning to Eckroad's cost classification [25], none of the sources cited above mention fixed upfront costs. A value snapshot published by CIBSE includes several fixed cost

[2]Note, the Damato data were reclassified as described in [115] by subtracting the \$95 kW^{-1} BOP estimate in table 3.4 from the original "Grid Integration" category and combining with PCS to give BOSH. The remainder of "Grid Integration" was combined with "Equipment Tax, fees and G&A" category to get an estimate of EPC.

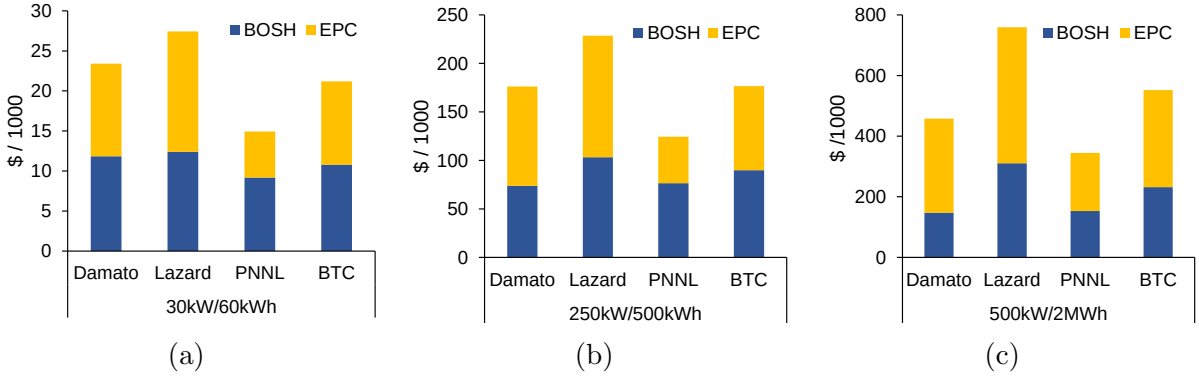

Figure 3.1: Comparison of LIB balance of system hardware (BOSH) and EPC cost estimates from PNNL model, Lazard model and the combined model applied in this work (BTC). Model estimates are compared to estimates for three particular behind-the-meter configurations made by Damato.

items associated with a 1 MW/1.8 MW h LIB installation in the UK, namely £40,000 for "Contract formation" and £45000 for "DNO network connection costs", although it is not made clear why a DNO connection would be required for a behind the meter project [124]. Fixed costs of $ 295000 for permitting are reported by NREL for a utility scale BESS co-installed with a large PV array, but the scale is not comparable with the present work, and it is not clear what proportion of the permitting would be attributable to the BESS.

Minke and Turek mention a fixed cost for PCS, but it is not clear if this is relevant to modular systems [125].

As there are no reliable data for fixed costs in the application analysed here, it has not been possible to include these in the DCF. This omission may bias the results slightly toward shorter duration systems.

3.4.7 Operation and Maintenance Costs

BESS installations will incur ongoing costs due to regular maintenance required to keep the systems operating at top performance. For data on these costs a number of publications were consulted, all published in 2019 or later.

Mongird *et al.* at PNNL applied a fixed O&M cost of $\$10\,\mathrm{kW}^{-1}$ p.a. to both LIB and VRFB systems in their comparison, based on a survey of other sources [115]. An

NREL survey of O&M costs for LIB systems gave a wider range of values, but it was acknowledged that the higher values included augmentation of the battery to counteract degradation [126]. The lower end figures given center around $\$10\,\mathrm{kW}^{-1}$, corroborating the data in [115]. Lazard apply a variable O&M cost of 0.8% of the total hardware costs in their behind the meter case study, but state that this includes augmentation [9].

A variable O&M cost of $\$0.0003\,\mathrm{kW}^{-1}\,\mathrm{h}^{-1}$ throughput is also reported by Mongird *et al.*, and is assumed to be a "catch-all for energy throughput-related costs that are not accounted for by cycle/calendar life and RTE". The variable costs reported in [126] show more variability, but average out at $\$0.0015\,\mathrm{kW}^{-1}\,\mathrm{h}^{-1}$. Assuming a single cycle per day, these cost estimates equate to $\$0.11\,\mathrm{kW}^{-1}\,\mathrm{h}^{-1}$ and $\$0.55\,\mathrm{kW}^{-1}\,\mathrm{h}^{-1}$ capacity per annum respectively, and are ignored in this analysis.

As degradation is dealt with explicitly in the revenue model, the $\$10\,\mathrm{kW}^{-1}$ figure for fixed O & M is used in all scenarios for both LIB and VRFB systems, and is incremented by 2 % each year to reflect inflation.

3.5 Conclusions

In order to address the research challenges identified in Section 2.4 it has been necessary to define a bottom up turnkey model for VRFB cost, add novel functionality to an existing model for use-case A, define use-case B, translate degradation models to both use-cases and develop a completely novel model for VRFB optimisation under variable efficiency. The role that these works played in generating the novel outcomes of this thesis is summarised graphically in Figure 1.1.

Chapter 4

The Co-optimisation of Revenue Streams Behind the Meter in the CAISO Market.

4.1 Introduction

In this chapter, the project economics of operation for VRFB and LIB systems are studied for site 281, which displays a load profile typical of the data set of commercial/industrial facilities hosted by EnerNoc [127]. An example week of load data from the summer is shown in Figure 4.1.

The site is active 7 days a week, and displays a broad load peak followed by a 6 h overnight trough. In the summer months, as shown in Figure 4.1, additional short load peaks occur during active hours, which may be due to air conditioning requirements.

The same SCE network tariff was applied as in Fisher *et al* [128], but the specific charges were updated to those in place at the time of writing [129]. The red zone peak demand charge k_3 has decreased in the interim, but the green zone charge k_1 has increased as shown in Table 4.1.

It is important to note that during winter, the red and yellow demand charge periods

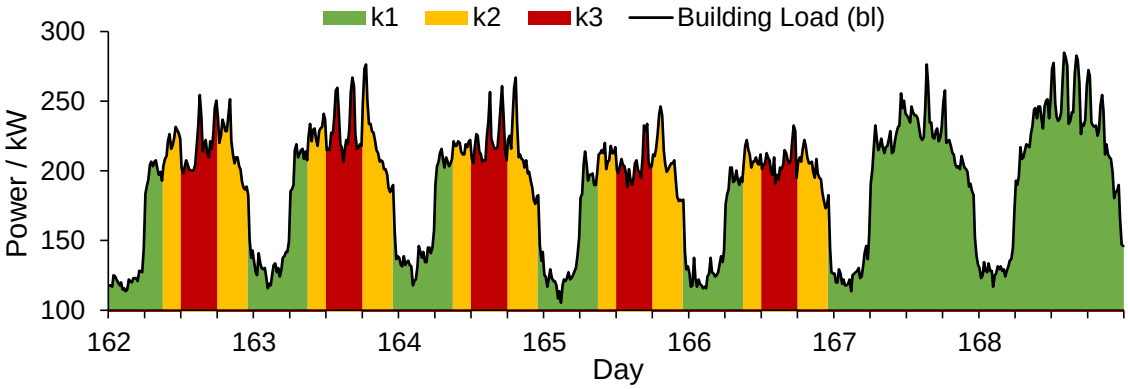

Figure 4.1: One week of load data for site 281 from June. The colours indicate the demand charge period, with k1 being the off-peak, k2 the shoulder and k3 the peak period.

Table 4.1: Retail energy charges EC (¢ $\mathrm{kW^{-1}\,h^{-1}}$) and demand charges DC (\$ $\mathrm{kW^{-1}}$) for the SCE tariff TOU8 option B in 2015 and 2019 (not corrected for inflation).

Year	EC_1	EC_2	EC_3	EC_4	EC_5	DC_{k1}	DC_{k2}	DC_{k3}
2015	6.81	8.90	6.29	8.75	14.2	15.57	22.06	38.52
2019	6.49	9.21	7.25	7.43	7.82	17.52	22.68	32.52

are not applied (see [128] for further details).

In Section 4.2.1, the modelling assumptions made in this chapter are outlined. In Section 4.3 the operation of the battery resulting from the linear programming optimisation described in Sections 4.2.2 and 4.2.3 is first examined in order to understand how the different properties of the two systems impact on revenue. The sensitivity of the model outputs to the degradation penalty and the demand charge weighting are studied in Section 4.4. In Section 4.5 the impact on revenue of the 1 h continuous energy requirement now imposed by CAISO is studied. In Section 4.6 the feasibility of performing regulation with a behind-the-meter BESS is assessed. Conclusions are drawn in Section 4.7.

4.2 Methods

The algebraic formulation for the schedule optimisation across multiple revenue streams is adapted from the work of Fisher *et al.* [10], where a linear programming approach was used to optimise the scheduling of BESS systems in a behind the meter application. In order to

focus in more detail on the battery operation the scenarios with PV were not studied. In the Fisher study, the benefits of PV was highly dependent on the export tariff assumptions and this would require an additional branch in the already large scenario tree in this work. In this section, the Fisher model is first described, followed by a series of novel extensions which improve the fidelity of the model, and allow for the enhanced degradation models defined for both VRFB and LIB in Section 3.3 to be applied post-optimisation. The regulation signal data are also updated, and a discussion made on the signal imbalance.

An additional constraint to enforce the CAISO continuous energy requirement on SOC during ancillary service bidding is also defined.

4.2.1 Model Assumptions

The DC round trip efficiency η_{DC} was set at 0.75 for the VRFB, as this appears to be achievable at high current density both at pilot scale [28] and commercially [14]. The efficiency of a VRFB is partly a design choice, involving a trade-off between area specific costs of the stack components and the additional revenue gained with higher efficiencies. This matter is revisited in Section 6.5. For the LIB system η_{DC} was set at 0.95 as in Fisher et al. For both systems, the η_{DC} values were multiplied by an inverter round trip efficiency of 0.96 giving round trip η_{AC} values of 0.72 and 0.91 for the VRFB and LIB systems respectively [115]. The SOC range was set at 0.15 to 0.95 for the LIB as in Fisher. For the VRFB the SOC range was reduced to 0.15 to 0.85, as discussed in Section 2.1.3. For the LIB, the BRC parameter which is used as a penalty to discourage the performance of low value transactions was set by default to $\$145\,\mathrm{kW}^{-1}\,\mathrm{h}^{-1}$. This is the 2030 price projection by PNNL (plus oversize to account for 0.8 SOC range) in their central scenario, hence there is an implicit assumption (borne out by the following results) that for a project starting in 2025 the LIB will not need replacing in the first 5 years [21].

Combining 2012 load data with wholesale market prices from later years as done in [10] is a potential source of inaccuracy, but unfortunately there is very little commercial/industrial load data available. A likely source of inaccuracy is mismatch between the day of week

index. For example, in summer months, the demand charge yellow and red sub-periods only occur during week days. If high AS prices also only occur on weekdays, then failing to match the indices may result in an overestimation of revenue, as the mutual exclusivity of revenue streams is not captured

In order to check for such patterns, 2019 market prices were analysed using a clustering technique reported elsewhere [130]. Clustering has the advantage of being able to detect profile shape, when compared to simple metrics such as average or maximum daily prices. Day ahead price data for June to September were analysed, as these months have the highest demand charges. The clustering in each of the AS markets are shown in Figure 4.2, and the clustering for the wholesale market is shown in Figure 4.3

The key finding of the cluster analysis is that for spinning reserve, up regulation, and locational marginal price (LMP, also referred to as wholesale price herein) there is a cluster with a high price peak (18:00 to 20:00) that is exclusively associated with week days, and is presumably caused by high early evening demand. Hence it is important to line up the indices. In this case study, this was achieved by simply starting the 2019 price data series on 30th December 2018 (a Sunday) to match the Sunday start for the 2012 load data.

In the down regulation data and the LMP data, there is also a clustering pattern that appears over a longer timescale. In both cases, the first six weeks of the summer period belong predominantly to a particular cluster. For the LMP, this cluster has a depressed midday price, whereas in the down regulation data, the midday price is increased. These patterns are likely weather related. Dealing with such patterns rigorously is outwith the scope of the present work, but would be important for the optimal operation of an installed battery.

4.2.2 Linear Programming Model Described by Fisher *et al.*

In the Fisher study, regulation was modelled as a single bidirectional service, i.e the battery must move it's setpoint by the product of the bid power and the regulation signal (-1 to

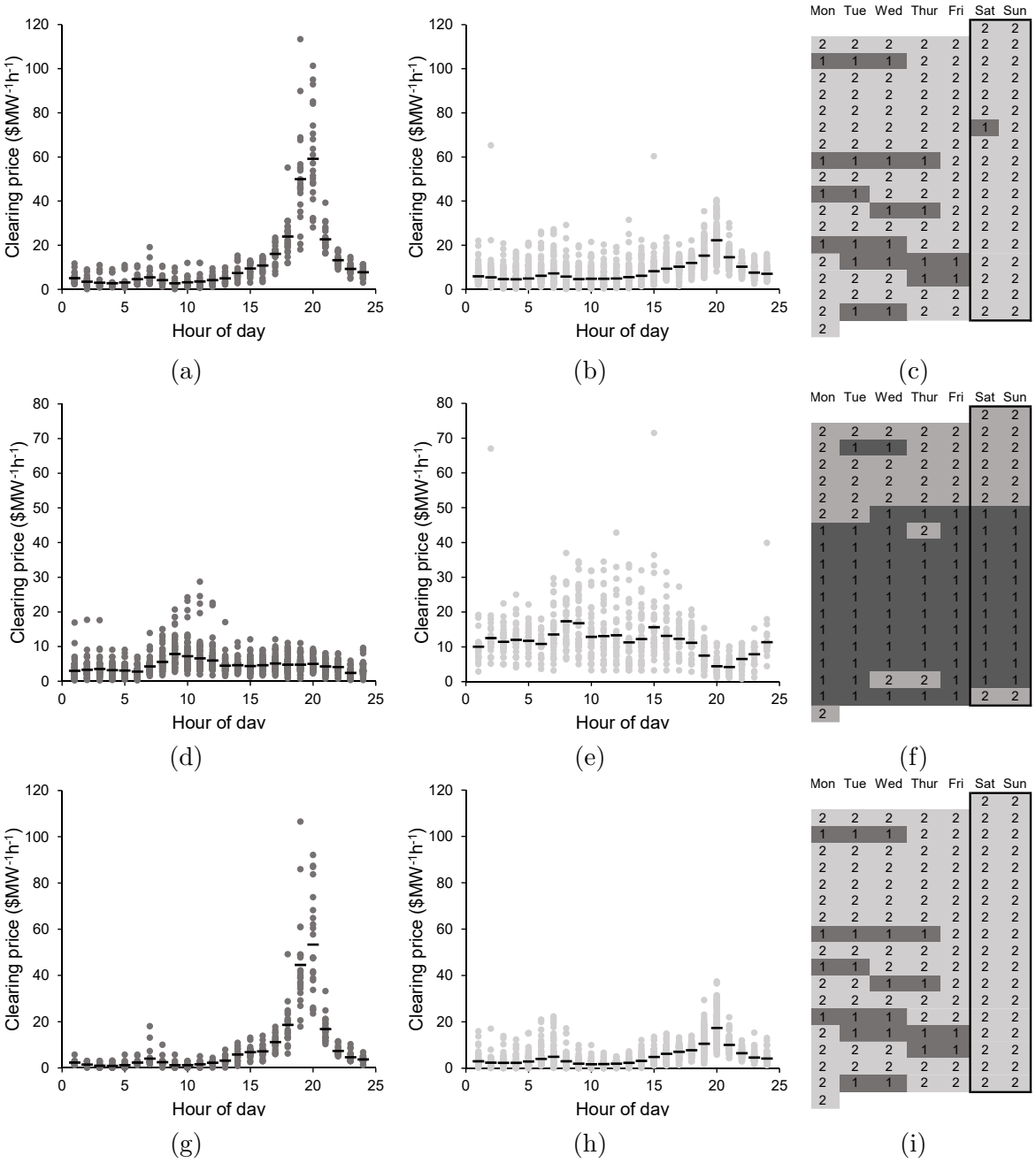

Figure 4.2: Clusters found for 2019 CAISO day ahead AS market clearing prices. (a) and (b); cluster 1 and 2 in up regulation, (d) and (e); cluster 1 and 2 in down regulation, (g) and (h): cluster 1 and 2 in spinning reserve. (c), (f) and (i) show which days in June to September 2019 fall into which clusters for the respective AS markets.

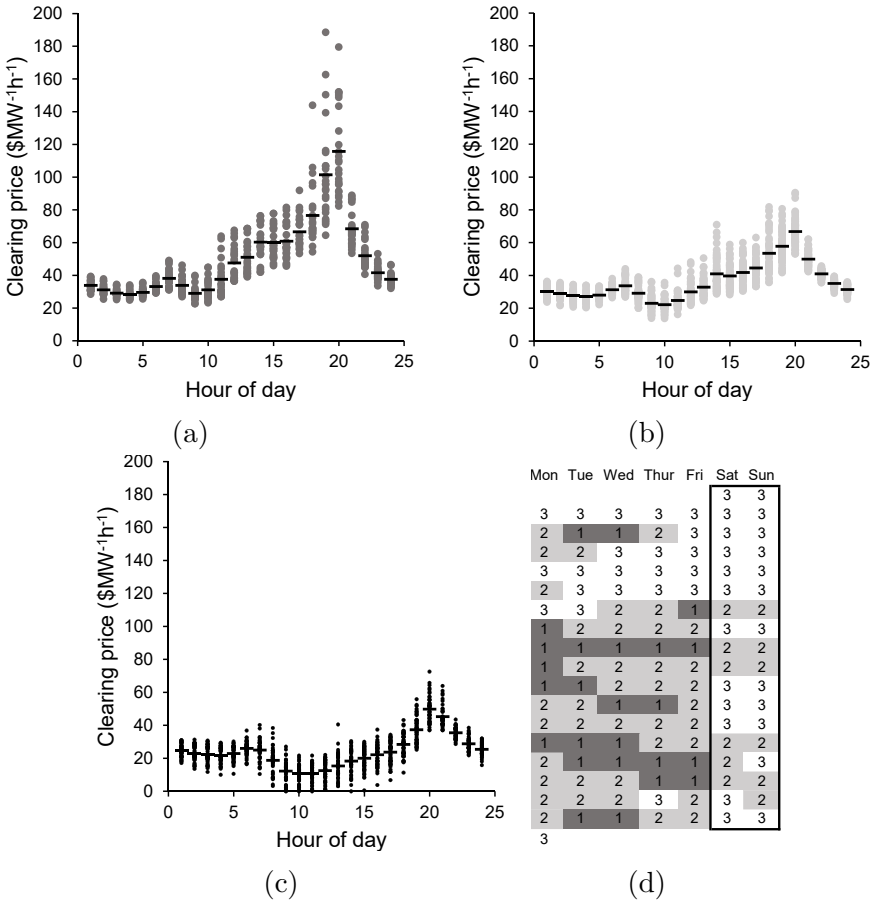

Figure 4.3: Clusters found for day ahead LMP clearing prices (a) 1, (b) 2, (c) 3. (d) shows which days in June to September fall into which clusters.

1). The cost objective was defined by:

$$minimise(\sum_{t \in T} [(LMP_t + EC_t) \cdot nl_t - REGP_t \cdot reg_t - SPINP_t \cdot spin_t]/4 + deg_t + \sum_{k \in K} DC_k \cdot pd_k) \tag{4.1}$$

Where t is a 15 min billing period within the optimisation window T, and k is a sub-set of T where a particular demand charge applies. reg_t and $spin_t$ are continuous decision variables representing, respectively, the net load at the facility, the regulation bid and the spinning reserve bid (kW). LMP_t and EC_t are the parameters wholesale and retail unit energy costs (\$ kW^{-1} h^{-1}), and $REGP_t$ and $SPINP_t$ are the parameters regulation and spinning reserve market clearing price (\$ kW^{-1} h^{-1} availability). deg_t is the degradation cost penalty term. In the final term, for each demand sub-period k, the peak demand variable pd_k (kW) is multiplied by the demand charge DC_k (\$ kW^{-1}). It should be noted that the billing for demand charge is based on a whole month, whereas the optimisation in [10] was performed over 36 h. The demand charge term is therefore a penalty term.

The dependent variable nl_t, net load is defined by:

$$nl_t = bl_t + c_t - d_t \tag{4.2}$$

Where bl_t is the exogenous variable original building load and c_t and d_t the continuous positive decision variables representing the BESS charging and discharging power setpoint.

The constraint on combined power output of the BESS, is defined by:

$$reg_t \leq \bar{P} - c_t - d_t - spin_t \tag{4.3}$$

where $\bar{P}$ is the maximum power rating of the BESS.

The set-point operation variables are constrained by:

$$0 \leq c_t, d_t \leq \bar{P} \tag{4.4}$$

In addition to the constraints on BESS power output, Fisher *et al.* also apply constraints on the energy balance. The state of charge at time t is first defined by:

$$SOC_t = SOC_{t-1} + (\sqrt{\eta} \cdot c_t - \frac{d_t}{\sqrt{\eta}} - reg_t \cdot ABSE \cdot (1 - \eta))/4 \tag{4.5}$$

where η is the round-trip energy efficiency of the BESS and $ABSE$ is the typical average energy throughput of the battery while performing regulation. In Fisher *et al.*, SOC is defined in kW h. This formulation assumes that the regulation signal averages to 0, and the SOC movement is purely discharge associated with losses. The state of charge at time t is constrained by:

$$\underline{SOC} \leq SOC_t \leq \overline{SOC} \tag{4.6}$$

Where $\overline{SOC}$ and $\underline{SOC}$ are the maximum and minimum permitted SOC values (in kW h respectively.

The authors then pose SOC head-room and foot-room constraints, defined by:

$$SOC_t + RDNE \cdot reg_t/4 \leq \overline{SOC} \tag{4.7}$$

$$SOC_t - RUNE \cdot reg_t/4 \geq \underline{SOC} \tag{4.8}$$

Where $RDNE$ and $RUNE$ are parameters representing near-worst case average regulation signal in the down and up directions over a 15 min period (kW h kW^{-1}). Fisher *et al.* set these at 0.1 and 0.2 respectively, based on the 97.5% percentile of the distribution of hourly average data taken from the PJM domain.

An auxiliary variable pd_k is next defined, representing the peak demand in each demand charge sub-period k. Under minimisation, this variable is forced to take the maximum value of the net load within k, using the constraint defined by:

$$nl_t \leq pd_k \;\; \forall t \in k \tag{4.9}$$

Lastly, Fisher *et al.* alluded to a "memory" constraint, that encodes previous peak demand information in the sliding window progression, but did not include the expression. In this work, this is interpreted as a constraint that avoids unnecessary discharge of the BESS to reduce the net load below the peak demand in the month so far. This constraint is defined by:

$$pd_k^{mth.} \leq pd_k \;\; \forall t \in k \tag{4.10}$$

Where $pd_k^{mth.}$ is the peak demand in sub-period k across all previous days of the present month. The value of this parameter is updated if necessary each time the sliding-window is progressed.

Note: in the formulation, no grid connection constraint is placed on nl_t. Charging the battery on top of a high load is disincentivised by the demand charges, so the pre-existing max import power is unlikely to be breached. Similarly, discharging the battery at times of low load is also disincentivised, so export of power is unlikely.

The cost of capacity degradation deg_t is defined by:

$$deg_t = \frac{\sqrt{\eta} \cdot c_t + \frac{d_t}{\sqrt{\eta}} + reg_t \cdot ABSE}{4 \cdot \overline{SOC}} \cdot CapDeg \cdot BRC \tag{4.11}$$

where the fractional term defines the energy throughput in cycles, $CapDeg$ the fractional capacity degradation that occurs per cycle, and BRC the expected replacement cost of the battery. $CapDeg$ is defined after Ciez and Whitacre [101] for the LIB by:

$$CapDeg = \left(\frac{SOC_{swing}}{1307.4} \right)^{0.95} \tag{4.12}$$

where SOC_{swing} is described as:

"The average depth of discharge reached by the battery in all previous months over all discharging events" but not defined mathematically.

4.2.3 Novel Extensions to Fisher Model

In the present work a number of novel additions have been made to the Fisher model in order to improve on the fidelity of the simulations. Firstly, the connection between the battery operation and degradation has been defined explicitly (it was not properly described by Fisher *et al.*). Secondly, a method has been defined for passing high resolution regulation signal through the degradation model, in order to more accurately capture the micro-cycles the BESS performs. Lastly a constraint on the SOC the BESS must carry to bid on the ancillary services market has been formulated.

4.2.3.1 Quantifying BESS Usage for Accurate Degradation Modelling

Firstly, SOC is expressed as a fractional term taking value 0 to 1. This was achieved by defining it by:

$$SOC_t = SOC_{t-1} + (\sqrt{\eta} \cdot c_t - \frac{d_t}{\sqrt{\eta}} - reg_t \cdot ABSE \cdot (1-\eta))/4C \tag{4.13}$$

where C is the working capacity of the BESS in kW h. The constraints defined by Equations (4.7) and (4.8) are similarly replaced by:

$$SOC_t + RDNE \cdot reg_t/4C \leq \overline{SOC} \tag{4.14}$$

$$SOC_t - RUNE \cdot reg_t/4C \geq \underline{SOC} \tag{4.15}$$

With $\overline{SOC}$ and $\underline{SOC}$ taking fractional values. The SOC constraint defined in Equation (4.6) was removed as it is redundant, as may be demonstrated by setting reg_t to 0.

The expression for the LIB capacity degradation cost penalty (Equation (4.11)) was redefined by:

$$deg_t = \frac{\sqrt{\eta} \cdot c_t + \frac{d_t}{\sqrt{\eta}} + reg_t \cdot ABSE}{8 \cdot C} \cdot CapDeg \cdot BRC \tag{4.16}$$

The Ciez and Whitacre form takes cycles as input, whereas the Fisher form is defined in energy throughput, and must hence be divided throughout by 2. As SOC is redefined as a fractional term, the $\overline{SOC}$ term on the denominator is replaced by C. It should be noted that Equation (4.11) would not have lead to modelling errors, it is a penalty term which the authors adjusted via the BRC parameter until the LIB would last the ten years of the project.

Secondly, for the post-optimisation calculation of degradation, the energy throughput was calculated using a rainflow counting algorithm. The rainflow counting algorithm was based on the ASTM standard method [131]. This method analyses the SOC profile of the implemented battery schedule, and breaks it down into whole cycles, where a round trip can be identified, and half cycles where only a charge or discharge occurs. For each of these events, values for SOC swing and mean SOC are returned (the latter is not called for in the Ciez and Whitacre model, but is required for the degradation model described in Section 3.3.2).

For the LIB, the absolute degradation resulting from a given schedule, in kW h of capacity, is then defined by:

$$\Delta_C = 0.2C_0 \left(0.5 \sum_{h \in H} SOC_{swing,h} CapDeg_h + \sum_{w \in W} SOC_{swing,w} CapDeg_w \right) \tag{4.17}$$

Where C_0 is the initial energy capacity of the LIB and H and W are respectively the set of half cycles and set of whole cycles performed. In this expression, SOC_{swing} represents energy throughput in cycles. For the former usage, half cycles must be divided by two to give full cycle equivalents. It is important to note that in [101] the $CapDeg$ expression was based on the number of cycles to reach a state of health of 0.8, hence a multiplier of 0.2 was incorporated to work in terms of actual capacity loss (see equation 7 in [101]).

During optimisation, the aging severity term $CapDeg$ in Equation (4.12) takes a historic average of SOC_{swing} as its input. In the present work, this is calculated as the

throughput weighted average of SOC_{swing} for all previous whole/half cycles, defined by:

$$SOC_{swing,hist} = \frac{0.5 \sum_{h \in H} SOC^2_{swing,h} + \sum_{w \in W} SOC^2_{swing,w}}{0.5 \sum_{h \in H} SOC_{swing,h} + \sum_{w \in W} SOC_{swing,w}} \tag{4.18}$$

which is a throughput weighted average (noting that SOC_{swing} serves as both a measure of depth of discharge and energy throughput in this formulation).

4.2.3.2 Accounting for Regulation Throughput in Degradation

An important component in the model applied here is the treatment of energy throughput due to regulation provision. Constant provision of frequency regulation has the potential to increase the equivalent full cycles per day above 1. In the Fisher model, energy throughput during regulation is used in the penalty term for degradation (Equation (4.11)), and also in the state of charge expression in Equation (4.5). It appears that when it comes to tracking the degradation that occurs, the authors look at the SOC profile, but they do not clarify whether the profile is at 15 min resolution or the 2 s resolution at which regulation is performed. This is a highly important distinction for the present application: at 15 min resolution, the regulation signal may be approximated as averaging to 0, hence the only effect of regulation is to slowly drain the battery via losses (Equation (4.5)). At 2 s resolution, the battery will be performing a large number of micro-cycles. Factoring this into the optimisation process is beyond the scope of the current work, as it would add considerable complexity. This is because the performance of regulation only involves cycling if the output of the battery changes sense. This is the case if only regulation is being performed, but if, say, the battery has bid 40 kW in regulation over an existing 40 kW charging setpoint, then the power output will only vary from 0 kW to −80 kW, so no cycles will be performed.

Because of this difficulty, an increased resolution treatment was restricted to the post-optimisation tracking of degradation. In order to avoid repetition of large iterative processes, the regulation signal data were smoothed to 30 s, which was found to preserve the micro cycle information, as illustrated in Figure 4.4.

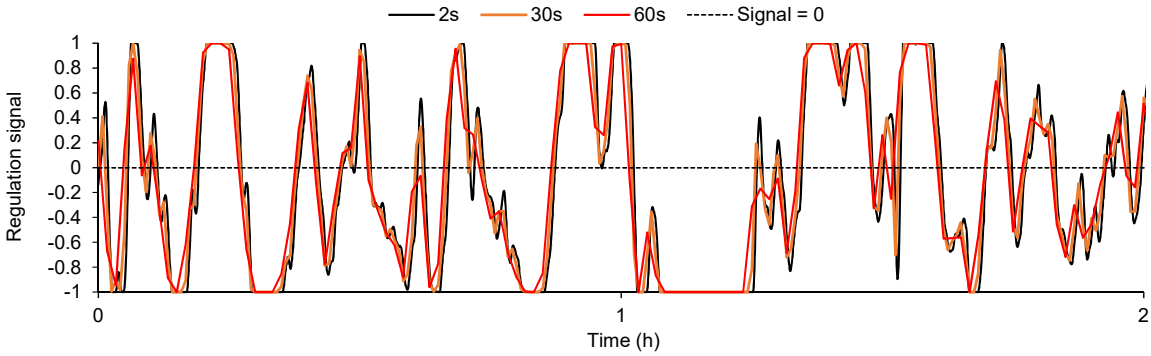

Figure 4.4: A sample of regulation signal from 11th July 2019 in raw form (2 s) and smoothed to 30 s and 60 s. The 30 s smoothing captures the movement from charge to discharge, whereas the 60 s smoothing misses some transitions.

The 30 s resolution state of charge profile taken as input for the rainflow counting algorithm is constructed as follows:

1. Construct schedule parameters c_τ, d_τ and reg_τ at the 30 s time-step by replicating the values of the variables c_t, d_t and reg_t from the optimal schedule.

2. Define the power flow at time τ by:

$$p_\tau = d_\tau - c_\tau + reg_\tau \cdot REGSIG_\tau \tag{4.19}$$

   where a positive value denotes discharging, and $REGSIG_\tau$ is the regulation signal.

3. Construct a 30 s resolution SOC profile using the conditions defined by:

$$p_\tau > 0 \implies soc_\tau = soc_{\tau-1} + \frac{p_\tau}{120\sqrt{\eta} \cdot C} \tag{4.20}$$

$$p_\tau < 0 \implies soc_\tau = soc_{\tau-1} + \frac{p_\tau \cdot \sqrt{\eta}}{120C} \tag{4.21}$$

There is some variation in the regulation signal distribution from day to day, as shown in Figure 4.5.

It may be observed that the distribution is not normal, with the signal spending a greater time at the maximum and minimum levels. It is possible that the regulation signal distribution correlates with exogenous variables such as the regulation price. However,

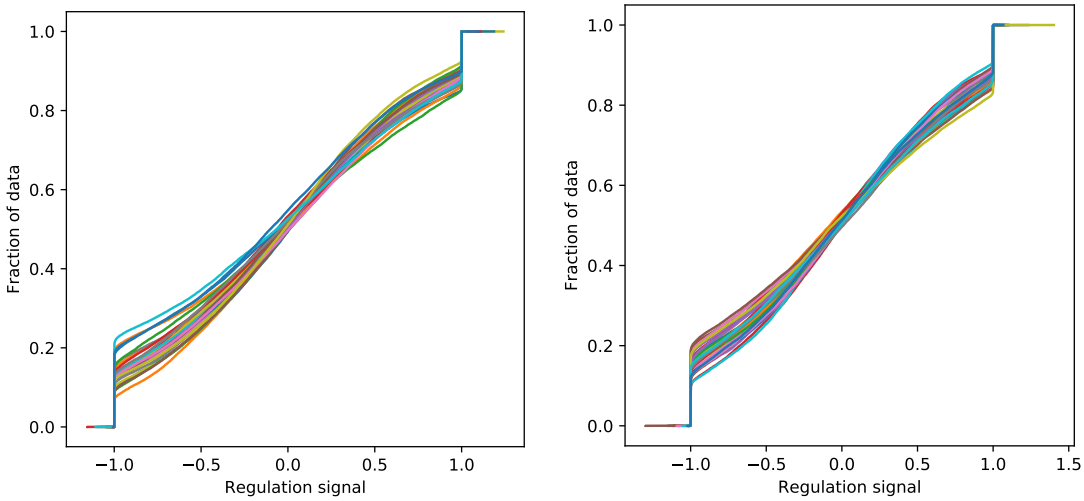

(a) (b)

Figure 4.5: Cumulative distribution plots of regulation signal data at 2 s resolution. Each line represents a day of signal. a) January 2019, b) July 2019.

because the regulation signal is drawn from the PJM domain, and the price data comes from CAISO, there is little value in trying to stitch together the time indices, and instead a random distribution is drawn from the 2019 data each day in the simulation. This is an area where the model could be improved in future.

The rainflow counting algorithm was then applied to the SOC profile resulting from the above process.

4.2.3.3 Regulation Signal Parameters

The parameters describing the regulation signal in the optimisation process were updated using 2019 dynamic regulation service data from the PJM jurisdiction, as the equivalent data is still not available for CAISO [132]. The RDNE and RUNE parameters, representing the near-worst case 15 min average in up and down direction were obtained as the 1.25 th percentile across the year of data. The distribution of 15 min averaged regulation signal data is shown in Figure 4.6:

It is assumed here that down regulation corresponds to a negative signal (as a generator would turn down its output). The distribution is slightly asymmetric, with the down regulation having a longer tail. This is reflected in the RDNE (1.25 th percentile of data)

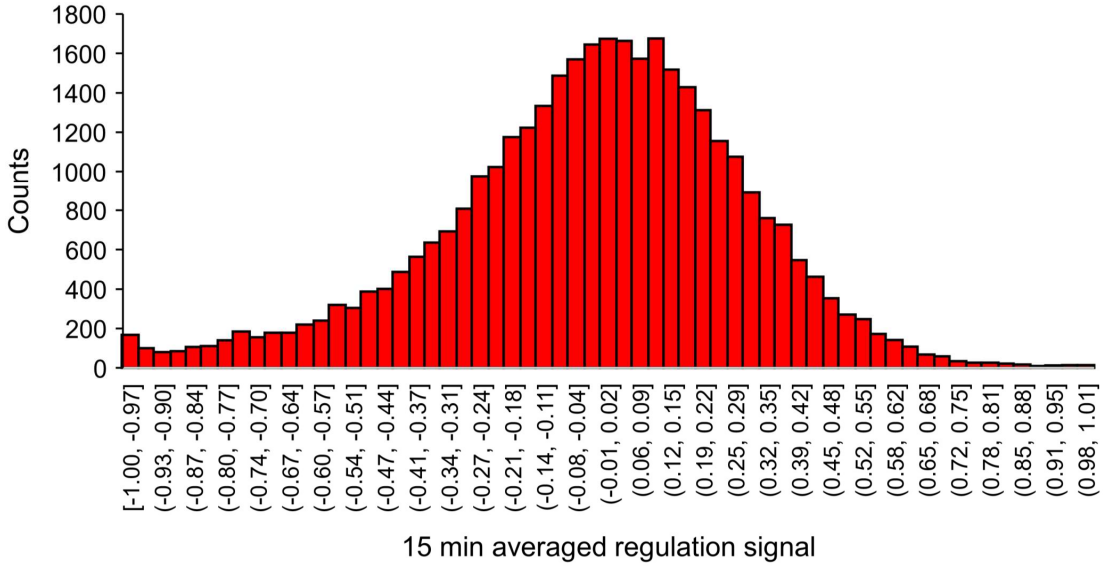

(a)

Figure 4.6: Distribution of 15 min averaged regulation signal from which RDNE and RUNE parameters are drawn.

value of 0.86 kW h kW^{-1} being considerably higher than the RUNE (98,75 th percentile of data) value of 0.63 kW h kW^{-1}. This means that the provision of regulation will be more constrained at high SOC than low SOC.

The ABSE metric, which is used in Equation (4.13) as an estimate of average energy throughput while performing regulation was obtained by taking the mean of the absolute values of the regulation signal data at 2 s resolution. For the 2019 data, the ABSE is 0.59 kW h kW^{-1} .

It is important to note that each of the above parameters have considerably larger values than were used in the work of Fisher *et al.*. For the RDNE and RUNE values, this is partly explained by the use of 60 min averaged data in the Fisher article, although this seems inappropriate given the 15 min timestep. Switching to 60 min averaging for the 2019 data used here would lower the RDNE and RUNE parameters, as shown in Table 4.2.

However, there is still a considerable difference in the RDNE and ABSE parameters between those calculated here and in the work of Fisher *et al.*, which raises the possibility that the regulation signal profile has changed between 2015 and 2019.

Table 4.2: Regulation Signal Parameters Reported by Fisher *et al.* and Those Obtained in the Present work.

Source	**time-step** (min)	**RDNE**	**RUNE**	**ABSE**
Fisher	60	0.1	0.2	0.26
This Work	60	0.40	0.22	0.59
	15	0.86	0.63	

4.2.3.4 Enforcement of the CAISO Continuous Energy Requirement

In the CAISO domain, BESS are classed as non-generator resources (NGR) [133, 134]. Such resources may bid for regulation services in two ways. In the traditional service, bidding for regulation does not preclude bidding on other markets, but there is a 60 min continuous energy requirement (which also applies to spinning reserve) [135]. In the regulation energy management (REM) service, the continuous energy requirement is only 15 min, but a bid for this service precludes bids in other markets. Fisher et al assumed that the BESS could bid into all markets with only a 15 min energy requirement, hence revenue will have been slightly overestimated. In this work, it is assumed that the BESS bids on the traditional service to be able to access all revenue streams, hence the CER constraint must be implemented. The definition of 1 h continuous dispatch is not made clear regarding regulation, as it could be 1 h of typical signal, or a worst case scenario. In this work, the same near worst case approach used to define $RDNE$ and $RUNE$, was used to define $CERD$ and $CERU$, except that the 1.25 th and 98.75 th percentiles were drawn from the distribution of regulation signal averaged to 1 h resolution. The 1 h continuous energy requirement is observed by replacing eqs. (4.14) and (4.15) with:

$$SOC_t + \frac{CERD \cdot reg_t}{C} \leq \overline{SOC} \tag{4.22}$$

$$SOC_t - \frac{(CERU \cdot reg_t + spin_t)}{C} \geq \underline{SOC} \tag{4.23}$$

Where CER is the continuous energy requirement in h.

CERD and CERU were given the values 0.40 and 0.22 from Table 4.2. Although these values are roughly half those of RDNE and RUNE, the regulation bid is more constrained

overall because the 4 in the denominator of eqs. (4.14) and (4.15) is removed. Also, $spin_t$ did not feature in the SOC headroom constraint previously, so this variable is now more constrained than before.

4.2.4 Data Sources and Processing Methods

The 2012 raw site load data downloaded from [127] were expressed in kW h per 5 min so were multiplied by 12 to obtain kW then averaged out to 15 min resolution to match the billing period. Data for day-ahead wholesale energy and ancillary service clearing prices for 2019 were downloaded from the OASIS portal [136]. The wholesale energy price was taken as the locational marginal price (LMP) at node HARBORG_7_N101, which corresponds geographically to site 767, and there is little variation between sites in the Southern California area. Ancillary service clearing prices were taken from the expanded CAISO region. In the work of Fisher *et al.*, up and down regulation clearing prices were summed to give a single series compatible with the formulation, so the same was done for the bidirectional case study. Despite day-ahead pricing being reported at 1 h resolution, bidding is at 15 min resolution, so the data were quadruplicated [137]. On the days each year where the clocks change, the data were either cropped or one hour was duplicated, so all days were 24 h long.

The same SCE network tariff for peak demand charges (DC_k) and electricity unit charges (EC) was applied as in Fisher *et al.* [128], but the specific charges were updated to those in place in 2019 [129].

4.3 The Revenue Stack

In this section, the operation of 2 h and 4 h duration VRFB and LIB systems is analysed in order to understand how the performance parameters of each system impacts on the short-term-optimal operation.

A snapshot of the optimal operation of the 2 h LIB system on the first weekday in July

is shown in Figure 4.7.

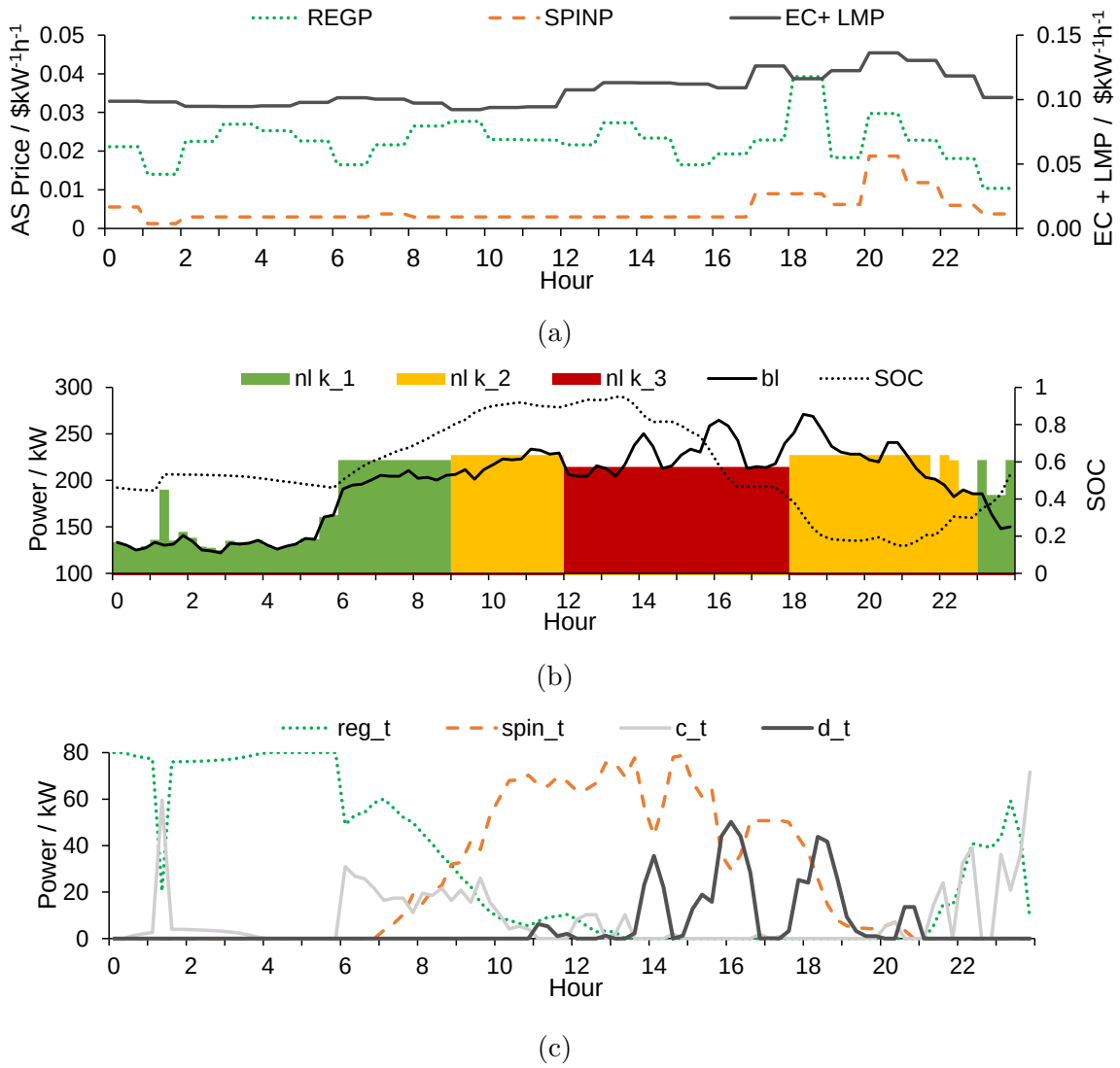

Figure 4.7: A snapshot of optimal operation of a 80 kW 2 h LIB battery. a) Price signals for 2nd July 2019. b) Original building load, net load (under each demand charge sub-period) and battery SOC. c) Portion of power capacity allocated to each service.

The price data for the AS markets, the wholesale market and the network energy charge are shown in Figure 4.7a. This is a typical summer weekday, with moderate price peaks for spinning reserve and regulation (from up service) in the early evening and a broad plateau in regulation price (from down service) from mid morning to early evening.

The SOC of the battery and the impact of operation on the facility net load are shown in Figure 4.7b. In the first six hours of the day the battery is primarily performing regulation, with a brief charge setpoint when the regulation price drops at 01:30. The SOC is maintained close to the center by offsetting regulation losses with a small charge

setpoint. This avoids the constraints associated with the $RDNE$ and $RUNE$ parameters. From 06:00 to 10:00 the battery mixes charging with regulation and spinning reserve provision according to respective price signals. From 11:00 to 21:00 the battery is primarily peak shaving, although spinning reserve bids are fit into the remaining discharge power headroom. It can be seen that the battery is performing peak shaving in both the yellow zone and the red zone, to avoid the penalties detailed in Table 4.1. Although the charge is highest in the red sub-period (k3), the battery does not discharge at full power because the derating required to further shave in the red zone would result in less benefit than saving the charge to shave in the following yellow zone (where the peak is narrower). The optimal operation includes charging the battery from 06:00 to 10:30 despite increasing the net load. This is because there was a higher net load in the green zone on the previous day (see Equation (4.10)).

In order to understand how the BESS type affects the optimal choice of revenue streams, simulations of one year of operation were performed for both battery types at 2 h and 4 h duration. The breakdown of the revenue generated and costs avoided by each system is shown in Figure 4.8.

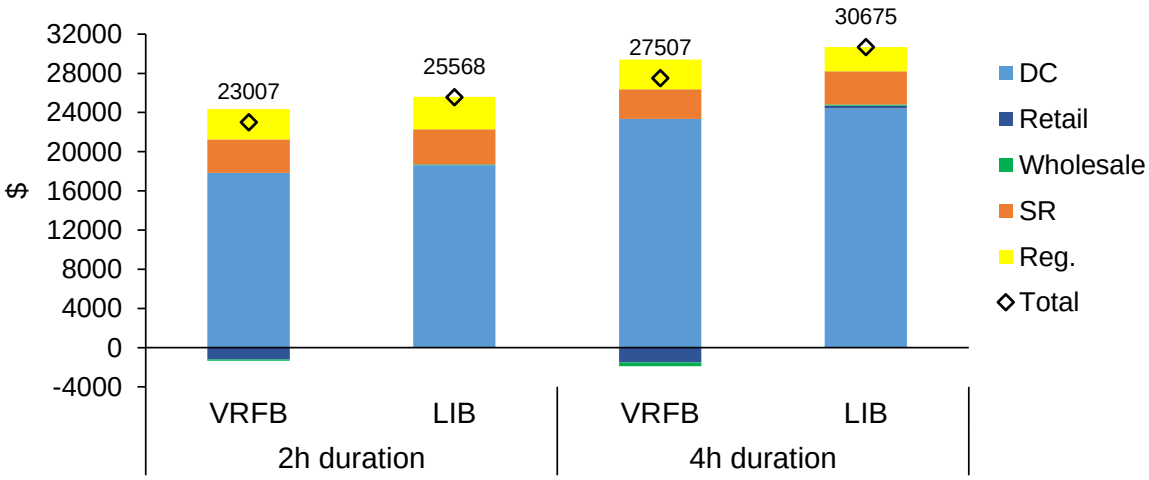

Figure 4.8: Breakdown of annual revenue for 2 h and 4 h VRFB and LIB systems at site 281. DC: demand charge avoidance, retail and wholesale unit energy price arbitrage and revenue from spinning reserve and regulation provision.

The first observation is that, as in [10] there are diminishing returns going from 2 h to

4 h duration for both battery types [10]. Doubling the duration only increases the total benefit by 20% for the both the LIB and the VRFB. The majority of the increase comes from demand charge avoidance. It can be seen in Figure 4.7 that the 2 h system is able to shave the brief sub-peaks on top of the base load profile in the red zone by approximately 50 kW, whereas the remaining load is essentially flat, so would require de-rating of the power output to reach 6 h. This is a general feature of peak shaving, as the peak is always at least as wide at the bottom as at the top. In this particular case, the benefit of the 2 h system is higher than it would be at some sites where the peak is broader.

The second observation is that for a given power and duration, the LIB system generates more revenue than the VRFB (11% more at 2 h duration and 12% more at 4 h). In terms of individual revenue streams, the VRFB has a net expenditure on energy costs, whereas the LIB system is close to break-even. This is because the round trip efficiency of the latter is considerably higher. In both cases, consideration of charging costs is subordinate to the performance of demand charge avoidance, spinning reserve and regulation.

The other differences between the revenue stack for the two battery types involve a complex trade-off between the remaining revenue streams. These are discussed further in the following section, with reference to two imperfectly posed aspects of the optimisation.

4.4 Sensitivity of Optimal BESS Operation to Degradation Penalty and Demand Charge Weighting

For demand charge avoidance, the higher efficiency of the LIB battery allows it to sustain a given power output for longer without draining the SOC, which explains why this revenue stream is larger for the LIB systems than the VRFB systems. That this benefit is partially offset at 4 h duration by a lower regulation revenue could be explained in two ways:

- The LIB system is able to perform more peak shaving, and doing so reduces the capacity available for regulation provision.

- The degradation penalty applied to the LIB system in Equation (4.11) discourages regulation provision.

In order to check the second of these explanations, the simulation was re-run with various BRC parameter values, giving the results shown in Figure 4.9.

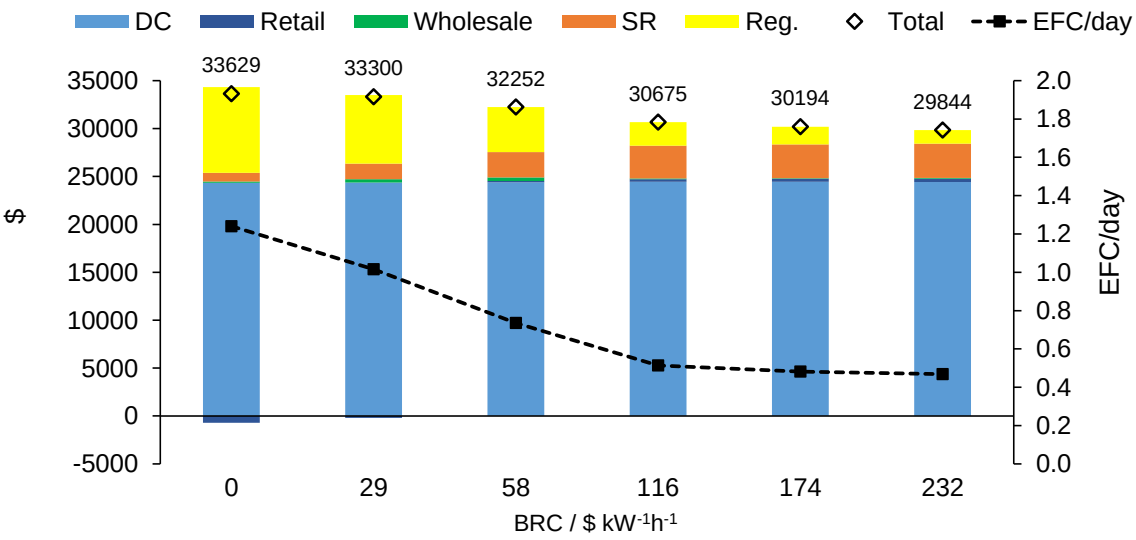

Figure 4.9: Annual breakdown of revenue stacks for a 4 h LIB system under different throughput penalties (BRC), and annual average equivalent full cycles per day.

It is clear that the degree of regulation provision is highly sensitive to the estimated battery replacement cost used in the throughput penalty term, so the second explanation above is feasible. The increase in regulation revenue when BRC is reduced is achieved at the expense of spinning reserve revenue, whereas the demand charge avoidance is constant across all cases. This again implies that the demand charge is the dominant revenue stream.

The downside of increasing regulation provision is that the energy throughput increases considerably, as will the rate of degradation. While the data in Figure 4.9 show that setting BRC at $\$58\,\mathrm{kW}^{-1}\,\mathrm{h}^{-1}$ will result in a 43% increase to equivalent full cycles compared to setting it at $\$116\,\mathrm{kW}^{-1}\,\mathrm{h}^{-1}$ for only 6% extra revenue, it is important to note that the

revenue accrues immediately, whereas the battery replacement may not occur for several years, and will hence be discounted in the cash flow analysis. This matter is dealt with in more detail in Chapter 5.

Although the provision of regulation appears to place a greater burden on the battery in this work than in previous work in the literature (see Section 4.2.3.3), it is important to note that the prices for ancillary service provision have increased since 2015. In 2015 the average clearing price for spinning reserve was $\$2.89\,\mathrm{MW}^{-1}\,\mathrm{h}^{-1}$ and the sum of the average clearing prices for up and down regulation was $\$7.81\,\mathrm{MW}^{-1}\,\mathrm{h}^{-1}$. In 2019 the respective prices were $\$6.10\,\mathrm{MW}^{-1}\,\mathrm{h}^{-1}$ and $\$21.07\,\mathrm{MW}^{-1}\,\mathrm{h}^{-1}$ [136].

In addition to the degradation penalty, there is another feature of the revenue optimisation that cannot be posed properly while maintaining a realistic optimisation window length. In the Fisher formulation (Section 4.2.2, the demand charge is applied directly in the objective function when optimising the BESS schedule for a 36 h period. This is not a faithful representation of reality, as the demand charge is applied monthly and the avoided cost not calculated until the end of the month. It is therefore possible that the demand charge avoidance is being over-weighted in the determination of the optimal schedule. As it is not realistic to optimise the schedule one month at a time due to forecasting issues, the demand charge is effectively a penalty term, and as such a sensitivity study should be carried out on it, as has been done above for the degradation penalty parameter BRC. To this end, one year simulations for both systems at 4 h duration were repeated with a weighting factor DCF applied to reduce the demand charge in Equation (4.1). The resultant changes to the revenue in the first year for the VRFB and LIB systems are shown in Figure 4.10.

The results show that across both the battery systems the maximum revenue is obtained when the demand charge coefficient is set at 0.0625. Up to 0.0625, reducing DCF increases the regulation revenue (partly offset by reduced spinning reserve revenue) with little impact on demand charge avoidance. Below DCF of 0.0625, the demand charge avoidance starts to fall off sharply for both BESS types. The increase to revenue is slightly greater for the LIB system, but there is also an increase to the number of equivalent full cycles per

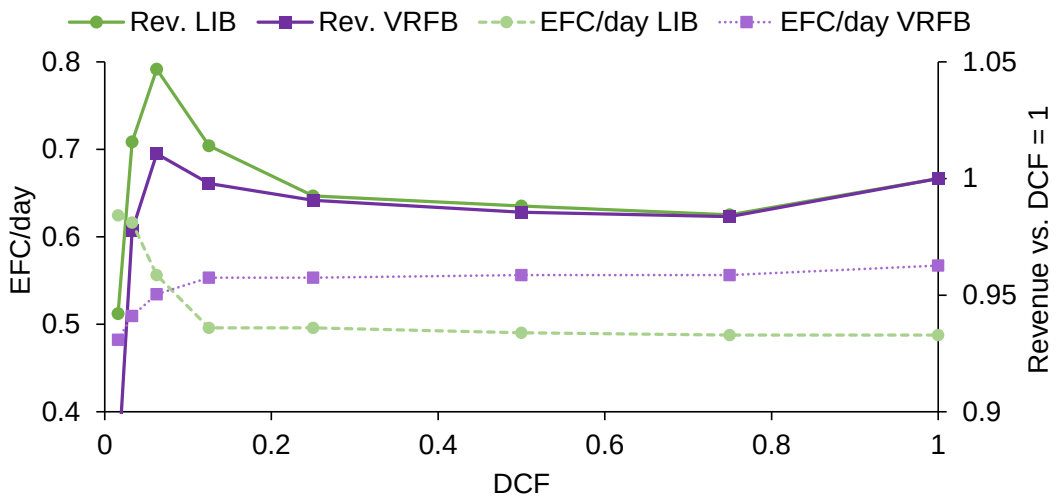

Figure 4.10: The dependence of revenue and daily energy throughput on the weighting (DCF) of the demand charge penalty function in the objective function (4 h duration BESS).

day, which will accelerate degradation. At the lowest values of DCF the VRFB exhibits a decreasing cycle rate, as peak shaving is discouraged and incremental regulation is not profitable due to the lower round trip efficiency, pushing the balance toward spinning reserve. This is clearly an area where care would have to be taken in performing an unsupervised operation. As the impact on the LIB is greater, and similar to that of the throughput penalty shown above, it will suffice to study the latter parameter further in Chapter 5. For the rest of this chapter, DCF is left at 1.

4.5 The Impact of the CAISO Continuous Energy Requirement

CAISO now applies a restriction on BESS that participate in multiple markets, such that any bid for ancillary services must be sustainable for 1 h [135]. This potentially reduces the revenue available, and might be expected to penalise shorter duration systems more. In order to test the impact of this continuous energy requirement (CER), the one year simulations for 2 h and 4 h systems were repeated following application of the additional constraint in Equations (4.22) and (4.23). The results are shown in Figure 4.11.

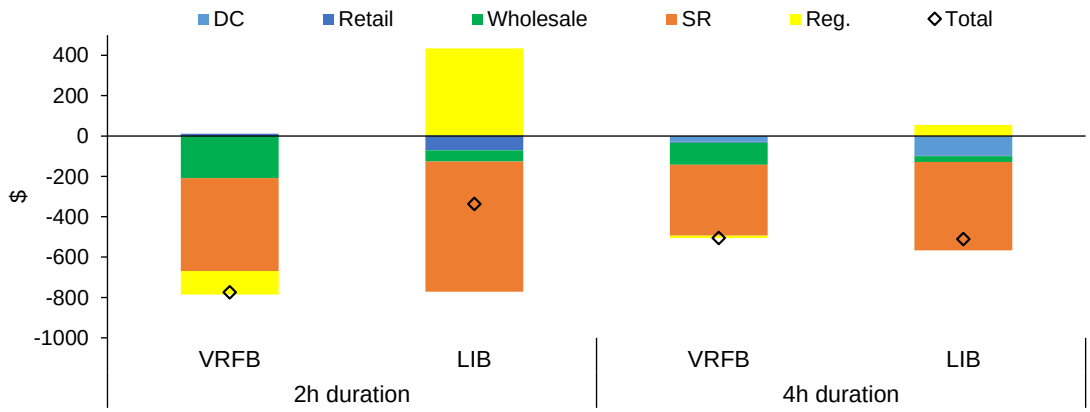

Figure 4.11: The change to the revenue stacks of 2 h and 4 h VRFB and LIB systems across one year, due to the 1 h continuous energy requirement that applies when bidding on multiple markets in the CAISO domain.

Overall the effect of the CER is modest, with a reduction in benefit of 3.4% and 1.3% for the VRFB and 1.8% and 1.7% for the LIB system at 2 h and 4 h respectively. The impact is largest for the 2 h VRFB as it has the lowest effective duration due to its lower efficiency. The greatest impact is seen in the spinning reserve stream, which was not previously subject to an energy constraint. At 2 h, the reduction in this stream is offset by an increase in regulation revenue for the LIB system, but not for the VRFB.

The CER is an important parameter, and if it is increased in the future then it will have an even greater impact on the project economics. The CER constraint is imposed from here onward for all case studies involving ancillary services.

4.6 Managing Risk Caused by Regulation Dispatch Uncertainty

It has been assumed so far that the regulation signal averages to zero, and hence the only impact on SOC from providing regulation would be a steady decrease due to the

round trip efficiency loss while performing micro-cycles. In order to avoid failing to honour the regulation provision, an additional SOC headroom cap has been applied via Equations (4.14) and (4.15), based on the near worst case net travel in a 15 min period, after [10]. However, given that regulation may in practice be performed for multiple consecutive periods, and that the signal is unpredictable, a risk exists that the SOC limit will be reached while trying to perform the service bid for the day ahead.

The first step was to look at how the signal varies with time at various time resolution settings, as shown in Figure 4.12:

It is clear that the signal is unbalanced over time periods that are considerably longer than the 15 min bidding window, and that these primarily occur in the down direction (charging). Even at a one year timescale, the average value of the signal is -0.023. There is no clear pattern to the variability. This is problematic for scheduling one day at a time, as the optimisation model makes no allowance for SOC travel due to signal imbalance, only a steady draining due to round trip efficiency.

Several previous studies have focused on regulation reliability. Campbell and Bradley reported on the reliability of distributed energy storage systems providing regulation, and introduced some terms which are helpful in the present analysis [138]. They defined $NZET$, the net zero energy time, as the minimum time over which the regulation signal will typically average to zero. They then showed that as this parameter increases, the storage duration required to reliably provide regulation also increases. As PJM signal data are being used in this work due to an absence of equivalent data for the CAISO region, it is useful to note that Campbell and Bradley reported $NZET$ values for 24 h samples of regulation data from CAISO and PJM of 8.25 h and >22 h respectively. This implies that the sustained imbalance problem is also relevant for CAISO. Based on the cited sample data, the problem may be less severe in CAISO, but it is difficult to tell based on such a small sample, given the inter-day variability shown in Figure 4.12d. In this section the possible consequences of the regulation signal imbalance on the ability to access the multiple revenue streams modelled above are analysed.

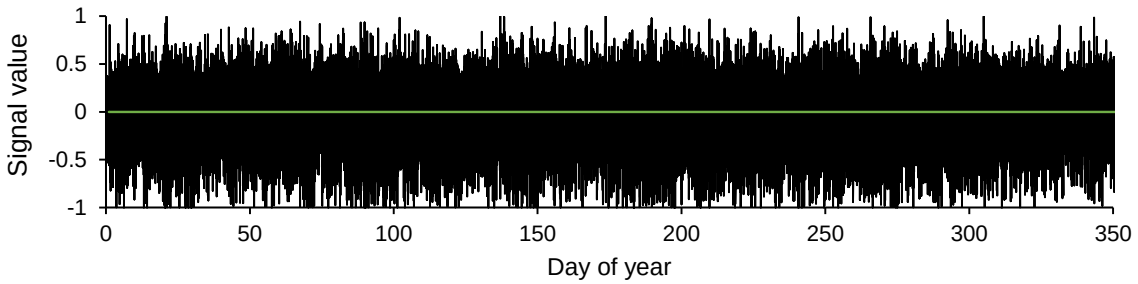

(a)

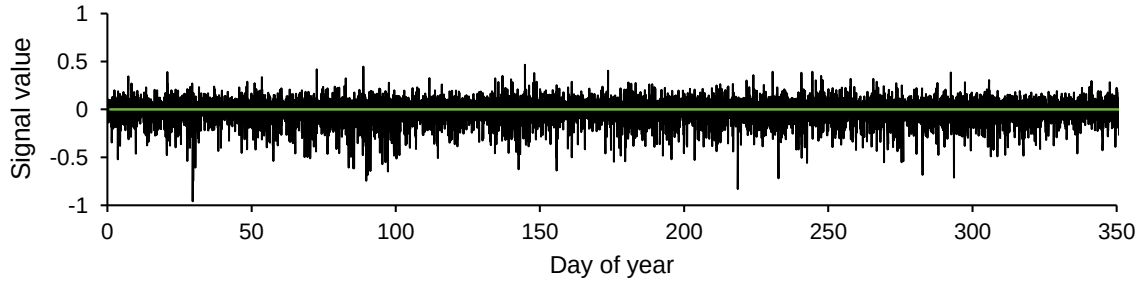

(b)

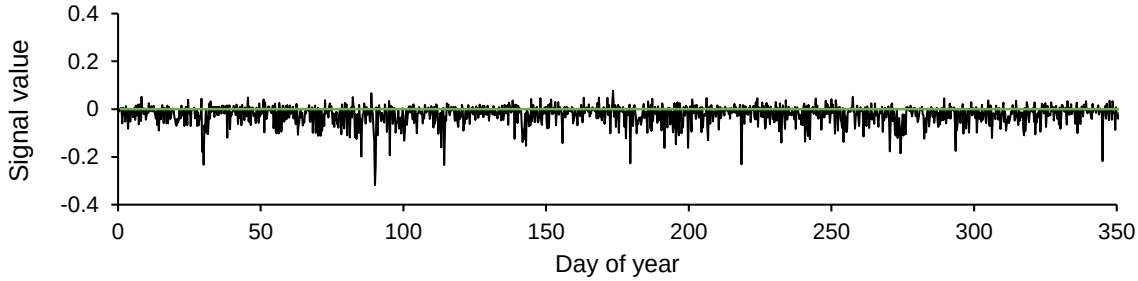

(c)

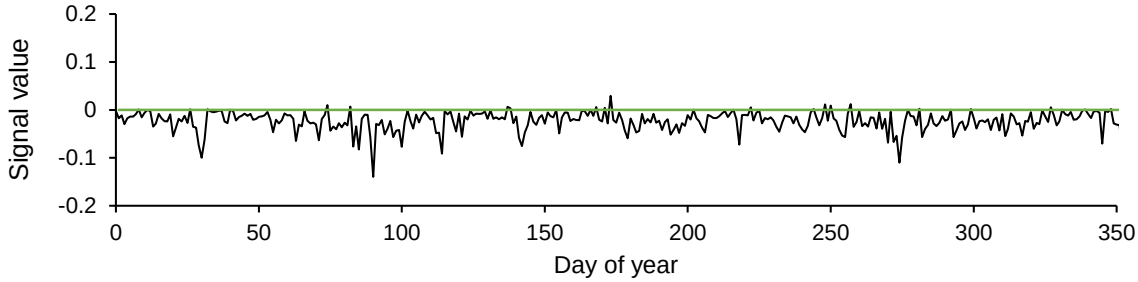

(d)

Figure 4.12: 2019 PJM RegD signal data averaged across increasingly large time periods. a) 15 min, b) 1 h, c) 6 h, d) 24 h.

4.6.1 Risk of Ejection from the Regulation Market

In CAISO there are two economic consequences to non-compliance in regulation provision. Firstly the performance component of the regulation payment (mileage) is multiplied by an accuracy metric, capturing how well the BESS output tracks the regulation signal [139]. However, the mileage payment is currently a much smaller revenue stream than the availability payment, and hence is not considered here. Secondly, there is also a threshold accuracy level below which the participant may be ejected from the market, which is set at 25% across a month, based on the accuracy in each 15 min period, weighted by the instructed mileage (i.e. the mileage performed if the signal is followed perfectly in that period) [134].

In this work, to calculate the accuracy metric after [140], the dispatch operating target (DOT), the set-point used as a baseline from which movement due to regulation is measured, is first defined for every 30 s period τ in the 15 min period t by:

$$DOT_\tau = d_t - c_t \tag{4.24}$$

The instructed movement for regulation (AGC control point) is next defined by:

$$AGC_\tau = reg_\tau \cdot REGSIG_\tau \tag{4.25}$$

Where $REGSIG_\tau$ is the regulation signal, lying between -1 and 1. The actual power output of the BESS is defined by:

$$P_\tau^{actual} = \begin{cases} DOT_\tau + AGC_\tau, & \text{if } DOT_\tau + AGC_\tau > 0 \text{ and } SOC_\tau > \underline{SOC} \\ & \text{or } DOT_\tau + AGC_\tau < 0 \text{ and } SOC_\tau < \overline{SOC} \\ 0, & \text{otherwise} \end{cases} \tag{4.26}$$

and the deviation from the instruction is defined by:

$$deviation_\tau = \left| DOT_\tau + AGC_\tau - P_\tau^{actual} \right| \tag{4.27}$$

The accuracy of regulation provision in the up and down services in a 15 min period are then defined by:

$$accuracy_t^{up} = \frac{\sum_\tau (AGC_\tau - deviation_\tau)}{\sum_\tau AGC_\tau} \tag{4.28}$$

and:

$$accuracy_t^{down} = \frac{\sum_\tau (AGC_\tau + deviation_\tau)}{\sum_\tau AGC_\tau} \tag{4.29}$$

Where AGC_t is negative for down regulation. In the case where $\sum_\tau AGC_t$ happens to be 0, the divide-by-zero error is dealt with by setting the accuracy to 0, as the mileage will also be 0, hence the value is moot in the weighting calculation.

With the CAISO definition of accuracy as just defined, performing regulation over a non-zero DOT may lead to a severe deviation if SOC hits the upper or lower bound. This is because when the SOC limit is hit, P_τ^{actual} falls to zero in the relevant direction and hence $deviation_\tau$ may be larger than AGC_τ, giving a negative accuracy number.

The consequences of such a violation are demonstrated in Figure 4.13, where it can be seen that due to SOC exhaustion while performing regulation over a charge setpoint, the deviation is larger than the target, which would give a negative accuracy value via Equation (4.29).

The mileage weighted accuracy calculation was performed following the schedule optimisation of both LIB and VRFB systems at 2 h and 4 h durations. Instructed mileage is defined as the total movement in the AGC control point (MW) during the 15 min period. For example if the AGC control point moved monotonically from + 50 MW to + 90 MW then back to + 50 MW, then an instructed mileage of 80 MW would be recorded. This means that greater weighting is given to measured performance in periods when the power output/input is changed more, and the bid is larger.

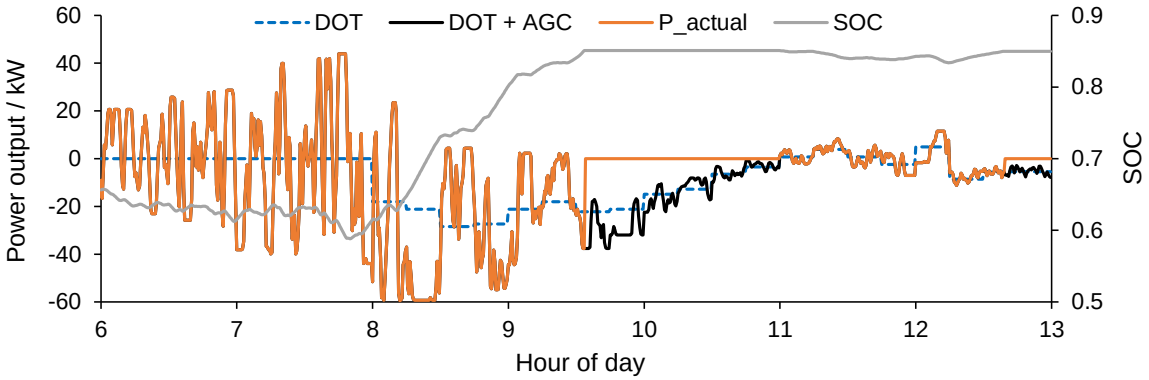

Figure 4.13: Example of a simulated regulation provision failure occurring at approx 09:30 due to maximum SOC being reached (2 h VRFB).

Monthly accuracy was calculated across one year using random samples of regulation signal from the PJM data and repeating the simulation to capture variability.The following assumptions were made:

- The battery follows the signal perfectly unless a SOC limit is reached.
- The SOC of the battery is re-balanced to the previously determined optimal value at the end of each day.

Simulated monthly accuracy data for 2 h and 4 h systems are shown in Figure 4.14.

The most important observation from Figure 4.14 is that although deviations do occur, even the shorter duration systems remain well above the 25% accuracy threshold. The benefit of longer duration is demonstrated, with improved accuracy for both battery types. The poorer accuracy of the VRFB, although not prohibitive in the present case study, merits investigation to aid general understanding. Across the year, the average regulation bid is 7.0 kW for the VRFB and 7.1 kW for the LIB system at 2 h. This, along with the similar regulation revenue seen in Figure 4.8 would imply that the two systems are performing regulation similarly.

In order to locate the source of the difference in accuracy, the schedule data for April were analysed at 15 min resolution, as plotted in Figure 4.15.

The LIB regulation bidding is more tightly concentrated in hours 8 to 20, which is when the price is highest, but also when peak shaving is typically performed. The VRFB

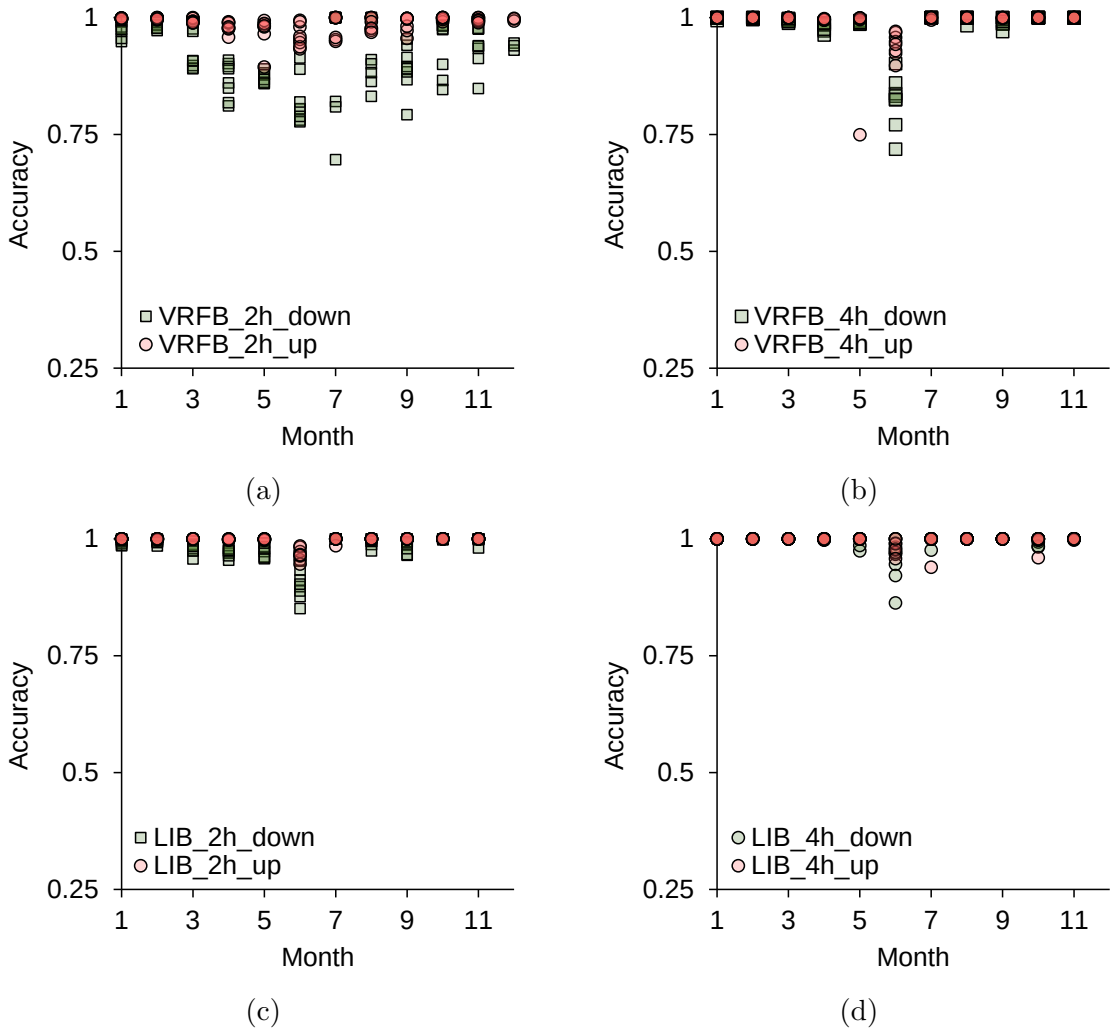

Figure 4.14: Monthly regulation accuracy turnout simulations (8 runs with random regulation signal data samples) for one year. (a) 80 kW/2 h VRFB, b) 80 kW /4 h VRFB, c) 80 kW/2 h LIB, d) 80 kW/4 h LIB.

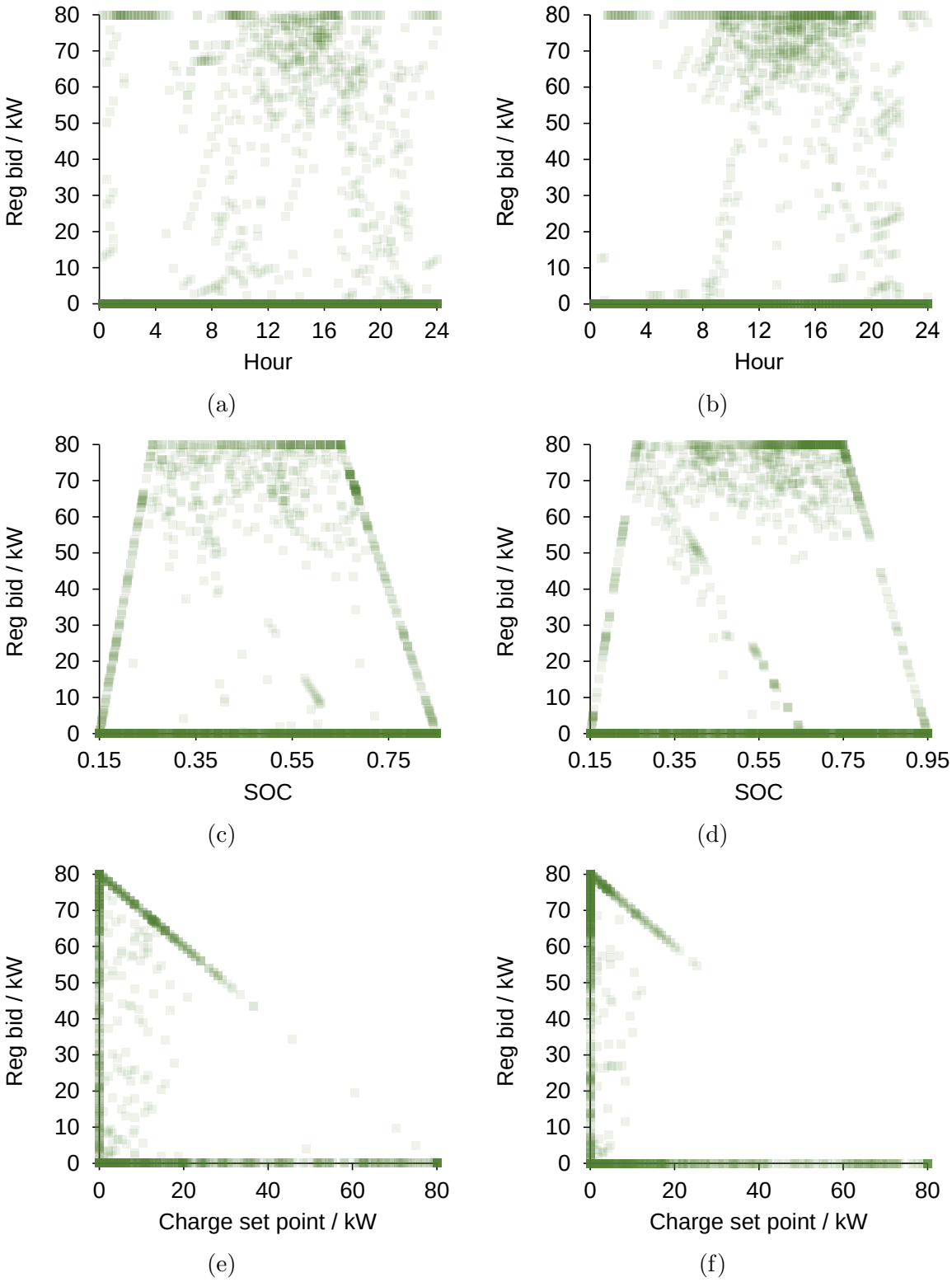

Figure 4.15: Correlations in April between regulation bid and: hour of day for (a) VRFB, b) LIB, modelled state of charge for (c) VRFB, d) LIB, and charge setpoint for e) VRFB f) LIB. (System ratings: 80 kW/2 h)

is not able to make as many bids in this window, as it is more constrained by energy limitations, both the shorter effective duration, and the greater modeled SOC drain from cycling. This means that more time must be allocated to charging in order to support peak shaving. On the other hand, it is able to make money outside of this period, as it does not have a minimum price set by degradation cost. The regulation vs. SOC plots show that the LIB is providing more regulation at higher SOC [1], which is riskier due to the down signal bias, hence it is unlikely that this is the cause of the poorer accuracy of the VRFB. Lastly, Figures 4.15e and 4.15f show that the average charge setpoint over which regulation is bid is clearly higher for the VRFB. Given the preceding illustration of the risk of this manoeuvre, this is the most likely explanation of the worse accuracy observed for the VRFB. In summary, the LIB will hit the upper SOC bound more often, but the consequences will not be as severe according to the CAISO accuracy definition.

It is possible that other frequency regulation services in other networks have stricter accuracy bounds, and hence additional measures may be required to ensure compliance. These might involve reserving power headroom in the period following a regulation bid so that either the regulation bid, or the DOT could be modified with a trade on the intra-day market. In principle, this should favour longer duration projects as the re-balancing could be delayed to hours outside of the regulation price peaks, hence avoiding de-rating. However, this benefit is irrelevant in the present case study. An approach that could reduce the severity of deviations from the AGC set point would be to make charging and regulation bidding mutually exclusive by employing a big M constraint of the type used later in Chapter 6.

A secondary issue is that any drift in SOC must be corrected at the end of each window, so as not to cause cumulative problems. It is anticipated that this could be done easily in physical terms as there is a slack period at night, but depending on the jurisdiction, there may be a small financial impact associated with trading.

[1] Note: this is the SOC anticipated by the optimisation model, not the turnout

4.6.2 Risk to Peak Demand Charge Avoidance

The regulation signal also poses a risk to demand charge avoidance. So far, the contribution of the regulation power output to the net load has been assumed to be 0. However, as shown in Figure 4.6 the dispatch often averages out to at least 50% of the bid power, especially in the down direction. Due to the nature of the billing, there only has to be one such event per month to cause a problem. In order to study this, the optimal DOT profile (15 min resolution) was combined with a random 24 h sample of regulation signal averaged to 15 min. In a one year test run, for a 2 h LIB system, the coincidence of high down regulation energy events with high load reduced the demand charge avoidance benefit from \$17415 to \$8851. This loss greatly outweighs the benefit of regulation provision, which was \$2411.

It is clear that in practice making assumptions about the average regulation signal behaviour will create unacceptable risk, and that additional controls on the power output of the battery are required. Such control may be achieved easily in the deterministic optimisation by redefining the peak demand (previously defined by Equation (4.9)) by:

$$nl_t + reg_t \cdot RRF \leq pd_k \quad \forall t \in k \tag{4.30}$$

Where RRF (regulation restriction factor) is a continuous variable that takes a value from 0 to 1 and allows the trade off between regulation revenue and demand charge avoidance to be probed. For the LIB 2 h battery, the one year simulation was run at RRF increments of 0.2, and repeated five times in order to capture the variability. The results are shown in Figure 4.16.

Failing to account for the contribution of regulation provision to the 15 min averaged net demand leads to a reduction in peak demand charge avoidance which is considerably greater than the regulation revenue. The need to set the RRF parameter at 0.6 or greater is seen for both 2 h and 4 h duration BESS, despite the battery being active in peak demand management for a smaller fraction of the time in the former. In both cases the

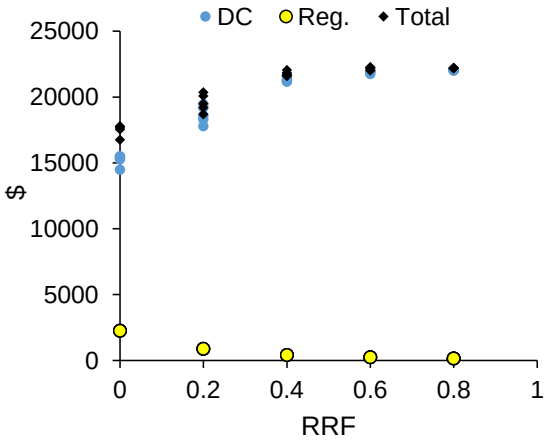

Figure 4.16: The trade-off between annual regulation revenue and demand charge avoidance, as determined by the regulation restriction factor, for a 80 kW/2 h LIB

regulation revenue is close to zero.

Applying a restriction to regulation provision all year round may not be the most appropriate approach however. As can be seen in Figure 4.17 the contribution of regulation to the revenue stack varies greatly from month to month. For example, in the months June-August, where peak charge avoidance is highest, there is already very little regulation revenue.

However, even if the higher regulation revenue seen from March to May was consistent from year to year, relaxing RRF to less than 1 in these months would still result in a net decrease in revenue as demand charge avoidance becomes negative, as shown in Figure 4.18

It is important to note that the degree of conflict between regulation provision and demand charge avoidance will vary with the load profile. As can be seen in Figure 4.7b, the time period in which peak demand is being managed by the battery (the flat region in the net load series) stretches from 06:00 to 22:00, completely overlapping with the times in which higher regulation prices are found in Figure 4.2.

Given separate regulation services may be bid for in the CAISO region, one seemingly attractive option is to bid solely for the up regulation service. However, the risk is essentially the same - if an up regulation bid is made, and the dispatched energy is lower than the averaged value used in the optimisation, then the actual demand will be higher

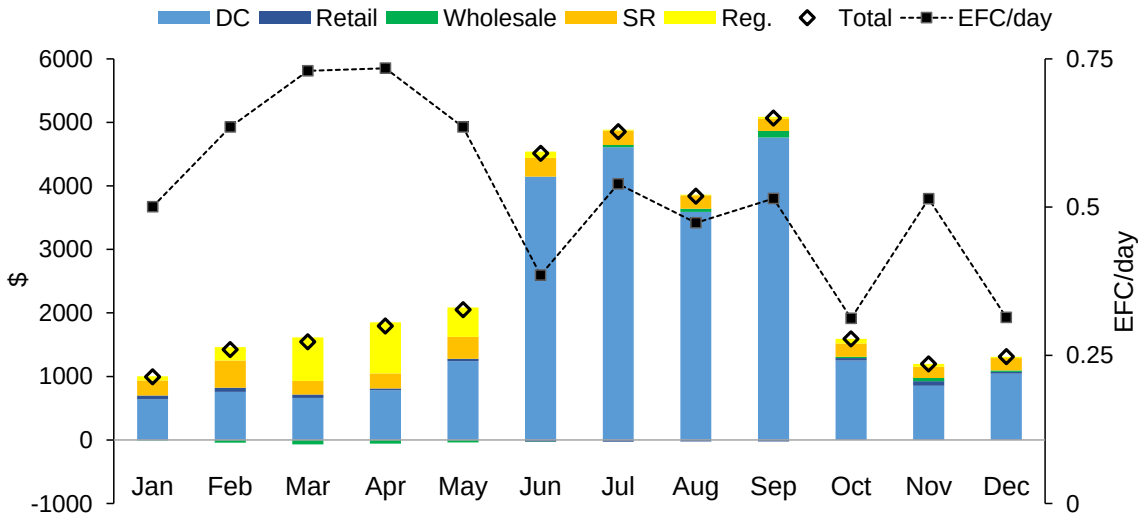

Figure 4.17: Monthly breakdown of revenue and cycle rate for a 80 kW/4 h duration LIB system with RRF set to 0.

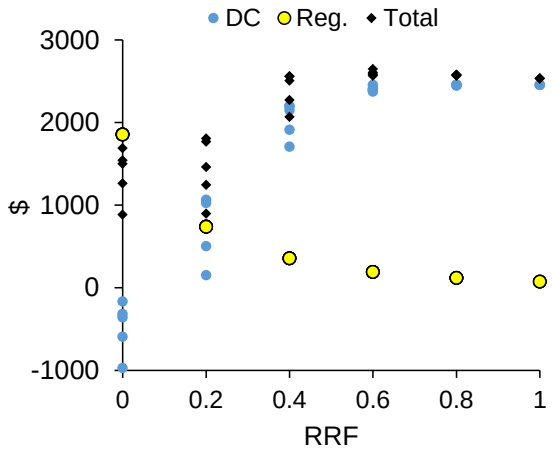

Figure 4.18: The trade-off between regulation revenue and demand charge avoidance from March to May for a 80 kW 2 h duration LIB.

than accounted for.

The above results plainly show that peak demand charge avoidance and regulation are not easily "stackable', and that for some load profiles, it will barely be worth trying to access this revenue stream. Additional problems may be encountered when attempting to aggregate multiple behind-the-meter BESS to form a single bid on the regulation market, as the individual load profiles will not be the same. The same issues are not raised when bidding for spinning reserve, as there is no scenario in which providing this service can increase the site load.

4.7 Conclusions

In this section, the maximum possible revenue obtainable by LIB and VRFB systems participating in the CAISO market from behind the meter at a commercial/industrail site has been estimated for 2019 price data using deterministic optimisation with the assumption of perfect forecasting. The following conclusions have been drawn:

- Looking at the revenue stacks for the LIB and VRFB systems, it is clear that an LIB system generates more revenue for a given nameplate installation. This is due primarily to the higher round trip efficiency of the LIB system, which allows more profitable provision of regulation, reduces the cost of charging and also gives a greater effective duration, allowing deeper peak shaving. It is therefore clear that efficiency is important for this application, and that this is an area where the assumed properties of the VRFB are a disadvantage.

- There are two features of the optimisation which cannot be posed accurately while maintaining a realistic optimisation window, and hence require sensitivity studies on the penalty terms. Reducing the penalty term for LIB degradation increases regulation revenue considerably, but leads to reduced spinning reserve revenue, and increased cycling. The demand charge penalty may also be varied, and reducing it leads to a slightly increased regulation revenue without compromising demand

charge avoidance.

- Two potential risks associated with providing regulation while performing other tasks have been studied. The first risk, that reaching SOC constraints may lead to penalisation for failure to follow the regulation dispatch signal was found to be small; deviations from the regulation signal when scheduling at the day-ahead do occur due to the upper SOC limit being reached, but the definition of accuracy by CAISO is sufficiently lenient for this not to matter.

  The second risk, that imbalance of the regulation signal at the 15 min timescale interferes with demand charge avoidance, was found to be very problematic. In fact, the loss in the latter service was considerably greater than the benefit of the former, even in the spring months where the regulation revenue is highest and demand charges lowest. In an attempt to manage this risk, the peak charge constraint was modified, and a sensitivity study performed on the de-rating of the regulation bid within the new constraint. The optimal solution was to set this parameter such that the regulation revenue is practically zero. It is important to note that these difficulties are somewhat site dependent. For site 281, the load peak is broad and overlaps with the periods in which regulation prices are highest.

- Going forward, the site 281 case study will be considered without regulation, as this service does not provide a meaningful contribution to the revenue stream once the risks are accounted for.

Chapter 5

Comparing the NPV of LIB and VRFB Projects at Site 281 using State of the Art Degradation Models.

5.1 Introduction

In this chapter, the project economics of behind the meter installations at site 281 are assessed, taking into account degradation using recently published models for both VRFB and LIB systems as described in Section 3.3. In Section 5.2.1 the assumptions behind the modelling work in this chapter are detailed. In Section 5.3, turnkey system prices output from the model described in Section 3.4.6 are compared for both BESS types at various durations. In Section 5.4, the impact of degradation is studied for each technology, and an optimal capacity maintenance strategy is chosen. In Section 5.5, the NPV for each technology at various durations are first reported, then the impact of the resource adequacy payment for capacity is studied. Lastly, a sensitivity study is performed on the relative economics of VRFB and LIB projects both with and without the spinning reserve revenue stream.

5.2 Methods

In this chapter, the revenue optimisation methods defined in Section 4.2 were combined with the bottom up cost models defined in Section 3.4 and the degradation models defined in Section 3.3 in order to simulate the project economics for use-case A. The model assumptions specific to this chapter are given in the following section.

5.2.1 Model Assumptions

In this section, the revenue due to optimised operation is combined with the system cost in order to establish the NPV of VRFB and LIB projects at a range of durations.

A key finding of the previous chapter was that the ability to provide regulation alongside peak shaving is dependent on the load profile at the site where the BESS is placed. For site 281, it is not deemed worthwhile to bid for regulation, as this results in loss of demand charge avoidance, hence for this case study the regulation bid is constrained to 0 at all times.

Projects are assumed to commence in 2025, which informs the modelling of DC module prices for both systems. The project life is set at ten years, as this is the typical lifetime of an inverter and hence a natural decision point on whether to invest in life extension. In cases where the LIB DC module reaches the end of its life before this point, the DC modules are replaced at the predicted price for that year (see Section 3.4.5), and the capacity is reset in the model. In the work of Fisher *et al.* [10], the degradation penalty term was increased until the battery lasted to the end of the project. However, this may not be the optimal strategy, as it involves delaying revenue. In the present work, where multiple durations are analysed this approach would also be too time consuming. Therefore any remaining value in the battery is assumed to be recovered at the $\$\,\mathrm{kW^{-1}\,h^{-1}}$ price in year ten (see Section 3.4.5).

For the VRFB it is assumed that the value of the electrolyte is recovered at the present price of $\$142\,\mathrm{kW^{-1}\,h^{-1}}$ of accessible duration, obtained by subtracting the tank cost from

the $\$145\,\mathrm{kW}^{-1}\,\mathrm{h}^{-1}$ total energy capacity price in Figure 5.1.

In both cases there are likely to be additional transaction costs associated with capacity restoration, for example the cost of dealing with the old modules in the LIB system, but researching these costs is outwith the scope of this work.

5.3 CAPEX Requirements for Turnkey Systems

For the following analyses a VRFB installed price was constructed from the bottom up for each system specification using the model described in Section 3.4.4 and the VRFB base scenario parameters given in Section 3.4.4.2. The modelled VRFB DC module pricing is shown for both present and near term time-frames in Figure 5.1.

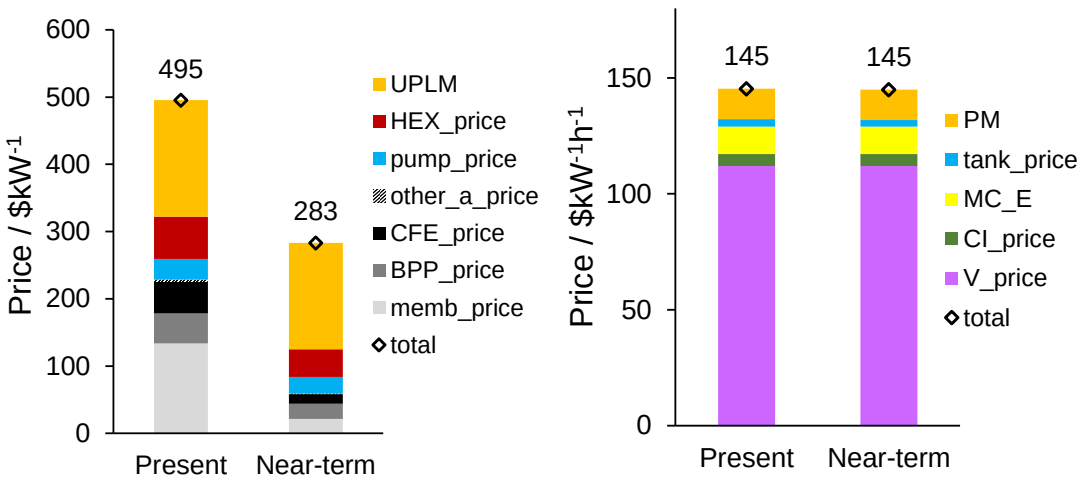

(a) (b)

Figure 5.1: Present and near-term price estimates for a VRFB DC module based on PNNL system [28] using the methodology described in Section 3.4.4. a) Price per kW. b) Price per accessible kW h as defined in Section 3.2

The present day price estimates in Figure 5.1b are close to estimates made by Viswanathan *et al.* for an earlier embodiment of a VRFB from the same research group [24]. For the "V-V Gen 2, Near term" scenario in that article, costs of $\$592\,\mathrm{kW}^{-1}$ and $\$132\,\mathrm{kW}^{-1}\,\mathrm{h}^{-1}$ were inferred from the two instances. The increased stack performance of the system considered here (e.g. current density of $219\,\mathrm{mA\,cm}^{-2}$ compared to $180\,\mathrm{mA\,cm}^{-2}$ for a similar efficiency) is partly responsible for the price in Figure 5.1 being lower than the cost in [24].

Considering the breakdown of costs in Figure 5.1, prices may drop considerably on a $\$\,\mathrm{kW}^{-1}$ basis, but not on a $\$\,\mathrm{kW}^{-1}\,\mathrm{h}^{-1}$ basis. It is of course possible that the margin on the latter will decrease, but this will not have a large effect as vanadium is the dominant cost.

The present price of a LIB DC module is set at \$194 $\mathrm{kW^{-1}\,h^{-1}}$ which is the central 2020 estimate of the DC storage block cost made by PNNL for the smallest power rating in their study (1 MW at 4 h duration). The near-term price is set at \$155 $\mathrm{kW^{-1}\,h^{-1}}$, which is the average of the above 2020 value and the 2030 estimate of \$116 $\mathrm{kW^{-1}\,h^{-1}}$ [21, 141]. These values are both divided by 0.8, the accessible SOC range, as discussed in as defined in Section 3.2. This coincidentally results in a price of \$194 $\mathrm{kW^{-1}\,h}$ for the near-term scenario.

It is assumed that the near-term price scenario for the VRFB - which is defined in [40] as occurring when a manufacturing scale of 1 GW h - 2 GW h per year is reached - will be achieved by 2025.

The turnkey prices for present day and near-term systems were calculated using the model described in Section 3.4.6 for a range of system durations, and the results are shown in Figure 5.2.

In the BTC model EPC costs scale primarily with energy rating, whereas the balance of system hardware costs scale primarily with power rating (see Equation (3.20)). Hence EPC costs make up an increasing proportion of the system price as duration increases.

The data in Figure 5.2 show that the VRFB is predicted to be 29% more expensive than the LIB at 2 h duration, 14% more expensive at 4 h duration and then approach the LIB price as duration increases further. Although the VRFB is cheaper on a DC \$ $\mathrm{kW^{-1}\,h^{-1}}$ basis by 6 h duration, the higher EPC costs stipulated in the model by the 1.7 footprint factor push the turnkey price higher.

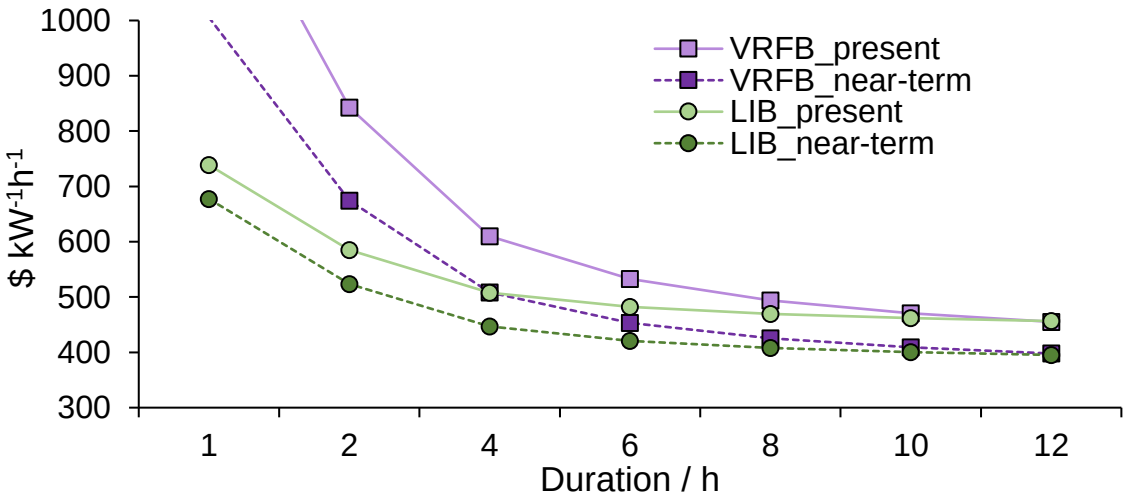

(a)

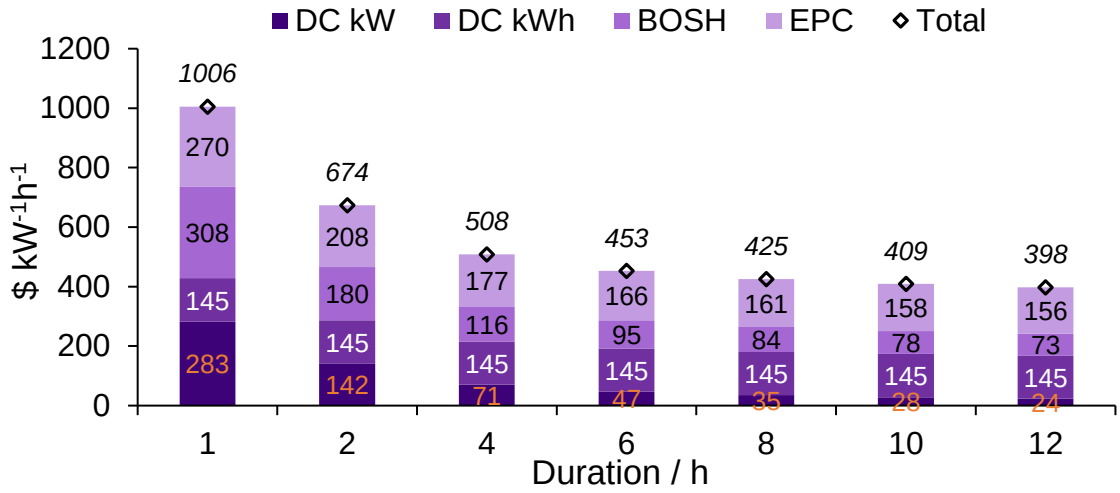

(b)

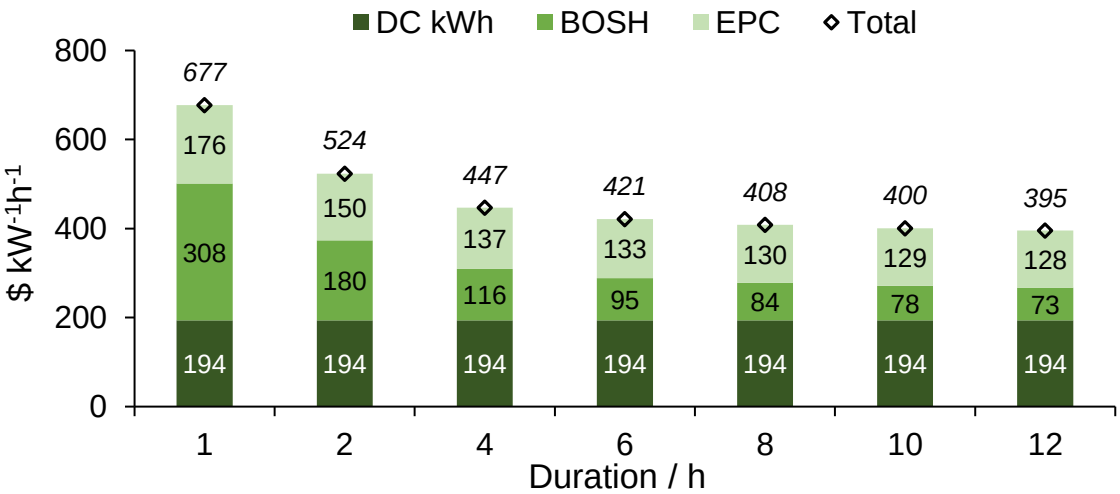

(c)

Figure 5.2: a) Comparison of turnkey price estimates for LIB and VRFB systems at a range of durations and both the present and near term DC module price scenarios. b) VRFB price component breakdown for the near-term scenario. c) LIB plot for same.

5.4 The Impact of Degradation

5.4.1 A Comparison of the Ciez and Whitacre and the Schmalstieg Degradation models

Before moving to the net present value calculation, it is important to understand the change to degradation prediction that comes from updating the model from that reported by Ciez and Whitacre [101] to that reported by Schmalstieg [102]. The primary difference between the two models is that the latter includes calendar aging, which occurs whether the battery is active or not, and is accelerated by high temperature and high SOC. For temperature, it is assumed that the LIB is stored outdoors, not air conditioned, and hence the cell temperature tracks the ambient temperature. Three sets of hourly data from 2012 were analysed, representing different climactic conditions in South California. These are shown in Figure 5.3.

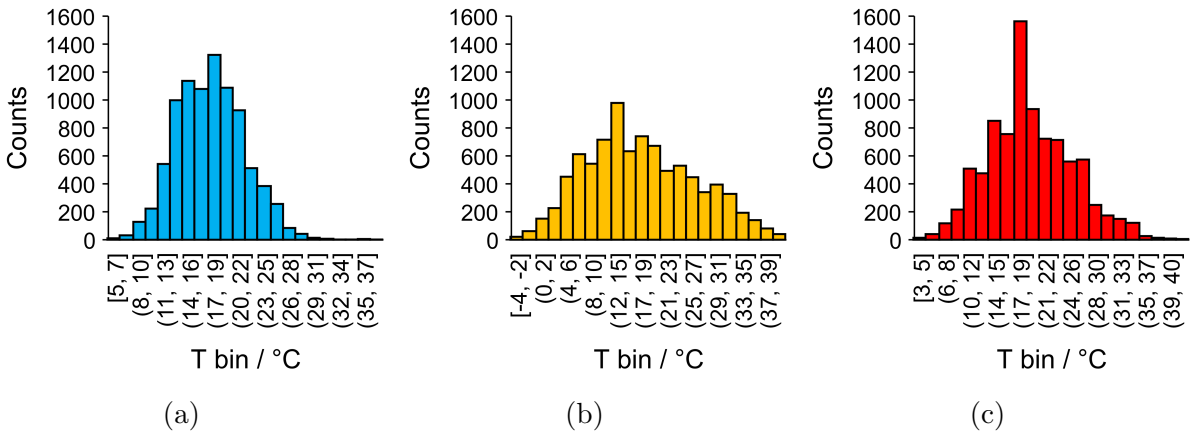

Figure 5.3: Hourly 2012 temperature data from weather stations at a) San Diego International Airport, b) March Air Reserve Base, c) Fullerton Airport.

The first two sets, from San Diego International Airport (SDIA), and March Air Reserve Base (MARB) have the same annual average of 17.5 °C, but the former has a narrower range due to the coastal location. The third data set is from Fullerton airport, to the east of Los Angeles which, with a similar inland position to MARB, but at a 29 m elevation as opposed to 468 m, has a higher average temperature of 19.5 °C.

These three temperature data sets were applied in the post optimisation calculation of

degradation for a 4 h LIB performing peak shaving, energy price arbitrage and bidding for spinning reserve at site 281. The degradation profiles are shown in Figure 5.4.

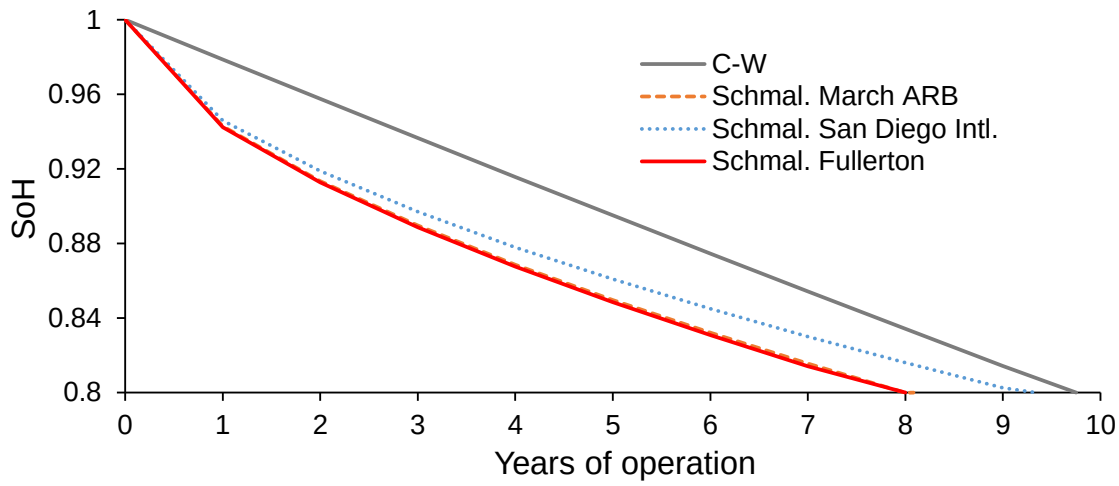

Figure 5.4: A comparison of modelled degradation for a 80 kW 4 h LIB operating behind the meter at site 281, by the Ciez and Whitacre model and the Schmalstieg model for three different ambient temperature scenarios in South California.

The results show that the Schmalstieg model predicts faster degradation than the Ciez and Whitacre model under each of the temperature scenarios. There is also a significant difference in lifetime expectation between the SDIA site and the other sites, despite this site having the same average annual temperature as the MARB site. Similarly, despite the Fullerton Airport site having a 2 °C higher average ambient temperature than MARB, the rate of degradation is the same. This is due to the non-linearity of the temperature dependence, (Equation (3.9)) with the more extreme upper temperature range at MARB compensating for the lower average. In the rest of this section the March AFB data are used, as this is closest weather station to site 281 for which hourly temperature data could be found (site 281 is listed as latitude 33.62 and longitude 116.62).

With BRC set to \$116 kW^{-1} h^{-1}, the LIB is predicted to last at least 8 years in a relatively hot South California location. This is due to a low cycle count, of 0.46 EFC/day on average in the first year of operation. The cycle count is low because price arbitrage revenue does not meet the hurdle rate imposed by the BRC penalty term, and because the peak shaving requirement is low. The latter merits further explanation. A feature of the load profile at Site 281 is that it varies considerably across a given month, hence it will not

be necessary to peak shave to the same extent each day. The historic demand constraint ensures that unnecessary shaving below the existing peak demand is not undertaken.

5.4.2 Optimising the Revenue/Lifetime Trade-off

As there is scope to utilise the battery further, the throughput penalty term BRC was varied in order to derive the optimal NPV across the 10 year project. The impacts on both lifetime and revenue are shown in Figure 5.5.

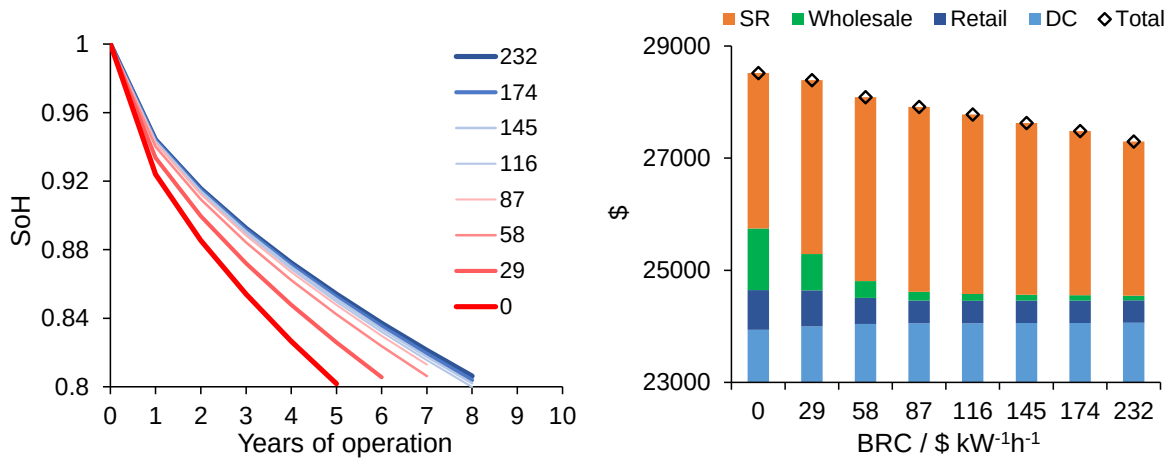

(a) (b)

Figure 5.5: a) State of health profile of an 80 kW/4 h LIB system at site 281 with various $ kW^{-1} h^{-1} BRC penalties. b) Corresponding revenue stacks.

It can be seen that relaxing the degradation penalty increases the revenue slightly, primarily due to increased wholesale energy price arbitrage, although some spinning reserve is sacrificed. Demand charge avoidance is barely altered. The lifetime expectation of the battery is significantly decreased however, as the cycle count is increased to 0.69 EFC/day when BRC is set to \$0 kW^{-1} h^{-1}. It can also be seen that even increasing BRC by 100% does not prolong the life of the LIB to 10 years.

The dependence of the modelled NPV upon BRC is shown in Figure 5.6.

The data in Figure 5.6 show that the dependence of NPV on BRC is slightly different for the 2 h and 4 h duration LIB. The longer duration system shows a broad plateau where changing BRC has little effect, although using the expected replacement cost of 145 kW^{-1} h does give the highest NPV by a negligible margin. The shorter duration system

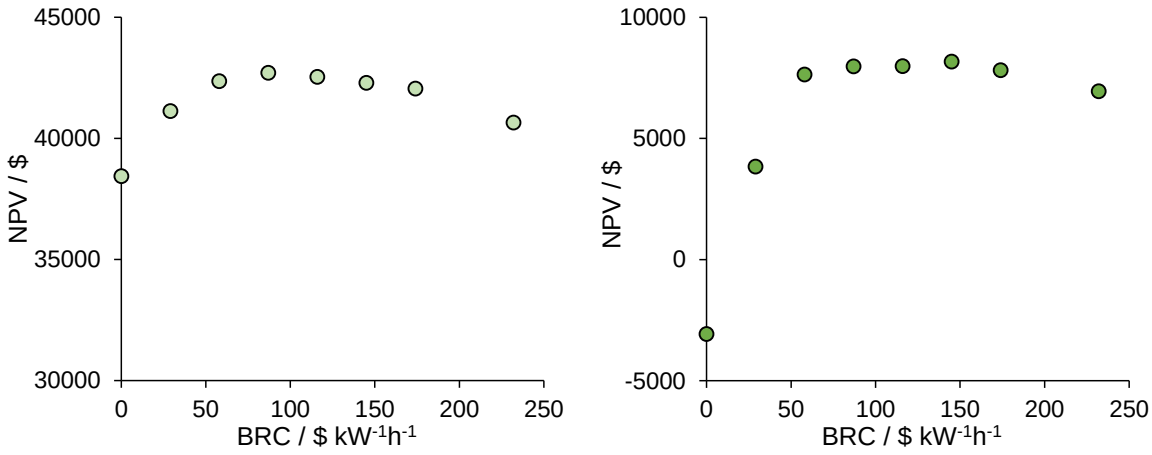

Figure 5.6: Net present value of 80 kW LIB performing energy price arbitrage, demand charge avoidance and spinning reserve at site 281, under various BRC penalty values. a) 2 h duration. b) 4 h duration.

has a clearer optimum, with BRC set 40% below the expected replacement cost. This is because the 2 h system generates more revenue per unit energy capacity and has a smaller replacement cost. It hence makes sense to use it more heavily.

The consequence of failing to factor degradation cost in the schedule optimisation is much worse for the 4 h LIB, which yields a negative NPV, unlike the 2 h system. From here on, BRC is set at 145 kW^{-1} h for a 4 h system and 87 kW^{-1} h for a 2 h system.

5.4.3 Managing SOC to Extend LIB Lifetime

So far the LIB SOC range has been set at 0.15-0.95, as it was by Fisher *et al.* [10]. However, the work of Schmalstieg *et al.* showed that spending time at high SOC, even while idle, accelerates calendar aging. For this reason, it may be more beneficial to set the SOC range at 0.1-0.9. For the 4 h LIB in the above scenario, this prolongs the life of the battery by 5 months. The NPV of the project is increased from $ 8176 to $ 10353. In practice, this would slightly alter the working voltage range of the LIB, but this is not deemed to be a significant effect.

Another way to reduce the rate of calendar aging is to avoid unnecessary time spent at high SOC. This may be done easily in the deterministic optimisation model by adding a

calendar aging cost term to the objective function. As the calendar aging term is linear with respect to SOC, it may be defined without simplification by multiplying the calendar aging expression in Equation (3.7) by BRC and the SOC range 0.8 (as the BESS is oversized by 1/0.8).

Overall the effect of this penalty term is slightly negative, reducing the revenue slightly but not extending the lifetime (to the nearest month), and reducing the NPV by to $ 10202. The alteration to the SOC range is kept in place for the rest of the chapter. The SOC penalty is not applied until it is revisited in the no spinning reserve scenario in Section 5.5.3

5.4.4 Optimisation of VRFB Maintenance Timing

Applying the degradation of Rodby *et al.* [23] there are two costs of degradation to be accounted for in the project:

- Cost of rebalance charge to reverse capacity fade daily due to vanadium ion crossover.
- Loss of revenue between maintenance visits as electrolyte decay reduces working capacity.

The corresponding costs were modelled in the manner defined in Sections 3.3.1 and 3.4.7. The impact of these two phenomena on the project economics was initially gauged by running a one year simulation of a 4 h system, the results of which are shown in Figure 5.7.

It may be observed in Figure 5.7 that the cost of re-balancing the electrolyte to counter vanadium ion crossover is very low, totalling only $ 54 per year. Figure 5.7 also shows that the drop in capacity due to electrolyte decay is 15% across the year. The VRFB generates $ 24842 in revenue, compared to $ 25579 if degradation is not modelled, a decrease of 3.9%. The diminishing returns in revenue with capacity were already demonstrated in Chapter 4, which explains why the drop in working capacity has a small impact. It is therefore likely that the re-balancing operation need only be performed annually, meaning

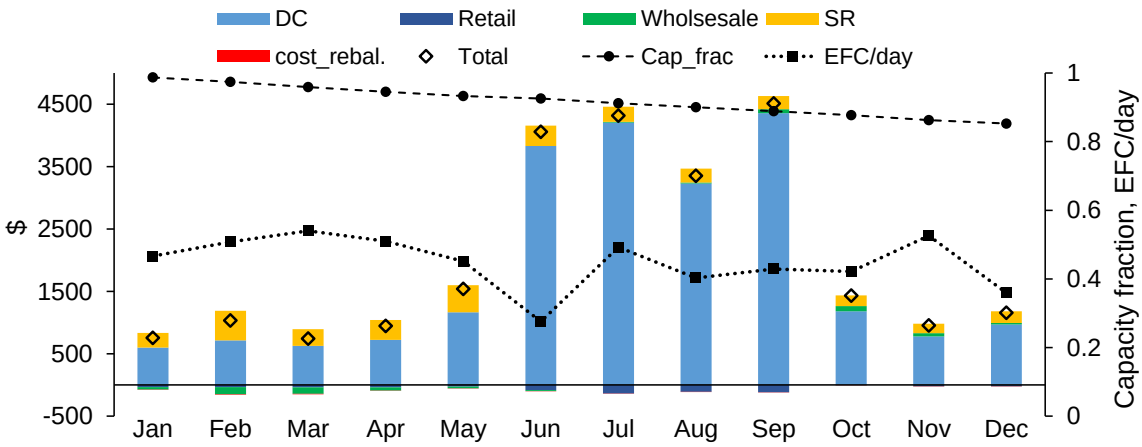

Figure 5.7: Monthly revenue stacks for a 4 h VRFB operating at site 281, including the cost of re-balancing which is barely visible. Also shown are the average equivalent full cycles per day, and the modelled reduction in working capacity due to electrolyte decay.

it could be combined with the maintenance visit already costed in the O & M budget (Section 3.4.7), minimising the additional cost.

Given the seasonality of the revenue streams in this case study illustrated in Figure 5.7 there is potential to reduce the economic impact of electrolyte decay by appropriate timing of the maintenance visit. It would make sense to restore the capacity in May ahead of the peak demand charge charge months. This strategy was simulated by adjusting the working capacity to 89% at the start of the simulation on 1st January, such that following a restoration at the end of April, it would reach 89% again by the end of the year. Doing so increases the simulated revenue to $ 25326, reducing the loss due to degradation to 1.0%. This strategy is employed for the rest of this chapter and in Chapter 6.

5.5 NPV Comparison of VRFB and LIB of Varying Duration at Site 281

The economics of 80 kW LIB and VRFB systems were compared at a range of durations for site 281, based on 2019 prices for retail and wholesale energy and spinning reserve provision, and temperature data from the March Reserve Base site. The results are shown

in Figure 5.8.

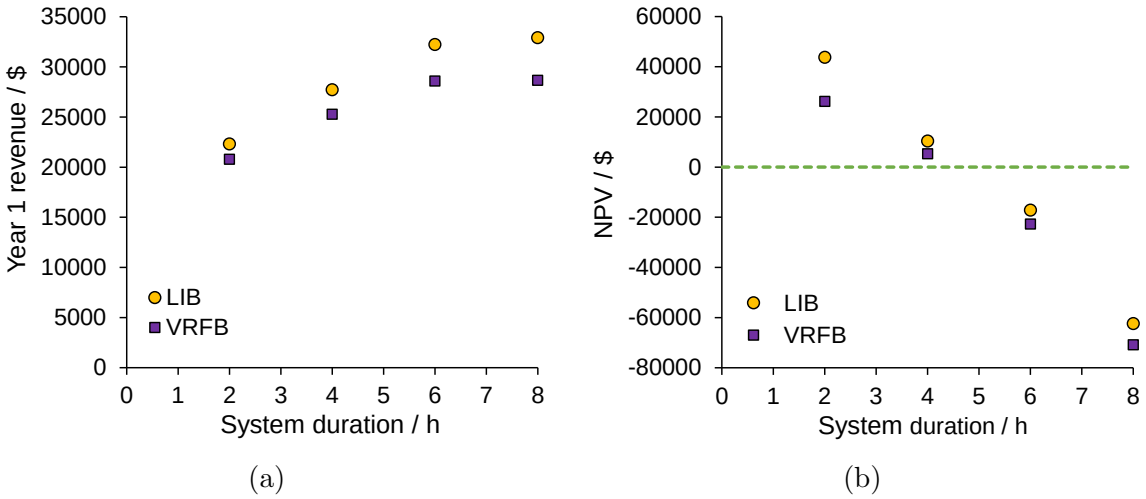

Figure 5.8: a) Simulated revenue in year 1 for 80 kW LIB and VRFB systems with a range of durations at site 281. (b) Simulated NPV of 10 year projects at 10% discount rate assuming energy and spinning reserve prices do not change from 2019 values.

Both BESS types give a positive NPV up to 4 h duration. The LIB gives a considerably higher NPV at 2 h duration, but the gap narrows at 4 h duration and above. The greater revenue from the LIB due to higher round trip efficiency, and the lower CAPEX clearly outweigh the costs associated with DC module replacement, which do not appear until at least year 8, and are hence heavily discounted. The residual value in the vanadium electrolyte is only realised at the end of year 10, and hence discounted by 61% in today's money.

Both LIB and VRFB systems show decreasing economic return as duration increases, particularly going from 6 h to 8 h. The decreasing marginal revenue clearly outweighs the decreasing marginal CAPEX in the overall balance.

In the following subsections a number of economic factors that may change the relative economic case for each system and duration are explored.

5.5.1 Impact of 4 Hour Duration Resource Adequacy Payments

In the CAISO domain, the need for multi-hour storage to replace peaker plant has been recognised with the introduction of a capacity ('resource adequacy') payment paid on a

per-kilowatt basis for storage with a duration of 4 h or above, although shorter duration systems can participate with fractional de-rating of the power bid [142]. This revenue stream was modelled by calculating the average working capacity of the battery each year, calculating the power de-rating to maintain a 4 h duration, and multiplying this by the monthly payment and 12. The payment was set at $\$3\,\mathrm{kW}^{-1}$ per month, which is the average for contracts for the coming four years as of 2018 [143]. The impact of the resource adequacy payment is shown in Figure 5.9.

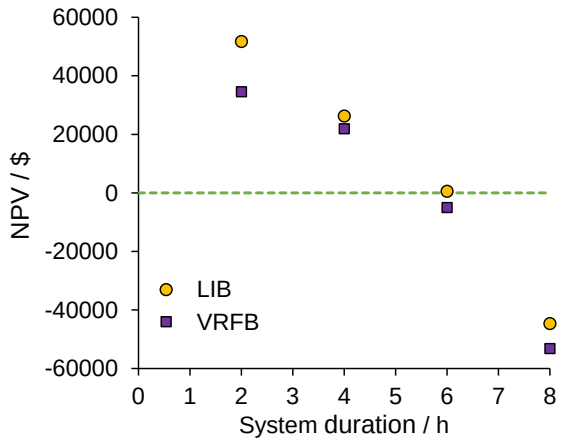

Figure 5.9: Simulated NPV of 10 year projects at 10% discount rate with addition of resource adequacy payment.

This additional revenue stream improves the economic case considerably, with the LIB now modelled as breaking even at 6 h duration and the VRFB very close to breaking even. It also reduces the project risk simply by being a separate source of revenue, for example if spinning reserve became unavailable. The 2 h LIB system still gives the highest NPV. The resource adequacy payment is included in the rest of this chapter.

5.5.2 An Economic Sensitivity Study on External Variables and VRFB Efficiency.

There are a number of factors relating to the use case of the battery that will clearly have a bearing on the relative economic merits of the two technologies. In this section a sensitivity study was performed on a selection of factors deemed to be most significant, in order to guide the selection of the most suitable applications for the VRFB. The following

two factors that would impact on the LIB were studied:

- Cycle rate: it was already demonstrated that reducing the penalty term BRC increases the cycle rate for the LIB. Adjusting this parameter allows the impact of higher cycle rates on LIB economics to be illustrated. In addition to the optimal values of \$145 $\mathrm{kW^{-1}}$ h and \$87 $\mathrm{kW^{-1}}$ h for the 4 h and 2 h LIB respectively, values of 29 $\mathrm{kW^{-1}}$ h and 0 $\mathrm{kW^{-1}}$ h were run for both durations to capture the variety seen in Figure 5.6.

- Cell temperature: In Figure 5.4, the change to LIB degradation rate moving from a coastal location to an inland location was demonstrated. Both the inland site MARB and the cooler coastal site SDIA were simulated for the LIB systems.

In addition, three factors specific to the VRFB system were studied:

- Footprint factor: the base case estimate of EPC costs for the VRFB system includes a 1.7 footprint factor, used by PNNL to account for the lower energy density of the VRFB compared to the LIB. In order to gauge the importance of reducing EPC costs, a lower value of 1.2 was also run.

- Electrolyte leasing: one approach to reducing the CAPEX requirement is to lease the vanadium electrolyte, which is arguably a non-depreciating asset. Lease rates of 6% and 8% of the electrolyte price are tested, with the assumption that an upfront lease payment is made in year 0.

- Round trip efficiency: the lower assumed efficiency of the VRFB has been shown to result in a lower revenue when compared to the LIB. For this reason, the impact of a modest improvement from 0.75 to 0.80 DC round trip efficiency was tested without any increase to system cost.

In order to gauge the combined effect of the above parameters, a full factorial study was run, at both 2 h and 4 h duration. The difference between the NPV predicted for the VRFB and that predicted for the LIB are shown for each scenario in Figure 5.10.

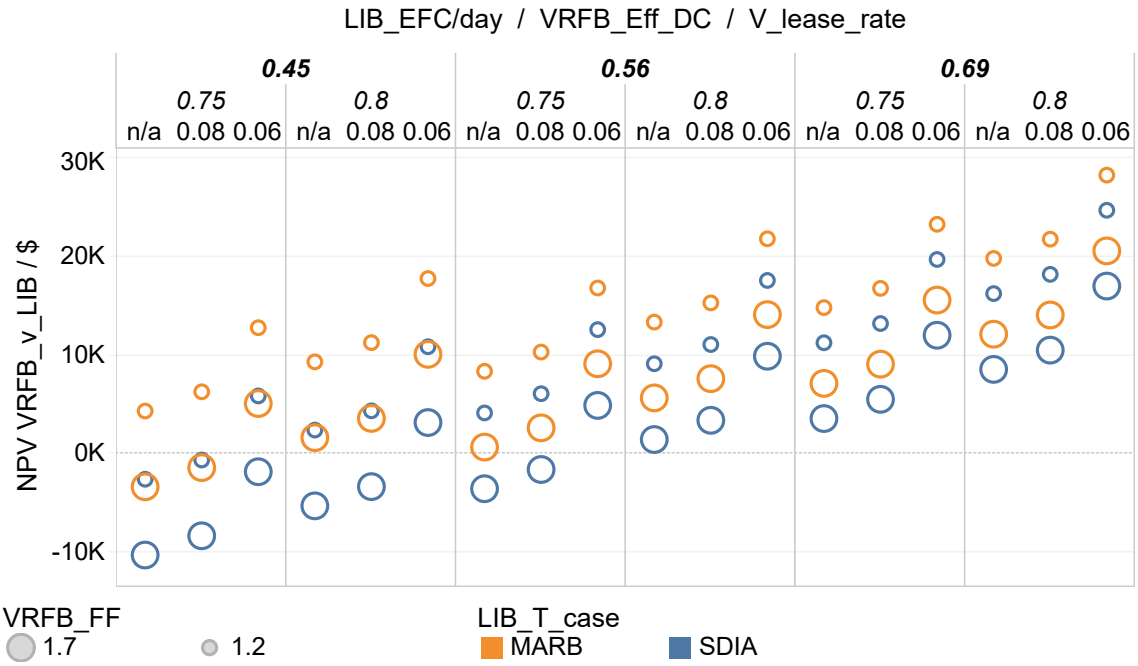

Figure 5.10: Results of sensitivity study for site 281 showing the NPV of the VRFB minus the NPV of the LIB under each scenario. Points shown are all 80 kW/4 h systems.

Before considering the data in Figure 5.10 it is important to note that that even under the combination of factors most advantageous to the VRFB, the LIB system always delivers a higher NPV at 2 h. Hence these comparison points are not shown in Figure 5.10. Thus the findings of Fisher *et al.* are shown to be robust under the set of economic, technological and environmental assumptions most favourable to the VRFB. As the NPV at 2 h duration is considerably higher than at 4 h, the short term, strictly economic choice would still be a 2 h LIB, despite the resource adequacy incentive.

At 4 h duration, there are a number of scenarios where a VRFB would be a better choice, and there are several useful findings. Firstly, all of the parameters tested have a meaningful effect on the relative economics of LIB and VRFB. Leasing the VRFB electrolyte has little effect at 8% p.a., but a notable effect at 6% p.a.. Where the LIB operates at 0.45 EFC/day, the climactic location has as much of an effect on the economic comparison as reducing the EPC costs of the VRFB. The effect of climate becomes less important at higher cycle rates, as the LIB will degrade quickly anyway. Reducing the EPC costs of VRFB systems is clearly important, and leads to the same NPV uplift regardless of the other parameter settings.

When the LIB is operated optimally and averages 0.45 EFC/day, the VRFB is still modelled as returning greater economic benefit at the hotter location if an electrolyte lease rate of 6% is available. Where the EFC/day is increased by adjusting the *BRC* penalty, the prospects for the VRFB improve, and progressively less optimistic combinations of factors are required to compete with the LIB system. It is important to remember that the higher LIB cycle rate cases are purely illustrative, and that an informed owner of a LIB would not set the *BRC* parameter this low. The circumstances in which a higher cycle rate might become necessary are discussed in the conclusions of this chapter.

5.5.3 An Economic Sensitivity Study of the No-Spinning-Reserve Scenario

As it may not be possible for the BESS owner to contract with an aggregator to provide spinning reserve, the economics of performing just energy arbitrage and peak shaving are studied in this section.

The 0.75 DC efficiency VRFB simulations were re-run with the spinning reserve bid variable constrained to 0. It was observed that the average cycle rate increased from 0.40 EFC/day and 0.45 EFC day to 0.63 EFC/day and 0.59 EFC/day for the 2 h and 4 h systems respectively. The higher cycle rate occurs because the spinning reserve and wholesale energy price peaks overlap, hence removing spinning reserve encourages energy price arbitrage, which requires cycling. The resultant increase in simulated capacity fade means the average working capacity is 91% of the fresh, compared to 94% in the spinning reserve scenario (in the simulations for the following sensitivity study, the starting capacity is adjusted downward to keep the annual cycle closed). For the LIB, at the default *BRC* settings, there is only a minor increase in cycle rate from 0.41 and 0.45 EFC/day to and EFC/day for the 2 h and 4 h systems respectively. Interestingly, despite this minor increase, the LIB lifespan is increased from 9.2 years to 80% SOH to 9.8 years.

As the use case clearly changes when spinning reserve is removed, the SOC penalty, which had negligible effect previously (Section 5.4.3 was revisited. In the no spinning

reserve case, the penalty pushes the average SOC across the year down from 0.320 to 0.305. This extends the lifetime of the LIB from 9 years and 3 months to 9 years and 5 months, which adds \$ 752 to the NPV, a 7% increase.

The impact of the SOC penalty on optimal LIB schedule is shown in Figure 5.11.

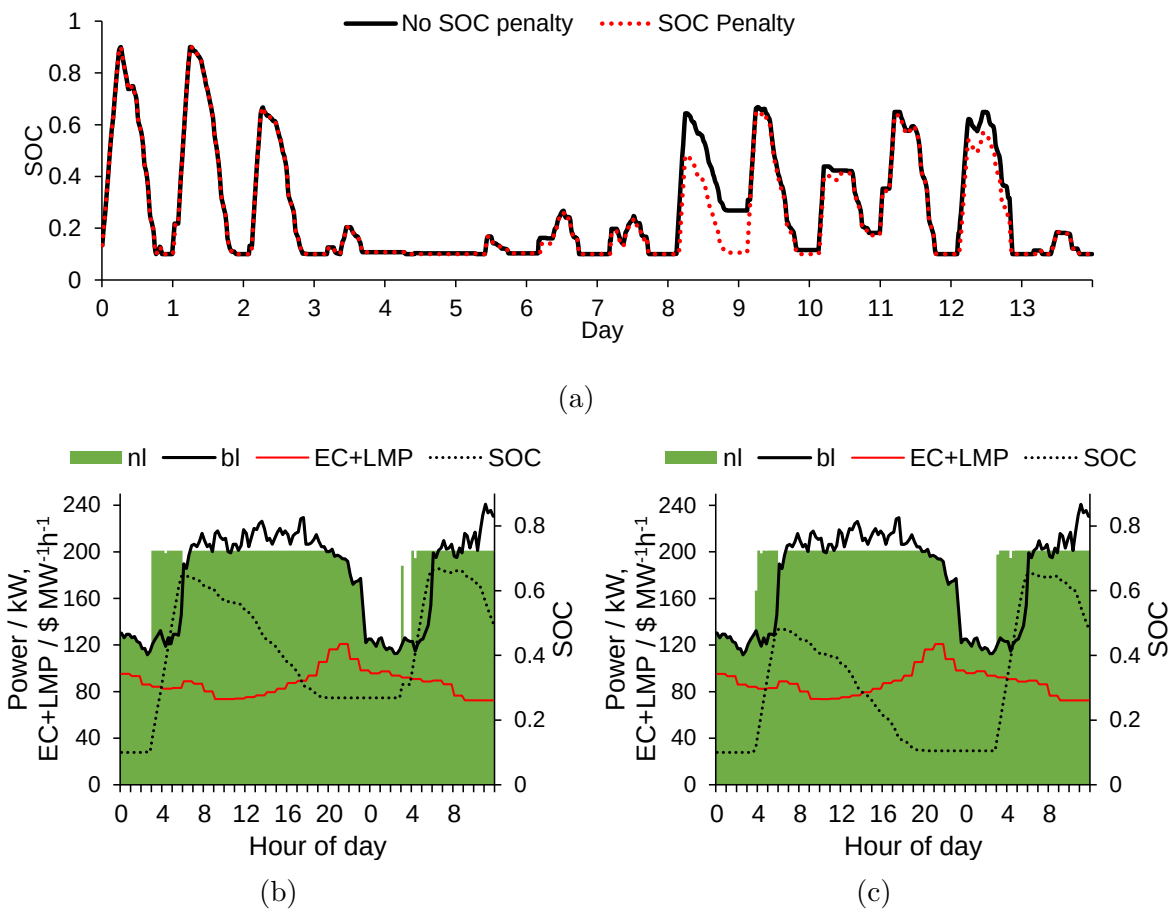

Figure 5.11: The impact of a SOC penalty on optimal scheduling of 80 kW 4 h LIB. SOC profiles for first two weeks in June with and without SOC penalty term a) and close up of day 9 operation without (b) and with (c) SOC penalty.

On day 9, where there is a notable difference between the two schedules, the requirement to peak shave is capped by the peak demand history, and the price profile does not support arbitrage. Without the SOC penalty, the battery charges close to the maximum SOC in hours 3-6 on day 9, and ends the day with a SOC of 0.27. With the SOC penalty in place the battery moves some of the charging in hour 3 to the same period the following day, despite the price being slightly higher (\$ 0.092 $\mathrm{kW^{-1}\,h^{-1}}$ vs. \$ 0.084 $\mathrm{kW^{-1}\,h^{-1}}$). This is done to minimise the average SOC throughout day 9.

The SOC penalty was hence applied to the LIB in the following sensitivity study, where the same parameters were varied as in Section 5.5.2. The results of this sensitivity study are shown in Figure 5.12.

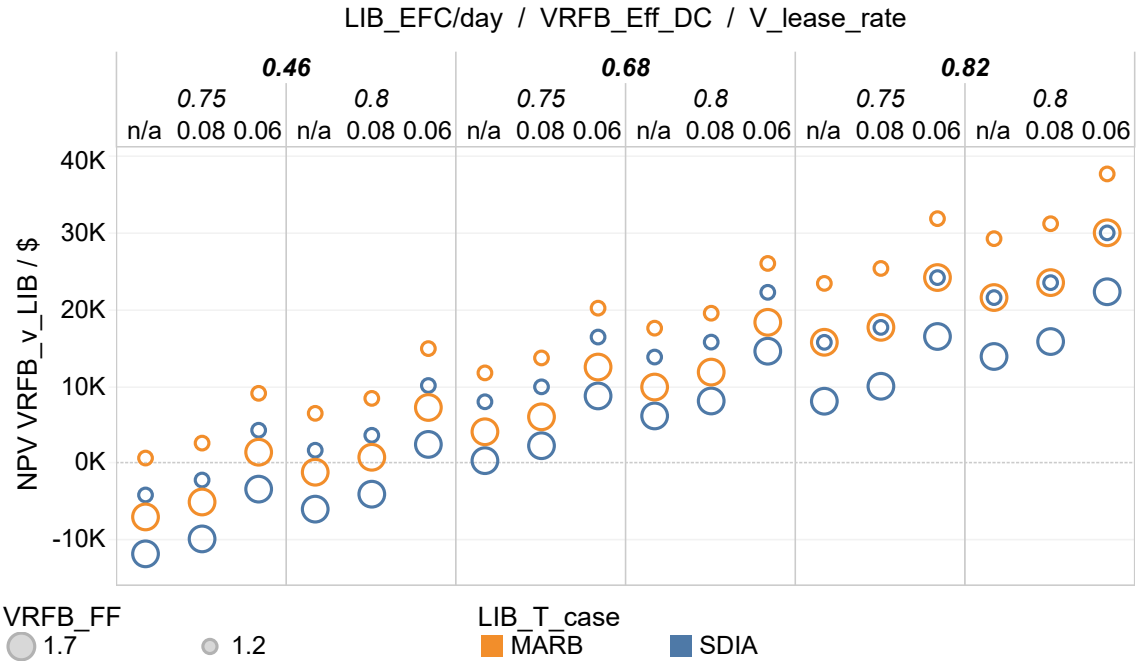

Figure 5.12: Results of sensitivity study for site 281 showing the NPV of the VRFB minus the NPV of the LIB under each scenario when spinning reserve is not included. Points shown are all 80 kW/4 h systems.

The main difference between Figure 5.12 and Figure 5.10 is that considerably higher cycle rates are performed by the LIB when the BRC penalty is not properly controlled. This would lead to an increased advantage for the VRFB. It also highlights again the importance of finding high cycle rate applications for VRFB deployment.

In the no spinning reserve case there are a few parameter combinations where the 2 h VRFB gives better economics than the LIB, which are not shown in Figure 5.12 for the sake of brevity. These all occur when the BRC term is set to 0, in which case the LIB performs 0.92 EFC/day on average, and requires replacement twice during the ten year project. The scenarios also all involve the higher temperature location and the reduced footprint factor for the VRFB. Overall it is fair to conclude that the VRFB is not competitive at 2 h in this case study too.

Lastly, it was found that the 4 h VRFB is still predicted to return a positive NPV

without spinning reserve under the base parameters (1.7 footprint factor, no electrolyte leasing and 0.75 DC efficiency).

5.6 Conclusions

Based on the results reported in this chapter, it is possible to make a number of important conclusions regarding the relative economic merit of LIB and VRFB systems for a behind the meter application in California, but also more generally.

- Figure 5.2 shows that the turnkey price estimate per kW h of storage is marginally higher for the VRFB than the LIB even for systems specified with 12 h duration. This is because the assumed 2025 LIB DC module price is only 34% higher than that of the VRFB electrolyte, and the difference is more than offset by the higher EPC cost of the latter (via PNNL's footprint factor).

- VRFB capacity fade due to vanadium crossover has a negligible effect on economics, as the cost of rebalancing is low. Electrolyte decay has a small impact as it reduces the average working capacity (0.92) if only corrected annually, This impact can be minimised by timing the maintenance for the start of the peak demand charge season.

- Using the more detailed degradation model developed by Schmalstieg *et al.* [102], it has been shown that the location of the installation will have a significant impact on the lifetime of the LIB assuming the system is not refrigerated. For example, a 4 h LIB installed at the MARB location is predicted to require replacement 15 months earlier than a unit installed at SDIA. The lifetime is not a simple function of average temperature; the SDIA location has the same average temperature as the MARB but the latter has a higher upper range. This is because the dependence on temperature is non linear. It was also shown that the optimal LIB operation at the MARB involves replacing the battery once in the ten year project. This is because once calendar aging is accounted for, the lifetime extension achievable by reducing

cycling is reduced.

- When the degradation penalty for the LIB is optimised, the most profitable system for the peak shaving/price arbitrage/spinning reserve scenario is always a 2 h LIB. This is because all revenue streams scale sub-linearly, except the resource adequacy payment, which scales linearly since de-rating is permitted. The findings of Fisher *et al.* [10] are hence shown to be robust to external assumptions that favour VRFB. Setting the degradation penalty correctly is more important for a longer duration system, as the cost of module replacement is higher. For a 4 h LIB, neglecting to apply a penalty on throughput results in a negative NPV, whereas a 2 h system still delivers a positive NPV.

- At 4 h duration, both LIB and VRFB can return positive NPV and there is more potential for the VRFB to compete with the LIB, as the cost of LIB degradation starts to cancel out the higher efficiency advantage of the LIB. However, VRFB competitiveness is predicated on either a greater than optimal cycle rate for the LIB, or at least two of the studied factors taking values that favour the VRFB. the LIB cycle rate by relaxing the degradation penalty below the optimal value, although the required cycle rate is lower in hotter environments, and when vanadium electrolyte leasing is available. When spinning reserve is not available, the potential cycle rate is increased further.

- The lower trip energy efficiency is an important disadvantage of the VRFB, with even a modest improvement from 0.75 to 0.85 having a significant impact.

Chapter 6

Optimising the Operation of a VRFB with a Novel Algebraic Model for Dynamic Efficiency

6.1 Introduction

In the previous chapter, it was shown that round trip efficiency is an important property, and that even a modest improvement in the assumed DC efficiency of the VRFB from 0.75 to 0.85 can make the difference between a VRFB and an LIB being the optimal choice at 4 h duration in the CAISO behind-the-meter scenario. A feature of the VRFB that distinguishes it from the LIB at the DC level is the significant variation in efficiency with C rate it exhibits.

In this chapter, the impact of these dynamic efficiency features are explored using the MIQP optimisation model described in Section 6.2.2. In Section 6.3, an efficiency profile for the VRFB reported at PNNL [28] is constructed and discussed. In Section 6.4, the optimal operation under the MIQP and LP optimisation methods are compared for the behind-the-meter case study with just peak-shaving and energy arbitrage, and the operational efficiency of the VRFB estimated. In Section 6.5 the model is then used

to determine the optimal choice of electrode area for the VRFB. In Section 6.6 the MIQP model is applied to study the benefits to VRFB system efficiency of independently scheduling sub-modules. The MIQP formulation also allows a voltage constraint to be applied, preventing combinations of SOC and current density that would lead to hydrogen evolution. The relevance of this constraint to actual operation is analysed in Section 6.7.

6.2 Methods

In this section, novel methods developed to address the variable VRFB efficiency research challenge are introduced. The core algebraic model is first defined, then the parametrisation is detailed. After this, a novel constraint on working Lastly, the process undertaken to achieve an acceptable solution in a reasonable time-frame using the Gurobi solver is described.

6.2.1 Model Assumptions

A detailed description of the assumptions made in the MIQP formulation for VRFB efficiency is given in Section 6.2.2.

6.2.2 Novel Mixed Integer-Quadratic Programming Model for Multiple VRFB Modules

In this section the mixed integer-quadratic programming formulation developed to allow a dynamic efficiency optimisation of the VRFB operation is described. There are three key differences between this formulation and the formulation used by Fisher *et al.* [10] (and the other LP formulations reviewed in Chapter 2):

- The coulombic and voltaic components are separated, allowing ohmic losses to be expressed as a convex quadratic function of current, with kinetic losses approximated as a scalar step instead of a logarithmic expression as seen in the Butler-Volmer

equation.

- Pumping and coulombic losses due to shunt currents and/or vanadium ion crossover are modelled as constants. Hence, an integer variable representing idle/active state is introduced, to allow the VRFB to be placed in an idle state when not in use. In this state it is assumed that the pump is off, and the coulombic losses are arrested due to the small electrolyte volume in the stack.

- All variables are indexed over the set of multiple VRFB modules S so that the schedule of individual modules can be optimised as an ensemble.

The model is formulated for the scenario where neither regulation or spinning reserve are accessible.

The objective function is therefore defined by:

$$minimise(\sum_{t \in T} \tau(LMP_t + EC_t) \cdot nl_t + \sum_{k \in K} DC_k \cdot pd_k) \tag{6.1}$$

Where τ is the model timestep in h. The net load at the site at time t is next defined by:

$$nl_t = bl_t + \sum_s P_{s,t}^{VRFB} \tag{6.2}$$

Where $P_{s,t}^{RFB}$ is the power to VRFB module s (kW) at time t, defined by:

$$\begin{aligned} P_{s,t}^{RFB} = ((A_s(I_{s,t}^c(OCV_{50\%,s} + V_s^a) + I_{s,t}^{c^2} ASR_s) + \delta_{s,t}^c P_s^{pump})/\sqrt{\eta_{inv.}} \\ -(A_s(I_{s,t}^d(OCV_{50\%,s} - V_s^a) - I_{s,t}^{d^2} ASR_s) - \delta_{s,t}^d P_s^{pump})\sqrt{\eta_{inv.}})/1000 \end{aligned} \tag{6.3}$$

Where $I_{s,t}^c$ and $I_{s,t}^d$ are continuous non-negative variables representing current density for charge and discharge ($\Omega\,\mathrm{m}^{-2}$) and $\delta_{s,t}^c$ and $\delta_{s,t}^d$ the binary variables representing active/idle charge and discharge status. The parameter A_s is the electrode area of the stack (m^2) as defined for the cost model in Equation (3.11), $OCV_{50\%,s}$ is the open cell stack voltage at 50% SOC, V_s^a the kinetic over-potential scalar, ASR_s the area specific resistance ($\Omega\,\mathrm{m}^2$)

and P_s^{pump} the fixed pump power (W).

The state of charge of VRFB module s at time t is defined by:

$$SOC_{s,t} = SOC_{s,t-1} + \frac{A_s.\tau}{C_s}(I_{s,t}^c - I_{s,t}^d - (\delta_{s,t}^c + \delta_{s_t}^d)I_s^{loss}) \tag{6.4}$$

Where I_s^{loss} is the constant approximation of the coulombic loss ($\mathrm{A\,m^{-2}}$) and C_s is the coulombic capacity of the battery, defined by:

$$C_s = \frac{1000P_{Inv.}}{OCV_{50\%_s}(\overline{SOC}_s - \underline{SOC}_s)N_S} \tag{6.5}$$

where h is the specified discharge duration in hours, and N_S the number of modules combined to provide the overall BESS capacity. This definition is consistent with the duration definition in Section 3.2, where the capacity is oversized to account for the reduced SOC range, but not the losses.

The constraint on SOC defined in Equation (4.6) is retained, with the addition of the s index. Next, four binary constraints are introduced to define the active/idle behaviour. For charging, the condition that the system be active when a non-zero current is flowing, and that the current density not exceed the maximum permitted are both enforced by:

$$I_{s,t}^c - \bar{I}_s^c \delta_{s,t}^c \leq 0 \tag{6.6}$$

Where $\bar{I}_s^C$ is the maximum permitted charge current density. The condition that the system be idle when zero current is flowing is enforced by:

$$I_{s,t}^c - \mu \delta_{s,t}^c \geq 0 \tag{6.7}$$

After Williams, where μ is a small positive non-zero number acting as a threshold for declaring the system idle [144]. The equivalent constraints for discharging are obtained by substituting the discharge specific variables and parameters. It is worth noting that Equation (6.7) is not strictly necessary under the objective in Equation (6.1), but without

it, errors are generated under the self-sufficiency objective defined later in Equation (7.5).

The charge and discharge states are constrained to be mutually exclusive by:

$$\delta^c_{s,t} + \delta^d_{s,t} = 1 \tag{6.8}$$

Again, Equation (6.8) is not strictly necessary under the objective in Equation (6.1), but reduces the solve time. It is however necessary to prevent erroneous behaviour in the self-sufficiency objective defined in Equation (7.5).

Lastly, given that the VRFB electrode area is specified so the stack is able to match the inverter rating during dispatch, charging at the maximum current density permitted for discharge would exceed the inverter rating. It was found to be far more efficient to enforce this condition by defining different charge and discharge current density bounds than by placing an extra constraint on the charge power of the VRFB. After calculating the electrode area A_s by Equation (3.11), the relationship between the maximum charge current density $\bar{I}^C_s$ and the inverter rating was defined by:

$$P_{Inv.} = N_s(A_s(\bar{I}^c_s(OCV_{50\%,s} + V^a_s) + \bar{I}^{c^2}_s ASR_s) + P^{pump}_s)/1000\sqrt{\eta_{Inv.}} \tag{6.9}$$

Which may be solved to obtain $\bar{I}^c_s$. The tightened bound on charge current density makes the VRFB operation more consistent with the LP formulation, where efficiency is encoded within the state of charge expression and the maximum input and output power are the same.

6.2.3 VRFB Parametrisation in the MIQP Model

The values assumed for the additional model parameters were derived from the performance data reported in [28] as follows. The highest performing inter-digitated stack design (IDD2s) was chosen, and the lowest electrolyte flow rate (400 $\mathrm{mL\,min^{-1}}$ per cell). For this embodiment, the maximum current density was set at 219 $\mathrm{mA\,m^{-2}}$ as this is the value

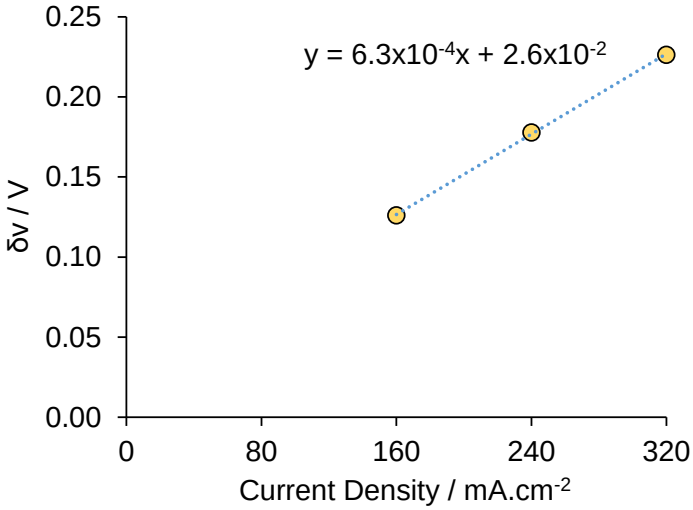

Figure 6.1: Plot of over-potential against current density for the studied PNNL VRFB embodiment. ASR_s the area specific resistance is derived as the gradient of the linear fit, and V_s^a the kinetic over-potential approximation as the zero current intercept.

that returns a round trip DC efficiency of 0.75 based on Equation (3.10). To obtain ASR_s and V_s^a, over-potentials δ_V for the PNNL system were first calculated for each of the three current density points by solving:

$$\eta_V = (1 + \delta_V)/(1 - \delta_V) \tag{6.10}$$

for δ_V, where η_V is the experimental round trip voltaic efficiency. ASR_s was derived as the gradient of the linear fit of δ_V versus current density, and V_s^a as the zero current intercept. The fit is shown in Figure 6.1 .

This approach makes the assumption of symmetrical charge/discharge voltaic losses.

Under the applied assumption of a near-fixed coulombic loss, the coulombic efficiency would be expected to increase non-linearly with current density, rapidly at first then levelling off toward 100%. This behaviour has been shown both experimentally [145, 146] and in a shunt current modelling study [147]. However, the PNNL system was not tested at low current density, making it difficult to set a value for I_{loss}. Also, the coulombic efficiency reported is practically constant at 0.976 - 0.974 from 160 mA cm^{-2} to 320 mA cm^{-2}, giving a range for I_{loss} from 1.9 mA cm^{-2} to 4.2 mA cm^{-2}. The increasing loss at higher current density may be related to the increased temperature of the electrolyte reported, which

could lead to higher ionic crossover and higher ionic conductivity leading to higher shunt currents. The coulombic loss calculated at the 1600 mA cm^{-2} test point was used, as this is not only most representative of the actual battery use range, but gave the best fit of the experimental data (see Figure 6.2).

It is important to note that shunt current magnitude increases with the number of cells in series in the stack [37]. Thus using small stack data may give an over-optimistic estimate of coulombic efficiency compared to a real system that aims for 24V or 48 V. In [28] the number of cells in the IDD2s test stack is not made explicit, but it is likely either 15 or 20, giving a voltage of either 22 or 29 V, which could run a 24 V system. However it may be desirable to have a 48 V stack; this issue is discussed further in Section 6.6.1.

The pumping power is assumed to be fixed, and is calculated by multiplying the sum of the maximum anolyte and catholyte flow (calculated by Equation (3.12)) by the pressure drop (34.5 kPa) and dividing by the assumed pump efficiency of 0.6.

The values of the above parameters for 1 kW of power output, based on the sizing process in Section 3.4.4 are given in Table 6.1.

Table 6.1: The parameters used to describe 1 kW of output from VRFB s in the MIQP model in the base scenario. All derived from data in [28].

Parameter	Value	Units	Source
A_s	0.354	m^2	Equation (3.11)
I_s^{loss}	2.9	mA cm^{-2}	
ASR_s	6.3e−4	mΩ cm^{-2}	
V_s^a	0.03	V	[28]
P_s^{pump}	3.5	W	
$\bar{I}_d, s$	219	mA cm^{-2}	
$OCV_{50\%,s}$	1.47	V	[17]

6.2.4 Maximum Cell Voltage Constraint

In order to constrain the maximum cell voltage during operation, the open cell voltage at time t is first defined by:

$$OCV_{s,t} = aSOC_{s,t} + b \tag{6.11}$$

Where a and b are coefficients describing a linear approximation of the OCV vs. SOC curve. The cell voltage during charging is then constrained by:

$$OCV_{s,t} + V_s^a + I_{s,t}^c ASR_s \leq V_{max} \tag{6.12}$$

Where V_{max} is the maximum permitted cell voltage.

6.2.5 Practicalities of Solving the MIQP Problem

As the MIQP problem involves integer variables for module active/idle status, a branch and bound process is used by the solver (Gurobi in this case). The default behaviour is to continue searching the solution tree until an integer solution is found that is within 0.01% of the solution to the LP relaxation (the LP relaxation will always give a solution at least as good as the integer solution, as the variables are allowed to take values between 1 and 0). Under the default settings, the problem is typically solved to this tolerance in less than 1 s, but in certain instances it takes considerably longer. Rather than increase the gap tolerance, a time limit was applied. This has the minor disadvantage of making the optimisation non-deterministic, i.e. a different solution may be returned depending on the computing resources available to the solver. However, it avoids the need to relax the gap tolerance every time to accommodate the few challenging instances. The time limit was set at 5 s initially, but longer times were required for the multiple module optimisation, as discussed in Section 6.6.

6.3 VRFB Dynamic Efficiency

In order to demonstrate the potential efficiency of the VRFB, the model developed in Section 6.2.2 was used to simulate cycles at varying current density. The results are shown in Figure 6.2.

It is important to bear in mind that for the linear programming formulation used in Chapters 4 and 5 it was necessary to pick a constant representative value for efficiency.

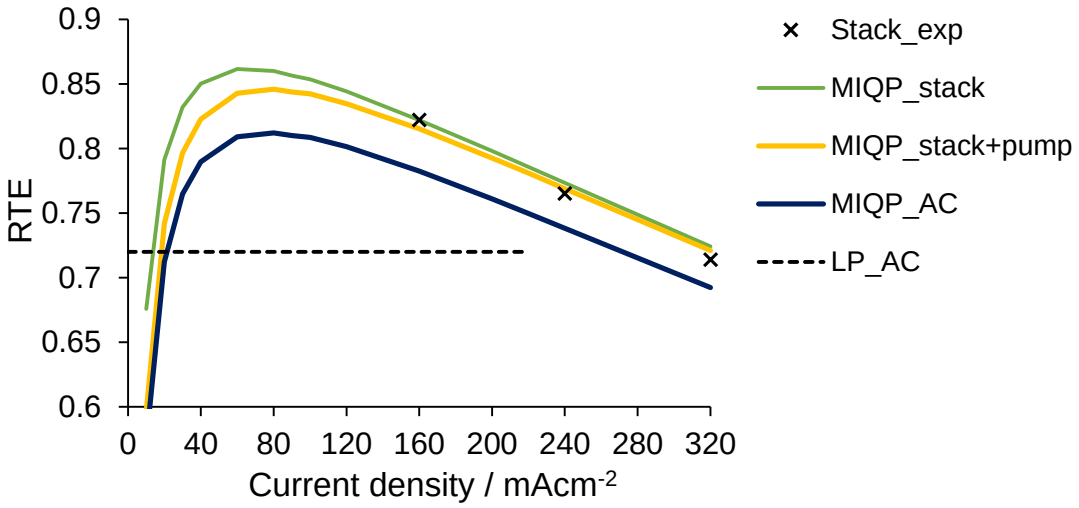

Figure 6.2: A comparison of experimental round trip stack energy efficiency data from the PNNL system [28] with the MIQP model output. Also shown is the linear approximation applied for AC efficiency in Chapters 4 and 5.

In order to be conservative the value at the highest permitted current-density was used (219 mA cm^{-2}, giving 0.75 DC efficiency and 0.72 AC efficiency). Figure 6.2 shows that this likely led to an underestimation of the modelled VRFB efficiency. In the MIQP model, below the current density cap of 219 mA cm^{-2} the AC efficiency is higher than 0.72 at all but the lowest current densities (<35 mA cm^{-2}), and reaches a maximum of 0.814 at 74 mA cm^{-1}. At 219 mA cm^{-2} the difference between the LP and MIQP model values for efficiency is mostly due to dropping the 2% each way balance of plant loss described in Section 3.4.4.2, most of which was attributed to pumping losses. For any other BOP losses, it should be remembered that no such losses are applied to the LIB in Chapter 7. In the PNNL system the improved electrode design means that the pumping power is only 3.5 W, or 0.35% of the 1 kW output at 219 mA cm^{-1}. The profile in Figure 6.2 implies that depending on the duty cycle, the VRFB economic performance could be closer to, or even exceed the optimistic 0.80 DC (0.77 AC) efficiency scenario simulated in Sections 5.5.2 and 5.5.3. This matter is discussed further in the following section.

6.4 MIQP Optimal VRFB Operation

In the previous section it was shown that the maximum efficiency of the modelled VRFB is achieved at 74 mA cm^{-2}. The advantage of the MIQP optimisation approach is the ability to aim for this point and avoid the high and low current unless there is an extreme in the price signal that merits high power, or shaving the load profile demands low power output.

An example of MIQP optimal operation is compared to LP optimal operation for a 80 kW/4 h VRFB on a Sunday in January in Figure 6.3.

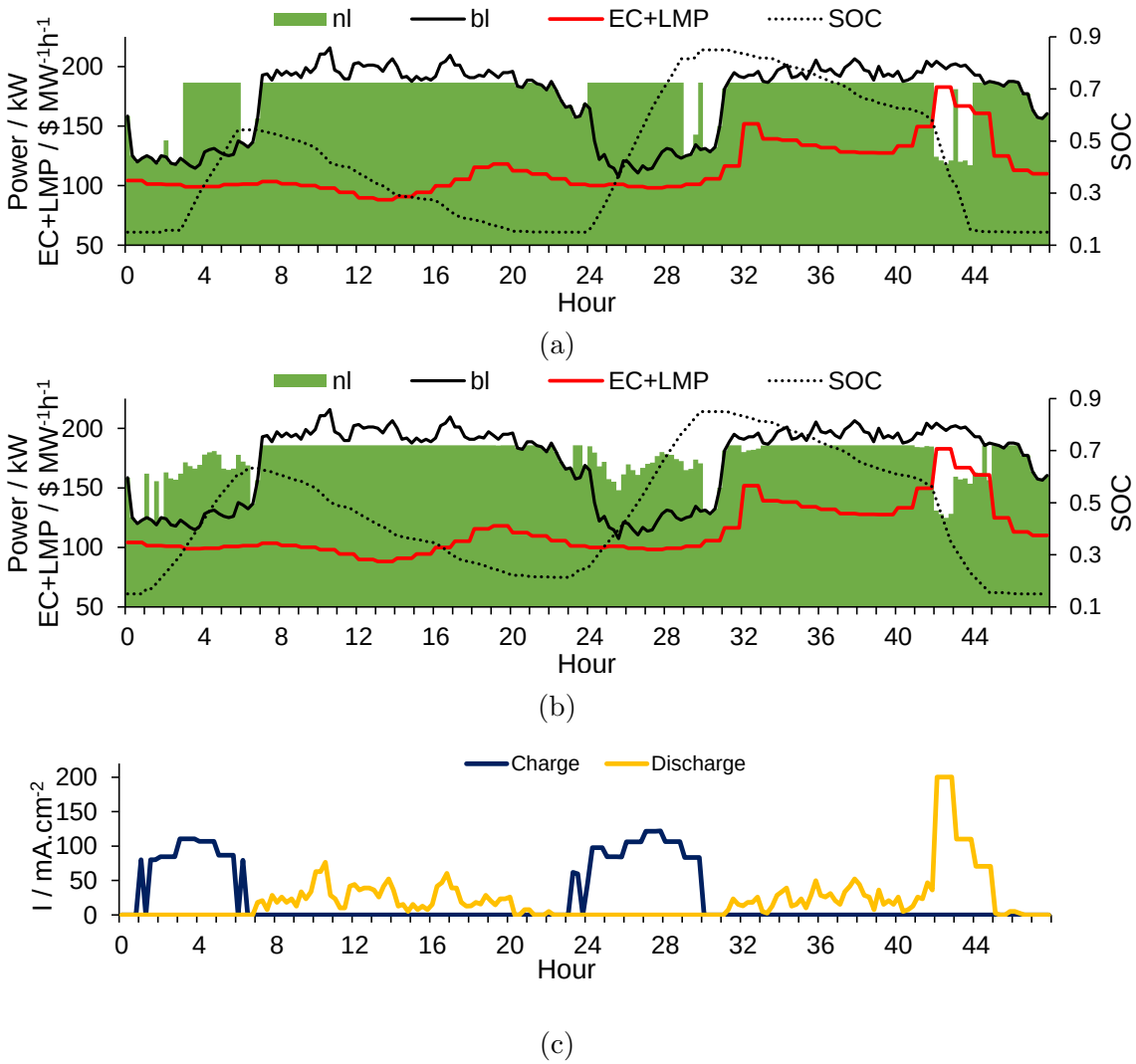

Figure 6.3: a) LP optimal operation for a 80 kW 4 h VRFB on 8th and 9th January. b) MIQP optimal operation for same BESS and day. c) Current density profile during MIQP operation.

In the LP optimal solution, on the first day the VRFB is charged at the highest power possible without compromising the peak shaving in the electricity price trough from hour

4 through hour 6. In the MIQP solution, the charging in these hours is reduced, and charging is carried out in hours 2, 3 and 7 as well. The slightly higher cost of electricity in hours 2, 3 and 7 ($\$101\,\mathrm{MW}^{-1}\,\mathrm{h}^{-1}$ versus $\$99\,\mathrm{MW}^{-1}\,\mathrm{h}^{-1}$ in hours 4 though 5) is more than compensated for by the higher efficiency that comes from moving the charging current closer to the optimal value of $74\,\mathrm{mA\,cm}^{-2}$ seen in Figure 6.2. Similarly, on the second day there is less peak shaving requirement, and the evening electricity price is high, so arbitrage is performed. The MIQP optimal solution entails spreading the discharge out to include hour 45 despite the slightly lower price here.

Although the charging current is close to the optimum, the discharging current is often well below it due to the peak shaving requirements. As the VRFB starts and ends the two days at 0.15 SOC, the round trip energy efficiency may be calculated by dividing the total discharged power by the total charging power. The round trip energy efficiency for the example days shown in Figure 6.3 was calculated to be 0.800. Across the whole year, the simulated operational AC efficiency was 0.786. This is above the higher value of 0.800 DC / 0.770 AC applied in the sensitivity study in Section 5.5.2. It is important to note that when the VRFB is required to operate at low current, the energy throughput is also low, so the low efficiency is assigned a low weighting in the overall performance.

6.5 Cost Benefit Analysis on Electrode Area

As the VRFB efficiency profile is expressed dynamically in the MIQP formulation, it is possible to study the optimal electrode area for a VRFB in this particular application. In the preceding economic analyses, the price of the VRFB was modelled under the assumption that it could cycle at maximum power (defined by the inverter rating) while achieving a 0.75 DC efficiency. In Figure 6.2 it can be seen that such a system could provide considerably higher output while achieving a DC efficiency of greater than 0.72. This approach is attractive because in the peak shaving application the battery operates at its maximum power output for only a small fraction of time anyway.

In the economic model, the power output of the VRFB was kept constant, but the

system cost recalculated by altering the maximum current in the stack area calculation in Equation (3.11) to the values in Table 6.2.

Table 6.2: Different electrode area cases for 1 kW of VRFB output and the corresponding maximum current densities for charge and discharge. 0.361 $m^2\,kW^{-1}$ is the base case used so far.

Electrode Area $m^2\,kW^{-1}$	$\bar{I}_s^d$ mA	$\bar{I}_s^c$ cm^{-2}
0.528	150	118
0.361	219	169
0.293	270	205
0.247	320	240

The impact on DC price per kW and turnkey price per kW h is shown in Figure 6.4.

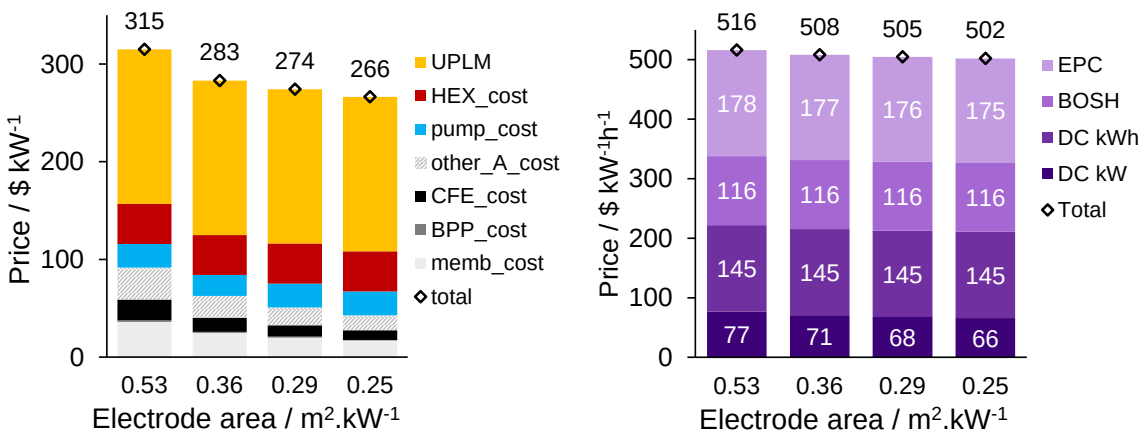

(a) (b)

Figure 6.4: a) DC boundary price of 1 kW of VRFB power under different electrode area cases.b) Turnkey price of 1 kW h of VRFB at 4 h duration.

The impact on system price is quite small as in the near term scenario the cost of the components that scale with area form a small proportion of the overall turnkey system price. The simulated operational efficiencies for 80 kW/2 h and 80 kW/4 h duration VRFB systems under each electrode area scenario are shown in Figure 6.5 along with the NPV resulting from a 10 year project.

The operational efficiency of the 4 h VRFB drops from a maximum of 0.790 at the largest electrode area to 0.773 at the smallest, and the 0.29 $m^2\,kW^{-1}$ gives the highest NPV by a very small margin. The 2 h VRFB however has a maximum efficiency of 0.780 at

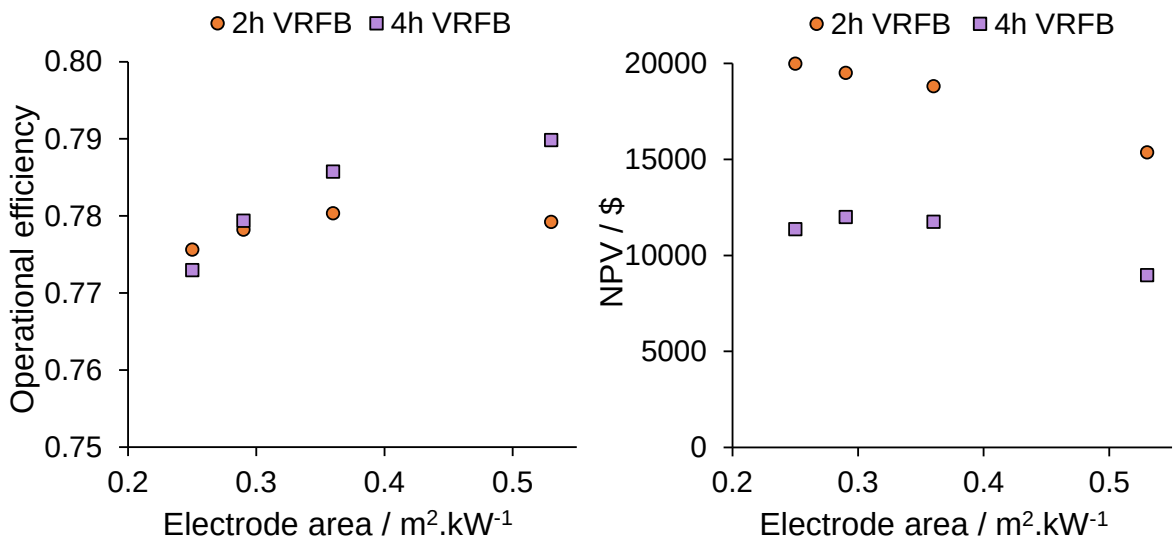

(a) (b)

Figure 6.5: a) Operational efficiency and b) NPV as a function of the electrode area and VRFB duration.

the base case electrode area of $0.36\,\mathrm{m^2\,kW^{-1}}$, and actually drops slightly to 0.779 when the electrode area is increased. The difference in efficiency profiles is due to the differing optimal operation at the two durations, which may be explained by reference to the $0.53\,\mathrm{m^2\,kW^{-1}}$ scenario where the difference is greatest. Histograms showing the distribution of current density during charging and discharging are shown for both durations in Figure 6.6.

During both charging and discharging, the 2 h duration VRFB displays more frequent operation at low current density. The difference is more pronounced during discharging, where the 4 h system very rarely discharges in the range $10\,\mathrm{mA\,cm^{-2}}$ to $20\,\mathrm{mA\,cm^{-2}}$, whereas the 2 h system frequently does.

This is due to the economic obligation to perform peak shaving. For example, as the load peak shown in Figure 6.3 is around 12 h long, both systems need to operate far below their maximum power output to deliver a flat net load. However, the 2 h system has to de-rate to a greater extent. The effect is not so pronounced at smaller electrode areas because the whole distribution is shifted to higher current densities.

The NPV predicted for the 4 h VRFB increases slightly when the electrode area is reduced to $0.29\,\mathrm{m^2\,kW^{-1}}$, but beyond this the drop in revenue due to the reduced efficiency offsets the CAPEX reduction. For the 2 h VRFB, the monotonic increase in NPV with

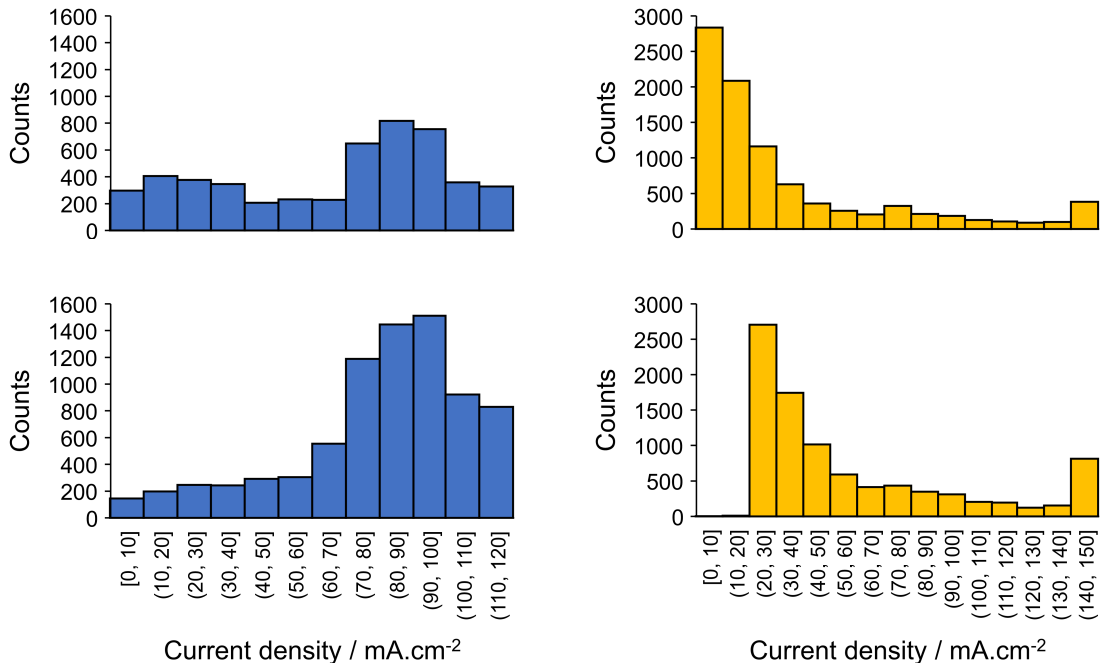

Figure 6.6: Histograms showing distribution of current density across all 15 min periods in the year for 2 h and 4 h duration VRFB. Left: charge, Right: discharge, Top: 2 h, Bottom: 4 h.

decreasing electrode area is more marked, as the components priced by area form a larger proportion of the overall CAPEX at shorter duration, and the revenue drops of more slowly for the reasons explained above.

In the preceding analysis it is assumed that pumping losses do not change as the electrode area is changed. In reality, if the electrode area is reduced while keeping the aspect ratio constant, the pump load will increase as the same same electrolyte flow must be pushed through a smaller cross section. Given the small contribution of pumping losses shown in Figure 6.2 it is not expected that this assumption leads to significant error. In practice, resizing the electrode would require a more detailed optimisation of the trade off between a long electrode to minimize shunt currents and a short electrode to minimise pump load.

6.6 Improving VRFB Efficiency With Independent Scheduling of Sub-Modules

Despite the efficiency aware optimisation achieved by the MIQP model introduced in Section 6.4, there is still a small efficiency performance gap when compared to the maximum predicted efficiency of 0.812 shown in Figure 6.2. This is primarily due to the nature of peak shaving, whereby the power required to achieve a flat net load varies with the load profile and there will be some periods where a very low power output is required, as exemplified in fig. 6.3. One option to reduce the low power commitments is to use several smaller modules. At low power requirement, some modules could be kept idle so that the few that are active would operate at a higher current. This problem is commercially relevant as several VRFB manufacturers are selling modular systems of around 10 kW (see Table 2.1) as opposed to larger bespoke systems, but to the best of the author's knowledge no research on this topic has been published.

In a large system, it would likely be excessive to specify independent control at the module level, and so modules may be paired or grouped to achieve a sensible trade-off between optimality of efficiency and complexity of the control system. The modular approach was tested by splitting the 80 kW 4 h system into two and three sub-systems. Given that this split increases the number of variables in the optimisation problem, a sensitivity study was first carried out on the required solution time, using the base case electrode area of $0.36\,\mathrm{m^2\,kW^{-1}}$. The results of this exercise are shown in Figure 6.7.

When the RFB is split into two modules, the operational efficiency of the battery continues to increase out to 20 s solve time, but shows negligible improvement at 40 s. When split into 3 modules, the solution improves at least until 40 s. For the base electrode area scenario, splitting the system into two independently controlled units results in an efficiency gain of just under 1 percentage point. Splitting into three modules gives a slightly higher efficiency at the longest solution time. A better solution may be obtainable with longer solve times and a greater number of modules, but the benefit is expected to be limited, and the time to run the simulations would be considerably longer. Hence the

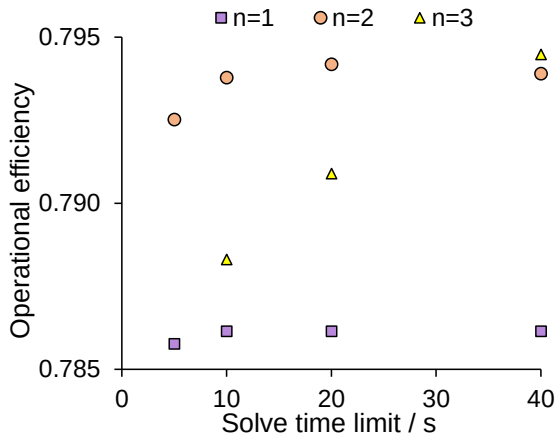

Figure 6.7: The variation in modelled operational efficiency of a 80 kW/4 h VRFB with $0.36\,\mathrm{m^2\,kW^{-1}}$ electrode area when divided into 2 or 3 sub-modules. Note: for the 3 module system the solver failed to find a feasible solution within the 5 s time limit in some instances.

two module case is studied in the rest of this section.

The optimal schedules for the two modules at 20 s solve time are shown in Figure 6.8 for the example day of the 2nd January. It may be observed in Figure 6.8c that although the overall power output during peak shaving does not change, the current density does. When the power requirement is low, then one of the two modules will be idled and the current density on the remaining module will be double that seen in Figure 6.8b. The lowest current density at which the solver activates both units is $58\,\mathrm{mA\,cm^{-2}}$. This may be understood by inspection of the efficiency profile in Figure 6.2, which shows that this is the highest current density where doubling the current density (turning one module off) would not lead to a poorer efficiency.

In Figure 6.5a it was shown that for the 4 h duration VRFB increasing the electrode area from the base case of $0.36\,\mathrm{m^2\,kW^{-1}}$ to $0.53\,\mathrm{m^2\,kW^{-1}}$ did not change the efficiency considerably. This was due to the drop in efficiency at low power output cancelling out the increase at high power output. However, as the modular approach allows low power output to be avoided, this study was revisited, and the various electrode scenarios were retested, giving the results shown in Figure 6.9.

As expected, the uplift in operational efficiency when the system is split into two

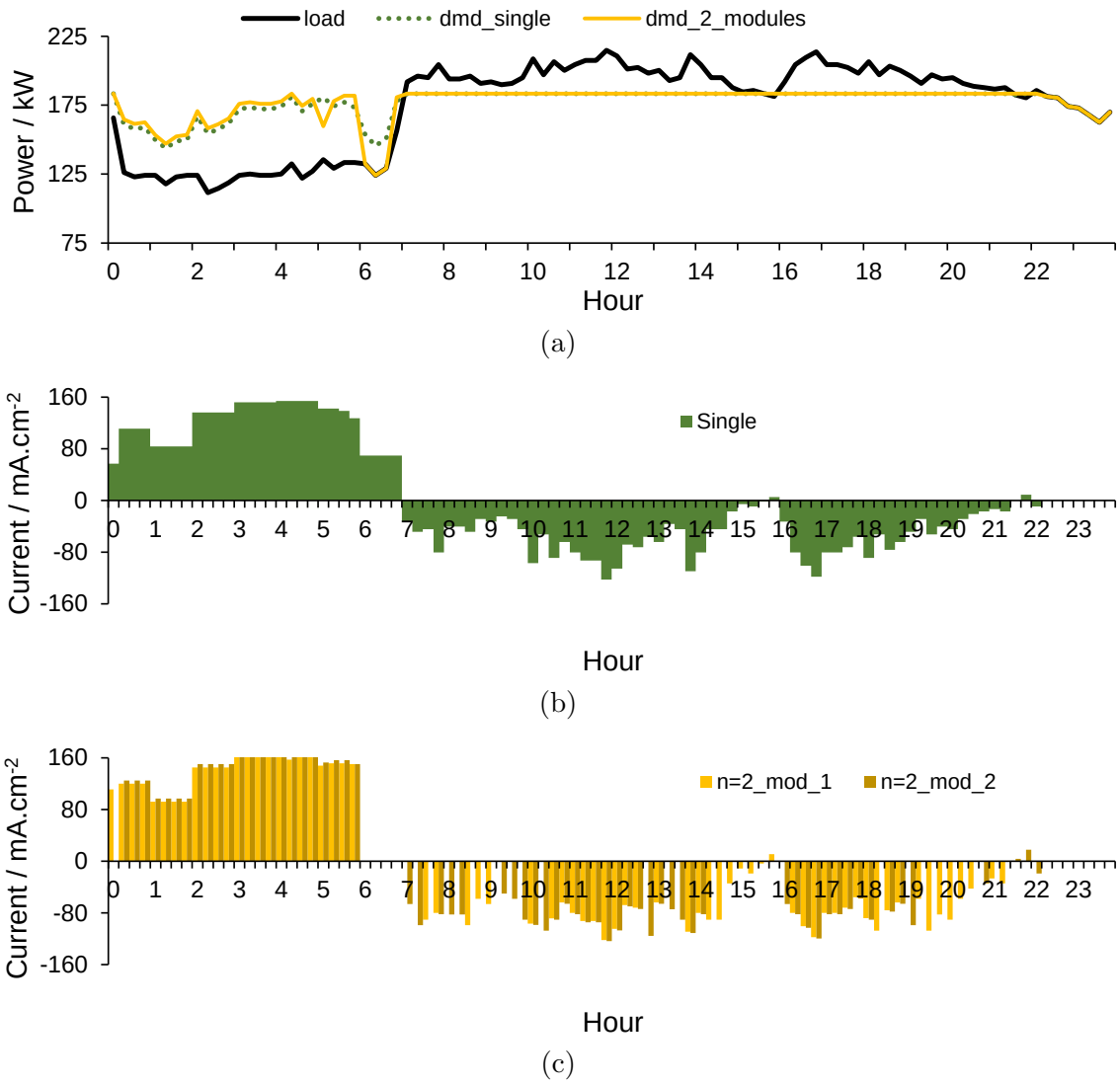

Figure 6.8: a) Comparison of optimal output of a 80 kW/4 h VRFB with 0.36 $m^2\,kW^{-1}$ electrode area on January 2nd when scheduled as a single module and as two modules. b) Optimal current density profile of single module. c) Optimal current density profiles for two modules.

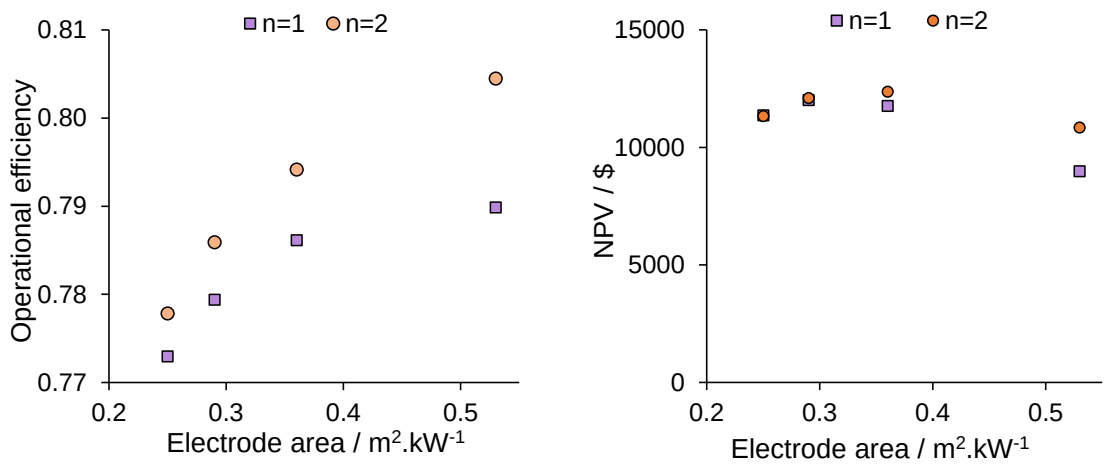

(a) (b)

Figure 6.9: a) Impact on efficiency of splitting 80 kW/4 h VRFB into 2 independently optimised modules under various electrode area scenarios. b) Impact on resulting NPV.

modules is greatest for the 0.53 $m^2\,kW^{-1}$ electrode area scenario. It is notable that the modelled average operational efficiency of 0.805 in this case is very close to the peak efficiency of 0.812 seen in Figure 6.2. Splitting the system into two modules alters the NPV optimum, with the 0.36 $m^2\,kW^{-1}$ design now predicted to give the highest NPV, albeit by a very small margin ($ 12368 versus 12097).

It is important to note that the above results are based on a single set of component cost assumptions. If lower prices for the stack components are realised, then the optimal electrode area will increase and vice versa.

6.6.1 Uncertainty in Fixed Losses

If the VRFB stack is required to supply 48 V rather than the 22 V - 29 V in the system parametrised here from [28], then the total shunt current may increase considerably. Xing *et al.* reported a 200% increase in shunt currents going from a 10 cell stack to a 20 cell stack [37] . Without a bottom up model it is not possible to determine what fraction of the coulombic loss in [28] is due to shunt currents and what fraction due to ionic crossover. Similarly, determining the scaling of shunt currents from 15-20 cells in [28] to the 33 or more required for 48 V is beyond the scope of this work. To test the impact of such an

increase, the coulombic loss was doubled from the 1.9 mA cm^{-2} applied in this work to 3.8 mA cm^{-2}. This leads to a reduced AC efficiency, particularly at low current density, as shown in Figure 6.10.

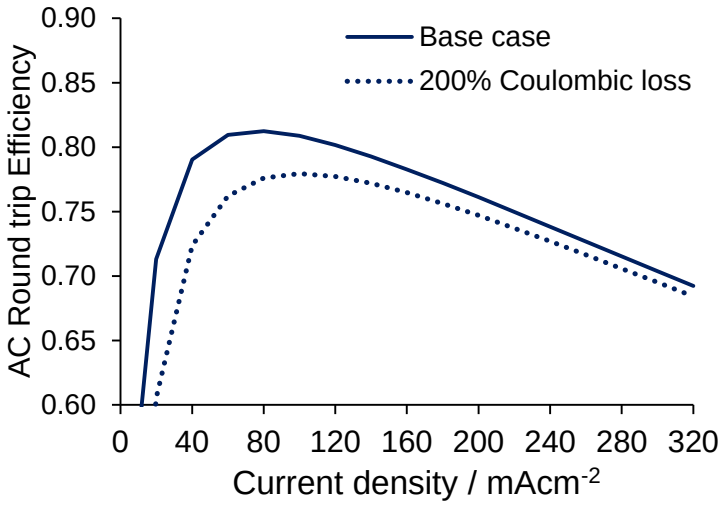

Figure 6.10: A comparison of efficiency profiles for the base case VRFB where a fixed coulombic loss of 1.9 mA cm^{-2} is assumed, and the scenario where the coulombic loss is doubled.

In this scenario the benefit of independent module optimisation is increased, as shown in Figure 6.11.

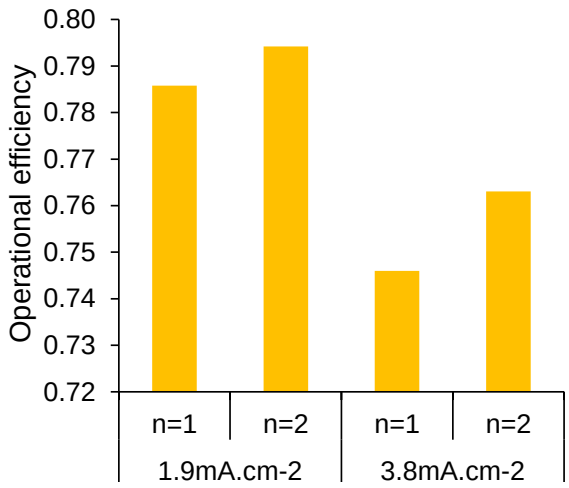

Figure 6.11: A comparison of the improvement to operational efficiency of a 80 kW/4 h VRFB due to modular control (n=2) when the coulombic losses are 1.9 mA cm^{-2} and 3.8 mA cm^{-2}.

In the base scenario the simulated operational efficiency went from 0.786 to 0.794 when the VRFB was split into two modules, an increase of 0.8 percentage points. In

the increased coulombic loss scenario the efficiency increases from 0.746 to 0.763, 1.7 percentage points. In Chapter 5 economic comparisons between LIB and VRFB were reported for the case where the VRFB DC efficiency is increased from 0.75 to 0.80, giving a 0.767 AC efficiency. By employing a modular control approach, the VRFB could achieve an efficiency very close to this value even if the full size stack has twice the coulombic losses of the modelled system. This would not be the case if the VRFB consisted of a single module, or multiple modules without independent control.

The same principle would also apply to pumping losses, for example, if the pump efficiency estimate of 0.6 is not achievable.

6.7 The Impact of Voltage Constraints on High Current Operation

While it may be desirable to increase the maximum current density in the stack, e.g. for the 2 h duration case in Section 6.5, there may be practical limitations to this approach. At higher current densities a larger over-potential is generated, so there is both the risk of hitting too high a voltage during charging and the possibility of hitting the low voltage cutoff prematurely. So far in this work, it has been possible for the VRFB to charge at the maximum current even at the highest SOC. This approach was used in [28], where in the highest current density case, the VRFB was charged until SOC 0.85 at 1.85 V. However, overcharging may lead to water splitting as a side reaction. This results in reduced coulombic efficiency, but more importantly electrolyte fade, as discussed in Section 2.1.3. The evolved gases can also cause a range of problems as described in [33] and [36]. The particular cell-voltage at which this side reaction initiates will depend on the particular electrode and electrolyte chemistry of the system.

Appropriate limits on voltage were estimated by reference to a commercial module produced by a company exploiting the PNNL mixed acid electrolyte [14]. The 14 kW module has a voltage range of 42 V to 67.2 V. Given that the evolution of macroscopic

bubbles of hydrogen and oxygen was reported to initiate at 1.70 V in [148], the number of cells in the stack of the commercial system was assumed to be 40, which gives an upper voltage limit of 1.68 V. The lower cell voltage limit is hence 1.05 V. To test whether these constraints might reduce the utility of the VRFB, the maximum and minimum voltages were calculated for the smallest electrode case in Section 6.5. The parameters a and b describing the gradient and intercept of the linear approximation of OCV versus SOC in eq. (6.11) were set at 0.267 and 1.33 respectively [17].

While discharging, given that the SOC is already constrained to be >0.15, the minimum voltage that could be reached at the highest discharge current density considered is 1.33 V + 0.15 x 0.267 V - 0.026 V - 320 mA cm^{-2} x 0.000 627 mΩ cm^2 = 1.14 V. Further constraining the minimum voltage is therefore unnecessary.

During charging, the maximum voltage according to the MIQP model is 1.33 V + 0.85 x 0.267 V + 0.026 V + 240 mA cm^{-2} x 0.000 627 mΩ cm^2 = 1.73 V. As this exceeds the 1.68 V limit, the constraint defined by Equation (6.12) was added.

The optimal electrode area scenario for the 4 h VRFB was also analysed (0.36 kW m^{-2} as shown in Figure 6.9b). In this case the maximum current density is already capped at 169 mA cm^{-2}, giving a maximum possible charge voltage of 1.69 V.

The relevance of the upper voltage constraint is shown in Figure 6.12, where the constraint is superimposed on scatter plots of 15 min charge current density versus SOC taken from the unconstrained case.

Figure 6.12 shows that without the voltage constraint there are very few instances in which the charging voltage exceeds 1.68 V, especially at 4 h duration.

The restriction on charging voltage does not reduce the revenue by a meaningful amount. For the 2 h VRFB the predicted NPV is reduced from \$ 20288 to \$ 20024. For the 4 h VRFB from \$ 11775 to \$ 11733. Given that only one point in the unconstrained 4 h VRFB schedule is outside of the boundary, it is surprising that even this small difference occurs. It is possible that the constraint is influencing the heuristics of the optimisation process in other ways.

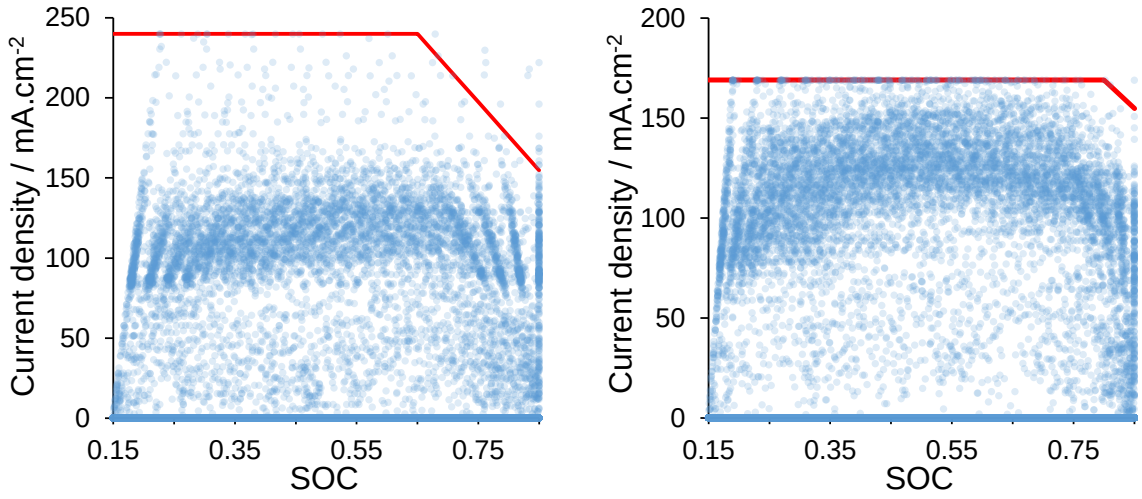

(a) (b)

Figure 6.12: Scatter plots of one year of 15 min charging current density versus SOC data for a) 2 h and b) 4 h VRFB operating without an upper cell voltage constraint. Each plot is superimposed with the minimum of the inverter constraint and the 1.68 V cell voltage constraint to show which schedule points would be forbidden by the latter.

The above results were obtained for a single module VRFB. Although in principle a VRFB with two modules could operate one module at more than the bound due to the inverter rating, this would not happen in the optimal schedule, as it was shown in Section 6.6 that above 58 mA cm^{-2} the optimal solution involves activating both modules.

It is foreseeable that there will be certain situations where the importance of such constraints increases, for example where the duration of the VRFB is longer and it would therefore have to charge at high current density for longer in the limited load trough. Also, if the area specific component costs were higher than modelled here, a smaller electrode area would be more attractive, resulting in higher current densities.

6.8 Conclusions

- In this chapter it has been estimated that the VRFB reported by PNNL is capable of operating at up to 0.86 round trip DC efficiency or 0.81 AC efficiency. Applying the introduced MIQP optimisation allows the best trade-off to be made between high current to exploit extreme prices, and moderate current to maximise efficiency.

At site 281, while performing peak shaving and energy arbitrage, the operational efficiency of the 80 kW/4 h is simulated at just under 0.79.

- For the present component price assumptions, a 2 h VRFB has a smaller optimum electrode area than a 4 h VRFB. This is partly because the stack components make up a greater fraction of the overall cost in the 2 h system. The other reason is that the 2 h system exhibits less drop-off in efficiency as electrode area is reduced. This is because decreasing efficiency at high power output is compensated for by increasing efficiency at low power output, which is more frequent for the 2 h while peak shaving.

- The existence of a peak in the efficiency versus current density plot in Figure 6.2 inspired the hypothesis that modularity can improve the operational efficiency further. This was studied by modelling the splitting of an 80 kW VRFB into 2 and 3 modules. By optimising the schedule of each module independently using the introduced formulation, the hypothesis was shown to be valid. The gain comes from idling one module when the current density falls below a threshold. For the 4 h VRFB, at the optimal electrode area, the efficiency was simulated as increasing from 0.786 to 0.794. The benefit of this approach is higher at the maximum electrode area, as this is where the lowest current densities are seen without the modular approach.

- When scaling up to a 48 V stack, the coulombic losses due to shunt current will likely increase. In a test where the coulombic loss was doubled, the multiple module optimisation showed a greater benefit, raising the operational efficiency from 0.746 to 0.763, which is just under the higher value (0.767) assumed in Chapter 5.

- Introducing an upper voltage constraint to avoid conditions which may damage the VRFB has very little impact on the overall performance, and was practically negligible for the 4 h system. This is due in part to the charge current already being capped by the inverter rating (to which the maximum discharge power is matched). It is also due to the MIQP operation which spreads out charging to maximise efficiency.

Chapter 7

A Comparison of LIB and VRFB Economics in Support of Self-Sufficiency from on-Site PV

7.1 Introduction

The results in Chapter 5 showed that VRFB are far more likely to exceed the economic potential of LIB when the required cycle count is high, but that such cycle rates do not currently arise in a market context in California. Higher cycle rates are likely to arise when an electrical grid domain moves to high PV power penetration. In a market context, the higher cycle rate would be stimulated by depression of the midday price and/or an increase in the price at other times, particularly the evening when demand is typically highest. Some evidence of this hypothesised effect is already being seen in domains with high PV penetration[149], but it is difficult to deconvolute from other factors, and even more difficult to extrapolate. In a micro-grid context, although the goal might be the same - to supply power demand reliably from variable renewable power - the problem may be studied without reliance on price data. Instead, a metric that captures the ability to match demand is typically used, such as self-sufficiency or self-consumption [150]. In this chapter the cost of providing self-sufficiency for site 281 is studied. Previous studies

have used the levelised cost of storage (LCOS) metric to explore the relative economics of different BESS under assumed cycle rates, but these tend to lack a sizing optimisation step. Additionally, the cycle rate will depend on the sizing, with longer durations resulting in lower cycle rates, which is an important consideration for LIB.

For an electrical grid based on variable renewable power the relationship between levelised cost of electricity and % of renewable energy in the generation mix is non-linear, and the cost v self-sufficiency gradient increases with the latter [151]. The same principle applies to self-sufficiency in a micro-grid context [86]. The exact shape of the profile will depend on the periodicity of the renewable power output. Southern California is an attractive location for 100% renewable energy projects, as the seasonal variation in solar irradiance is relatively minor, hence a shorter duration storage should be required than in higher latitudes or areas with more variable weather.

Given that self-sufficiency and levelised cost of storage are both important objectives, this chapter focuses on the use of grid searches to estimate the Pareto set of power/duration points for each BESS type, where a better result in one objective cannot be achieved without sacrificing the other objective [152]. For the grid search, the linear programming optimisation described in Section 7.2.2 is used for both BESS types.

In Section 7.2.1 the assumptions underpinning the modelling work are described.

In Section 7.3, the case-study involves installing the BESS at site 281 to increase the self-consumption of PV from a pre-existing rooftop installation. The levelised cost of storage is compared for each BESS type, based on the incremental PV consumed on-site.

In Section 7.4, the study is expanded to include the sizing of the PV installation, as the benefit of increasing the size will be different for the VRFB and LIB due to the differing round trip efficiencies. Within this section, the Pareto fronts for LIB and VRFB under the base scenario are first compared in detail in Section 7.4.1. In Section 7.4.2 a sensitivity study is performed on the impact on the economic comparison of changing the following parameters: Climate, Projected LIB price, VRFB electrolyte leasing, VRFB EPC costs and VRFB stack cost. In Section 7.4.3 the impact of modifying the optimal operation to

avoid unnecessary high SOC for the LIB is demonstrated.

In Section 7.5 the model for hybrid BESS optimisation introduced in Section 7.2.4 is applied to check whether deploying a system combining LIB and VRFB can reduce the cost of self-sufficiency.

In Section 7.6 the MIQP model for SSR optimisation introduced in Section 7.2.3 is applied to study the optimal behaviour of the VRFB.

Lastly, the base scenario comparison of LIB and VRFB is repeated for a second site in order to check whether the findings are consistent.

7.2 Methods

In this section an MILP method for maximising the self-sufficiency of a site with BESS and PV installed is first introduced. Next, the MIQP formulation for variable VRFB efficiency defined in Section 6.2 is incorporated within the use-case. Lastly, a novel MILP model for a hybrid LIB:VRFB system is introduced, which uses penalty terms to drive preferential charging of the VRFB.

7.2.1 Model Assumptions

In this chapter both MILP and MIQP optimisation methods are used to maximise self-sufficiency. In both cases the optimisation assumes that all demand is equally important to satisfy.

For the VRFB, the AC efficiency of 0.71 used in Chapters 4 and 5 was revised to 0.78 given the findings on operational efficiency in Chapter 6.

In the interest of balance, the LIB efficiency was also revised. Literature data on internal resistances for an NMC cell similar to the one tested by Schmalstieg *et al.* [102] were obtained from an experimental study [153], summed and used to calculate the round trip efficiency at various C-rates, as shown in Figure 7.1. In doing this, it is assumed that,

unlike in the VRFB, there are no fixed losses associated with the LIB system at the DC boundary, and that the coulombic efficiency is 100%.

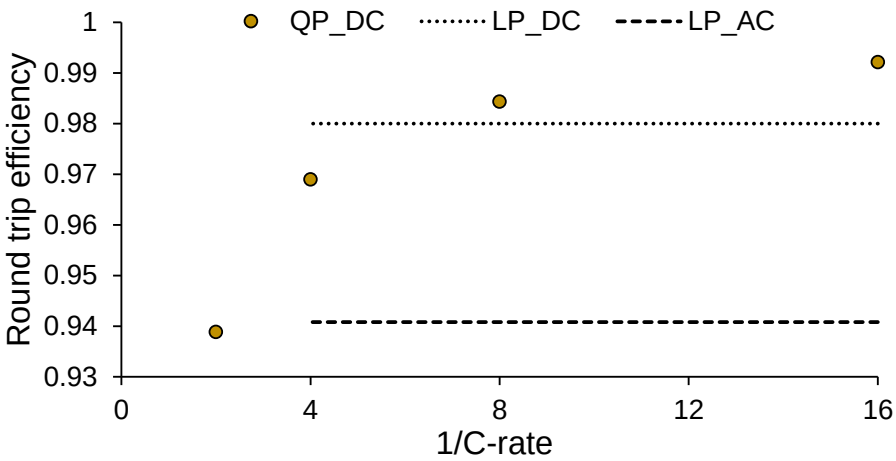

Figure 7.1: Approximation of round trip efficiency for a 2.6 A h Li-ion cell using a quadratic model, and the linear approximation applied in this chapter where studied durations are >4 h.

Initial scoping work for the following case study showed that the optimal duration for self-sufficiency from PV is greater than 4 h. Therefore, the round trip efficiency of the LIB will only vary between 0.97 and 0.99, and assuming a DC round trip efficiency of 0.98 will only lead to +/- 1% error across the entire output range. It is hence appropriate to use a MILP approach, which has the benefit of reducing the optimisation time considerably as the relaxation required for the quadratic equality constraint described in Section 7.2.3 can be avoided. The AC efficiency applied here is slightly higher than the 0.90 advertised for a commercial turnkey system at C/4, and this the discrepancy is probably due to additional parasitic loads such as cooling. Such losses are not included for the VRFB either. This matter is discussed further in Section 8.1.

In this case study the inverter is sized to the maximum BESS discharge power. In situations where high self-sufficiency is being targeted, the BESS power rating is considerably higher than the building load, and power transfer from the PV array to the BESS could be done by DC. Hence the inverter cost is likely higher than necessary. The cost is also based on bidirectional power conversion, and this would not be necessary in a pure self-sufficiency scenario.

7.2.2 MILP Formulation for Maximising PV Self-Sufficiency Ratio

The following MILP formulation was applied to analysis of both LIB and VRFB systems as performed in Chapter 7.

The net load at the site at time t is first defined by:

$$nl_t = bl_t - P_t^{PV} + c_t - d_t \tag{7.1}$$

Where P_t^{PV} is the power output of the photo-voltaic array. The continuous positive variables for net import and net export $P_t^{Imp.}$ and P_t^{Exp} are next introduced. These are then constrained to take the value the nl_t when appropriate and 0 otherwise by:

$$nl_t = P_t^{Imp.} - P_t^{Exp.} \tag{7.2}$$

and:

$$P_t^{Exp.} - M(\delta_t^{Exp.}) <= 0 \tag{7.3}$$

$$P_t^{Imp.} - M(1 - \delta_t^{Exp.}) <= 0 \tag{7.4}$$

Where $\delta_t^{Exp.}$ is a binary indicator variable which takes the value 1 for export and M is an arbitrarily large constant. The constraints in Equations (7.2) to (7.4) are taken from [154]. [1]

The objective of maximising self-sufficiency is identical to minimising imports, and is hence defined by:

$$minimise(\tau \sum_t P_t^{Imp.} - SOC_{final}C.Pen._{Fill} + SOC_{mean}C.Pen._{Delay}) \tag{7.5}$$

The second and third terms in the objective are penalties for controlling SOC. The first

[1]Note: care must be taken when setting M in this case study, as it must be larger than the possible import or export across all PV array sizes and load profiles studied otherwise there may not be a feasible solution.

of these ensures that when there is an overall surplus of PV in the optimisation window, the BESS will store as much of it as possible. SOC_{final} is the SOC in the last period of the optimisation window, and $Pen._{Fill}$ is the penalty term which was set at 0.1. The second penalty ensures that if there is a greater surplus than the BESS can store, the BESS is charged as late as possible so that SOC_{mean}, the mean SOC, is minimised. For LIB systems, the penalty $Pen._{delay}$ was set to 0.01, so as to be secondary to the carry-over incentive. This is not relevant to the VRFB, so $Pen._{delay}$ is set to 0. The BESS capacity C is included for consistency of units.

The self sufficiency ratio is subsequently calculated by:

$$SSR = 1 - \frac{\tau \sum_t P_t^{Imp.} + E_{rebal.}C}{\tau \sum_t bl_t} \tag{7.6}$$

Where $E_{rebal.}$ is the energy cost of continually rebalancing 1 kW h of VRFB capacity, defined by removing the price terms from Equation (3.2).

Of course, in a true islanded system, the power import would be a deficit, but this makes no difference to the mathematical representation.

7.2.3 MIQP Multiple VRFB Module Formulation

The MIQP, multi-module version of the formulation is defined by replacing the definition of net load in Equation (7.1) with:

$$P_t^{Imp.} = bl_t - P_t^{PV} + \sum_s P_{s,t}^{RFB} \tag{7.7}$$

With $P_{s,t}^{RFB}$ as defined in Equation (6.3). This complicates the model formulation as equality constraints are non-convex. This issue is dealt with on-board by the Gurobi solver using a bilinear relaxation, but the solve time increases.

7.2.4 Hybrid System MILP Formulation

In the self-sufficiency case-study in Chapter 7, the benefit of hybrid BESS comprising LIB and VRFB is studied. In order to do this the definition of nl_t in Equation (7.1) was adapted, with the discharge power d_t being replaced with $d_{VRFB,t} + d_{LIB,t}$ etc. In order to ensure that the VRFB is cycled preferentially, it was necessary to introduce a new objective defined by:

$$\begin{aligned} minimise(\tau \sum_t P_t^{Imp.} + Pen._{priority} \tau \sum_t d_{LIB,t} - \\ (SOC_{final,LIB} + SOC_{final,VRFB}) C.Pen._{Fill} + SOC_{mean,LIB} C.Pen._{Delay}) \end{aligned} \tag{7.8}$$

By setting $Pen._{priority}$ to 0.8, the penalty was larger than the loss in self-sufficiency due to the lower round trip efficiency of the VRFB, but not large enough to prevent the LIB cycling if the VRFB is full.

7.3 Economic Comparison of LIB and VRFB in a Constrained PV Scenario

So far in this work, the case studies have centred on Site 281, which is classed as "Grocer/Market". This building has a floor area of 4543 m^2, and it is assumed that it is a single storey building, hence has the same roof area. Following [155] a usable fraction of 70% is assumed . Multiplying the usable area by an assumed efficiency of 20% results in a PV rating of 636 kWp. The output of this solar array was modelled at 36.62° latitude and −116.3° longitude for 2012 using the PVGIS satellite image irradiance model [156]. The slope and azimuth of the panels were assumed to be 10° and 0° respectively, and it is assumed that there is negligible horizon impingement. The total annual output of the PV array is modelled as 1123 MW h, compared to the total consumption of 1584 MW h, meaning that a maximum SSR of 71% is achievable. The SSR with no BESS installed is 43%. There are no buildings in the data set that have a higher floor area to average load

ratio.

In this section, it is assumed that the PV is already installed, hence the metric of interest is the LCOS, the cost of the additional electricity that is made available to the site by installing a BESS.

Although tools such as the genetic algorithm NSGA II are able to find this set unsupervised, in the author's experience the process can take several hours even when the time to evaluate a single point is a few seconds. Given that the time to evaluate one power/duration point is 10 min it was deemed faster to perform the search manually, starting with the BESS power rating of half the peak surplus PV.

The Pareto fronts of the sets shown in Figure 7.2 exhibit a minimum for both BESS types because as the duration is increased from 4 h, the marginal cost of storage (see Figure 5.2) initially falls faster than the marginal energy throughput. Above a certain point however the drop in energy stored accelerates as the sides of the PV surplus parabola are reached. This inflection point is reached at progressively shorter durations as power rating is increased.

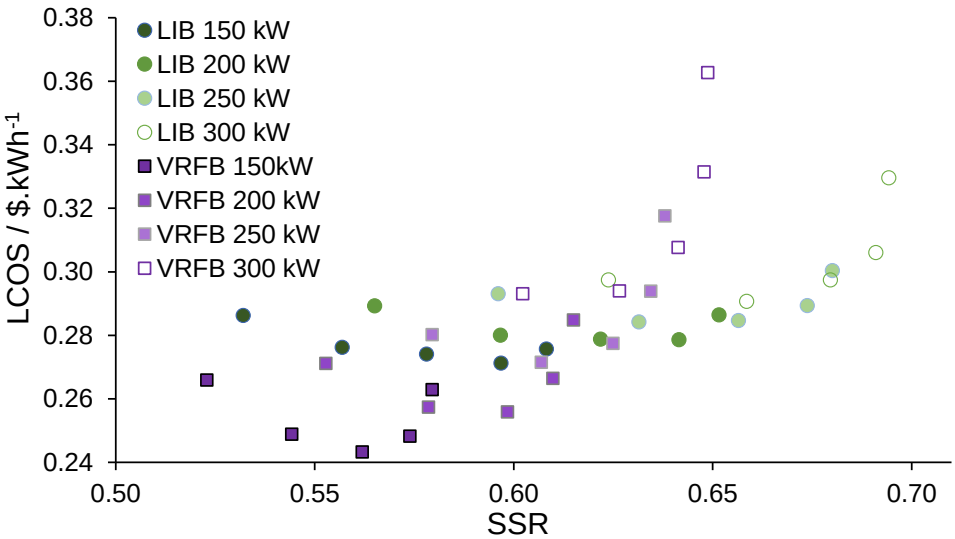

Figure 7.2: Levelised cost of storage versus self sufficiency ratio for LIB and VRFB systems retrofitted at site 281 to increase self consumption of rooftop PV. At each power rating, usable durations of 4, 5, 6, 7 and 8 h were simulated (shortest duration gives lowest SSR). The maximum theoretical SSR is 71% and the SSR with no BESS installed is 43%.

It can also be seen in Figure 7.2 that when a smaller BESS is specified, the VRFB is the

more economical choice, giving a lower LCOS for a given SSR. However, once the BESS are sized to provide SSR greater than approximately 0.6, the LIB becomes preferable. There are two factors at play here, the first being cycle rate. The cycle rate is higher for the smaller BESS, as the PV surplus is frequently greater than the BESS capacity, hence the battery will fill and discharge on most days. For example, at 150 kW / 6 h duration, the VRFB and LIB perform 0.58 and 0.69 EFC per day respectively, or 0.83 and 0.86 cycles relative to the restricted SOC ranges. This high cycle rate leads to replacement of the LIB after 5 years and 7 months. Given that the BESS durations in this application are longer than in the case study in the preceding chapters, degradation carries a higher cost.

As the BESS size is increased, the cycle rate decreases, as the number of days on which the battery may be filled with PV decreases. At 200 kW / 6 h, where the LIB becomes the preferred BESS, the VRFB and LIB are performing 0.55 and 0.66 EFC per day respectively, and the LIB gains 5 months of life.

The second factor, round trip efficiency, becomes more important at high SSR, where PV output is the limiting factor. As the VRFB has a lower efficiency, for a given power/duration specification it can never deliver as high an SSR as the LIB if there is an overall deficit of PV power. This can be seen in the trends of LCOE versus SSR, with the VRFB line reaching a vertical asymptote at 65%, while the LIB line reaches a similar asymptote at 70%. Given that the SSR with no BESS is 43% the ratio of the improvement due to each BESS at 300 kW / 6 h ((65 - 43) / (70 - 43) = 0.81) is very similar to the ratio of their respective efficiencies (0.78 / 0.94 = 0.83).

This raises an issue for VRFB proponents - to achieve a high SSR the VRFB requires a larger PV array than the LIB in order to cover the additional round trip losses. This must hence be factored into the overall project economics. Of course, when aiming for high self-sufficiency, it will likely be necessary to have the array oversized for the majority of days in order to have sufficient supply on days with lower solar irradiance. This matter forms the subject of the next section.

7.4 A Comparison in a Non-Constrained PV Scenario

As long as the majority of days see an overall deficit of PV power, then the VRFB will be unable to reach the SSR that the LIB can, due to the greater losses. However, when there is an overall surplus of PV in a daily cycle, the losses become less important. However, for this to happen a larger PV installation is required, with an associated cost increase. The VRFB may catch up with the LIB considerably below 100% SSR if the PV output or load varies considerably from day to day, as there may be multi day periods of PV deficit which even considerable over-sizing cannot overcome.

In this section, the installed PV power is varied to study the overall economics of the project. Where the BESS is not the only component being installed in the project, it is appropriate to use levelised cost of electricity as a metric [86]. The cost of the PV installation (CAPEX and OPEX) is added to the numerator of the levelised cost calculation (Section 3.4.2), and the denominator is modified to be the combination of PV supplying the load directly and through the BESS. With the PV panels included in the cost analysis, it is more appropriate to model a 20 year project. To do this the following assumptions are made:

- Inverters are replaced in year ten [106] for the same cost as at the start of the project ($\$205\,\mathrm{kW}^{-1}$).
- VRFB stack kW components are replaced at end of year ten, using the cost of $\$283\,\mathrm{kW}^{-1}$ from Section 5.3.
- The first 640 kWp of PV is assumed to be installed on the roof, at a cost of $1650 per kWp, achieved by removing the inverter field from the 2020 price reported for commercial rooftop PV by NREL [106]. Additional PV is assumed to be ground mounted and cost $1280 per kWp, which is midway between the rooftop value and the utility scale fixed mount cost of $900 per kWp (excluding inverter) from the same source. To the total cost is applied the investment tax credit (ITC), which, for projects installed after 2023, will give a 10% rebate on PV installations [157].

- An annual PV O&M cost of \$19 kW^{-1}p is applied after [106].
- A discount rate of 5% is applied, as for the rooftop PV case in [106].
- The PV panel output decreases at a rate of 0.5% per year [158].

7.4.1 Base Scenario

The search for the LCOE/SSR Pareto front was first carried out using the base scenario parameters described in Chapter 5. The results for LIB and VRFB installations are shown in Figure 7.3.

In order to increase the SSR at the site, it is necessary to increase both the PV and the BESS energy capacity. As the duration is constrained by both the hours of PV surplus and the ability to discharge fully into the site load, the latte is primarily achieved by increasing the power rating. In the lower SSR range shown, the optimal duration is 7.5 h in some places, but at higher SSR 6.5 h/7 h is more typical.

At a given SSR target, the required VRFB capacity is greater than the required LIB capacity. For example, at 0.95 SSR, the optimal VRFB specification is 600 kW/7 h whereas the optimal LIB specification is between 500 kW and between 6.5 h and 7 h. This is due to the effective capacity of the VRFB being lower due to its lower efficiency. However, the installed PV capacity is the same in both cases, at 160% over-sizing. This is because the PV over-sizing is dictated primarily by the seasonal variation.

Despite the greater VRFB capacity requirement, in this scenario, the VRFB gives a lower LCOE than the LIB, and the gap is consistent across the Pareto front at approximately ¢0.7 kW^{-1} h^{-1}. This is slightly surprising, as the LIB cycle-rate is much lower at high SSR, which should benefit the LIB economics. The 400 kW/6 h LIB that delivers 0.875 SSR performs 0.698 EFC per day and requires replacement in 6 years and 9 months, whereas the 600 kW/6 h LIB that delivers 0.952 SSR performs 0.546 EFC per day and requires replacement in 7 years and 11 months. However, the larger capacity at high SSR means that although the cost is delayed, it is higher. Also, at high SSR the VRFB also benefits,

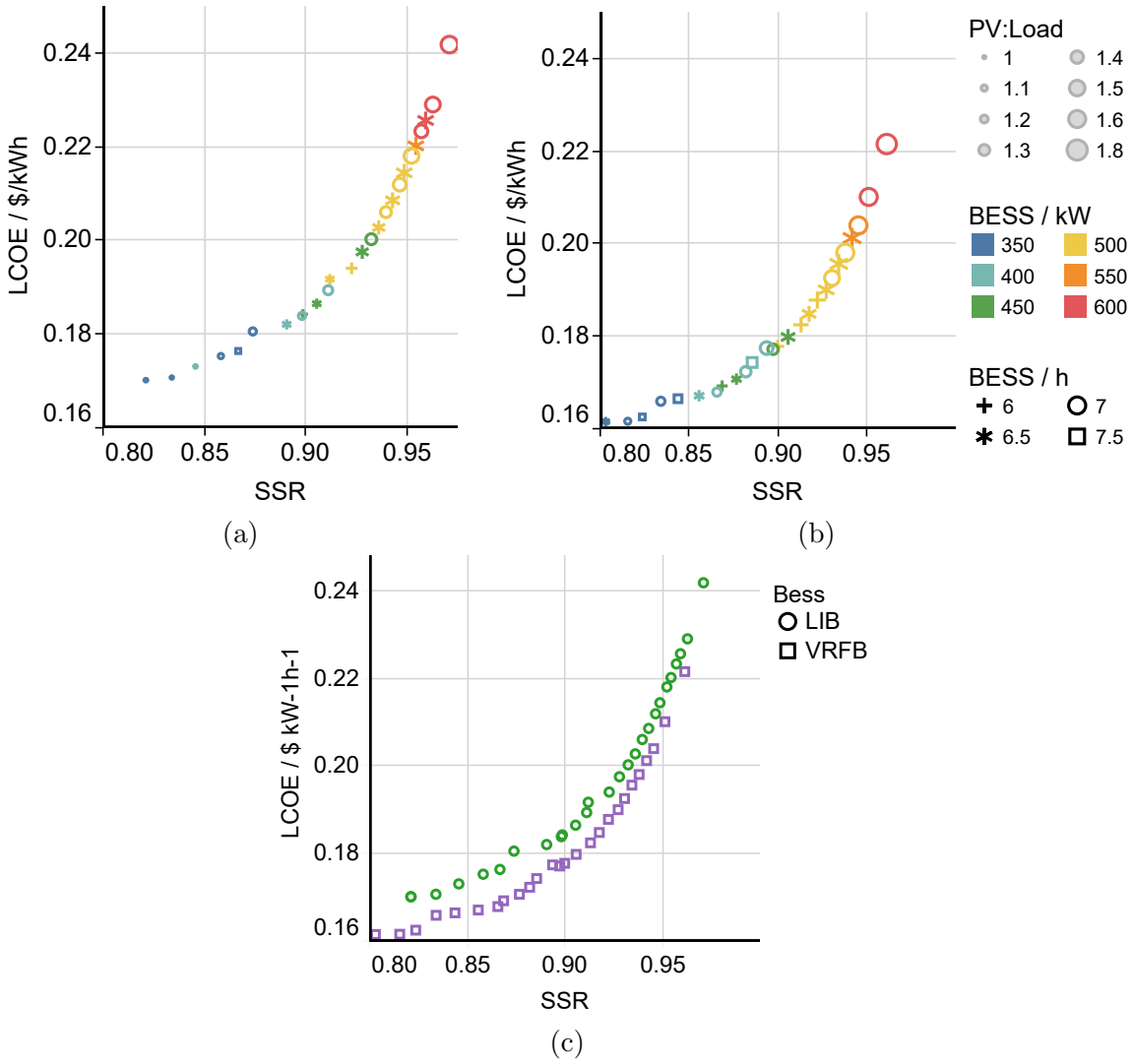

Figure 7.3: The results of a grid-search of the PV power / BESS power / BESS duration space to find the approximate Pareto fronts for maximisation of SSR and minimisation of LCOE at site 281. PV:load is the ratio of simulated annual PV output to annual building load. a) LIB, b) VRFB. The comparison of the approximate Pareto fronts is shown in c).

in this case from the PV over-sizing mentioned above.

7.4.2 Economic Sensitivity Study

In this section, the impact of changing several economic parameters is investigated, in order to gauge the robustness of the results. As the base case comparison showed that the VRFB gives a lower LCOE for self sufficiency ratios at least as high as 0.96, to test the robustness of the VRFB advantage, parameters were changed to tip the balance in favour of the LIB. The LIB DC module price was reduced to the low end projection made by [21] (see Section 3.4.5), and the ambient temperature was reduced by simulating the San Diego site, and then by subtracting 2 K from that temperature series. On the VRFB side, electrolyte leasing and EPC reductions were tested as these were shown to be important in Section 5.5.2. A high stack cost case was also modelled, in which only half of the projected reduction in stack cost by 2025 is achieved, giving a DC price of 389 kW^{-1} for both the initial CAPEX and the year ten replacement.

Approximate Pareto fronts for the various cases are shown in Figure 7.4.

On the LIB side of the comparison, the future price of the DC modules is the dominant factor. Under the mid price projection, the LIB LCOE is greater than or equal to the base VRFB LCOE at all points on the front in all temperature scenarios. Under the low price assumption, the LIB LCOE is equal to or less than the base VRFB LCOE under all temperature assumptions.

Temperature also has an important impact, with the reduction from the March Air Reserve Base site to the San Diego site with the -2 K offset reducing the LCOE by approximately ¢0.5 $\mathrm{kW}^{-1}\,\mathrm{h}^{-1}$ at 0.82 SSR and ¢0.7 $\mathrm{kW}^{-1}\,\mathrm{h}^{-1}$ at higher SSR. The drop is greater at high SSR as the LIB module replacement comprises a higher proportion of the overall expenditure. Further reductions in ambient temperature will show decreasing impact due to the Arrhenius type behaviour reported by Schmalstieg *et al.* [102]. At low SSR, reducing the temperature counter-intuitively reduces the modelled SSR. This is due to the non-linear nature of degradation. As the degradation slows, the LIB spends more

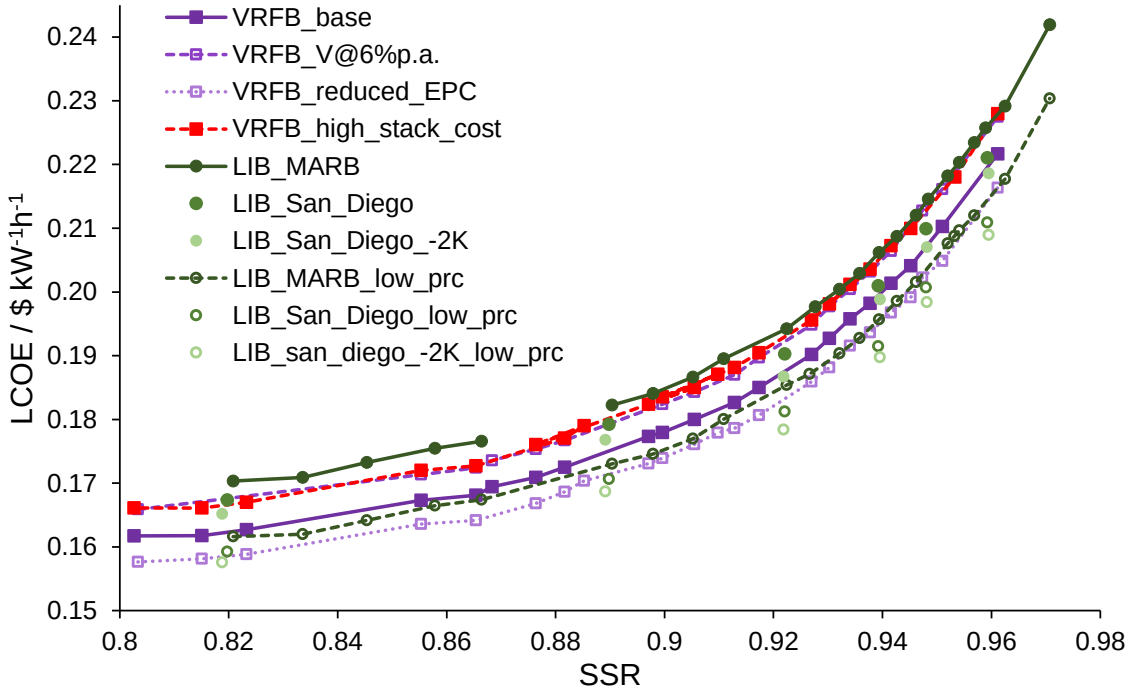

Figure 7.4: A sensitivity study on environmental and economic factors affecting the relative economic performance of LIB and VRFB systems providing self-sufficiency at site 281. For the VRFB, only one parameter is changed from the base case at a time.

of the project at a reduced working capacity. This effect is not as strong at high SSR, as the lifetime is longer due to reduced cycle-rate. Hence the slower drop in working capacity due to temperature reduction dominates.

On the VRFB side, leasing at 6% actually has a negative impact on LCOE. This is because the discount rate is 5% and the project life is 20 years, hence the total discounted lease payment is higher than the CAPEX minus the discounted residual value in the base case.

Reducing the footprint factor from the 1.7 average from [115, 121] to 1.2 reduces the LCOE by about ¢0.4 $kW^{-1}\,h^{-1}$. In a 2021 cost comparison, PNNL reported the EPC costs for LIB and VRFB systems as being approximately the same [21, 159], so the lower figure may be more appropriate.

In the high stack cost case, the VRFB front goes from being roughly equivalent to the low price LIB front, to being roughly equivalent to the mid price LIB front.

Overall, the economics of self-sufficiency of the LIB and VRFB are quite similar, and the distributions of Pareto fronts overlap.

7.4.3 Extending LIB lifetime by SOC control

The experimental work of Schmalstieg *et al.* showed that calendar aging is accelerated when the LIB is at high SOC[102]. In Chapter 5 it was shown that applying a degradation penalty to SOC, as has been done previously for throughput, leads to a small modelled increase in NPV in the CAISO market case study by delaying the LIB module replacement.

In this section the impact of such a strategy on the self-sufficiency economics of LIB systems is studied. In order to reduce the average SOC within the MILP formulation, it is necessary to extend the optimisation window and apply a penalty on average SOC as described in Section 7.2.2. This way, the LIB will still aim to store surplus at the end of the 48 h, but do this as late as possible. As only the first day of this schedule is implemented, on consecutive days with PV surplus, the LIB will not spend time at a higher SOC than necessary.

The impact of the SOC consideration is greatest in the summer months, as shown in Figure 7.5.

In summer the high PV output leads to a smaller residual load, and the cycle rate required of the BESS is smaller. When the optimisation window is 24 h the LIB fills with surplus PV and rarely discharges fully. Extending the optimisation window to 48 h and applying the penalty on average SOC forces the LIB to only store what it requires to cover any shortfall the following day. This reduces the average SOC across the first year of operation from 0.45 to 0.39, and increases the lifetime from 6 years and 9 months to 7 years and 1 month. The impact is greater for the larger LIBs specified to provide higher SSR. In these cases the LIB is cycled less, and in the 24 h optimisation sits idle at a high SOC for a greater fraction of the time. For the 600 kW/6.5 h LIB paired with the 1440 kWp PV array, the SOC penalty reduces the mean SOC from 0.57 to 0.33, extending the lifetime from 8 years and 6 months to 11 years and 9 months.

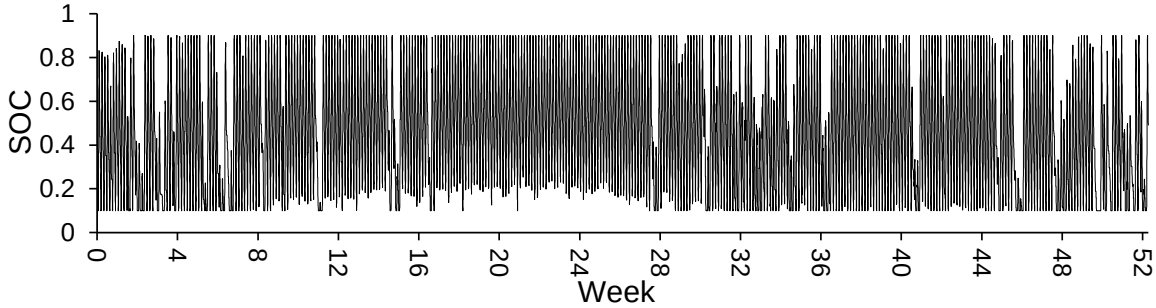

(a)

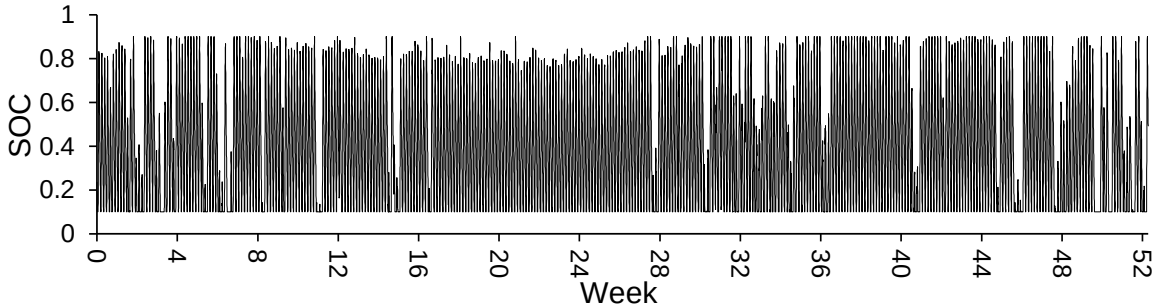

(b)

Figure 7.5: Comparison of SOC profile of a 1080 kW/6 h LIB across one year of operation providing self sufficiency at site 281 when paired with a 1080 kWp PV array (120% oversizing). a) 24 h optimisation. b) 48 h optimisation with penalty on mean SOC.

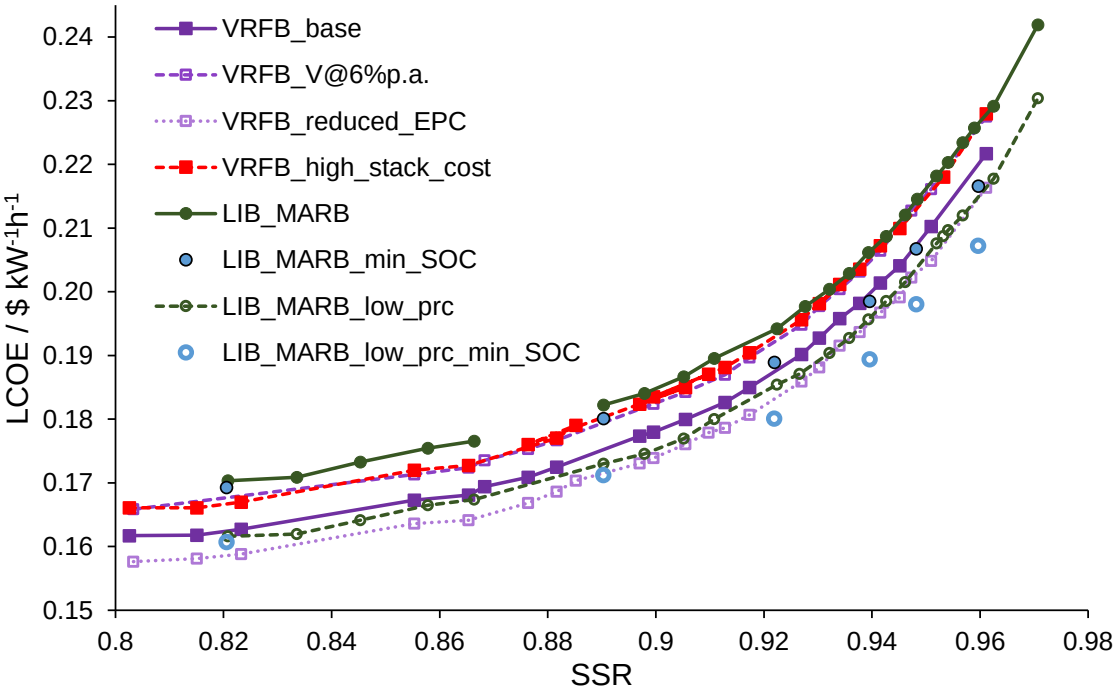

Figure 7.6: An illustration of the modelled effect of a SOC minimisation strategy for LIB under mid price and low price scenarios. VRFB data are shown for comparison.

Several points on the LIB Pareto front shown in Figure 7.4 were re-run using the 48 h optimisation. Figure 7.6 shows how the LCOE falls at various points on the Pareto front.

The decrease in LCOE is greatest at higher SSR for the reasons outlined above. Overall the SOC minimisation strategy does not result in a meaningful change to the VRFB / LIB comparison at low SSR, but at high SSR it can push the balance in favour of the LIB.

Although a perfect forecast has been assumed here, it is likely that most of the benefit seen above could be realised in a real project as the forecast requirement is only 48 h, and the total energy demand of the site does not vary much from day to day.

7.5 Evaluating the Benefit of Hybrid LIB/VRFB Systems

The findings in Chapter 5 show that VRFB gain an advantage relative to LIB when the application cycle rate is high, although the picture is more complicated in the present case

study. By using both technologies in a hybrid system it should be possible to perform the daily cycling with a suitably sized VRFB, and the less frequent cycling for days of higher net load with an LIB. Site 281 is active 7 days a week, and hence the variability in the load profile comes primarily from PV output fluctuations, with summer days giving longer hours of net PV surplus.

In this section the results of an MILP co-optimisation of several VRFB:LIB hybrid combinations are compared to the individual systems. A snapshot of the optimal schedule for the 75:25 VRFB:LIB hybrid at the 500 kW/6 h specification is shown in Figure 7.7.

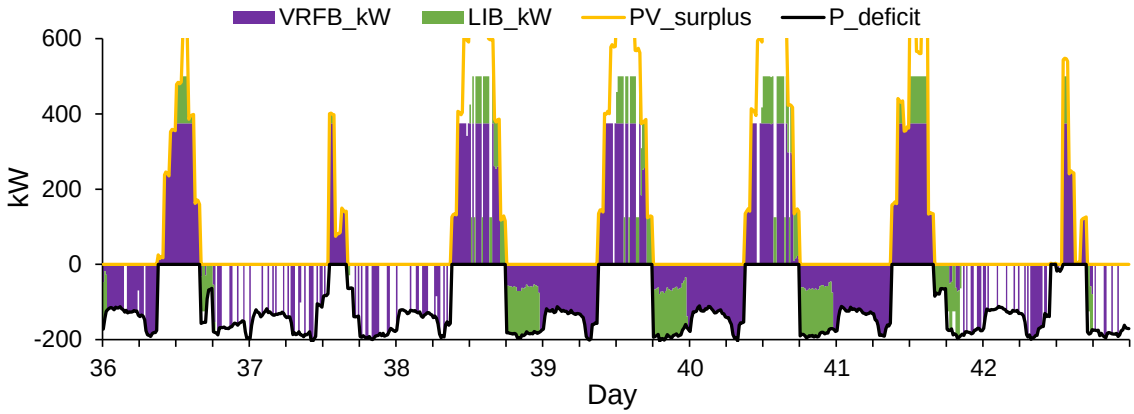

(a)

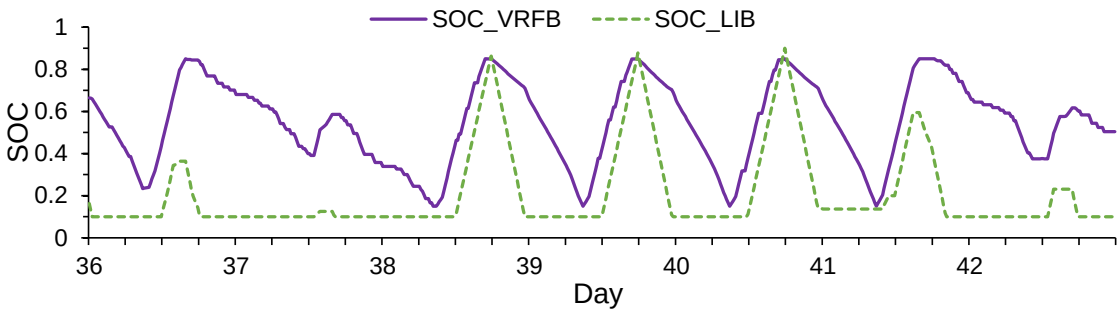

(b)

Figure 7.7: A snapshot of the optimal operation at site 281 during February of a hybrid BESS consisting of a 375 kW/6 h VRFB and a 125 kW/6 h LIB paired with a 1350 kWp PV array.

The hybrid schedule optimisation is successful in that the VRFB is charged preferentially. If the LIB must be charged, this is done as late as possible, and once the system moves to a power deficit the LIB discharges first. It is also worth noting that because the BESS power must be specified to make the most of the available PV, it will typically be oversized

relative to the discharge requirements. Hence using the load profile to guide the ratio of VRFB to LIB power rating is not particularly useful.

The impact of the hybridisation on the cycle-rate and lifetime of the LIB component is shown in Figure 7.8. The data show that hybridisation has the expected effect of reducing the LIB cycle-rate and extends the lifetime. The lifetime extension is greatest at high SSR, where the overall system is oversized hence the VRFB can cover a higher proportion of the overall duty.

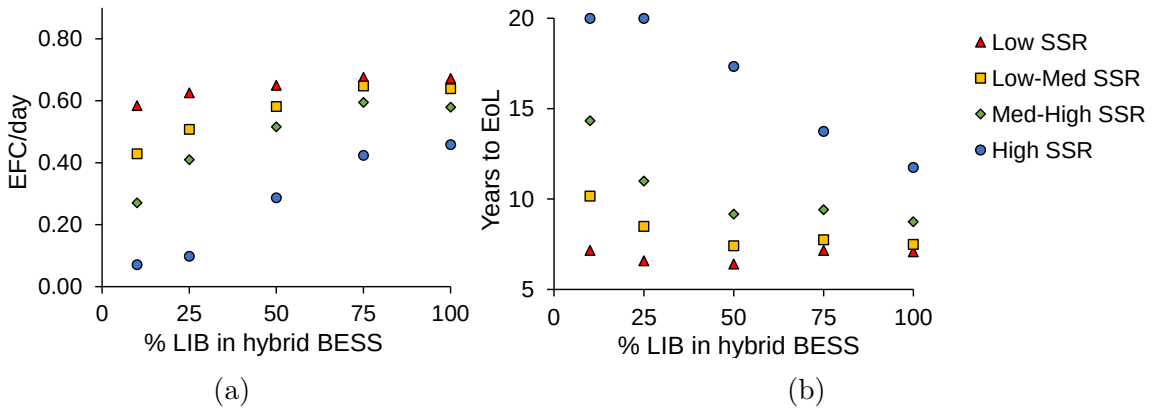

Figure 7.8: The variation in LIB cycle rate (a) and lifetime (b) due to varying the fraction of the hybrid BESS it comprises. Results are shown for four SSR scenarios.

Generating a full Pareto front in SSR and LCOE for the hybrid system is outwith the scope of this work, as adding two new dimensions, LIB:VRFB power ratio and LIB:VRFB duration ratio would greatly increase the computation and data processing time. Hybridisation was hence evaluated at four points for site 281:

- PV: 1080 kWp, BESS: 400 kW/6 h
- PV: 1170 kWp, BESS: 400 kW/6.5 h-7 h
- PV: 1350 kWp, BESS: 500 kW/6 h
- PV: 1440 kWp, BESS: 600 kW/6.5 h

These points were chosen as they lie on the Pareto front for both BESS types (except the 1170 kWp point, in which case the duration was set at 6.5 h for the LIB and 7 h for

the VRFB). The ratio of the VRFB power rating to LIB power rating (assuming each has its own inverter) was varied at each point, and the resultant LCOE versus SSR data are shown in Figure 7.9.

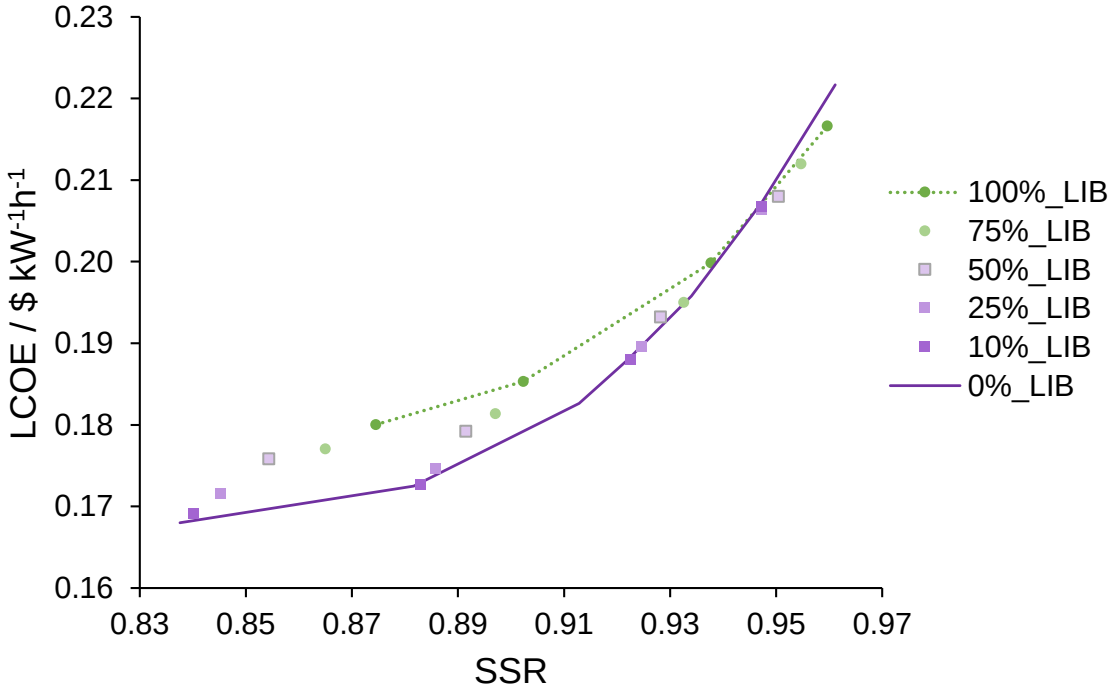

Figure 7.9: A comparison of the economics of hybrid VRFB:LIB systems with those of the optimal single BESS systems. 0% VRFB indicates a 100% LIB system.

The results in Figure 7.9 show that there is no economic benefit to deploying a hybrid system, as at each SSR point the hybrid systems simply follow a trend between the pure VRFB and pure LIB points, and do not move outside of the two Pareto fronts. This is somewhat surprising given the increases to LIB lifetime seen in the hybrid cases. However, it is important to note the trade-offs. As the LIB size is reduced, it contributes less to the overall provision of SSR, and hence the round trip efficiency of the hybrid system decreases.

7.6 Achievable VRFB Round Trip Efficiency While Providing Self Sufficiency

Having used a fast MILP optimisation to find the power / duration specification of VRFB that would give the lowest LCOE at a range of SSR targets, it is important to test whether the assumed 0.78 round trip AC efficiency could be achieved in practice. This figure was obtained in Chapter 6 as the operational AC round trip efficiency that could be achieved by performing an MIQP optimisation of the peak shaving and energy arbitrage schedule of a VRFB consisting of a single module. As the use case has changed, and the optimal duration is higher than the 2 h and 4 h in Chapter 6 this figure may not be appropriate.

A one year simulation was run for three VRFB specifications from low, mid and and high SSR sections of the Pareto front in Figure 7.3b. The modeled operational efficiency in each case is shown in Table 7.1

Table 7.1: Simulated operational efficiency values of VRFB at three specifications from different sections on the approximate Pareto front for maximisation of SSR and minimisation of LCOE at site 281.

Case	**PV** (kWp)	**VRFB Power** (kW)	(h)	**SSR (LP model)**	**LCOE (LP model)** ($ kW^{-1} h^{-1})	**Eff. RT (MIQP model)**
Low SSR	1080	400	6.5	0.855	0.167	0.798
High SSR	1440	600	7	0.951	0.210	0.798

Despite the variable efficiency of the VRFB shown in Figure 6.2, the operational AC efficiency is close to the peak modelled efficiency of 0.81, and exceeds the value of 0.78 assumed in the preceding grid search. The operational efficiency also varies remarkably little across the Pareto front despite a 50% increase to VRFB power rating from the low SSR case to the high one. In order to better understand this behaviour, the distribution of current density modeled while maximising SSR across a year of operation was plotted for the three specifications in Table 7.1, as shown in Figure 7.10.

The data shown in Figure 7.10 show that two opposing effects are at play in determining the operational efficiency of the VRFB as the SSR target is increased. On the discharge side, as the power rating of the VRFB is increased to facilitate increased SSR, the current

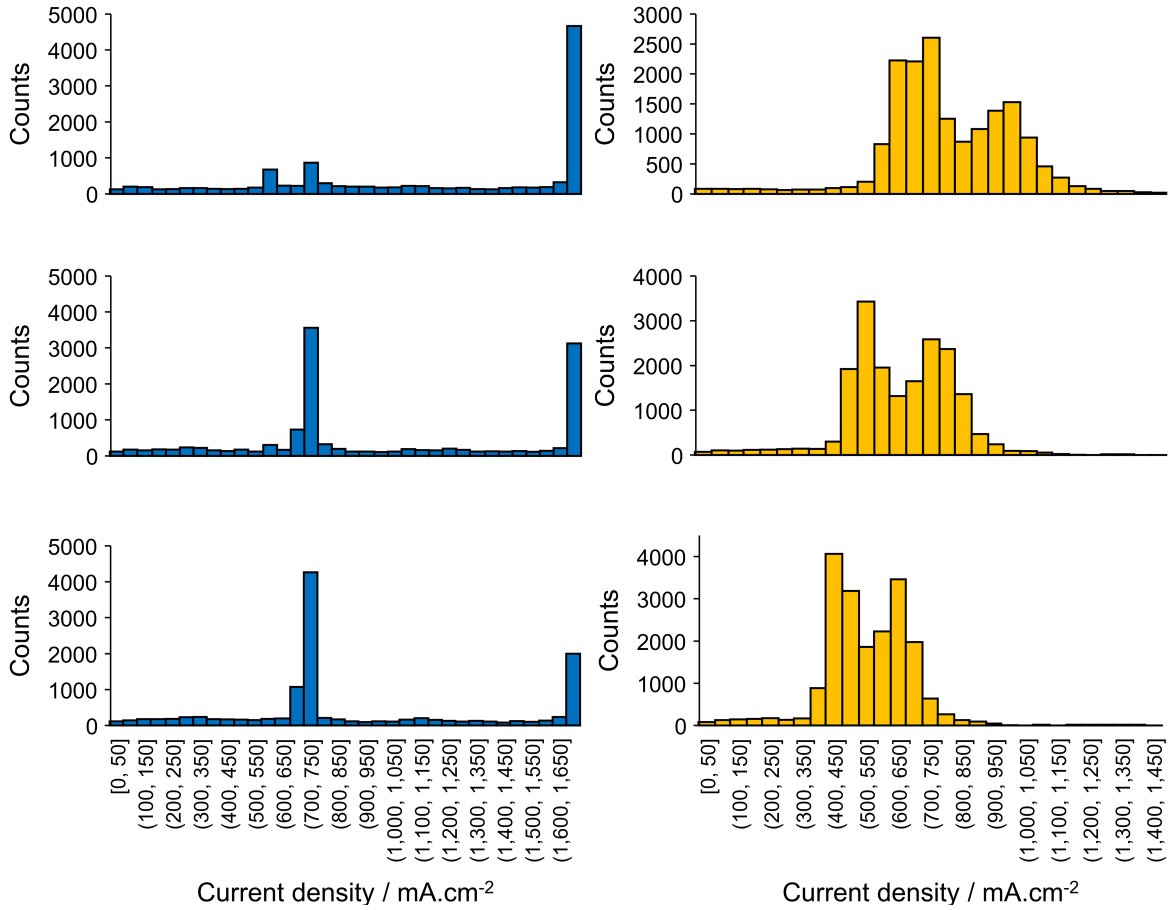

Figure 7.10: Histograms showing distribution of current density across all 15 min periods in the year for discharge and charge in three SSR scenarios. Left: charge, Right: discharge, Top: low SSR case, Middle: Mid SSR case, Bottom: High SSR case.

density at which the VRFB must operate to follow the load falls. In the low SSR case, 90% of the data fall between 51 mA cm^{-2} and 107 mA cm^{-2}, close to the optimal value of 74 mA cm^{-2} shown in Figure 6.2. In the high SSR case, the whole range shifts to lower values, and 90% of the data lie in the range 42 mA cm^{-2} to 73 mA cm^{-2}, below the optimal current density. Hence there is a small drop in discharging efficiency going from low to high SSR. The bimodal distribution of current density is due to the clear distinction between hours when the building is in use and hour in which it is empty, as shown in Figure 4.1.

On the charging side, the distribution is quite different, showing standout peaks at the maximum current density of 169 mA cm^{-2} permitted by the inverter rating and at the maximum efficiency point of 74 mA cm^{-2}. The relative size of these two peaks is related to the degree of PV surplus. Where the PV surplus exceeds the available capacity of the VRFB, there is some flexibility in when the VRFB may be charged. In this case, the VRFB will charge at the maximum efficiency point as much as possible. However, given the duration of the VRFB is close to the length of the PV surplus period, it will not be possible to charge fully at 74 mA cm^{-2} (unless the VRFB has carried over charge from the previous day), hence the VRFB switches between this value and the maximum permitted. Where the PV surplus is less than the VRFB capacity, the VRFB will simply charge at whatever current is required to consume all of the available PV. In the high SSR case, with the largest PV array, the days of surplus become more common and hence in the histogram the peak at 74 mA cm^{-2} is highest, and the charging efficiency is also highest. This cancels out the poorer discharge efficiency at high SSR.

7.7 Load Profile Dependence

The duty cycle required of the BESS will depend on the load profile at the site, and this is hence a source of variability in the economic analysis. Site 767 differs from site 281 in that the load peak in the day is briefer, and the power consumption on weekends is much reduced, as shown in Figure 7.11.

Grid searches were also performed (at lower resolution) to find the approximate Pareto

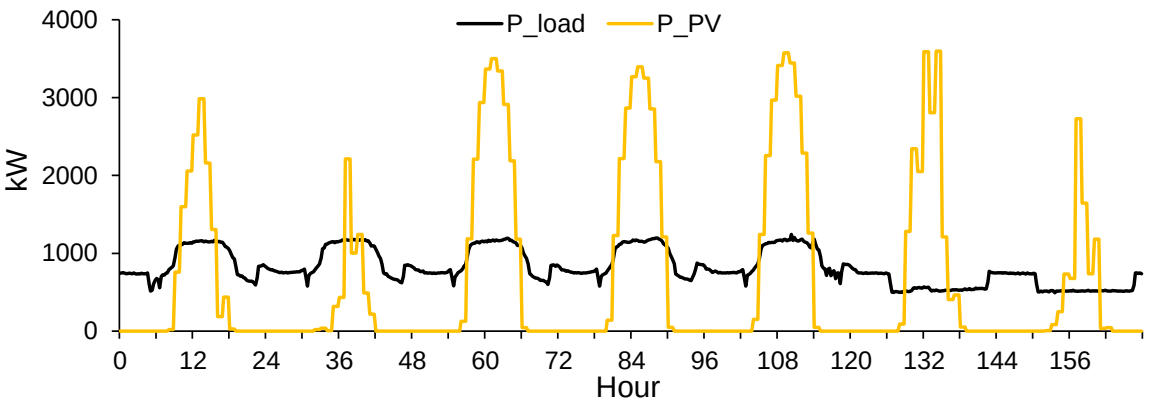

Figure 7.11: The load profile and PV array output for a week in February (starting Monday) at site 767. The PV array is sized at 5 MWp for 120% provision of site energy consumption across the year.

front for VRFB and LIB systems at site 767. The PV and BESS power ratings were increased according to the ratio of the average load at site 767 to that at site 281. The resultant approximate Pareto fronts for the VRFB and LIB systems are shown in Figure 7.12

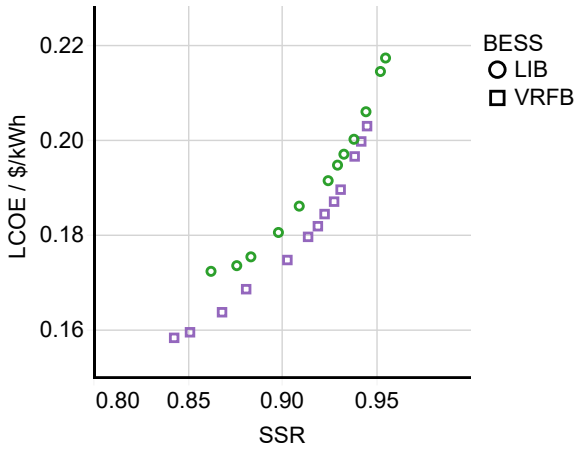

Figure 7.12: Approximate Pareto fronts for maximisation of SSR and minimisation of LCOE with LIB and VRFB systems at site 767. For comparison with Figure 7.3c.

Overall the results from site 767 are very similar to those at site 281. The LIB appears to perform better relatively at high SSR.

The operational efficiency modelled using the MIQP optimisation is also very similar to that reported in Table 7.1 for the optimal VRFB specifications at site 281 , as shown in Table 7.2.

Table 7.2: Simulated operational efficiency values of VRFB at three specifications from different sections on the approximate Pareto front for maximisation of SSR and minimisation of LCOE at site 767.

Case	**PV** (kWp)	**VRFB Power** (kW)	(h)	**SSR (LP model)**	**LCOE (LP model)** ($ kW^{-1} h^{-1})	**Eff. RT (MIQP model)**
Low SSR	5400	1800	6.5	0.858	0.163	0.798
Mid SSR	6600	2300	6	0.922	0.185	0.799
High SSR	6600	2800	7	0.949	0.203	0.797

7.8 Conclusions

- Under the base economic scenario, and with the March Air Reserve Base temperature data, a VRFB gives a slightly lower LCOE from 0.8 to 0.95 SSR for site 281. This is despite a larger VRFB capacity being required for a given SSR. Under the low price projection for LIB modules, the LIB LCOE is the same as the base scenario VRFB LCOE at the lower end of the SSR range and just below it at the higher end of the range. Temperature is again a significant factor; taking the San Diego International Airport data and applying a minus 2 K offset, the LIB becomes more cost effective across the entire range by at least ¢0.4kW^{-1} h^{-1}.

- Employing a strategy to minimise the SOC of the LIB by avoiding unnecessary charging has a marked benefit on the LCOE at high SSR. This is because the LIB is oversized for the summer months, and is hence at risk of charging fully but not discharging fully. This leads to a high SOC being carried which accelerates calendar aging. With an SOC minimisation strategy in place, the LIB is predicted to be the cheapest option at SSR greater than 0.9, even in the mid price scenario.

- Overall the LCOE data do not vary by a large range across the BESS types under the different scenarios; at 0.82 SSR, the LCOE varies from \$0.181 kW^{-1} h^{-1} for the mid price LIB at MARB, to \$0.158 kW^{-1} h^{-1} for the low EPC case VRFB and the low temp/low price case for the LIB. At 0.95 SSR, there is a similar range, from \$0.215 kW^{-1} h^{-1} for the mid price LIB at MARB, to \$0.198 kW^{-1} h^{-1}, for the low price LIB with SOC minimisation (and the low temp cases are predicted to be lower

again).

- A method has been introduced to optimise a hybrid BESS comprising a LIB and a VRFB, such that the VRFB always charges and discharges first, to protect the LIB from degradation. Despite this approach increasing the lifespan of the LIB, there is no hybrid benefit, simply a blending effect.

- Despite the variable nature of VRFB efficiency, and the drop in efficiency at low power output, the operational efficiency while providing self-sufficiency at both site 281 and site 767 is modelled as 0.80 at the AC boundary. This is very close to the maximum modeled efficiency of 0.81. The high efficiency is due in part to the PV and BESS sizing requirements for high SSR, whereby the average discharge current density lies in an optimal range. The MIQP model is able to maximise the efficiency when there is a daily PV surplus by reducing the charge power to perform as much charging as possible at the optimal current density of $74\,\mathrm{mA\,cm^{-2}}$. The estimate of 0.78 AC efficiency assumed in the economic analyses hence includes a small contingency.

Chapter 8

Conclusions

This thesis has addressed the question of whether vanadium redox flow batteries (VRFB) offer economic advantages over lithium-ion batteries (LIB) for behind the meter applications at a commercial/industrial site in California.

In the course of answering the posed question, a number of original contributions have been made to the field of TEA of these BESS:

- A bottom up price model for the turnkey VRFB has been introduced which breaks both DC module costs and installation costs into \$ kW^{-1} and \$ $kW^{-1}\,h^{-1}$ components.

- State of the art models for both LIB [102] and VRFB degradation [23] have been applied for the first time to a multiple revenue stream market case study and a PV self-sufficiency case study.

- The economics of VRFB and LIB for supporting LIB self-sufficiency have been analysed using a multi-objective optimisation that explores the BESS power / BESS duration / PV power space.

- For the VRFB, where efficiency varies significantly with power output, an MIQP model has been introduced to consider this during optimisation of operation. The introduced model has been defined for both case studies, although in the market

study, it does not cover ancillary services.

- Using the above model, the operational efficiencies of optimally sized VRFB have been studied for both use cases in order to determine whether previous assumptions on VRFB efficiency are valid.

- The MIQP model has also been applied to study the benefit of independent scheduling of multiple VRFB sub-modules to avoid the poor efficiency that occurs at low power output.

- A TEA of a hybrid VRFB-LIB system has been performed for the PV self-sufficiency case study applying a penalty method to prioritise VRFB cycling.

In Chapter 2, a review of promising flow battery technologies was made, and the key figures of merit determined. Although a wide range of chemistries and configurations have been demonstrated at the lab scale, the VRFB has the highest power area specific power density at present, which is crucial from a cost perspective for the case studies considered in this work. Both VRFB and hybrid zinc/bromine flow batteries have been commercialised, but the latter does not incorporate power and energy decoupling. A review of performance models highlighted the significant variation in VRFB efficiency with power output.

The literature search also yielded a detailed empirical LIB degradation model that includes the temperature and SOC dependence of calendar aging [102]. At the time of writing this model had only been applied to a TEA of energy arbitrage [103]. Similarly, a recently published empirical model for reversible capacity fade in VRFB was found [23].

Lastly, a review of TEA found that for VRFB these tend to be split into those which focus on the bottom up costs of VRFB and include a cursory application study if any, and those which give a detailed analysis of the application side, including optimisation of operation, but use a basic representation of the BESS. Of the latter, there are more studies on LIB than VRFB. There are a few notable exceptions to this categorisation - the work of Nguyen *et al.* on optimal VRFB sizing and operation in a micro-grid and

the work of Reniers *et al.* (published during this work) on optimising LIB operation to minimise degradation being stand-out examples [20, 103].

It was concluded that there was a gap in the literature for a high level techno-economic analysis with enhanced modelling of degradation for both systems and operational efficiency for the VRFB. In Chapter 3 the modelling methods employed in this work were described, and necessary definitions made. The methods pertain to the three following components of the overall TEA.

- Installed cost of each system at various durations.
- Technical performance of each system; round trip efficiency and degradation rate.
- Economic benefit of each system under optimal operation.

In Chapter 4 the formulation of Fisher *et al.* was applied to analyse the short-term optimal operation of VRFB and LIB performing peak-shaving, energy price arbitrage and ancillary service provision from behind the meter in the CAISO region. It was shown that both the peak shaving aspect and the LIB degradation aspect are reliant on penalty terms due to time frame mismatch, and these should hence be optimised on a per application basis. It was also demonstrated that providing regulation from behind the meter would be uneconomical from this site. The regulation request frequently averages to greater or less than 0 over a double digit number of hours, which poses a risk to peak shaving that outweighs the regulation revenue. This will of course be dependent on the domain, as some regulation services may have a signal that averages to 0 over a much shorter time-frame than the CAISO and PJM ones do. Also, a site with low load during the regulation price peaks may be suitable.

In Chapter 5, the CAISO case study was studied over a ten year project length, with the model of Fisher *et al.* augmented to include the enhanced degradation models and predictions of turnkey LIB/VRFB prices. The results of the bottom up price modelling were first reported, showing that the predicted prices for 2025 installations are 29% higher for the VRFB than the LIB at 2 h, 14% higher at 4 h and % higher at 6 h.

For the VRFB, the degradation cost associated with ionic crossover is negligible, assuming this can be automated and performed continually. The degradation due to capacity fade has a greater impact, and if corrected by an annual visit, is predicted to result in an average working energy capacity of 0.91-0.94 of the fresh value depending on the cycle rate. As peak shaving is the dominant revenue stream and is seasonal, the economic impact in this case study can be minimised by performing maintenance at the end of May.

For the LIB, the rate of degradation has been shown to be dependent on ambient temperature, assuming no air conditioning is applied. At a hotter site such as March Air Reserve Base, it is not possible to prolong the LIB battery life to ten years as calendar aging occurs regardless of the cycling. This contrasts with the outcome of cycle degradation only models such as the one employed by Fisher *et al.* in the same case study. At the San Diego International Airport site, although the average temperature is the same, the LIB does last the full ten years, as the maximum temperature is lower. In any case, extending the lifetime by increasing the throughput penalty is not the optimal strategy given the low modelled cost of module replacement and 10% discount rate.

Overall the highest NPV is returned by a 2 h LIB, although both LIB and VRFB give positive NPV at 4 h duration, and are around breakeven at 6 h duration with inclusion of the CAISO resource adequacy payment. A subsequent sensitivity showed that none of the studied scenarios predict a 2 h VRFB giving higher NPV than a 2 h LIB. At 4 h duration there is some scope for a VRFB to return a higher NPV, and increasing the efficiency to 0.80, reducing the EPC costs, leasing the electrolyte at 6% p.a. and the ambient temperature were all shown to be significant factors. Most importantly, removing the throughput penalty on the LIB (a sub-optimal strategy in this application) increases the EFC/day from 0.46 to 0.82, in which case the 4 h VRFB gives a higher NPV under all studied scenarios. This indicates that VRFB companies must focus on high cycle rate applications as well as hot climates to outperform LIB on a purely economic basis.

In Chapter 6 the MIQP optimisation model for dynamic VRFB efficiency was demonstrated for the CAISO case study where only peak shaving and energy arbitrage are

performed. The main impact of the MIQP optimisation is that charging is spread out where there is a prolonged period of similar electricity price in order to move the current density as close as possible to the peak efficiency point. The same applies on the occasions where discharging occurs for energy arbitrage. When performing peak shaving there is no flexibility in the operation, and the MIQP discharge profile is the same as the LP one. By doing this, the VRFB is modelled to achieve an operational efficiency of 0.787, which is higher than the 0.768 assumed in the higher efficiency scenario in Chapter 5.

The MIQP model was then used to study the impact of varying the electrode area. Increasing the electrode area from the base case taken from the Reed system has a negative impact on economics under the component price assumptions, as the gain in efficiency does not outweigh the additional cost.

The MIQP was also applied to optimise the operation of a VRFB where multiple sub-modules may be independently activated and idled. In the case of two modules, idling one unit when the required power is low allows the minimisation of parasitic coulombic and pumping losses. Under the base assumptions this approach increases the operational efficiency from 0.786 to 0.794. The importance of this strategy is linked to the magnitude of the quasi-fixed losses; in a case where the coulombic losses are doubled, the operational efficiency is increased from 0.746 to 0.763, double the gain. The gain is also highest in the largest electrode case, as this is where the lowest current densities occur, although this does not change the choice of electrode area.

Lastly, as the MIQP model assumes a constant voltage in the optimisation, a linear voltage constraint was applied to check whether damaging high voltages would occur when charging at high SOC. This was not found to be a problem, as both the cap imposed by the inverter rating and the efficiency consideration discourage high charge current density.

In Chapter 7 a second case study was analysed, in which the LIB/VRFB is used to improve the self-sufficiency of the commercial/industrial site in combination with PV. In the first analysis, the PV was assumed t be already installed on the rooftop and the LIB/VRFB retrofitted. At lower SSR, the VRFB is predicted to give a lower LCOE as

the cycle rate is high. As the LIB/VRFB size is increased, the VRFB LCOE becomes the higher, and reaches a vertical asymptote at lower SSR due to its lower efficiency.

In the second analysis, Pareto fronts for maximisation of SSR and minimisation of LCOE were generated by varying the BESS power and duration and the PV array size. Both LIB and VRFB are predicted to achieve self-sufficiency ratios (SSR) of up to 0.95 while keeping the LCOE below ¢20 $\mathrm{kW^{-1}\,h^{-1}}$. The impact of the lower VRFB efficiency is reduced by the need to oversize the PV array in both cases to cope with seasonal variation. That said, a larger VRFB than LIB is specified at all SSR targets. Despite this, an optimally sized VRFB system is predicted to marginally outperform an optimally sized LIB system (i.e. by ¢1 $\mathrm{kW^{-1}\,h^{-1}}$ in LCOE) up to the low nineties for SSR when the LIB module price follows a mid projection. Under the low end LIB module cost projection LCOE fronts overlap with those of the case case VRFB. At higher SSR values, assuming the LIB SOC can be minimised effectively, the LIB becomes the economically optimal choice, due to the reduction in cycle rate that comes with over-sizing. The minimisation of SOC requires more forecasting to delay charging where possible.

Electrolyte leasing at 6% p.a. actually increases the VRFB LCOE in this case study, as the discount rate is 5% and the project term 20 years. Other factors like reductions in EPC cost for the VRFB, and variation in ambient temperature for the LIB have a less noticeable (though still meaningful) effect on LCOE than they did on the NPV in Chapter 5. This is partly because NPV is an absolute measure whereas LCOE is more proportional, and partly because the LCOE also contains the PV CAPEX, which makes up more than 50% of the project cost. In this application, a duration of 6 to 7h is optimal - increasing the duration to span days with lower PV output is not beneficial as the variation in output is primarily seasonal.

A similar analysis was run for a different site, chosen because the load profile was markedly different, and the results were similar, except that the VRFB LCOE passe above that of the LIB at a lower SSR value.

Applying the MIQP formulation to the SSR objective, it was found that the operational

efficiency was remarkably consistent at 0.80 across the different sizing scenarios at both sites. This is due to reductions in discharge efficiency cancelling out increases to discharging efficiency and vice versa. During charging the optimal schedule involves spending as much time as possible at the most efficient current-density, but switching between this and the maximum current density if the VRFB would not fill using just the former.

Lastly, the introduced hybrid optimisation method was used to study combinations of LIB and VRFB at four different overall sizes drawn from the Pareto fronts. The approach successfully reduces the predicted degradation of the LIB by dispatching the VRFB first, but no hybrid benefit was observed, just a blending effect.

The results of this work provide important insights for a number of entities in the BESS field.

- VRFB manufacturers: the demonstrated sensitivity of LIB to high temperatures suggests that it should be a priority to promote VRFB systems in regions with hot climates. Pairing with PV in desert regions such as Saudi Arabia would be an ideal application. The efficiency gains achievable by optimising multiple modules as an ensemble should motivate the development of a suitable control system, and the model introduced could be used to inform the minimum module sizing requirements for a given application.

- LIB system designers: the notable reduction in LCOE due to minimising the SOC of the LIB system where possible implies that it will be worth the expense of installing a more sophisticated control system that includes forecasting to avoid storing more PV output than necessary to cover the coming days.

- BESS project developers in California: in use-case A it was found that a 6 h duration BESS could break-even, and in use-case B, durations of 6 h to 7.5 h could support a high self-sufficiency ratio without passing the knee point of diminishing returns. Hence 6 h appears to be a suitable duration to deploy in this region. The analysis of regulation provision showed that there is conflict between the provision of regulation and peak demand charge avoidance, due to imbalanced regulation signal. Crude

analyses that assume stacking of these two revenue streams hence risk overestimating the profitability of behind-the-meter projects.

8.1 Further Work

During the course of this work, a number of important subjects for further research were identified but not pursued due to time constraints. The most important of these are described in the following sections.

8.1.1 Temperature and Degradation Modelling

In both the CAISO case study and the PV self-sufficiency case study, the effect of ambient temperature is shown to be important for the lifetime of LIB, and hence the economics of LIB projects. However, the assumption that the LIB cell temperature matches the ambient temperature is crude. In reality there are opposing drivers for cell temperature that may impact on the actual temperature experienced by the cells. On one side, thermal inertia may prevent the upper or lower extremes of the ambient temperature range being reached. On the other side, there will be some warming due to resistive losses and other physical phenomena [103]. Zhang *et al.* tested NMC cylindrical cells at various C rates [160]. The C/5 data reported are most appropriate for the present use as they correspond to a 4 h system duration once the 80% SOC window is factored in. The average temperatures at the end of discharge for these respective discharge rates were 26 °C and 24 °C, compared to an ambient temperature of 22 °C. The range of temperatures is similar to those reported by Li *et al.* for natural and forced convection tests on a MnO cathode pouch cell [161]. It is therefore possible that the temperature of the LIB cells is slightly underestimated in this work, especially given that the above experimental data were collected on single cells rather than modules. There is a clear need for further analysis like that of Reniers *et al.* [103].

The necessary PV array over-sizing for high self-sufficiency ensures that there will be

PV power surplus on summer days when the temperature is highest. There is therefore scope for actively cooling the LIB cells without a loss of utility, although this would require additional CAPEX. This is an important subject from both an economic and a sustainability perspective, so a TEA is merited.

In this work a major assumption is made regarding the LIB lifetime, namely that the battery would be retired once a state of health of 80% is reached. This is a commonly used end of life definition; although it may derive from vehicular applications, it is also the case that aging begins to accelerate around this point. This has recently been attributed to cathode degradation due to high potentials that are experienced once the anode degrades below a threshold [162]. However, the degree to which this phenomenon may be delayed or circumvented by reducing the SOC window has not been established to the best of the author's knowledge, and hence remains an important research question.

It is also important to highlight that in this work, the degradation model is based on a specific commercial product from 2014, and that there are likely to be cells now available with better degradation characteristics. For this reason testing the lifetime of current products would provide useful insight. However, this would ideally be carried out at the pack level to address the temperature issue described above.

The VRFB is also sensitive to temperature due to the V(V) species solubility issue at high temperature. Although this problem is mitigated by the mixed acid electrolyte studied in this work [17], no modelling studies have been published showing that there are no constraints on operation. Given that VRFB display relatively high resistive losses, they will generate more heat than an LIB, although the electrolyte will act as a large thermal store. This is an important point for VRFB deployment, as it has been shown in this work that high temperatures favour a VRFB over a LIB. This area is ripe for further optimisation work and it is likely that the MIQP optimisation would also benefit heat management.

8.1.2 Non-Deterministic Modelling

The deterministic algebraic modelling approach applied in this thesis is valid for comparing the maximum benefit that LIB and VRFB systems could give under the perfect forecasting assumption. However, there are a number of ways in which the field performance might fall short of that reported here. Load profiles are most variable at the top, for example at site 281 the 80 kW/2 h BESS only shaves short duration peaks that lie on top of a broader peak, and these peaks occur at different times each day. Attempting to optimise the schedule of the BESS with a forecast in this situation might lead to the battery charging on a peak, which would be very costly. Hence in a real time dispatch scenario, an algorithm would be used to decide a threshold for peak shaving as in [142]. Under uncertainty, a 2 h BESS would require a greater de-rating than a 4 h BESS to avoid the risk of premature SOC exhaustion, as there is more uncertainty in the top part of the load profile.

The benefits to the VRFB system efficiency resulting from multiple module operation demonstrated in this work also benefit from the perfect forecasting assumption. In reality, an algorithmic approach would be required, for example, in determining when to bring a second module online in the case of rising PV output. Work has already been done in this area for a LIB/VRFB hybrid [163] but not for the multiple module VRFB problem. The optimisation model introduced here would be useful for training machine learning processes such as decision trees, which are based on thresholds.

8.1.3 Lithium Iron Phosphate Chemistry

In this thesis the analysis of LIB economics has been confined to the NMC cathode chemistry. The cost of replacing these cells twice in a 20 year PV self-sufficiency project is the primary reason why VRFB give comparable economics despite their lower efficiency and higher CAPEX. The lithium iron phosphate (LFP) chemistry has the advantages of lower cell costs and higher cycle life [21]. Its lower energy density has meant that the annual production is not yet at the scale of NMC, which has been driven by portable applications. However, given the above advantages it is likely that LFP will become the preferred chemistry for stationary storage, and hence the technology that VRFB will need to compete against. For this reason, it would be informative to repeat the analysis performed in Chapter 7 for systems based on LFP cells. Degradation models similar to that applied herein for NMC have more recently been published for LFP cells [164] and could be adapted to fit in the overall modelling framework.

References

[1] International Energy Agency (IEA), "Renewables 2018," 2018. [Online]. Available: https://www.iea.org/renewables2018/ (Accessed: 2018-11-07).

[2] "BP Statistical Review of World Energy," BP, Tech. Rep., 2018.

[3] ERCOT, "ERCOT Quick Facts for 2017," 2017. [Online]. Available: https://www.dropbox.com/s/vcrbv143x9u8y6c/ERCOT_Quick_Facts_for_2017_2518.pdf?dl=0 (Accessed: 2018-11-06).

[4] California Energy Commission, "Total system electric generation," 2018. [Online]. Available: https://www.energy.ca.gov/almanac/electricity_data/total_system_power.html (Accessed: 2018-11-21).

[5] Drax Group, "Drax electric insights," 2018. [Online]. Available: www.electricinsights.co.uk (Accessed: 2018-10-24).

[6] Climate Action Tracker, "Countries." [Online]. Available: https://climateactiontracker.org/countries/ (Accessed: 2021-10-08).

[7] Neoen, "Hornsdale Power Reserve — Australia's Big Battery," 2021. [Online]. Available: https://hornsdalepowerreserve.com.au (Accessed: 2021-10-08).

[8] I. Staffell and M. Rustomji, "Maximising the value of electricity storage," Journal of Energy Storage, vol. 8, pp. 212–225, nov 2016.

[9] Lazard, "LAZARD'S LEVELIZED COST OF STORAGE ANALYSIS —VERSION 5.0," 2019. [Online]. Available: https://www.lazard.com/media/451087/lazards-levelized-cost-of-storage-version-50-vf.pdf (Accessed: 2020-09-27).

[10] M. Fisher, J. Apt, and J. F. Whitacre, "Can flow batteries scale in the behind-the-meter commercial and industrial market? A techno-economic comparison of storage technologies in California," Journal of Power Sources, vol. 420, pp. 1–8, 2019.

[11] "The cellcube." [Online]. Available: https://www.cellcube.com/the-cellcube-1 (Accessed: 2021-04-22).

[12] "Vanadium flow batteries." [Online]. Available: https://invinity.com/solutions/vanadium-flow-batteries/ (Accessed: 2021-04-22).

[13] Sumitomo, "Redox Flow Battery—Products—Sumitomo Electric Industries, Ltd." [Online]. Available: https://sumitomoelectric.com/sites/default/files/2021-04/download_documents/Redox_Flow_Battery_En.pdf (Accessed: 2021-04-22).

[14] UET, "UniEnergy Technologies," 2020. [Online]. Available: https://uetechnologies.com (Accessed: 2021-04-22).

[15] "VRB-ESS® Sustainable, Scalable and Safe Energy Storage." [Online]. Available: https://vrbenergy.com/wp-content/uploads/2020/07/VRB_Gen2x_Brochure.pdf (Accessed: 2021-04-22).

[16] Panasonic, "Panasonic NCR18650B Lithium ion battery specification." [Online]. Available: https://www.batteryspace.com/prod-specs/NCR18650B.pdf (Accessed: 2018-07-16).

[17] S. Kim, M. Vijayakumar, W. Wang, J. Zhang, B. Chen, Z. Nie, F. Chen, J. Hu, L. Li, and Z. Yang, "Chloride supporting electrolytes for all-vanadium redox flow batteries," Physical Chemistry Chemical Physics, vol. 13, no. 40, p. 18186, 2011.

[18] "Prospects for Long-Life Batteries in Waterway Transportation." [Online]. Available: https://www.maritime-executive.com/editorials/prospects-for-long-life-batteries-in-waterway-transportation (Accessed: 2021-10-08).

[19] V. Jülch, "Comparison of electricity storage options using levelized cost of storage (LCOS) method," Applied Energy, vol. 183, pp. 1594–1606, 2016.

[20] T. A. Nguyen, M. L. Crow, and A. C. Elmore, "Optimal sizing of a vanadium redox battery system for microgrid systems," IEEE Transactions on Sustainable Energy, vol. 6, no. 3, pp. 729–737, 2015.

[21] K. Mongird, V. Viswanathan, J. Alam, C. Vartarian, and V. Sprenkle, "2020 Grid Energy Storage Technology Cost and Performance Assessment," PNNL, Tech. Rep., 2020.

[22] L. da Silva Lima, M. Quartier, A. Buchmayr, D. Sanjuan-Delmás, H. Laget, D. Corbisier, J. Mertens, and J. Dewulf, "Life cycle assessment of lithium-ion batteries and vanadium redox flow batteries-based renewable energy storage systems," Sustainable Energy Technologies and Assessments, vol. 46, p. 101286, 2021.

[23] K. E. Rodby, T. J. Carney, Y. Ashraf Gandomi, J. L. Barton, R. M. Darling, and F. R. Brushett, "Assessing the levelized cost of vanadium redox flow batteries with capacity fade and rebalancing," Journal of Power Sources, vol. 460, no. April, 2020.

[24] V. Viswanathan, A. Crawford, D. Stephenson, S. Kim, W. Wang, B. Li, G. Coffey, E. Thomsen, G. Graff, P. Balducci, M. Kintner-Meyer, and V. Sprenkle, "Cost and performance model for redox flow batteries," Journal of Power Sources, vol. 247, pp. 1040–1051, 2014.

[25] S. Eckroad, "Vanadium Redox Flow Batteries: An In-Depth Analysis," The Electric Power Research Institute, Tech. Rep. 3, 2007. [Online]. Available: http://www.paredox.com/foswiki/pub/Trash/TrashAttachment/EPRI_-_Vanadium_Redox_Flow_Batteries_2007_.pdf

[26] S. Weber, J. F. Peters, M. Baumann, and M. Weil, "Life Cycle Assessment of a Vanadium Redox Flow Battery," Environmental Science & Technology, vol. 52, no. 18, pp. 10 864–10 873, 2018.

[27] M. Skyllas-Kazacos and F. Grossmith, "Efficient Vanadium Redox Flow Cell," Journal of The Electrochemical Society, vol. 134, no. 12, p. 2950, 1987.

[28] D. Reed, E. Thomsen, B. Li, W. Wang, Z. Nie, B. Koeppel, J. Kizewski, and V. Sprenkle, "Stack Developments in a kW Class All Vanadium Mixed Acid Redox Flow Battery at the Pacific Northwest National Laboratory," Journal of The Electrochemical Society, vol. 163, no. 1, pp. A5211–A5219, 2016.

[29] R. Dmello, J. D. Milshtein, F. R. Brushett, and K. C. Smith, "Cost-driven materials selection criteria for redox flow battery electrolytes," Journal of Power Sources, vol. 330, pp. 261–272, 2016.

[30] K. T. Cho, P. Albertus, V. Battaglia, A. Kojic, V. Srinivasan, and A. Z. Weber, "Optimization and Analysis of High-Power Hydrogen/Bromine-Flow Batteries for Grid-Scale Energy Storage," Energy Technology, vol. 1, no. 10, pp. 596–608, 2013.

[31] R. M. Darling and M. L. Perry, "The Influence of Electrode and Channel Configurations on Flow Battery Performance," Journal of the Electrochemical Society, vol. 161, no. 9, pp. A1381–A1387, 2014.

[32] K. G. Gallagher, S. E. Trask, C. Bauer, T. Woehrle, S. F. Lux, M. Tschech, P. Lamp, B. J. Polzin, S. Ha, B. Long, Q. Wu, W. Lu, D. W. Dees, and A. N. Jansen, "Optimizing Areal Capacities through Understanding the Limitations of Lithium-Ion Electrodes," Journal of The Electrochemical Society, vol. 163, no. 2, pp. A138–A149, 2016.

[33] G. Kear, A. A. Shah, and F. C. Walsh, "Development of the all-vanadium redox flow battery for energy storage: A review of technological, Financial and policy aspects," International Journal of Energy Research, vol. 36, no. 11, pp. 1105–1120, 2012.

[34] D. Aaron, Z. Tang, A. B. Papandrew, and T. A. Zawodzinski, "Polarization curve analysis of all-vanadium redox flow batteries," Journal of Applied Electrochemistry, vol. 41, no. 10, pp. 1175–1182, 2011.

[35] Q. Chen, M. R. Gerhardt, and M. J. Aziz, "Dissection of the Voltage Losses of an Acidic Quinone Redox Flow Battery," Journal of The Electrochemical Society, vol. 164, no. 6, pp. A1126–A1132, 2017.

[36] L. Wei, M. C. Wu, T. S. Zhao, Y. K. Zeng, and Y. X. Ren, "An aqueous alkaline battery consisting of inexpensive all-iron redox chemistries for large-scale energy storage," Applied Energy, vol. 215, pp. 98–105, 2018.

[37] F. Xing, H. Zhang, and X. Ma, "Shunt current loss of the vanadium redox flow battery," Journal of Power Sources, vol. 196, no. 24, pp. 10 753–10 757, 2011.

[38] S. König, M. R. Suriyah, and T. Leibfried, "Model based examination on influence of stack series connection and pipe diameters on efficiency of vanadium redox flow batteries under consideration of shunt currents," Journal of Power Sources, vol. 281, pp. 272–284, 2015.

[39] R. A. Potash, J. R. McKone, S. Conte, and H. D. Abruña, "On the Benefits of a Symmetric Redox Flow Battery," Journal of The Electrochemical Society, vol. 163, no. 3, pp. A338–A344, 2016.

[40] S. Ha and K. G. Gallagher, "Estimating the system price of redox flow batteries for grid storage," Journal of Power Sources, vol. 296, pp. 122–132, 2015.

[41] Lazard, "Lazard's levelised cost of storage v2.0," 2016. [Online]. Available: https://www.lazard.com/media/438042/lazard-levelized-cost-of-storage-v20.pdf (Accessed: 2020-07-21).

[42] Redflow, "Installation and Operation Manual ZBM2 (3kW/10kWh)," 2018. [Online]. Available: https://redflow.com/wp-content/uploads/2018/03/ZBM2-Installation-and-Operation-Manual-CE-V2.9.pdf (Accessed: 2018-11-18).

[43] L. F. Arenas, A. Loh, D. P. Trudgeon, X. Li, C. Ponce de Leon, and F. C. Walsh, "The characteristics and performance of hybrid redox flow batteries with zinc negative electrodes for energy storage," Renewable and Sustainable Energy Reviews, vol. 90, pp. 992–1016, 2018.

[44] J. Winsberg, T. Hagemann, T. Janoschka, M. D. Hager, and U. S. Schubert, "Redox-Flow Batteries: From Metals to Organic Redox-Active Materials," Angewandte Chemie International Edition, vol. 56, no. 3, pp. 686–711, 2017.

[45] J. Noack, N. Roznyatovskaya, T. Herr, and P. Fischer, "The Chemistry of Redox-Flow Batteries," Angewandte Chemie International Edition, vol. 54, no. 34, pp. 9776–9809, 2015.

[46] Y. K. Zeng, T. S. Zhao, X. L. Zhou, L. Zeng, and L. Wei, "The effects of design parameters on the charge-discharge performance of iron-chromium redox flow batteries," Applied Energy, vol. 182, pp. 204–209, 2016.

[47] EnergyStorageSense, "Flow Batteries — Energy Storage Sense." [Online]. Available: http://energystoragesense.com/flow-batteries/ (Accessed: 2018-07-12).

[48] D. P. Scamman, G. W. Reade, and E. P. L. Roberts, "Numerical modelling of a bromide-polysulphide redox flow battery. Part 2: Evaluation of a utility-scale system," Journal of Power Sources, vol. 189, no. 2, pp. 1231–1239, 2009.

[49] K. Lin, Q. Chen, M. R. Gerhardt, L. Tong, S. B. Kim, L. Eisenach, A. W. Valle, D. Hardee, R. G. Gordon, M. J. Aziz, and M. P. Marshak, "Alkaline quinone flow battery," Science, vol. 349, no. 6255, pp. 1529–1532, 2015.

[50] B. Huskinson, M. P. Marshak, C. Suh, S. Er, M. R. Gerhardt, C. J. Galvin, X. Chen, A. Aspuru-Guzik, R. G. Gordon, and M. J. Aziz, "A metal-free organic-inorganic aqueous flow battery," Nature, vol. 505, no. 7482, pp. 195–198, 2014.

[51] Y. Yang, G. Zheng, and Y. Cui, "A membrane-free lithium/polysulfide semi-liquid battery for large-scale energy storage," Energy & Environmental Science, vol. 6, no. 5, p. 1552, 2013.

[52] Chemours, "Chemours—Nafion—Markets & Applications—Fuel Cells." [Online]. Available: https://www.chemours.com/Nafion/en_US/apps/fuel-cell.html (Accessed: 2017-09-20).

[53] 3M, "3M Redox Flow Battery Components for Energy Storage and Fuel Cell — 3M United States." [Online]. Available: https://www.3m.com/3M/en_US/company-us/all-3m-products/~/All-3M-Products/Energy/Power-Storage-and-Conversion/Battery-Materials/Redox-Flow-Battery-Components/?N=5002385+8709319+8710671+8710697+8711017+8731905+8743457+3294857497&rt=r3 (Accessed: 2018-07-11).

[54] AGC, "AGC launches the new brand "FORBLUE™", serving the expanding needs for chemical separation |News |AGC," 2017. [Online]. Available: http://www.agc.com/en/news/detail/1196110_2814.html (Accessed: 2018-07-12).

[55] W. Wang, Z. Nie, B. Chen, F. Chen, Q. Luo, X. Wei, G. G. Xia, M. Skyllas-Kazacos, L. Li, and Z. Yang, "A new Fe/V redox flow battery using a sulfuric/chloric mixed-acid supporting electrolyte," Advanced Energy Materials, vol. 2, no. 4, pp. 487–493, 2012.

[56] T. Janoschka, N. Martin, U. Martin, C. Friebe, S. Morgenstern, H. Hiller, M. D. Hager, and U. S. Schubert, "An aqueous, polymer-based redox-flow battery using non-corrosive, safe, and low-cost materials," Nature, vol. 527, no. 7576, pp. 78–81, 2015.

[57] K. Gong, X. Ma, K. M. Conforti, K. J. Kuttler, J. B. Grunewald, K. L. Yeager, M. Z. Bazant, S. Gu, and Y. Yan, "A zinc–iron redox-flow battery under $100 per kW h of system capital cost," Energy Environ. Sci., vol. 8, no. 10, pp. 2941–2945, 2015.

[58] D. Reed, E. Thomsen, W. Wang, Z. Nie, B. Li, X. Wei, B. Koeppel, and V. Sprenkle, "Performance of Nafion® N115, Nafion® NR-212, and Nafion® NR-211 in a 1 kW class all vanadium mixed acid redox flow battery," Journal of Power Sources, vol. 285, pp. 425–430, 2015.

[59] C. Minke and T. Turek, "Economics of vanadium redox flow battery membranes," Journal of Power Sources, vol. 286, pp. 247–257, 2015.

[60] X. L. Zhou, T. S. Zhao, L. An, Y. K. Zeng, and X. B. Zhu, "Performance of a vanadium redox flow battery with a VANADion membrane," Applied Energy, vol. 180, pp. 353–359, 2016.

[61] T. Zawodzinski, "Comparative Study of Different Membrane Types for Redox Flow Batteries." [Online]. Available: http://www.polyacs.net/Workshops/15FuelMat/images/Speakers/zzztomzforasilomar2015.pdf (Accessed: 2018-07-12).

[62] S. Roe, C. Menictas, and M. Skyllas-Kazacos, "A High Energy Density Vanadium Redox Flow Battery with 3 M Vanadium Electrolyte," Journal of The Electrochemical Society, vol. 163, no. 1, pp. A5023–A5028, 2016.

[63] D. Bryans, V. Amstutz, H. H. Girault, and L. E. Berlouis, "Characterisation of a 200 kw/400 kwh vanadium redox flow battery," Batteries, vol. 4, no. 4, 2018.

[64] X. Z. Yuan, C. Song, A. Platt, N. Zhao, H. Wang, H. Li, K. Fatih, and D. Jang, "A review of all-vanadium redox flow battery durability: Degradation mechanisms and mitigation strategies," International Journal of Energy Research, vol. 43, no. 13, pp. 6599–6638, 2019.

[65] "UKRFB Network Workshop 2020." [Online]. Available: https://sites.google.com/view/ukrfbnetwork/workshops/workshop-jul-2020 (Accessed: 2020-08-17).

[66] A. Bhattarai, N. Wai, R. Schweiss, A. Whitehead, G. G. Scherer, P. C. Ghimire, T. M. Lim, and H. H. Hng, "Vanadium redox flow battery with slotted porous electrodes and automatic rebalancing demonstrated on a 1 kW system level," Applied Energy, vol. 236, pp. 437–443, 2019.

[67] N. Poli, M. Schäffer, A. Trovò, J. Noack, M. Guarnieri, and P. Fischer, "Novel electrolyte rebalancing method for vanadium redox flow batteries," Chemical Engineering Journal, 2020.

[68] Rongke Power, "Rongke Power Container Products." [Online]. Available: http://www.rongkepower.com/chuneng?lang=en (Accessed: 2018-07-12).

[69] Dow Centre, "Techno-Economic Analysis - Dow Centre - The University of Queensland, Australia." [Online]. Available: http://www.dowcsei.uq.edu.au/technology (Accessed: 2018-07-13).

[70] M. Lauer, "Methodology guideline on techno economic assessment (TEA)." [Online]. Available: https://ec.europa.eu/energy/intelligent/projects/sites/iee-projects/files/projects/documents/thermalnet_methodology_guideline_on_techno_economic_assessment.pdf (Accessed: 2018-07-13).

[71] W. Hu, Z. Chen, and B. Bak-Jensen, "Optimal operation strategy of battery energy storage system to real-time electricity price in Denmark," in IEEE PES General Meeting, PES 2010. IEEE, 2010, pp. 1–7.

[72] C. J. Barnhart and S. M. Benson, "On the importance of reducing the energetic and material demands of electrical energy storage," Energy & Environmental Science, vol. 6, no. 4, p. 1083, 2013.

[73] D. Weißbach, G. Ruprecht, A. Huke, K. Czerski, S. Gottlieb, and A. Hussein, "Energy intensities, EROIs (energy returned on invested), and energy payback times of electricity generating power plants," Energy, vol. 52, pp. 210–221, 2013.

[74] W. Li, G. Joós, and J. Bélanger, "Real-time simulation of a wind turbine generator coupled with a battery supercapacitor energy storage system," IEEE Transactions on Industrial Electronics, vol. 57, no. 4, pp. 1137–1145, 2010.

[75] D. D. Banham-Hall, G. A. Taylor, C. A. Smith, and M. R. Irving, "Flow Batteries for Enhancing Wind Power Integration," IEEE Transactions on Power Systems, vol. 27, no. 3, pp. 1690–1697, 2012.

[76] B. Ge, W. Wang, D. Bi, C. B. Rogers, F. Z. Peng, A. T. De Almeida, and H. Abu-Rub, "Energy storage system-based power control for grid-connected wind

power farm," International Journal of Electrical Power and Energy Systems, vol. 44, no. 1, pp. 115–122, 2013.

[77] L. Gelažanskas, A. Baranauskas, K. A. Gamage, and M. Ažubalis, "Hybrid wind power balance control strategy using thermal power, hydro power and flow batteries," International Journal of Electrical Power & Energy Systems, vol. 74, pp. 310–321, 2016.

[78] M. Zhang, M. Moore, J. S. Watson, T. A. Zawodzinski, and R. M. Counce, "Capital Cost Sensitivity Analysis of an All-Vanadium Redox-Flow Battery," Journal of the Electrochemical Society, vol. 159, no. 8, pp. A1183–A1188, 2012.

[79] A. Crawford, V. Viswanathan, D. Stephenson, W. Wang, E. Thomsen, D. Reed, B. Li, P. Balducci, M. Kintner-Meyer, and V. Sprenkle, "Comparative analysis for various redox flow batteries chemistries using a cost performance model," Journal of Power Sources, vol. 293, pp. 388–399, 2015.

[80] R. M. Darling, K. G. Gallagher, J. A. Kowalski, S. Ha, and F. R. Brushett, "Pathways to low-cost electrochemical energy storage: a comparison of aqueous and nonaqueous flow batteries," Energy Environ. Sci., vol. 7, no. 11, pp. 3459–3477, 2014.

[81] O. Schmidt, A. Hawkes, A. Gambhir, and I. Staffell, "The future cost of electrical energy storage based on experience rates," Nature Energy, vol. 2, p. 1, 2017.

[82] S. van der Linden, "Bulk energy storage potential in the USA, current developments and future prospects," Energy, vol. 31, no. 15, pp. 3446–3457, 2006.

[83] "List of all balancing services — National Grid UK." [Online]. Available: https://www.nationalgrid.com/uk/electricity/balancing-services/list-all-balancing-services (Accessed: 2018-04-19).

[84] S. Sabihuddin, A. E. Kiprakis, and M. Mueller, "A numerical and graphical review of energy storage technologies," Energies, vol. 8, no. 1, pp. 172–216, 2015.

[85] S. X. Chen, H. B. Gooi, and M. Q. Wang, "Sizing of energy storage for microgrids," IEEE Transactions on Smart Grid, vol. 3, no. 1, pp. 142–151, 2012.

[86] M. Arbabzadeh, J. X. Johnson, R. De Kleine, and G. A. Keoleian, "Vanadium redox flow batteries to reach greenhouse gas emissions targets in an off-grid configuration," Applied Energy, vol. 146, pp. 397–408, 2015.

[87] J. García-González, R. M. R. de la Muela, L. M. Santos, and A. M. Gonzalez, "Stochastic joint optimization of wind generation and pumped-storage units in an electricity market," IEEE Transactions on Power Systems, vol. 23, no. 2, pp. 460–468, 2008.

[88] G. He, Q. Chen, C. Kang, P. Pinson, and Q. Xia, "Optimal Bidding Strategy of Battery Storage in Power Markets Considering Performance-Based Regulation and Battery Cycle Life," IEEE Transactions on Smart Grid, vol. 7, no. 5, pp. 2359–2367, 2016.

[89] A. Oudalov, R. Cherkaoui, and A. Beguin, "Sizing and optimal operation of battery energy storage system for peak shaving application," in 2007 IEEE Lausanne POWERTECH, Proceedings. IEEE, 2007, pp. 621–625.

[90] S. M. Vaca, C. Patsios, and P. Taylor, "Enhancing frequency response of wind farms using hybrid energy storage systems," in 2016 IEEE International Conference on Renewable Energy Research and Applications, ICRERA 2016. IEEE, 2017, pp. 325–329.

[91] L. Johnston, F. Díaz-González, O. Gomis-Bellmunt, C. Corchero-García, and M. Cruz-Zambrano, "Methodology for the economic optimisation of energy storage systems for frequency support in wind power plants," Applied Energy, vol. 137, pp. 660–669, 2015.

[92] J. A. Mellentine, W. J. Culver, and R. F. Savinell, "Simulation and optimization of a flow battery in an area regulation application," Journal of Applied Electrochemistry, vol. 41, no. 10, pp. 1167–1174, 2011.

[93] I. L. Gomes, H. M. Pousinho, R. Melício, and V. M. Mendes, "Stochastic coordination of joint wind and photovoltaic systems with energy storage in day-ahead market," Energy, vol. 124, pp. 310–320, 2017.

[94] J. Lei and Q. Gong, "Operating strategy and optimal allocation of large-scale VRB energy storage system in active distribution networks for solar/wind power applications," IET Generation, Transmission & Distribution, vol. 11, no. 9, pp. 2403–2411, 2017.

[95] T. Sayfutdinov, C. Patsios, J. W. Bialek, D. M. Greenwood, and P. C. Taylor, "Incorporating variable lifetime and self- discharge into optimal sizing and technology selection of energy storage systems," IET Smart Grid, vol. 1, no. 1, pp. 11–18, 2018.

[96] C. Bordin, H. O. Anuta, A. Crossland, I. L. Gutierrez, C. J. Dent, and D. Vigo, "A linear programming approach for battery degradation analysis and optimization in offgrid power systems with solar energy integration," Renewable Energy, vol. 101, pp. 417–430, 2017.

[97] M. R. Sarker, M. D. Murbach, D. T. Schwartz, and M. A. Ortega-Vazquez, "Optimal operation of a battery energy storage system: Trade-off between grid economics and storage health," Electric Power Systems Research, vol. 152, pp. 342–349, 2017.

[98] T. K. A. Brekken, A. Yokochi, A. von Jouanne, Z. Z. Yen, H. M. Hapke, and D. A. Halamay, "Optimal Energy Storage Sizing and Control for Wind Power Applications," IEEE Transactions on Sustainable Energy, 2011.

[99] A. Maheshwari, N. G. Paterakis, M. Santarelli, and M. Gibescu, "Optimizing the operation of energy storage using a non-linear lithium-ion battery degradation model," Applied Energy, vol. 261, no. December 2019, p. 114360, 2020.

[100] Y. Shi, B. Xu, Y. Tan, and B. Zhang, "A Convex Cycle-based Degradation Model for Battery Energy Storage Planning and Operation," in Proceedings of the American Control Conference, vol. 2018-June. IEEE, 2018, pp. 4590–4596.

[101] R. E. Ciez and J. F. Whitacre, "Comparative techno-economic analysis of hybrid micro-grid systems utilizing different battery types," Energy Conversion and Management, vol. 112, pp. 435–444, 2016.

[102] J. Schmalstieg, S. Käbitz, M. Ecker, and D. U. Sauer, "A holistic aging model for Li(NiMnCo)O2 based 18650 lithium-ion batteries," Journal of Power Sources, vol. 257, pp. 325–334, 2014.

[103] J. M. Reniers, G. Mulder, S. Ober-Blöbaum, and D. A. Howey, "Improving optimal control of grid-connected lithium-ion batteries through more accurate battery and degradation modelling," Journal of Power Sources, vol. 379, pp. 91–102, 2018.

[104] B. Zakeri and S. Syri, "Electrical energy storage systems: A comparative life cycle cost analysis," pp. 569–596, 2015.

[105] E. Hittinger, T. Wiley, J. Kluza, and J. Whitacre, "Evaluating the value of batteries in microgrid electricity systems using an improved Energy Systems Model," Energy Conversion and Management, vol. 89, pp. 458–472, 2015.

[106] R. Fu, D. Feldman, R. Margolis, M. Woodhouse, K. Ardani, R. Fu, D. Feldman, R. Margolis, M. Woodhouse, and K. Ardani, "U.S. Solar Photovoltaic System and Energy Storage Cost Benchmark: Q1 2020," NREL, Tech. Rep., 2021.

[107] R. Austin, "Solar Inverter Efficiency - What is the Most Efficient Solar Inverter? - Understand Solar," 2017. [Online]. Available: https://understandsolar.com/solar-inverter-efficiency (Accessed: 2021-06-01).

[108] C. Minke and T. Turek, "Materials, system designs and modelling approaches in techno-economic assessment of all-vanadium redox flow batteries – A review," Journal of Power Sources, vol. 376, pp. 66–81, 2018.

[109] Investopedia, "Which segments of the chemical sector have the highest profit margins?" [Online]. Available: https://www.investopedia.com/ask/answers/060115/which-segments-chemicals-sector-have-highest-profit-margins.asp (Accessed: 2020-05-08).

[110] "Live Vanadium Price, News and Articles." [Online]. Available: https://www.vanadiumprice.com/ (Accessed: 2018-08-23).

[111] AliBaba. [Online]. Available: https://www.alibaba.com/showroom/bulk-hydrochloric-acid.html (Accessed: 2020-05-14).

[112] ——. [Online]. Available: https://www.alibaba.com/showroom/bulk-sulphuric-acid.html (Accessed: 2020-05-14).

[113] "PREMIUM MAGNETIC-DRIVE SEALLESS CENTRIFUGAL PUMPS DB & SP SERIES." [Online]. Available: https://voigtabstore.com/content/DB/brochure.pdf (Accessed: 2020-05-18).

[114] B. Bowen. [Online]. Available: https://www.icis.com/explore/resources/news/2017/06/08/10114252/us-hydrochloric-acid-prices-jump-higher-on-outages/ (Accessed: 2020-05-14).

[115] K. Mongird, V. Fotedar, V. Viswanathan, V. Koritarov, P. Balducci, B. Hadjerioua, and J. Alam, "Energy storage technology and cost characterization report," Pacific Northwest National Laboratory, Tech. Rep. PNNL-28866, 2019.

[116] S. Kim, E. Thomsen, G. Xia, Z. Nie, J. Bao, K. Recknagle, W. Wang, V. Viswanathan, Q. Luo, X. Wei, A. Crawford, G. Coffey, G. Maupin, and V. Sprenkle, "1 kW/1 kWh advanced vanadium redox flow battery utilizing mixed acid electrolytes," Journal of Power Sources, vol. 237, pp. 300–309, 2013.

[117] McKinsey & Company, "The new rules of competition in energy storage," 2018. [Online]. Available: https://www.mckinsey.com/industries/electric-power-and-natural-gas/our-insights/the-new-rules-of-competition-in-energy-storage (Accessed: 2020-).

[118] R. Fu, T. Remo, and R. Margolis, "U.S. Utility-Scale Photovoltaics-Plus-Energy Storage System Costs Benchmark," NREL, Tech. Rep., 2018.

[119] Lazard, "Lazard's levelised cost of storage v3.0," 2017. [Online]. Available: https://www.lazard.com/media/450338/lazard-levelized-cost-of-storage-version-30.pdf (Accessed: 2020-07-21).

[120] Z. Li, M. S. Pan, L. Su, P.-C. Tsai, A. F. Badel, J. M. Valle, S. L. Eiler, K. Xiang, F. R. Brushett, and Y.-M. Chiang, "Air-Breathing Aqueous Sulfur Flow Battery for Ultralow-Cost Long-Duration Electrical Storage," Joule, vol. 1, no. 2, pp. 306–327, 2017.

[121] E. Minear, "Energy storage technology and cost assessment: Executive summary," 2018. [Online]. Available: https://www.epri.com/#/pages/product/000000003002013958/?lang=en-US (Accessed: 2020-09-27).

[122] G. Damato, "Energy storage cost analysis : Executive summary of 2017 methods and results," 2017. [Online]. Available: https://www.epri.com/#/pages/product/000000003002012046/?lang=en (Accessed: 2020-09-28).

[123] "Inside construction of the world's largest lithium ion battery storage facility," 2016. [Online]. Available: https://www.utilitydive.com/news/inside-construction-of-the-worlds-largest-lithium-ion-battery-storage-faci/431765/ (Accessed: 2020-04-22).

[124] CIBSE, "Cost model - battery storage." [Online]. Available: https://www.cibsejournal.com/technical/cost-model-battery-storage/ (Accessed: 2020-04-29).

[125] C. Minke, U. Kunz, and T. Turek, "Techno-economic assessment of novel vanadium redox flow batteries with large-area cells," Journal of Power Sources, vol. 361, pp. 105–114, 2017.

[126] W. Cole, A. W. Frazier, W. Cole, and A. W. Frazier, "Cost Projections for Utility-

Scale Battery Storage Cost Projections for Utility- Scale Battery Storage," NREL, Tech. Rep. June, 2019.

[127] EnerNOC, "Open data," 2013. [Online]. Available: https://open-enernoc-data.s3.amazonaws.com/anon/index.html (Accessed: 2021-10-08).

[128] OpenEI, "U.S. Utility Rate Database," 2016. [Online]. Available: https://openei.org/apps/USURDB/rate/view/5571b5545457a38e37db22a4 (Accessed: 2019-07-23).

[129] OpenEI, "U.S. Utility Rate Database," 2019. [Online]. Available: https://openei.org/apps/USURDB/rate/view/5d9abde65457a3cd5061b9f1 (Accessed: 2020-02-20).

[130] D. Roberts and S. Brown, "Identifying calendar-correlated day-ahead price profile clusters for enhanced energy storage scheduling," Energy Reports, vol. 6, pp. 35–42, 2020.

[131] "E1049-85 standard practices for cycle count- ing in fatigue analysis. 85(reapproved):1–10," 1997.

[132] PJM, "RTO Regulation Signal Data," 2020. [Online]. Available: https://www.pjm.com/-/media/markets-ops/ancillary/regulation-signal-posting-010220.ashx?la=en (Accessed: 2020-04-27).

[133] B. Xu, Y. Dvorkin, D. S. Kirschen, C. A. Silva-Monroy, and J. P. Watson, "A comparison of policies on the participation of storage in U.S. frequency regulation markets," IEEE Power and Energy Society General Meeting, vol. 2016-Novem, 2016.

[134] CAISO, "Business Practice Manual for Market Operations, Version 68," 2020. [Online]. Available: https://bpmcm.caiso.com/BPMDocumentLibrary/MarketOperations/BPM_for_MarketOperations_V68_redline.pdf (Accessed: 2020-11-19).

[135] "Appendix K Ancillary Service Requirements Protocol (ASRP)," 2019. [Online]. Available: http://www.caiso.com/Documents/AppendixK-AncillaryServiceRequirementsProtocol-ASRP-asof-Dec3-2019.pdf (Accessed: 2020-11-19).

[136] CAISO, "Oasis," 2020. [Online]. Available: http://oasis.caiso.com

[137] California ISO, "Day-Ahead Market Enhancements Phase 1 : Fifteen-Minute Granularity Third Revised Straw Proposal," CAISO, Tech. Rep., 2019.

[138] T. Campbell and T. H. Bradley, "A model of the effects of automatic generation control signal characteristics on energy storage system reliability," Journal of Power Sources, vol. 247, pp. 594–604, 2014.

[139] CAISO, "Settlements & Billing BPM Configuration Guide: Regulation Up Mileage Settlement (CC 7251) Version 5.1." [Online]. Available: https://bpmcm.caiso.com/BPMDocumentLibrary/SettlementsandBilling/ConfigurationGuides/AncillaryServices/BPM-CGCC7251RegulationUpMileageSettlement_5.1.doc (Accessed: 2020-11-19).

[140] CAISO, "Pay Performance Regulation Accuracy Model Calculator." [Online]. Available: http://www.caiso.com/Documents/PayPerformanceRegulationAccuracyModelCalculator.xls (Accessed: 2020-11-24).

[141] PNNL, "Energy storage cost and performance database." [Online]. Available: https://www.pnnl.gov/ESGC-cost-performance (Accessed: 2021-03-02).

[142] A. W. Frazier, W. Cole, P. Denholm, D. Greer, and P. Gagnon, "Assessing the potential of battery storage as a peaking capacity resource in the United States," Applied Energy, vol. 275, no. June, p. 115385, 2020.

[143] C. P. U. Commision, "2018 resource adequacy report." [Online]. Available: https://www.cpuc.ca.gov/RA/ (Accessed: 2021-05-04).

[144] H. P. Williams, Model Building in Mathematical Programming, 5th ed. Wiley, 2013.

[145] Z. Yuan, Y. Duan, H. Zhang, X. Li, H. Zhang, and I. Vankelecom, "Advanced porous membranes with ultra-high selectivity and stability for vanadium flow batteries," Energy and Environmental Science, vol. 9, no. 2, pp. 441–447, 2016.

[146] W. Lu, Z. Yuan, Y. Zhao, X. Li, H. Zhang, and I. F. Vankelecom, "High-performance porous uncharged membranes for vanadium flow battery applications created by tuning cohesive and swelling forces," Energy and Environmental Science, vol. 9, no. 7, pp. 2319–2325, 2016.

[147] A. Tang, J. McCann, J. Bao, and M. Skyllas-Kazacos, "Investigation of the effect of shunt current on battery efficiency and stack temperature in vanadium redox flow battery," Journal of Power Sources, vol. 242, pp. 349–356, 2013.

[148] L. Wei, T. S. Zhao, Q. Xu, X. L. Zhou, and Z. H. Zhang, "In-situ investigation of hydrogen evolution behavior in vanadium redox flow batteries," Applied Energy, vol. 190, pp. 1112–1118, 2017.

[149] A. Rai and O. Nunn, "On the impact of increasing penetration of variable renewables on electricity spot price extremes in Australia," Economic Analysis and Policy, vol. 67, 2020.

[150] M. B. Roberts, A. Bruce, and I. MacGill, "Impact of shared battery energy storage systems on photovoltaic self-consumption and electricity bills in apartment buildings," Applied Energy, vol. 245, pp. 78–95, 2019.

[151] P. Denholm, D. J. Arent, S. F. Baldwin, D. E. Bilello, G. L. Brinkman, J. M. Cochran, W. J. Cole, B. Frew, V. Gevorgian, J. Heeter, B. M. S. Hodge, B. Kroposki, T. Mai, M. J. O'Malley, B. Palmintier, D. Steinberg, and Y. Zhang, "The challenges of achieving a 100% renewable electricity system in the United States," Joule, vol. 5, no. 6, pp. 1331–1352, 2021.

[152] M. Akbari, P. Asadi, M. K. B. Givi, and G. Khodabandehlouie, "Artificial neural network and optimization," in Advances in Friction-Stir Welding and Processing. Woodhead Publishing, 2014, pp. 543–599.

[153] V. Muenzel, A. F. Hollenkamp, A. I. Bhatt, J. De Hoog, M. Brazil, D. A. Thomas, and I. Mareels, "A comparative testing study of commercial 18650-format lithium-ion battery cells," Journal of the Electrochemical Society, vol. 162, no. 8, pp. A1592–A1600, 2015.

[154] D. Aguilar-Dominguez, J. Ejeh, A. D. Dunbar, and S. F. Brown, "Machine learning approach for electric vehicle availability forecast to provide vehicle-to-home services," Energy Reports, vol. 7, pp. 71–80, 2021.

[155] SolarStrap, "Photos." [Online]. Available: https://solarstrap.com/commercial-solar-panel/ (Accessed: 2021-08-16).

[156] European Commission, "Photovoltaic geographical information system (pvgis)." [Online]. Available: https://re.jrc.ec.europa.eu/pvg_tools/en/tools.html (Accessed: 2021-08-11).

[157] US Department of Energy, "Guide to the Federal Investment Tax Credit for Commercial Solar Photovoltaics." [Online]. Available: https://www.energy.gov/sites/prod/files/2020/01/f70/GuidetotheFederalInvestmentTaxCreditforCommercialSolarPV.pdf (Accessed: 2021-30-08).

[158] D. C. Jordan and S. R. Kurtz, "Photovoltaic degradation rates - An Analytical Review," Progress in Photovoltaics: Research and Applications, vol. 21, no. 1, pp. 12–29, 2013.

[159] "Energy storage cost and performance database." [Online]. Available: https://www.pnnl.gov/ESGC-cost-performance (Accessed: 2021-09-06).

[160] G. Zhang, L. Cao, S. Ge, C.-Y. Wang, C. E. Shaffer, and C. D. Rahn, "In Situ

Measurement of Radial Temperature Distributions in Cylindrical Li-Ion Cells," Journal of The Electrochemical Society, vol. 161, no. 10, pp. A1499–A1507, 2014.

[161] Z. Li, J. Zhang, B. Wu, J. Huang, Z. Nie, Y. Sun, F. An, and N. Wu, "Examining temporal and spatial variations of internal temperature in large-format laminated battery with embedded thermocouples," Journal of Power Sources, vol. 241, pp. 536–553, 2013.

[162] W. M. Dose, C. Xu, C. P. Grey, and M. F. L. De Volder, "Effect of Anode Slippage on Cathode Cutoff Potential and Degradation Mechanisms in Ni-Rich Li-Ion Batteries," Cell Reports Physical Science, vol. 1, no. 11, 2020.

[163] L. K. Gan, J. Reniers, and D. Howey, "A hybrid vanadium redox/lithium-ion energy storage system for off-grid renewable power," in 2017 IEEE Energy Conversion Congress and Exposition, ECCE 2017, vol. 2017-January. IEEE, 2017, pp. 1016–1023.

[164] M. Schimpe, M. E. von Kuepach, M. Naumann, H. C. Hesse, K. Smith, and A. Jossen, "Comprehensive modeling of temperature-dependent degradation mechanisms in lithium iron phosphate batteries," Journal of The Electrochemical Society, vol. 165, pp. A181–A193, 2018.